SOUTH WEST AFRICA
SUIDWES-AFRIKA

DEPARTMENT OF ECONOMIC AFFAIRS
DEPARTEMENT VAN EKONOMIESE SAKE

GEOLOGICAL SURVEY
GEOLOGIESE OPNAME

DAMARAN STRUCTURAL AND METAMORPHIC GEOLOGY OF AN AREA SOUTH-EAST OF WALVIS BAY, SOUTH WEST AFRICA/NAMIBIA

by/deur

E. W. SAWYER

MEMOIR 7

G.P.-S.

SOUTH WEST AFRICA
SUIDWES-AFRIKA

DEPARTMENT OF ECONOMIC AFFAIRS
DEPARTEMENT VAN EKONOMIESE SAKE

GEOLOGICAL SURVEY
GEOLOGIESE OPNAME

MEMOIR 7

DAMARAN STRUCTURAL AND METAMORPHIC GEOLOGY OF AN AREA SOUTH-EAST OF WALVIS BAY, SOUTH WEST AFRICA/NAMIBIA

by/deur

E. W. SAWYER, M.Sc.

Thesis submitted in partial fulfilment of the degree of Master of Science at the University of Cape Town
Tesis voorgelê om gedeeltelik te voldoen aan die vereistes ter verkryging van die graad Magister Scientiae aan die Universiteit van Kaapstad

Local/Plaaslik R2,02
4% GST/AVB.... R0,08
R2,10
Abroad/Buitelands R2,50
Post Free/Posvry

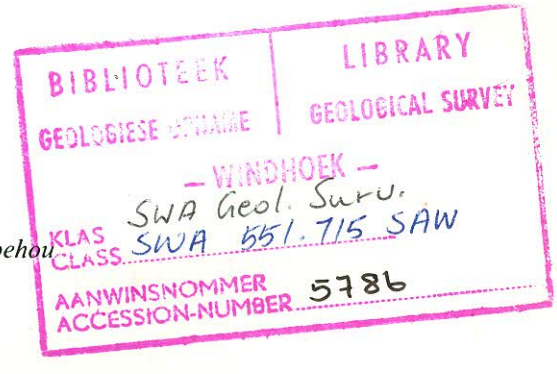

Printed by the Government Printer, Bosman Street/Private Bag X85, Pretoria, 0001
Gedruk deur die Staatsdrukker, Bosmanstraat/Privaatsak X85, Pretoria, 0001

Obtainable from the above address or from the Geological Survey, P.O. Box 2168, Windhoek
Verkrygbaar van bostaande adres of van die Geologiese Opname, Posbus 2168, Windhoek

ISBN 0 621 06066 6

28489—1

CONTENTS

DAMARAN STRUCTURAL AND METAMORPHIC GEOLOGY OF AN AREA SOUTH-EAST OF WALVIS BAY, SOUTH WEST AFRICA/NAMIBIA

ABSTRACT

Three main sedimentological, structural and metamorphic zones are recognised, the Central Zone in the north-west, bordered on the south by the Okahandja Lineament Zone, and the easternmost Trough Zone.

Lithologies and sedimentary structures indicate the Damara succession (from the base upwards—Nosib Group, Rössing, Chuos and Karibib Formations) to have been largely deposited in shallow water in the Central Zone. The Tinkas Member (in part a lateral equivalent of the Karibib Formation and partly the basal portion of the Kuiseb Formation) is characteristic of the Okahandja Lineament Zone and appears to have been of turbidite origin derived from the Central Zone and deposited on a continental slope.

The first three regional deformations and the two metamorphisms (M_1 synchronous with the second deformation and M_2, late to post the third deformation) can be directly correlated in the Central Zone and the Okahandja Lineament Zone, indicating similar tectono-metamorphic histories. The M_1 event occurred just after the intrusion of the pre-tectonic Salem Granite and is considered to be due to an early phase of subduction of a north-westerly dipping plate (700–650 Ma.). M_2 is believed to be due to the final stages of closure of the north-easterly trending Damara Sea. Thus the Central Zone represents a lower pressure/high temperature metamorphic belt. Both M_1 and M_2 are recognised in the Trough Zone, and on that basis the first two and perhaps the third deformations can be correlated with Trough Zone events.

Thermodynamic consideration of reaction equilibria for two Central Zone M_2 pelitic assemblages yield $T=652 \pm 25$ °C, $P=4{,}25 \pm 0{,}3$ kb, $X_{H_2O}=0{,}12$. In the Trough Zone calculated reaction equilibria for three M_2 pelitic assemblages indicate $T=605 \pm 25$ °C, $P=7{,}3 \pm 1{,}2$ kb, $X_{H_2O} \simeq 0{,}5$. Consideration of calc-pelite and calc-silicate assemblages in the Okahandja Lineament Zone suggests $T=585 \pm 25$ °C, $P=4{,}0 \pm 1{,}0$ kb, $X_{H_2O} \simeq 0{,}9$ for M_2.

Geothermal gradients in the Central Zone and the Okahandja Lineament Zone were about 40 °C. km^{-1} during M_2 whereas that of the Trough Zone was about 22 °C. km^{-1}. The two areas are thus characterised as low-pressure and high-pressure metamorphic belts respectively.

Diapiric structures in the Central Zone formed during M_2 with metamorphism serving to accelerate dome growth on a gravitationally unstable boundary between dense Damara metapelites and marbles and less dense pre-Damara granitic gneisses. Calculated dome spacing derived from a simple two-layer model representative of the Damara cover on the granitic basement are similar to those determined in the field.

A total of 50 to 80 per cent shortening is calculated from F_2 folds, deformed pillows and variolites for the second Trough Zone deformation. A similar order of shortening is obtained from third-generation folds in the Okahandja Lineament Zone.

Ten kilometres of uplift occurred in the Trough Zone after M_2 and before the emplacement of the Donkerhuk Granite. Uplift occurred along a subvertical lineament having the characteristics of a 'median tectonic line' at the very eastern edge of the Okahandja Lineament Zone. Uplift is considered to be due to isostatic rebound of continental crust at the southern edge of the Trough Zone which was partly overthrust and deeply buried by the Central Zone crustal block during the final stages of a continent—continent collision.

Finally the Donkerhuk Granite intruded along the line of uplift and thermally metamorphosed adjacent country rocks. Mineral assemblages from the aureole north of Hope Mine indicate $T=700° \pm 20$ °C, $P=4{,}6 \pm 1{,}0$ kb. During the emplacement of the granite fourth- and fifth-generation folds were formed in the Hope area of the Trough Zone.

UITTREKSEL

Drie hoof- sedimentologiese, strukturele en metamorfe sones word onderskei: die Sentraalsone in die noordweste, aan die suide begrens deur die Okahandja Lineamentsone, en die Trogsone in die ooste.

Litologieë en sedimentêre strukture dui daarop dat die Damara-opeenvolging (van die basis opwaarts—Groep Nosib, en Formasies Rössing, Chuos en Karibib) in die Sentraalsone grootliks in vlak water afgeset is. Die Lid Tinkas (gedeeltelik 'n laterale ekwivalent van die Formasie Karibib en gedeeltelik die basale gedeelte van die Formasie Kuiseb) is kenmerkend van die Okahandja Lineamentsone en blyk van turbiditiese oorsprong, afkomstig van die Sentraalsone en op 'n kontinentale helling afgeset, te wees.

Die eerste drie regionale vervormings en die twee metamorfoses (M_1 gelyktydig met die tweede vervorming en M_2, laat tot na die derde vervorming) kan in die Sentraalsone en die Okahandja Lineamentsone direk gekorreleer word, duiende op soortgelyke tektono-metamorfe geskiedenisse. Die M_1-gebeurtenis het net na die indringing van die voortektoniese variëteit van die Suite Salemgraniet plaasgevind en word beskou te wyte te wees aan 'n vroeë fase van subduksie van 'n noordweshellende plaat (700 tot 650 Ma). M_2 word beskou as die finale stadia van sluiting van die noordoosstrekkende Damarasee. Die Sentraalsone verteenwoordig dus 'n laer druk/hoër temperatuur metamorfe gordel. Beide M_1 en M_2 word in die Trogsone herken en op daardie basis kan die eerste twee en moontlik die derde vervorming met gebeure in die Trogsone korreleer word.

Termodinamiese oorwegings van reaksie-ekwilibria vir twee M_2 pelitiese versamelings van die Sentraalsone dui op $T=652 \pm 25$ °C, $P=4{,}25 \pm 0{,}3$ kb, $X_{H_2O}=0{,}12$. In die Trogsone dui berekende reaksie-ekwilibria vir drie M_2 pelitiese versamelings op $T=605 \pm 25$ °C, $P=7{,}3$ kb $\pm 1{,}2$ kb, $X_{H_2O} \simeq 0{,}5$. Oorweging van kalkpeliet- en kalksilikaatversamelings in die Okahandja Lineamentsone suggereer $T=585 \pm 25$ °C, $P=4{,}0 \pm 1{,}0$ kb, $X_{H_2O} \simeq 0{,}9$ vir M_2.

Geotermiese gradiënte in die Sentraal- en Okahandja Lineamentsone was ongeveer 40 °C. km^{-1} gedurende M_2 terwyl dié van die Trogsone ongeveer 22 °C. km^{-1} was. Die twee gebiede word dus respektiewelik as lae druk en hoë temperatuur metamorfe gordels karakteriseer.

Diapiriese strukture het in die Sentraalsone tydens M_2 gevorm met metamorfose om koepelgroei op 'n gravitasionele onstabiele grens tussen digte Damarametapeliete en -marmers en minder digte voor-Damaragranietgneise te versnel. Berekende koepelspasiëring, soos afgelei van 'n eenvoudige tweelaagmodel verteenwoordigend van die Damaradekking op die granitiese vloer, is soortgelyk aan dié in die veld bepaal.

'n Totaal van 50 tot 80 persent verkorting is van F_2-plooie, vervormde kussings en variëteite vir die tweede Trogsonevervorming bereken. 'n Soortgelyke orde verkorting is vir derdegenerasie plooie in die Okahandja Lineamentsone verkry.

Tien kilometer opheffing het in die Trogsone ná M_2 en vóór die inplasing van die Donkerhukgraniet plaasgevind. Opheffing het langs 'n subvertikale lineament met die kenmerke van 'n 'mediaan tektoniese lyn' op die oostelike rand van die Okahandja Lineamentsone plaasgevind. Opheffing word beskou te wyte te wees aan isostatiese terugsprong van kontinentale kors by die suidelike rand van die Trongsone, wat gedeeltelik oorgeskuif en diep begrawe is deur die korsblok van die Sentraalsone tydens die finale stadia van 'n kontinent—kontinentbotsing.

Ten slotte het die Donkerhukgraniet langs die lyn van opheffing ingedring en die aangrensende wandgesteentes termies gemetamorfoseer. Mineraalversamelings van die oureool noord van die Hope-myn dui op $T=700\ °C \pm 20\ °C$, $P=4{,}6 \pm 1{,}0$ kb. Tydens die inplasing van die graniet het vierde- en vyfdegenerasieplooie in die Hope-gebied van die Trogsone gevorm.

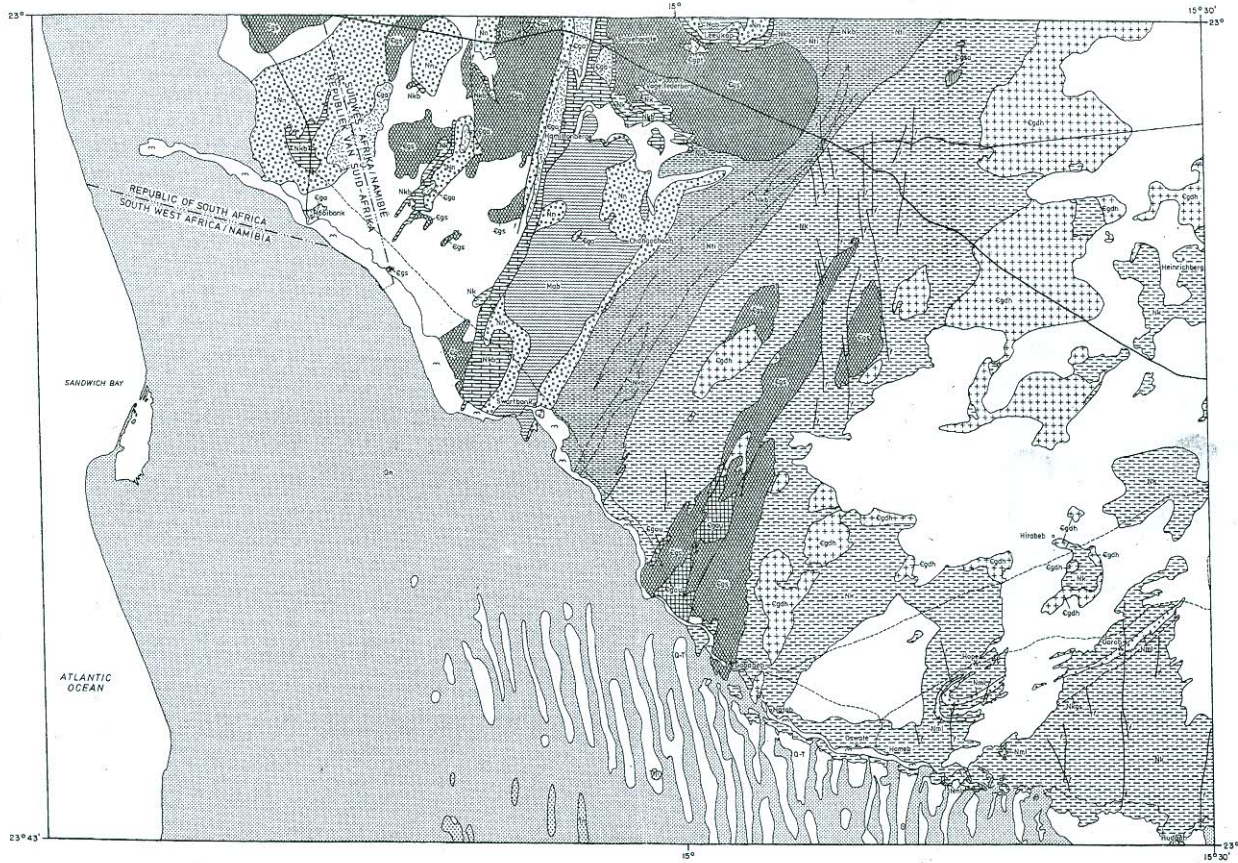

Alluvium

Aeolian sand, sandsea of the Namib Desert

Sand, soil, calcrete, silcrete, gypcrete west of 15°E

Reddish semi-consolidated aeolian sand with subordinate calcrete layers

Light grey, medium-grained, muscovite-biotite adamellite, scattered garnet and microcline $\mathfrak{e}$ sts in places — DONKERHUK GRANITE

Phenocryst in places

Dark grey hornblende-biotite-quartz diorite — POST-TECTONIC QUARTZ-DIORITE

Pink protoclastic medium-grained granite and adamellite, locally porphyritic — SAMUT GRANITE

Red foliated granite

Pinkish foliated (protomylonitic) granite and adamellite — AUSSINANIS GRANITE

Grey-pink, coarse-grained, foliated, porphyritic to aphyritic adamellite and granodiorite — SALEM GRANITIC SUITE

FORMATION	SUBGROUP	GROUP
Pelitic schist, metagraywacke, graphitic schist (Nkgs)		
MATCHLESS MEMBER (Nml) Amphibole schist, metabasite, pillow lava	(Nk) KUISEB	KHOMAS
TINKAS MEMBER (Nt) Dark, fine-grained pelitic schist, calc-silicate fels		
Calcitic and dolomitic marbles, minor schist and calc-silicate fels	(Nkb) KARIBIB	
Pebbly schist	(Nc) CHUOS	
Quartzite, arkose, conglomerate; calc-silicate fels	KHAN AND ETUSIS	SWAKOP / NOSIB
Paragneiss, augengneiss, schist, quartzite, conglomerate, calc-silicate fels, marble		ABBABIS METAMORPHIC COMPLEX

DAMARA SEQUENCE

Locality — Natab

Main roads

Other roads

International boundary

10 0 10 20 30 Kilometres

Folder I.1 – Geological map of the area

Voufiguur I.1 – Geologiese kaart van die gebied

1. INTRODUCTION

1.1 GENERAL

The area investigated is situated south-east of Walvis Bay in the Namib Desert of South West Africa/Namibia. Covering some 5 000 km² it is bounded by latitude 23°S along its northern edge and longitude 15°30′E at its eastern edge, and the Kuiseb River to the south and west. Exposures on the south bank of the Kuiseb and those present between sand dunes were also mapped (Folder 1.1).

The mapping project was initiated as part of Geological Survey's programme of mapping economically interesting areas in South West Africa/Namibia. The detailed description of the stratigraphy, outcrop and rock-types has been dealt with elsewhere (Sawyer 1979) and only a brief summary of the rock types will be given in Section 2.

1.2 PREVIOUS WORK

The earliest geological work was carried out in the area centered around the copper deposits at Hope and Gorob. A shaft was also sunk near Homeb, at what was thought to be a nickel occurrence. Between 1953 and 1954 the Bethlehem Steel Company undertook some reconnaissance mapping over the western part of the present area. The Hope–Gorob area was investigated by Rand Mines in 1957 and 1958, and recently in detail by the Johannesburg Consolidated Investment Company. The staff of the Desert Research Station at Gobabeb are engaged in geomorphological and ecological work within the confines of the Namib–Naukluft Park.

1.3 PRESENT INVESTIGATION

During mapping it became apparent that the area could be divided into four distinct structural and metamorphic domains (see Fig. 1.1). Three of these areas, the Central Zone, the Trough Zone and the Okahandja Lineament Zone have an important bearing on the sedimentological, structural and metamorphic evolution of the Damara Orogen. The aureole around the Donkerhuk Granite forms the fourth zone.

The sedimentological aspect has been dealt with elsewhere (Sawyer 1979). Here an attempt is made at establishing the deformation history of each zone and of correlating the deformation events between the various zones. An investigation of mineral-fabric relations is intended to resolve the metamorphic history and to fix metamorphic events within the tectonic framework. To define the conditions of metamorphism within each subzone a thermodynamic approach to reaction equilibria of selected low-variance mineral assemblages is used.

It is proposed that a combination of structural and metamorphic data obtained from each of the three subzones will enable new constraints to be placed upon a model attempting to explain the evolution of the Damara Orogen.

1.4 CHOICE OF UNITS

For the thermodynamic calculations, units based on the c.g.s. system are used in order to remain compatible with the bulk of available literature. Thus, for example, kilobars and calories are used in preference to pascals and joules respectively.

2. STRATIGRAPHY

2.1 INTRODUCTION

As far as possible the lithostratigraphic names approved by the South African Committee for Stratigraphy for subdivisions of the Damara Sequence and its intrusives have been adhered to. An informal nomenclature has, however, been employed for some Damara intrusives and rock units of the pre-Damara Abbabis Complex for which lithostratigraphic names have not yet been coined.

The stratigraphy is outlined in Table 2.1.

2.2 PRE-DAMARA ABBABIS COMPLEX

Pre-Damara rocks occur in the cores of several antiformal structures just west of the Okahandja Lineament Zone. Large parts of these basement rocks have undergone Damara reconstitution producing high-grade gneisses which have locally suffered partial melting to form red granite, red gneissic granite or buff leucocratic granite.

Four pre-Damara divisions have been recognised. Medium- to coarse-grained quartzo-feldspathic gneisses, quartzites, micaceous quartzites and cordierite schists constitute the "lower metasedimentary sequence". In the Swartbank area the "lower metasedimentary sequence" is overlain, probably unconformably, by the "upper metasedimentary sequence" consisting of calc-silicate rocks and marble near the base passing into a sequence of gneisses, schists and glassy quartzites. The rocks of both the lower and upper metasedimentary sequences are considered to be metasediments because of varied appearance, thin banding and rare cross-lamination.

The eastern part of the pre-Damara contains a large body of coarse-grained augen gneiss of very uniform appearance. Rare cross-cutting contacts with the "lower metasedimentary sequence", occasional xenoliths and aplitic dykes indicate this to be an ortho-augen gneiss derived from a porphyritic granite of batholithic proportions intruded into older pre-Damara metasediments.

Several metamorphosed dolerite dykes of two distinct ages intrude the ortho-augen gneiss and the "lower metasedimentary sequence" and represent the youngest pre-Damara rocks.

The pre-Damara rocks have a strong foliation, often striking east–west, contrary to the Damara trend. However, the Damara fabric is seen at the margins of pre-Damara outcrop areas, and it is probable that the rocks underwent at least one tectonic and metamorphic event before the Damara overprint.

2.3 DAMARA SEQUENCE

2.3.1 Nosib Group

The Nosib Group rocks are divided into a lower Etusis Formation and an upper Khan Formation. In the Leeukop Antiform (Folder 1.1), however, the sequence is rather mixed and the Nosib commences with Khan facies rocks interfingering with Etusis facies higher in the sequence. Nosib rocks occur only west of the Okahandja Lineament Zone.

2.3.1.1 *Etusis Formation*

The Etusis Formation buries a topography of up to 800 m relief on the pre-Nosib surface. The topographic lows are filled with locally derived material from the underlying pre-Damara. The development of a basal schistose metarudite is thus local. Above the metarudite is a thick sequence of pink or buff feldspathic medium-grained quartzites and meta-arkoses which are often cross-bedded and cross-laminated with heavy-mineral segregation laminae. Clean-washed metarudite bands are also present. In the Rooibank area especially, some Etusis Formation rocks contain up to 75 per cent microcline and may represent reworked acid extrusives. The derivation of the Etusis appears to have been largely

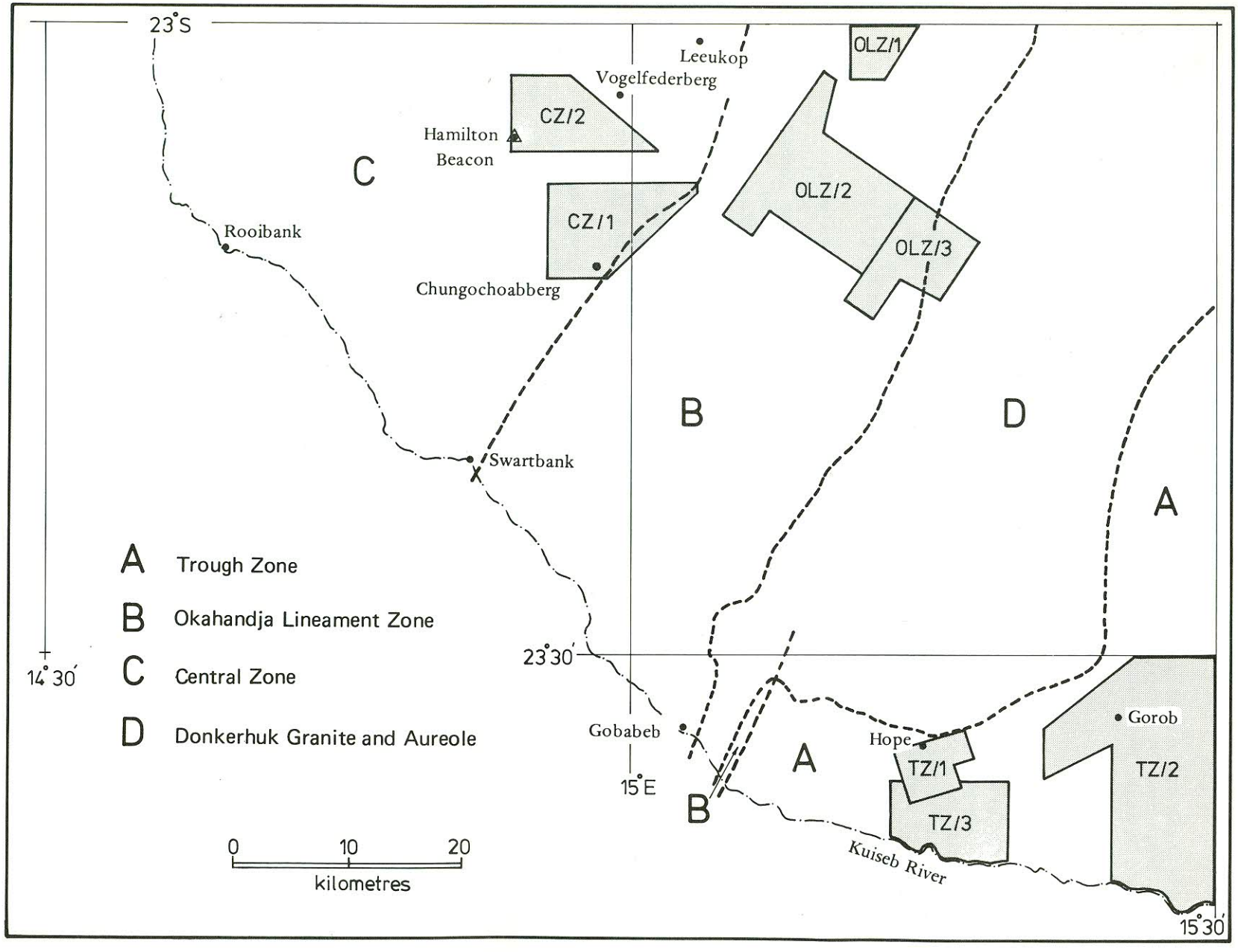

Fig. 1.1 — Major tectono-metamorphic zones and location of structural subzones.
Belangrikste tektono-metamorfe sones en ligging van strukturele subsones.

Table 2.1—STRATIGRAPHIC SEQUENCE WITHIN AREA MAPPED

DAMARA INTRUSIVES	POST-TECTONIC		Donkerhuk Granite ‡ Samut granite * Post-tectonic quartz diorite The Red Granites	
	PRE- and SYN-TECTONIC		Aussinanis Granite Salem Granite Suite	
DAMARA SEQUENCE	SWAKOP GROUP	KHOMAS SUBGROUP	Kuiseb Formation Karibib Formation Chuos Formation	Matchless Member Tinkas Member
			Rössing Formation	
	NOSIB GROUP		Khan Formation Etusis Formation	
PRE-DAMARA			Abbabis Complex	* Metadolerites * Ortho-augen gneiss * Upper metasedimentary sequence * Lower metasedimentary sequence

* Denotes informal term. ‡ Name not yet submitted to SACS for approval.

from the north-west, based on palaeocurrent estimates made from cross-bedding and cross-laminations.

2.3.1.2 *Khan Formation*

Typically the rocks are pale greenish-grey in colour, and fairly massive, occasionally banded but generally lacking in fissility. The texture is granoblastic to granoblastic-polygonal and fine to medium grained. Although there is rarely a shape orientation the rocks are generally not gneisses in the sense of Miyashiro (1973b), Spry (1969) and Winkler (1976), because of lack in fissility. The term fels (Winkler 1976) is appropriate with regard to the hand specimen and thin section appearance of these rocks. Quartz and plagioclase are ubiquitous whilst garnet, wollastonite, scapolite, microcline, epidote, clinozoisite, calcite, diopside-hedenbergite, amphibole and sphene may also be present. Near the base of the formation metarudites are locally developed, especially where Khan rocks underlie Etusis rocks as in the Leeukop area (Sawyer 1979).

In migmatite areas both the Etusis and Khan Formations have undergone partial melting to form either red gneiss or red homogeneous granite and rarely leucocratic granite.

2.3.2 Swakop Group

2.3.2.1 *Rössing Formation*

The Rössing Formation has been recognised in only two small areas, viz the Leeukop Antiform and south-west of Chungochoabberg, both west of the Okahandja Lineament. With a maximum thickness of about 10 m, it consists of a medium- to coarse-grained grey-blue marble up to 3 m thick at the base which is overlain by thinly banded greenish-brown, medium-grained calc-silicate rocks. The Rössing Formation rocks overstep the Nosib in the Leeukop Antiform, but elsewhere in the mapped area are bounded by a disconformity at the base.

2.3.2.2 *Chuos Formation*

Chuos Formation rocks crop out only to the west of the Okahandja Lineament Zone where these show rapid thickness variations. These may rest unconformably upon pre-Damara, Nosib or Rössing rocks but the angular discordance is small.

In the extreme west the Chuos is some 30 m thick and comprises a blackish ferruginous quartzite of variable iron content at the base overlain by greenish-white calc-silicate rocks. In the eastern part of its outcrop the Chuos is considerably thicker with the development of a ferruginous quartzite at the base, followed by thick schist, micaceous quartzite, schistose metarudite, and pebbly schist units. Dark-green, hard, medium- to coarse-grained glassy calc-silicate bands are numerous at the base and again at the top of the succession. Yellowish-brown, grey or bluish fine- to medium-grained dolomitic marbles occur only near the base.

Nowhere has evidence (e.g. striated clasts) been found to suggest a glacial orig.n for the schistose metarudite and pebbly schist units. These do, however, contain a wide range of clast-types, -sizes and -shapes.

2.3.2.3 *Karibib Formation*

The Karibib Formation occurs only in the Central Zone and is largely a carbonate sequence with lesser amounts of pelitic material. South of Vogelfederberg the base rests discordantly (up to 60°) upon the Chuos Formation, whilst in the Leeukop Antiform the Karibib oversteps Chuos and Rössing rocks. Further west the Karibib Formation rests directly on rocks of the Nosib Group, thus indicating the existence of a major unconformity between the Karibib and Chuos Formations.

In most places the succession begins with a few metres of schist and calc-silicate rocks followed by the main marble sequence. The calc-silicate rocks occur either as dark-greenish bands within the marble or as light greenish-blue bands in the schists. The calc-silicates are medium grained with rare scapolite crystals reaching 50 mm in length. Quartz, plagioclase, diopside-hedenbergite and sphene are ubiquitous with frequent hornblende, tremolite, carbonate, epidote and clinozoisite while garnet and scapolite (mizzonite) are rare. The schists are dark and fine grained, often with small cordierite porphyroblasts. These also occur as laterally discontinuous lensoid intercalations within the marbles.

The bulk of the Karibib Formation consists of massive yellow, greenish, brown, pink, white and grey marbles. The colour reflects the mineralogy which covers the range from pure dolomite to pure calcite to siliceous marble. Deformation of the marbles has been intense, producing a strong banded appearance perhaps reflecting attenuated bedding. Grain size ranges from 0,5 mm to 300 mm with the fine-grained marbles tending to be dolomitic. Minerals frequently occurring are calcite, dolomite, forsterite, antigorite, tremolite, and phlogopite with occasional chondrodite, microcline, plagioclase and talc.

A maximum thickness of about 1 000 m is reached in the Hamilton Mountains, but the formation thins markedly to the south-west, where schists are virtually absent.

2.3.2.4 *Kuiseb Formation*

The youngest rocks of the Damara Sequence belong to the Kuiseb Formation. All metasediments cropping out in and east of the Okahandja Lineament Zone belong to this formation. West of the Lineament the formation is much thinner and in most cases its position is taken by Salem Granite.

Many rock types are present, but in terms of volume, pelitic schists are by far the most important constituents. In addition to plagioclase, biotite and quartz, the Trough Zone pelites may contain garnet, staurolite, muscovite and kyanite; the Okahandja Lineament pelites may contain muscovite, cordierite, andalusite and rarely garnet or staurolite; the Central Zone pelites may contain garnet, sillimanite, cordierite and microcline. Grain size varies from fine to medium, although porphyroblasts (e.g. cordierite, staurolite and kyanite) may reach 100 mm in length.

Calc-silicate rocks occur widely in the Kuiseb Formation although volumetrically minor. Quartz and plagioclase (labradorite) are common to all samples examined with lesser amounts of garnet, diopside, amphibole, biotite, epidote, clinozoisite and carbonate. The glassy varieties of calc-silicate rock generally contain porphyroblastic quartz.

Quartzites, micaceous quartzites and marbles are very rare, although adjacent to the Matchless Member siliceous marble, calc-silicate rocks, magnetite quartzite, sericite quartzite and graphitic schists are locally developed.

Two members of the Kuiseb Formation are recognised:

Tinkas Member—Being the lowermost part of the Kuiseb Formation it is only present in and just west of the Okahandja Lineament Zone. The sequence of marbles, calc-silicates, pelites, semipelites and metagreywackes may in part be considered to be a lateral and upward facies change from the Karibib Formation, thickening rapidly eastwards into the Lineament Zone.

Characteristically the metapelites are strongly cleaved, dark bluish-grey schists of fine grain size frequently containing cordierite and andalusite. Calc-silicate rocks may have a bluish-green colour due to epidote and hornblende or a pale-green colour resulting from diopside. The marbles vary from pure carbonate to very siliceous types and may be white, buff, pinkish or grey in colour. Marbles of the Tinkas Member may possibly be correlated with those of the Karibib Formation but no direct connection has been proved. Scant palaeocurrent indicators in Tinkas metagreywackes point to a source area to the west. Clasts in the greywackes are frequently crystals of feldspar or small granitic fragments.

Matchless Member—Rocks belonging to this member constitute a prominent linear feature in the mapped area ending in a fold structure at the Hope Mine. However, small isolated bodies on the Kuiseb River and thin bands as far west as Gobabeb are also considered to belong to this member. The Matchless rocks are intercalated with schists of the Kuiseb Formation.

The rocks are typically dark-green amphibole-bearing schists and massive metagabbros. Epidote-banded amphibole schists represent deformed pillow lavas resembling those of Zermatt*. A minor amount of more basic material is also present. Metamorphosed dolerite dykes may be seen cross-cutting the amphibole-bearing rocks, but the dykes do not penetrate adjacent metapelites, possibly suggesting a tectonic emplacement of the amphibole-bearing rocks. Elsewhere, however, an intimate interlayering with pelitic schist and even gradational contacts suggest a non-tectonic relationship.

2.4 DAMARAN IGNEOUS ROCKS

2.4.1 Salem Granite Suite

Rocks of the Salem Granite Suite crop out in large areas west of the Okahandja Lineament Zone, and over a limited area within the Lineament (Folder 1.1). Rocks of this suite are intruded by the Aussinanis Granite, red homogeneous and buff leucocratic granites, the Donkerhuk Granite, and in the Leeukop area by a post-tectonic quartz diorite.

Characteristically the principal rock type is a greyish-pink coarse-grained porphyritic adamellite or locally a granodiorite. Aphyric adamellite, granodiorite and quartz diorite are minor constituents of the suite. In the majority of cases there is a marked foliation in the rock although small unfoliated portions are present in the Okahandja Lineament Zone. Field and thin-section evidence suggest that the penetrative foliation is tectonic, indicating that the Salem Granite Suite is largely pre- or syn-tectonic, whilst small parts of it (in the Lineament Zone) are clearly post-tectonic. The position of the Salem Granite in the Central Zone is generally where rocks of the Kuiseb Formation would be expected. This association has caused some workers (Miller 1973) to suggest an origin by partial melting of the Kuiseb Formation. This hypothesis is not acceptable since it requires an even earlier high-grade metamorphic event (for which no evidence can be found), as the main metamorphic episode post-dates much of the deformation (Section 7).

2.4.2 Aussinanis Granite

The Aussinanis Granite intrudes the Salem Granite Suite in the Gobabeb area. The granite is important since it contains a protomylonitic fabric having the same orientation as the Okahandja Lineament Zone schistosity. The fabric in the Salem rocks must thus also be tectonic in this vicinity. The Aussinanis fabric is marked by a layering of fine-grained recrystallised quartz and feldspar, distinct planes being 1–2 mm apart. The rocks vary from

* Personal communication: J. G. Ramsay.

granite to adamellite in composition, are generally medium grained and locally weakly porphyritic. Both muscovite and biotite occur, with small amounts of allanite and rarely hornblende. Donkerhuk Granite intrudes the Aussinanis Granite, but lacks a planar fabric.

2.4.3 Red Granites

Field relations (Sawyer 1979) show that the different varieties of red granite, viz the red gneissic, red homogeneous and buff leucocratic granites are contemporaneous and have interrelated origins. The use of an informal name is deemed necessary since no collective name has been accepted by the South African Committee for Stratigraphy. The Sopiehoogte vicinity contains virtually all Red Granite types present in the area mapped.

The gneissic variety is, as the name indicates, a dark-red gneissose rock of granitic composition. It appears at first glance to be older than the other two, but nebulitic and gradational as well as cross-cutting contacts occur and indicate a related origin. The red gneissic granite occurs through migmatisation of either pre-Damara or Nosib rocks; leucosomes (Mehnert 1968) that developed parallel to the regional fabric give rise to the gneissose appearance. The fabric is continuous with that of adjacent unaffected country rock. In some areas where partial melting is extensive, as in the Nosib at Rooibank, neosomes (Mehnert 1968) have coalesced to give rise to irregular nebulitic patches of red homogeneous or rarely buff coloured leucocratic granite within the gneissic portion. In the Leeukop Antiform, pre-Damara gneisses show a gradation via a nebulitic stage to red homogeneous and buff leucocratic granite. In places both the red homogeneous and buff leucocratic granites contain small oriented microcline phenocrysts and a weak tectonic foliation. Rarely (e.g. south of Vogelfederberg) the red homogeneous granite passes into a grey granite of identical texture and mineralogy, the colour difference being ascribed to differences in the state of oxidation of included Fe-bearing opaque minerals. Although called red homogeneous granite it is also leucocratic and has a similar texture and mineralogy to the volumetrically less abundant buff leucocratic granite. Many outcrops show the buff leucocratic granite to cross-cut the red homogeneous variety and mixing of the melt is often indicated by a pinkish streaky granite suggesting a virtually contemporaneous origin.

All varieties of Red Granites occur only in the Central Zone. The red gneissic granite is confined to antiforms where Nosib and pre-Damara rocks occur whilst the other two varieties are often found intruding the Salem Granite Suite in synformal areas.

2.4.4 Post-tectonic Quartz Diorite

South of Leeukop a dark-grey biotite-hornblende quartz diorite intrudes foliated Salem Granite (Folder 1.1). The quartz diorite contains xenoliths and xenocrysts derived from the porphyritic adamellite country rock; the rock itself is unfoliated. The lack of named geographical features near to the quartz diorite precludes a formal name.

2.4.5 Samut Granite

The Samut granite occurs as two small bodies in the north-eastern part of the Okahandja Lineament (Folder 1.1). The smaller northern body is in part a slightly porphyritic adamellite, the remainder and the whole of the larger southern body is a cataclastic (protoclastic) (Higgins 1971) clinopyroxene-bearing granite. Associated aplites are also cataclastic. There are numerous fracture-cleavage planes and minor mylonitic bands oriented subparallel to structures in the Okahandja Lineament. It is probable that this granitic rock was intruded during the last stages of movement in the Lineament, and that protoclasis accompanied intrusion.

2.4.6 Donkerhuk Granite

Typically a fine- to medium-grained light-grey granite to adamellite, it contains both muscovite and biotite with occasional garnet. Locally small feldspar phenocrysts are present. The marginal parts may be melanocratic or coloured. There is an extensive thermal aureole. Numerous pegmatites and aplites are associated with the granite, the earliest of these are deformed by late movements of the Okahandja Lineament Zone whereas the later granite stocks, notably the smaller ones north of Gobabeb deform the " breccia bands" by forceful intrusion. Country-rock sheets and xenoliths are common in the granite whilst lit-par-lit injection migmatites are common in the country rock. Donkerhuk Granite intrudes the Aussinanis Granite and units of the Salem Granite Suite in the Gobabeb area.

3. STRUCTURAL GEOLOGY

3.1 INTRODUCTION

During mapping it became evident that the area could be divided into four distinct zones (Fig. 1.1), each characterised by its own structural style and metamorphic assemblages, viz A. The Trough Zone; B. The Okahandja Lineament Zone; C. The Central Zone and D. The Donkerhuk Granite Aureole. Zones A, B and C are of significance in the history of the Damara Orogen, whilst Zone D is essentially post-tectonic and post-regional metamorphism.

In broad terms the Trough Zone is characterised by a strongly pervasive schistosity dipping 30–50° northwestwards which is axial-planar to tight, almost isoclinal, folds. Locally, as at the Hope Mine, schistosity is folded. Characteristic mineral assemblages include kyanite, staurolite and garnet.

The Okahandja Lineament Zone is defined as a structural domain characterised by a near-vertical, strongly pervasive schistosity or cleavage, striking about 30° east of north and axial-planar to elongated domes and basins or very tight, nearly isoclinal folds. Movement parallel to the cleavage planes is evident from rotated porphyroblasts, off-set pegmatites, and mylonite and breccia bands parallel to the regional schistosity. Porphyroblastic minerals are andalusite and cordierite with rare garnet and staurolite.

In the Central Zone the major trend strikes northeastwards and although axial planes vary in orientation these are moderately to steeply dipping north-westwards. Hinge directions plunge fairly constant northwards. The outcrop pattern is generally complex due to dome- and basin-like structures and considerable granite intrusion. The metamorphic conditions were essentially high-grade with sillimanite and/or cordierite-microcline assemblages.

The Donkerhuk Granite Aureole surrounds a large post-tectonic intrusion of adamellite accompanied by migmatisation and buckling of the country-rock schistosity.

The Okahandja Lineament Zone has an important position separating the Central Zone from the Trough Zone. The boundary between the Lineament Zone and the Central Zone is generally fairly sharp and defined by a change in orientation of schistosity from vertical to dipping steeply westward. It coincides with the appearance of Chuos, Karibib and Nosib rocks and the isograd muscovite+quartz out. Along the southern margin of the area the boundary is placed about 10 km east of

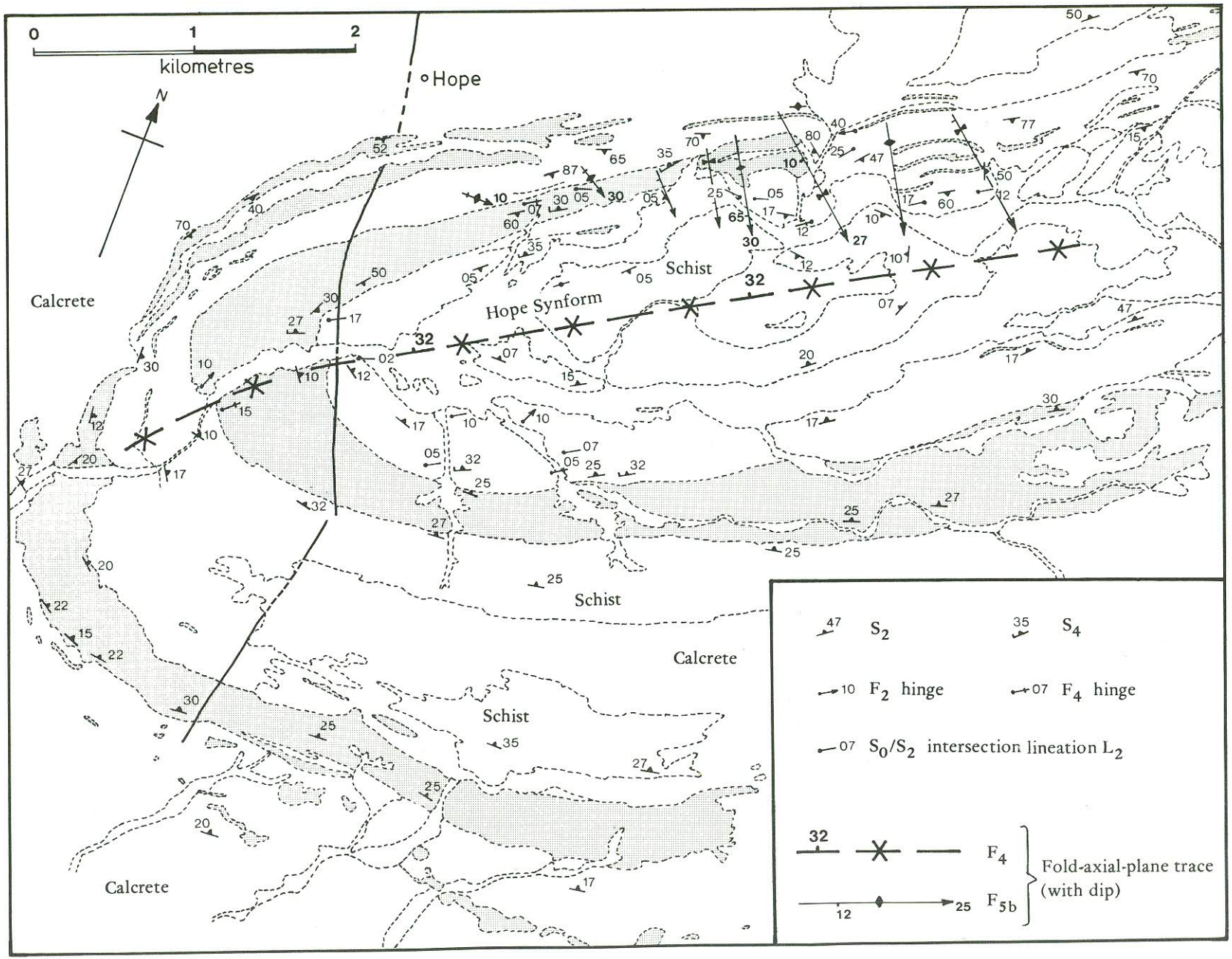

Fig. 3.1 — Structural details of subzone TZ/1:The Hope Synform. For correlation of fabric elements see Table 4.1. Matchless Member shaded.
Struktuurgegewens van subsone TZ/1:Die Hope-sinform. Vir korrelasie van maakselelemente verwys Tabel 4.1. Lid Matchless donkerkleurig aangetoon.

Gobabeb and is again fairly abrupt over about 1 km, marked by a steepening of schistosity from east to west. The exact relationship between the schistosities of the two zones is not clear because of the effect of the Donkerhuk Granite (Section 9).

Since the major zones are extensive and not uniformly exposed, detailed studies of a number of subzones from each of the three major zones (A, B and C) were made.

3.2 NOMENCLATURE AND CONVENTIONS USED

The structural elements are designated in age order for each zone. The convention adopted is that of Turner and Weiss (1963) where S denotes a planar penetrative fabric, L a linear penetrative fabric and F a folding of the fabric; suffixes 1, 2, 3 . . . denote which generation a particular fabric element belongs to. Bedding is referred to as S_0. When describing the geometrical properties of folded surfaces, e.g. interlimb angle, attitude of hinge line, and dip of axial plane the terms defined by Fleuty (1964) are used. In the description of folded layers the terms parallel and similar are used in the sense of Turner and Weiss (1963); for folds which have been more accurately measured the scheme of Ramsay (1967, p. 365) is used with the fold class stated. S_e and S_i respectively, refer to fabric external to and enclosed in poikiloblasts.

Orientations of planes give the dip direction and the amount of dip, i.e. 235/70. Linear elements are orientated by trend and plunge. Structural data are plotted on Schmidt equal-area-projection stereographic nets.

Since no single structural subzone contains all the fabric elements, Tables 3.1, 3.2 and 3.3 show the distribution of the observed elements together with the main characteristics for each zone. It is conceded that the nomenclature of these tables implies a knowledge of the sequence of structural events discussed in Section 4. The interrelationship of fabric elements evolved in Section 4 is used here to eliminate excessive descriptive repetition. The correlation of Section 4 is based largely on field observations summarised under the heading "effect on pre-existing fabrics" in the tables mentioned.

3.3 TROUGH ZONE STRUCTURAL GEOMETRY

The distribution and main characteristics of the penetrative fabrics observed in the Trough Zone are given in Table 3.1.

3.3.1 Subzone TZ/1: The Hope Synform

This subzone lies immediately to the south and east of the Hope Mine (Fig. 1.1), and includes the large synformal structure (the Hope Synform) delineated by the Matchless Member (Fig. 3.1).

3.3.1.1 *Fabric Elements*

Including bedding, four penetrative planar elements can be seen, although two are of minor local significance. Linear fabric elements are either S-surface intersections or rods.

Planar Elements—Contacts between pelitic schist and the Matchless Member rocks may be bedding in a few cases. Generally this is uncertain although the contact may be at a small angle to the dominant schistosity S_2 (see below). Contacts between metapelite and the Matchless Member metagabbro may represent an intrusive contact; there is, however, some doubt because of the strong effect of later boudinaging, folding and foliation development. Bedding contacts between calc-silicate rocks and metapelite are frequently observed.

The transposition of S_0 into S_2 is common (Turner and Weiss 1963, Fig. 5–26, domain IV; Hobbs *et al.* 1976, Fig. 31). Such transposition incorrectly suggests

Table 3.1—MAIN CHARACTERISTICS OF TROUGH ZONE PENETRATIVE FABRIC ELEMENTS

Element	Occurrence	Main features	General orientation	Effect on pre-existing fabrics
S_0	TZ/1, 2 & 3	Bedding, variation of lithology, mineralogy, grain-size or colour. Possibly also represents some contacts between Matchless Member rocks and metapelites	Variable but generally NW	—
S_1	TZ/2	Biotite foliae, parallel layers 1–2 mm thick, up to 10 mm apart; internal fabric in some porphyroblasts	Variable but generally NW	Discordant to S_0
F_1	TZ/2	Tight to isoclinal, moderately inclined gently plunging folds	Hinge 310/17; axial plane 355/40	Folds S_0. S_1 axial-planar?
S_2	TZ/1, 2 & 3	Schistosity, parallel orientation of muscovite and usually biotite in pelites; also frequent elongation of quartz and plagioclase, hornblende y-z (100) crystallographic planes parallel S_2 in Matchless Member schists; numerous quartz veins often with pinch-and-swell structure also parallel to S_2	TZ/1 340/25; TZ/2 325/32 and TZ/3 variable	Transposes S_0 (especially calc-silicate layers) into L_2 cleavage mullions Crenulates and transposes S_1
F_2	TZ/1, 2 & 3	Tight to isoclinal, gentle to moderately inclined and plunging folds, nearly reclined. S_2 defines axial plane; hinge parallel to L_2	TZ/1 hinge variable; TZ/2 hinge 355/30 and TZ/3 hinge variable	Folds S_0 and S_1. Type E interference pattern with F_1
S_3	TZ/2	Crenulation cleavage, common in pelites, rare in Matchless Member rocks	280/50	Crenulates S_0, S_1 and S_2 and intersection with S_2=L_3
S_4	TZ/1 & 3	Weak crenulation cleavage, rare quartz veins parallel S_4	TZ/1 332/32, TZ/3 345/40	Intersection with S_2 defines L_4
F_4	TZ/1 & 3	Close to tight moderately inclined subhorizontal asymmetric folds, S_4 axial planar	Hinge TZ/1 050/10	Folds S_0, S_2 and L_2
S_{5a}	TZ/1 West	Crenulation cleavage in micaceous schists (migmatitic in TZ/3)	TZ/1 010/45	Intersection with S_2 defines L_5
—	TZ/3 N.W.	—	TZ/3 average 345/15	—
F_{5a}	TZ/1 West	Kink folds, chevron or parallel gently plunging moderately inclined; S_{5a} axial planar	TZ/1 hinge (L_5) 042/15	Folds S_2
—	TZ/3	—	TZ/3 hinge (L_5) 320–010/15	—
F_{5b}	TZ/1 North	Medium-scale folds of varying geometry from west to east	Variable	Folds S_2, S_4 and L_4

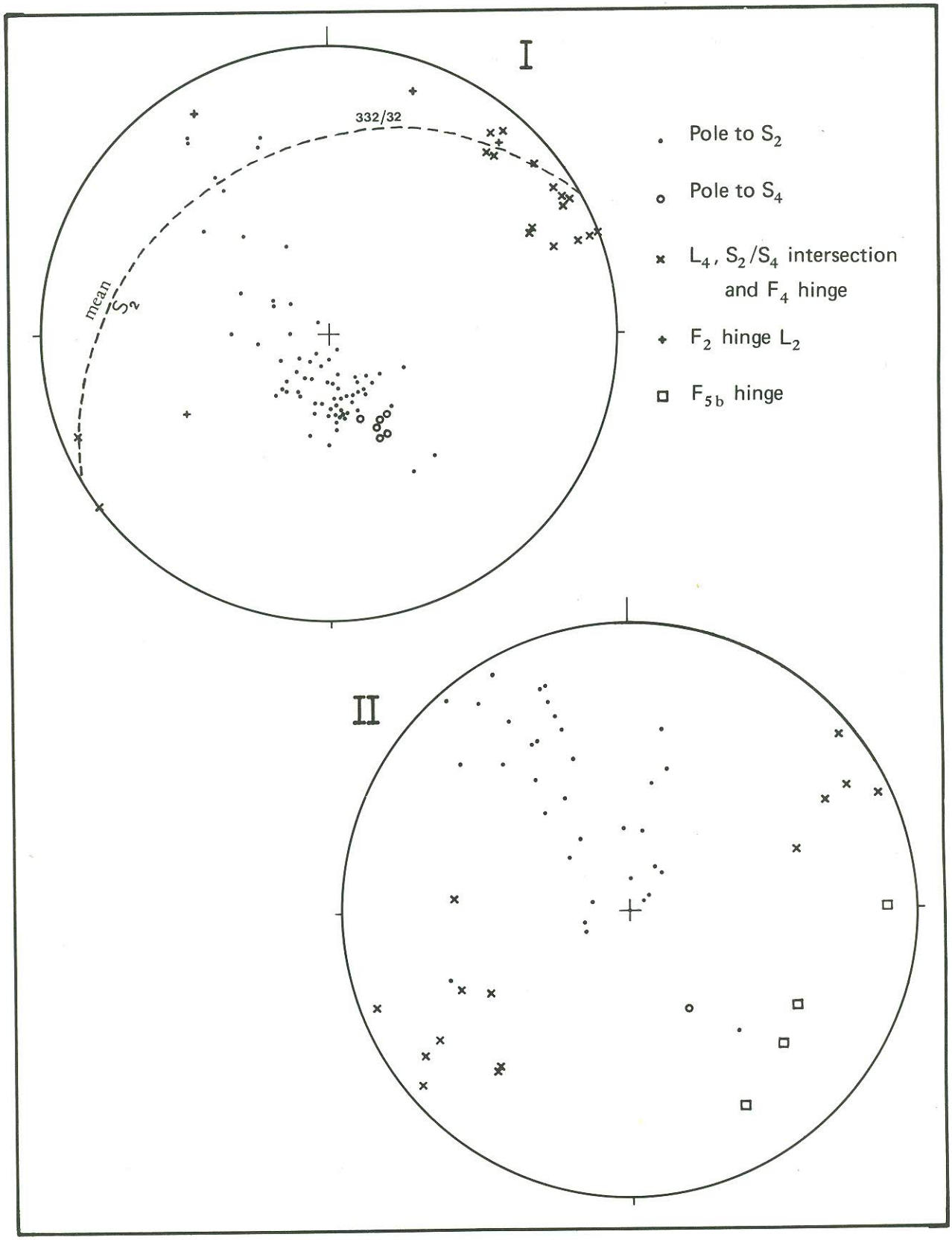

Fig. 3.2 – Fabric-element orientations in subzone TZ/1. I. Hope Synform excluding the northern limb where affected by F_5 folds. II. Hope Synform, northern limb. For correlation of fabric elements see Table 4.1.

Maakselelementoriëntasies in subsone TZ/1. I. Hope-sinform, uitgesluit die noordelike vleuel waar deur F_5 plooie geaffekteer. II. Hope-sinform, noordelike vleuel. Vir korrelasie van maakselelemente verwys Tabel 4.1.

that S_0 and S_2 are parallel, which generally is not the case (Fig. 4.1A). Further evidence for transposition (Turner and Weiss 1963, p. 117) of S_0 by S_2 comes from occasional small isolated, rootless, almost isoclinal fold closures found with limbs parallel to S_2, the dominant schistosity. Where S_2 is oblique to S_0 (e.g. a calc-silicate band) the latter may be transposed step-like into cleavage mullions.

The orientation of the S_2 schistosity varies as a result of later folding, but the mean in the relatively undisturbed southern part of the subzone is 340/25. For the northern part dips average 150/60 and are locally overturned.

A widespread but weak second cleavage S_4 reorientates S_2 parallel minerals. On average S_4 crenulation planes are 5 mm to 10 mm apart. S_4 is steeper than S_2 on the southern limb but shallower than S_2 on the northern limb of the Hope Synform.

In the river gorge at the Hope Synform closure a sporadically occurring crenulation cleavage S_{5a} is developed in mica-rich layers.

Linear Elements—The L_2 lineation is defined by elongated calc-silicate fels cleavage mullions and hinges of F_2 minor folds. In a few cases quartz veins parallel to S_2 are rodded along L_2, whilst in rare cases hornblende needles in Matchless Member amphibole schists also lie parallel to L_2. The general trend and plunge of L_2 vary due to later folding.

Biotite lineation L_4 on S_2 planes has a constant orientation over the subzone except in the northern part where later folding reorientates L_4 (Fig. 3.2).

Although quartz rods are frequently found parallel to L_2 and very rarely parallel to L_4, these commonly have orientations of only local significance, dependent to some extent upon the orientation of the initial vein relative to S_2. It is also probable that there are several ages of vein emplacement.

3.3.1.2 *Minor Folds*

Rarely rootless F_2 minor folds can be seen transposed in S_2; these intrafolial folds may be up to 200 mm in length and are best recognised as small folded quartz veins in metapelitic rocks. F_2 folds range in size from tens of millimetres to metres and belong to class 1C (Ramsay 1967), occasionally with very attenuated limbs. In one extreme case the measured wavelength was 300 mm and the amplitude 5 m. Limbs are frequently sheared out leaving a closure and only a thin vestige of a limb. Interlimb angles seldom exceed 7°. Hinge orientation L_2 has been disturbed by later folding over the whole subzone, but generally plunge northwards. Quartz veins folded by F_2 are frequently rodded parallel to L_2.

Widely occurring on both the northern and southern limbs of the Hope Synform are minor F_4 folds, generally of millimetre-scale having Z-shaped profiles on the southern and S-shaped profiles on the northern limb. F_4 folds belong to class 1C.

In the closure of the Hope Synform several F_{5a} kink folds are present but are only of local significance and confined to very micaceous pelites.

F_6 kink-type folds occur in the same area and often show dilation of folded S_2 cleavage planes in hinge zones. Hinges plunge gently northwards (010/15) with axial planes 270/52. These folds are of local importance and commonly occur with joint planes.

3.3.1.3 *Major Folds*

The most striking feature of this subzone both on maps and aerial photographs is the very large F_4 fold closing to the south-west. Folding of S_2 indicates this structure to be a synform. A stereographic plot of poles to S_2 from the closure and southern limb is shown in Figure 3.2 I whilst Figure 3.2 II shows poles to S_2 for the northern limb affected by later folding. Poles to S_4 (Fig. 3.2 I) give a tight grouping on the π girdle to S_4 poles, suggesting S_4 to be axial-planar to F_4. Lineation L_4 approximates to the F_4 hinge.

Using the evidence that S_4 is axial-planar to F_4 minor folds, then Figure 3.1 can best be interpreted by making F_4 a major synform with a mean axial plane 332/32 plunging 050/10 at the closure. Effects of later folding cause the hinge line to be undulose (non-cylindrical). The Hope Synform is asymmetric with a short northern limb.

Smaller-scale, but still important fold structures (F_{5b}) on the northern limb of the Hope Synform increase in size from west to east and show a concomitant change in hinge orientation from 090/20 to 150/20 (Fig. 3.2 II). The axial planes also change orientation from near-vertical in the west to dipping moderately south-west further east. Thus upright folds become reclined eastwards, enabling the easternmost folds to significantly affect the outcrop distribution by folding pelitic schists from north of the amphibole schists southwards over the Matchless Member thus giving rise to its discontinuous outcrop. Figure 3.2 II shows the scattering of L_4 due largely to F_{5b} folds.

3.3.1.4 *Major Faults and Discontinuities*

A subvertical fracture trend with apparently little vertical or lateral displacement traverses the closure of the Hope Synform. Some granitic dykes are intruded along a similar trend which is also parallelled by quartz- and calcite-filled tension gashes in the same area.

3.3.2 Subzone TZ/2: The Gorob Area

This subzone lies to the north and south-east of Gorob and includes rocks from both north and south of the Matchless Member (see Fig. 3.3).

3.3.2.1 *Fabric Elements*

Including bedding S_0, four penetrative planar-fabric elements are present, but only two (S_0 and S_2) are present everywhere. Five basic types of linear-fabric elements are recorded, and principally have two trends. Others are of purely local significance.

Planar Elements—On a large scale the bedding (S_0) trend is shown by the outcrop of a graphitic schist just south of the Matchless Member. At outcrop, bedding contacts between graphitic and pelitic schists are often gradational or disrupted by the strong regional schistosity S_2. In metapelites bedding is clearly shown on aerial photographs, but S_0 may be virtually impossible to establish at outcrop unless calc-silicate rocks are present. Frequently even sizeable (up to 10 m) fragments of calc-silicate rocks become transposed into S_2. Thus S_0 is only unambiguously seen in some fold closures where it is at a high angle to S_2. Within the Matchless Member differences in rock type probably reflect degrees of deformation, as for example when a continuous gradation from metagabbro to hornblende schist occurs. At a few places spotted amphibole schists containing deformed variolites (having pressure shadows) represent primary structure concentric to pillow lava structures in epidote-banded and amphibole schists.

S_0 generally dips north-westwards and cleavage(S_2)-bedding relations indicate that steep limbs (F_2) are overturned.

At two localities, A and B in Figure 3.3, a locally penetrative fabric S_1 is seen to be oblique to bedding S_0. The fabric is crenulated by S_2 and rarely by S_3. Biotite flakes comprising S_1 are oriented parallel to S_2 or occa-

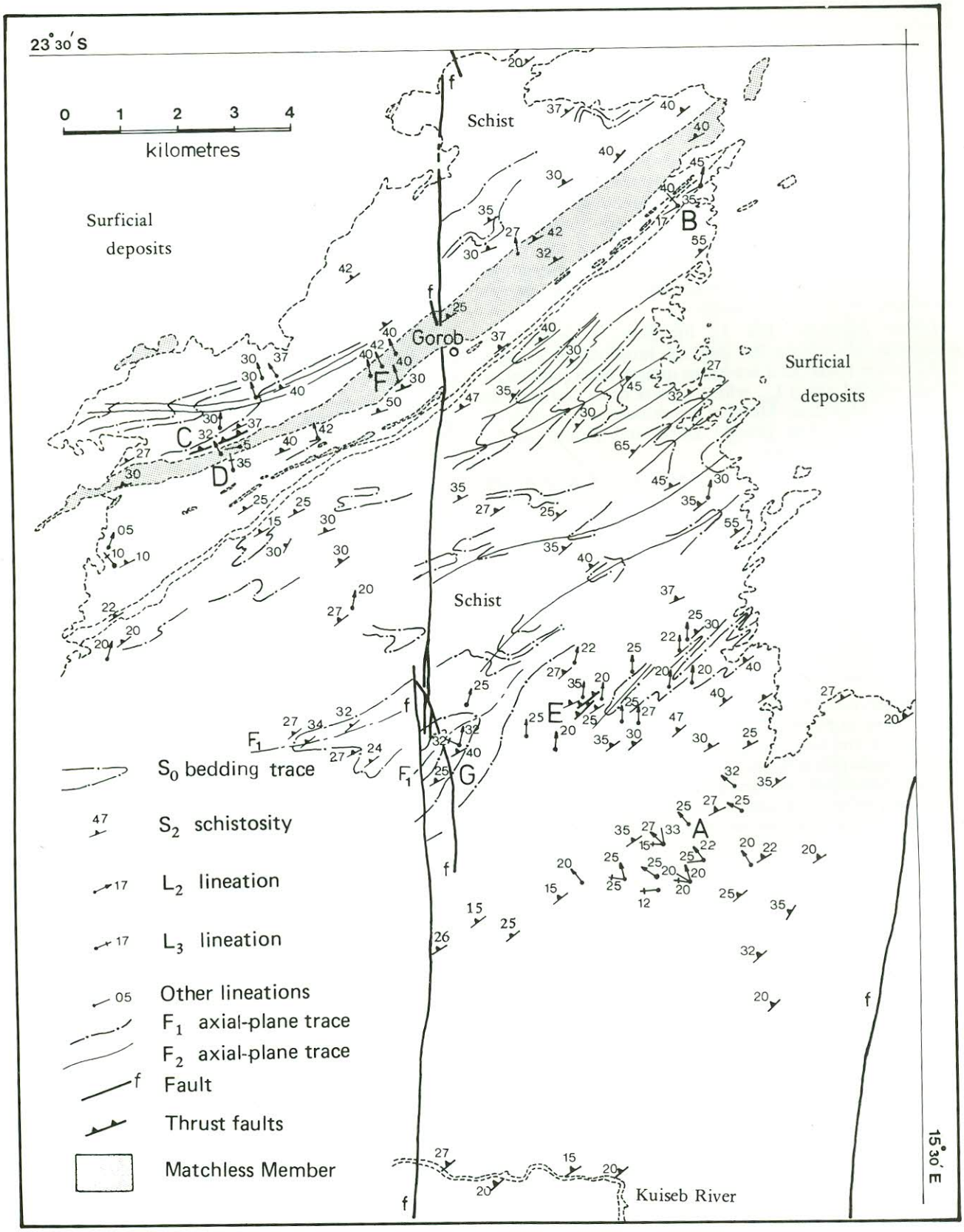

Fig. 3.3 – Structural details of subzone TZ/2. For correlation of fabric elements see Table 4.1. A–G refer to localities mentioned in the text.
Struktuurgegewens van subsone TZ/2. Vir korrelasie van maakselelemente verwys Tabel 4.1. A–G verwys na lokaliteite in die teks genoem.

sionally S_3 (Fig. 4.1A). S_1 does not appear to be related to folding.

Parallelism of biotite and especially muscovite in metapelites define the dominant S_2 schistosity, but in some schists muscovite parallels S_2 whilst porphyroblastic biotite, garnet, staurolite and kyanite have random orientations.

Small rootless F_2 folds and calc-silicate cleavage mullions indicate transposition of S_0 by S_2. Schistosity may be enhanced in highly micaceous rocks (which appear to be depleted in quartz) adjacent to S_2—parallel quartz segregation lenses. Small quartz-plagioclase knots of metamorphic origin present in some Matchless Member schists are elongated parallel to S_2. The degree of elongation of the knots increases rapidly adjacent to minor shear zones (150–200 mm wide) parallel to S_2. The orientation of S_2 is slightly variable as shown in Figure 3.4.

S_3 crenulation cleavage planes are 5–10 mm apart but are rare in amphibole schists. Post-tectonic growth of garnet in S_3 has occurred, especially along the S_2 and S_3 intersection (L_3). At D (Fig. 3.3) S_3 deforms both kyanite and staurolite, but later growth of both mineral species post-dates S_3. The orientation of S_3 is shown in Figure 3.4. Steeper dips tend to occur in the north of the subzone.

Linear Elements—Calc-silicate cleavage mullions occurring either singly or in trains and F_2 fold hinges define the L_2 lineation (Figs 3.3 and 3.4). The orientation of L_2 in Figure 3.3 shows marked differences in trend at localities A, E and F which may reflect later deformation, sliding (thrusting) along S_2 planes as at E, or orientation of S_0 due to pre-existing F_1 folds.

In many cases quartz rods lie parallel to L_2. L_2 mineral lineations occur as oriented amphiboles and garnet trains at cleavage mullion margins, or as oriented biotite flakes growing in the pressure shadows of quartz rods. Some Matchless Member amphibole schists contain pillows, epidote-amphibole pods (boudins) and ellipsoidally deformed variolites, all of which are elongated parallel to L_2.

L_3 occurs as biotite streaks or rarely as trains of garnets on S_2. In amphibole schists oriented hornblende crystals or hinges of S_3 crenulations define L_3.

Mineral lineations are abundant throughout the subzone, but cannot all be related to L_2 or L_3. Amphibole needles parallel to the S_3 strike direction have been observed in two widely separated localities within the Matchless Member. Prismatic biotite crystals in some metapelites locally define a lineation, especially near to quartz veins and rods, becoming seemingly random a few hundreds of millimetres away from the veins. Quartz rods are a prominent lineation, but the orientation is often irregular even in a single outcrop.

3.3.2.2 *Minor Folds*

At one locality F_1 deformed a biotite-rich layer (S_0) in a metapelite, with an axial plane 355/40 and hinge 310/17. The biotites of the layer have subsequently been reoriented parallel to S_2 at 330/20 (Fig. 4.1B). At locality G (Fig. 3.3) interference between F_1 and F_2 folds gives rise to an interference pattern resembling type E (Ramsay 1967, p. 531).

F_2 minor folds are common throughout the subzone, although less so in the Matchless Member. Characteristically these are of class 1C and have amplitudes far in excess of wavelength. Because of shearing along S_2 it is commonplace for one or other limb to be absent.

F_3 microfolds are best developed in micaceous schists and are often markedly asymmetric with small amplitude: wavelength ratios.

Occasionally, folds of differing hinge orientation and tightness are found, but generally plunge northwards. These are invariably defined by folded quartz veins having an orientation oblique to S_2. These veins may have been injected during F_2 formation, or were alternatively folded by a late flattening normal to S_2 (Section 7).

3.3.2.3 *Major Folds*

Figure 3.3 shows the outlines of the larger (F_2) folds as structural form lines depicting S_0. The large fold shown at G is a large F_1 synform since interference patterns are associated with it on aerial photographs (also Fig. 3.2), and S_2 can be seen to cut F_1 axial-plane traces at angles of 60°.

F_2 folds change in profile from S-shaped near B (Fig. 3.3) to M-shaped just north of locality E and Z-shaped at E. This may reflect a large F_2 synform between B and E.

Interference between the postulated F_2 synform and the north-eastward continuation of the F_1 structure at G may be responsible for the brachy-antiform just north of E.

3.3.2.4 *Major Faults and Discontinuities*

At E (Fig. 3.3) two thrust planes sensibly parallel to S_2 displace S_0 giving rise to a narrow zone where calc-silicate bands are extensively sheared and quartz lenses far more flattened than in adjacent schists. Just north of the Matchless Member at C (Fig. 3.3) kyanite-bearing schists terminate abruptly and a 40-m-wide zone contains intensively stretched and sheared quartz veins parallel to S_2. This zone possibly represents a small thrust.

A major north–south post-Damara fault crosses the subzone near Gorob. The fault has a down-throw to the east and, in the Gorob area, a strike displacement of about 75 m and an estimated dip separation of 50 m.

3.3.3 Subzone TZ/3

This subzone lies south of TZ/1 (Fig. 3.5) and extends to the south bank of the Kuiseb River.

3.3.3.1 *Fabric Elements*

Apart from the bedding there is only one penetrative planar element present over the whole area. However, locally penetrative planar elements do occur. Linear elements are common and are manifested as fold hinges, mineral lineations, rods and intersection of S planes.

Planar Elements—Bedding, S_0, is often seen in pelitic schists, whilst the contact between Matchless Member rocks and metapelites is generally parallel to S_2. The exceptions, however, are the massive metagabbros which are often present as pod-like bodies in the metapelite. It is possible that these contacts represent primary igneous ones, although some bodies may be large boudins.

The dominant planar fabric over the whole subzone is the S_2 schistosity (Figs 3.5 and 3.6), to which both quartz veins in metapelites and epidote bands in the Matchless Member are parallel.

An incipient crenulation cleavage S_4 is present in a small area (A in Fig. 3.5) and is axial-planar to an F_4 minor fold in amphibole schists of the Matchless Member.

In the north-west of the subzone the S_{5a} crenulation cleavage is developed in schists showing signs of migmatisation with coarsening of grain size.

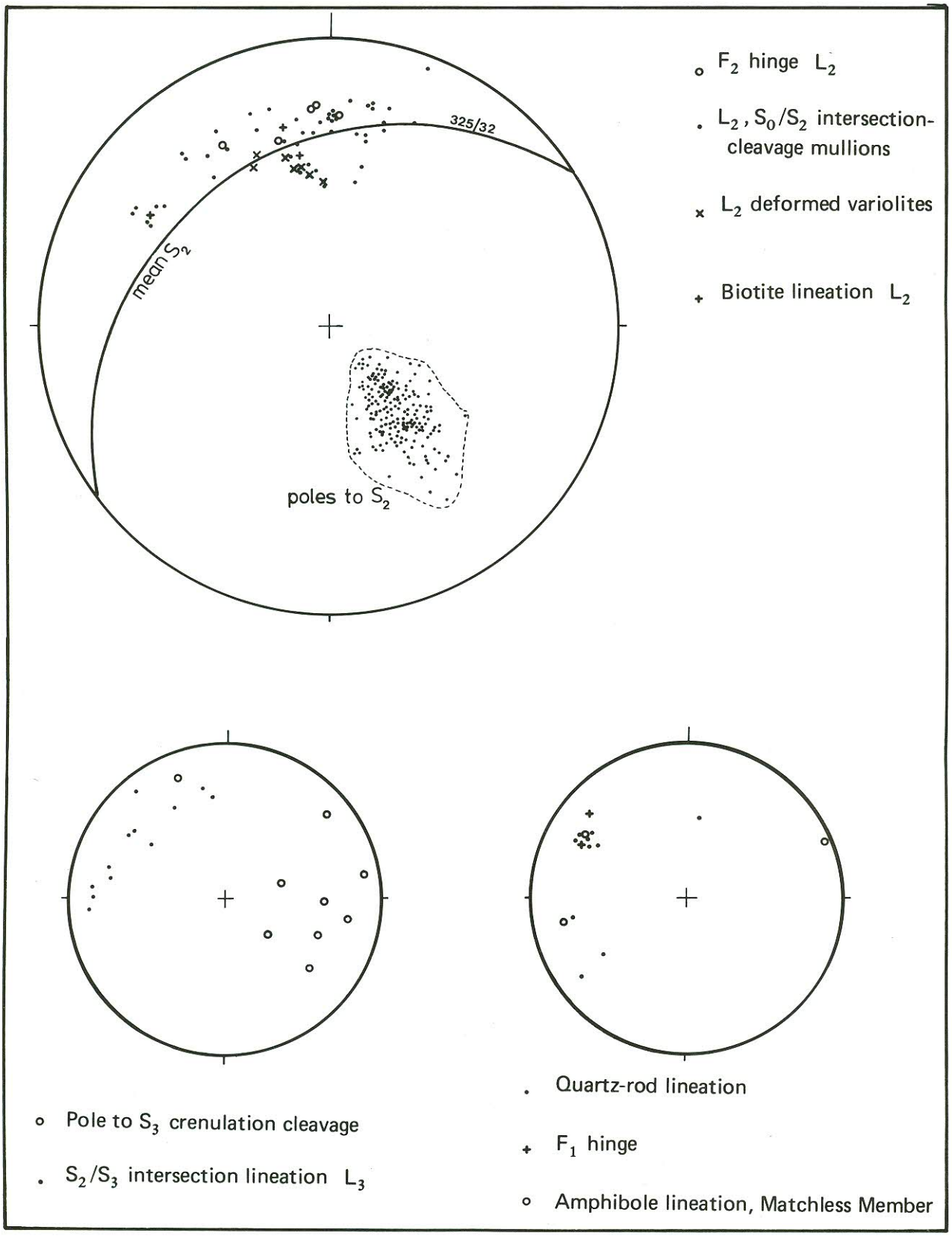

Fig. 3.4 – Fabric-element orientations in subzone TZ/2. For correlation of fabric elements see Table 4.1.
Maakselelementoriëntasies in subsone TZ/2. Vir korrelasie van maakselelemente verwys Tabel 4.1.

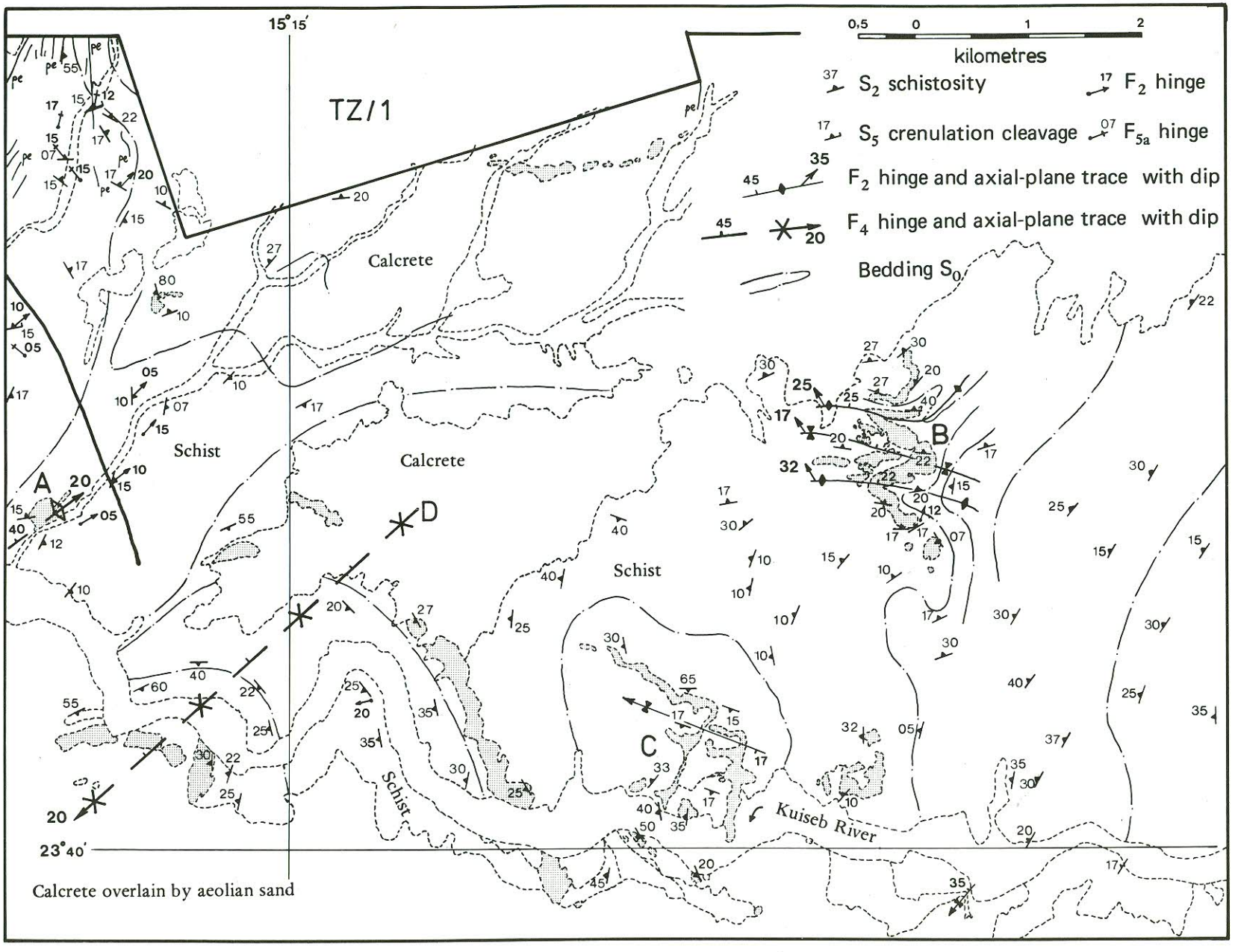

Fig. 3.5 — Structural details of subzone TZ/3. Matchless Member shaded. A — D refer to localities mentioned in the text.
Struktuurgegewens van subsone TZ/3. Lid Matchless donkerkleurig aangetoon. A — D verwys na lokaliteite in die teks genoem.

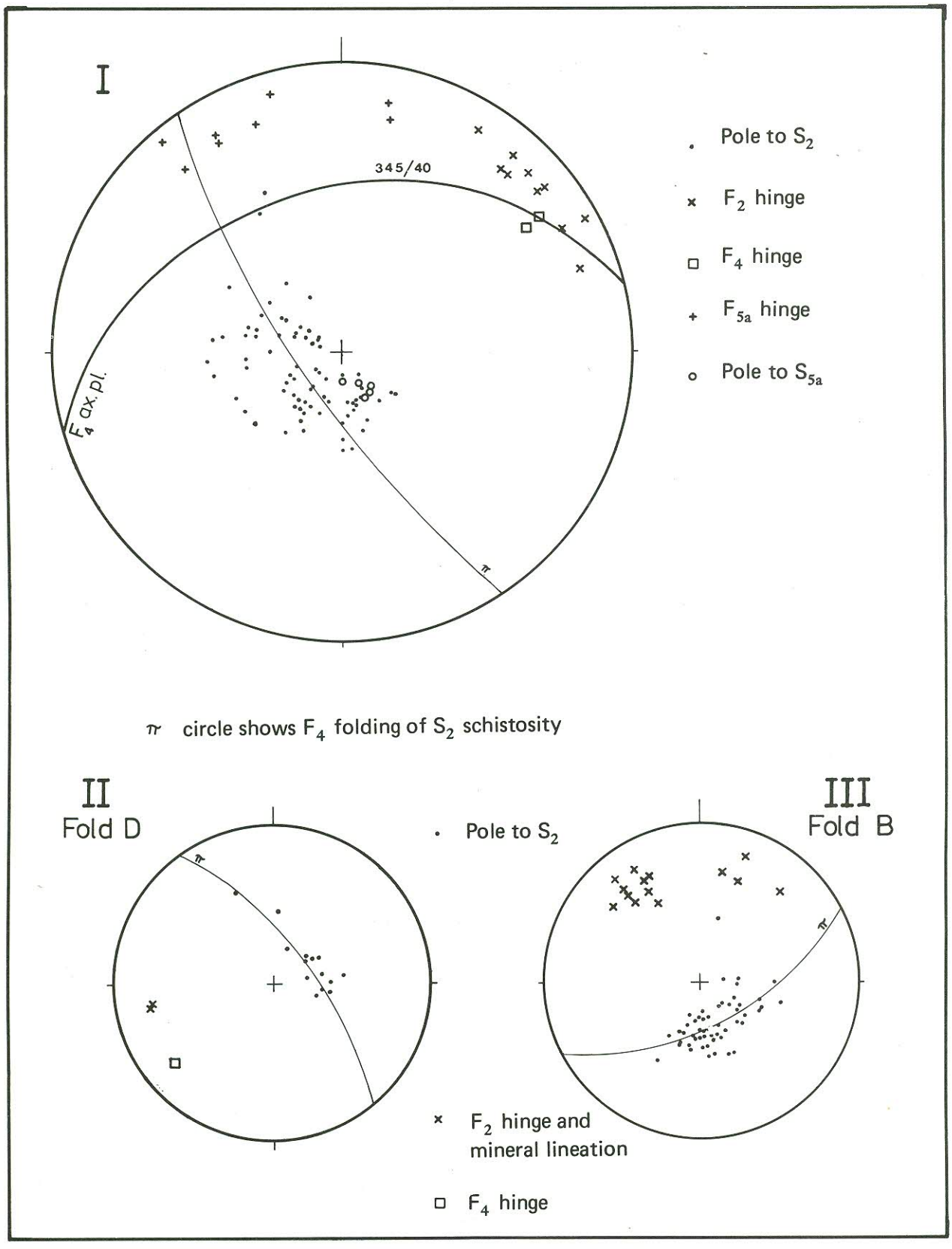

Fig. 3.6 — Fabric-element orientations of subzone TZ/3. I refers to the western half of the subzone, whilst II and III refer to folds shown in Figure 3.5. See Table 4.1 for correlation of fabric elements.
Maakselelementoriëntasies van subsone TZ/3. I verwys na die westelike helfte van die subsone terwyl II en III na plooie soos in Figuur 3.5 aangedui, verwys. Sien Tabel 4.1 vir korrelasie van maakselelemente.

Linear Elements—The L_2 lineation is defined by cleavage mullions, minor F_2 fold hinges and occasional quartz rods. It is however, consistently found that L_2 lies to the right of the down-dip direction of S_2 (as it does in TZ/2). The orientation of L_2 varies due to later folding (Fig. 3.6).

The L_4 lineation at A (Fig. 3.5) is a mineral striping on S_2 planes and trends 053°, parallel to F_4 fold hinges. A sporadically developed L_4 lineation on Fold D (Fig. 3.6) plunges south-westwards as seen on S_2 planes.

Hinges of F_{5a} minor folds and occasional quartz rods define the L_5 lineation which varies in azimuth orientation, although its plunge is consistent at about 15° in the S_5 plane.

3.3.3.2 *Minor Folds*

Class 1C F_2 minor folds range in size from tens of millimetres up to 100 m, and for these folds amplitude may exceed wavelength by 20:1. The Matchless Member rocks of Fold B (Fig. 3.5) commonly contain amphibole clusters elongated parallel to F_2 hinges (i.e. L_2).

F_4 minor folds at A in Figure 3.5 have an axial plane of about 345/40 and a plunge of 055/20. Folds are generally asymmetric with a short south-eastern limb to the main antiform and closely resemble F_4 minor folds of the southern limb of the Hope Synform (TZ/1).

Minor F_{5a} folds are of millimetre- or metre-scale occurring in migmatised schists in the north-western part of the subzone.

3.3.3.3 *Major Folds*

Major F_2 folds give rise to the outcrop pattern of the Matchless Member rocks in the eastern part of the subzone at C (Fig. 3.5). The fold geometry is complicated by the presence of large bodies of metagabbro which appear to have resisted deformation and in some cases form large boudins or pinch-and-swell structures. The folds are essentially of class 1C but have various hinge orientations due to later refolding. Initially these probably plunged north-westwards.

A large F_4 synform is clearly seen on the Kuiseb River (D, Fig. 3.5). Both S_2 and F_2 are reoriented by the fold, the axial plane of which possibly dips north-westwards whilst the plunge is 230/20, in contrast to F_4 minor folds at A in Figure 3.5. The axial-plane trace trend is essentially similar to that of the Hope Synform, the two folds being separated by a large antiformal region (Section 4).

Other folds can be seen from the structural form lines plotted on Figure 3.5; these folds are disharmonic and probably related to the intrusion of the Donkerhuk Granite (Section 4).

3.3.3.4 *Major Faults and Discontinuities*

There are no major faults in this subzone, although the southern continuation of a fault crossing the Hope Synform closure penetrates into the northern part of the subzone.

3.4 OKAHANDJA LINEAMENT ZONE STRUCTURAL GEOMETRY

Table 3.2 summarises the distribution and main features of the penetrative fabric elements observed.

3.4.1 Subzone OLZ/1

This subzone lies wholly within the outcrop area of the Tinkas Member of the Kuiseb Formation (Figs 1.1 and 3.7) and displays the most characteristic structural style of this zone.

3.4.1.1 *Fabric Elements*

Four planar elements are present including bedding, but only two have a wide distribution. Two major linear trends are present due to fold hinges and intersection of S surfaces.

Planar Elements—Bedding S_0 is readily seen over the whole subzone because of the varied lithology of calc-silicate rocks and marbles in pelitic types.

S_3, a strong schistosity in metapelites, is a mylonitic compositional layering (Vernon 1974) in calc-silicate bands and is the dominant fabric element of the subzone.

Table 3.2—MAIN CHARACTERISTICS OF THE OKAHANDJA LINEAMENT ZONE PENETRATIVE FABRIC ELEMENTS

Element	Occurrence	Main features	General orientation	Effect on pre-existing fabrics
S_0	OLZ/1, 2, 3	Bedding, variations in lithology, mineralogy, grain size or colour	Variable	—
S_1	OLZ/2 & 3	Biotite laminae. Parallel layers 1–2 mm thick up to 10 mm apart discordant to S_0	Variable	—
F_1?	OLZ/1	Isoclinal gently inclined subhorizontal folds	—	Folds S_0. S_1 axial planar?
F_2	OLZ/3	Tight to isoclinal gently inclined subhorizontal folds on cm scale	Axial plane dips NW, hinge N—S	Folds S_0 and S_1
S_3	OLZ/1, 2 & 3	Schistosity, parallel orientation of muscovite and biotite in most pelites; also elongation of quartz and plagioclase. Mylonitic layering in calc-silicate rocks	OLZ/1, 318/80; OLZ/2, 310/90 and OLZ/3, 115/80	Intersection with $S_0=L_{3a}$ and intersection with $S_1=L_{3b}$
F_3	OLZ/1, 2 & 3	Tight to isoclinal upright moderately plunging folds. S_3 axial-planar. Class 1C tending to class 2. Hinges parallel to L_{3a}	Hinge OLZ/1 232/37; OLZ/2 040/10 and 220/05; OLZ/3, 027/30 and 202/20	Folds S_0 and S_1
S_{4a}	OLZ/1, 2, 3	Crenulation cleavage in hinges of F_{4a} folds	300/77	Intersection with $S_3=L_4$
F_{4a}	OLZ/1, 2, 3	Close-tight steeply inclined moderately plunging folds. S_{4a} axial-planar	Hinge 217/40	Folds S_0, S_1, S_3 and L_{3a}
S_{4b}	OLZ/1, 3	Fracture cleavage, rarely crenulation cleavage in hinges of F_{4b} folds	280/75 and 095/82	—
F_{4b}	OLZ/1, 3	Close-tight steeply inclined moderately plunging folds. S_{4b} axial-planar	Hinge 200/45 and 007/37	Folds S_3 and some pegmatites
S_5	OLZ/2, 3	Mylonitic layering associated with 'breccia bands'	Parallel to S_3	—
F_5	OLZ/2, 3	Conjugate kink folds associated with 'breccia bands'	Variable	Folds S_0 and S_3
S_6	OLZ/3	Crenulation cleavages associated with Donkerhuk Granite emplacement	Variable	Crenulates S_0 and S_3
F_6	OLZ/3	Locally developed kink folds	Variable	—
		Close-tight parallel moderately inclined gently plunging minor folds	Hinge 210/12 axial plane 300/35	Folds S_0 and S_3

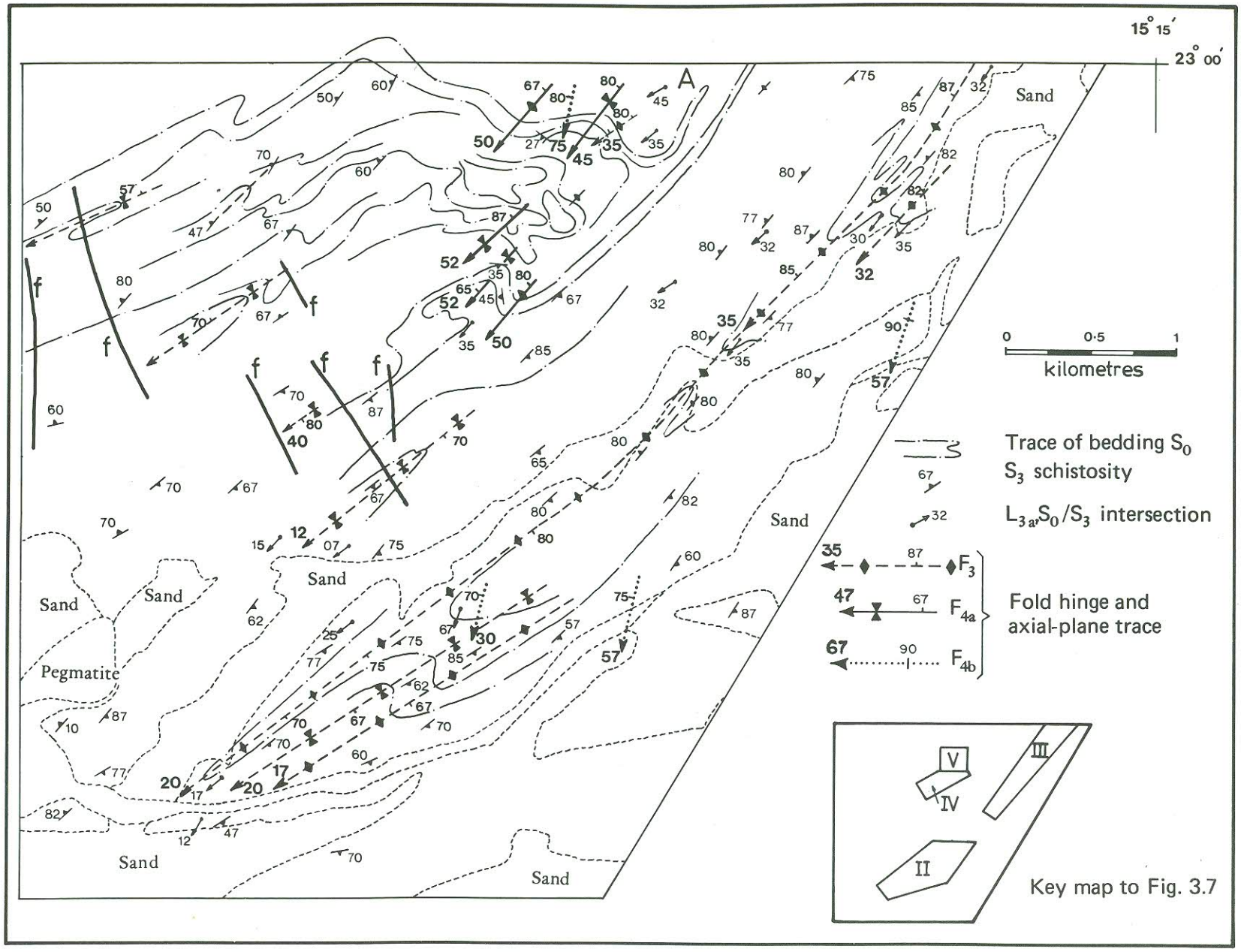

Fig. 3.7 — Structural details of subzone OLZ/1. See Table 4.1 for correlation of fabric elements. Locality A referred to in the text.
Struktuurgegewens van subsone OLZ/1. Verwys Tabel 4.1 vir korrelasie van maakselelemente. In teks word na lokaliteit A verwys.

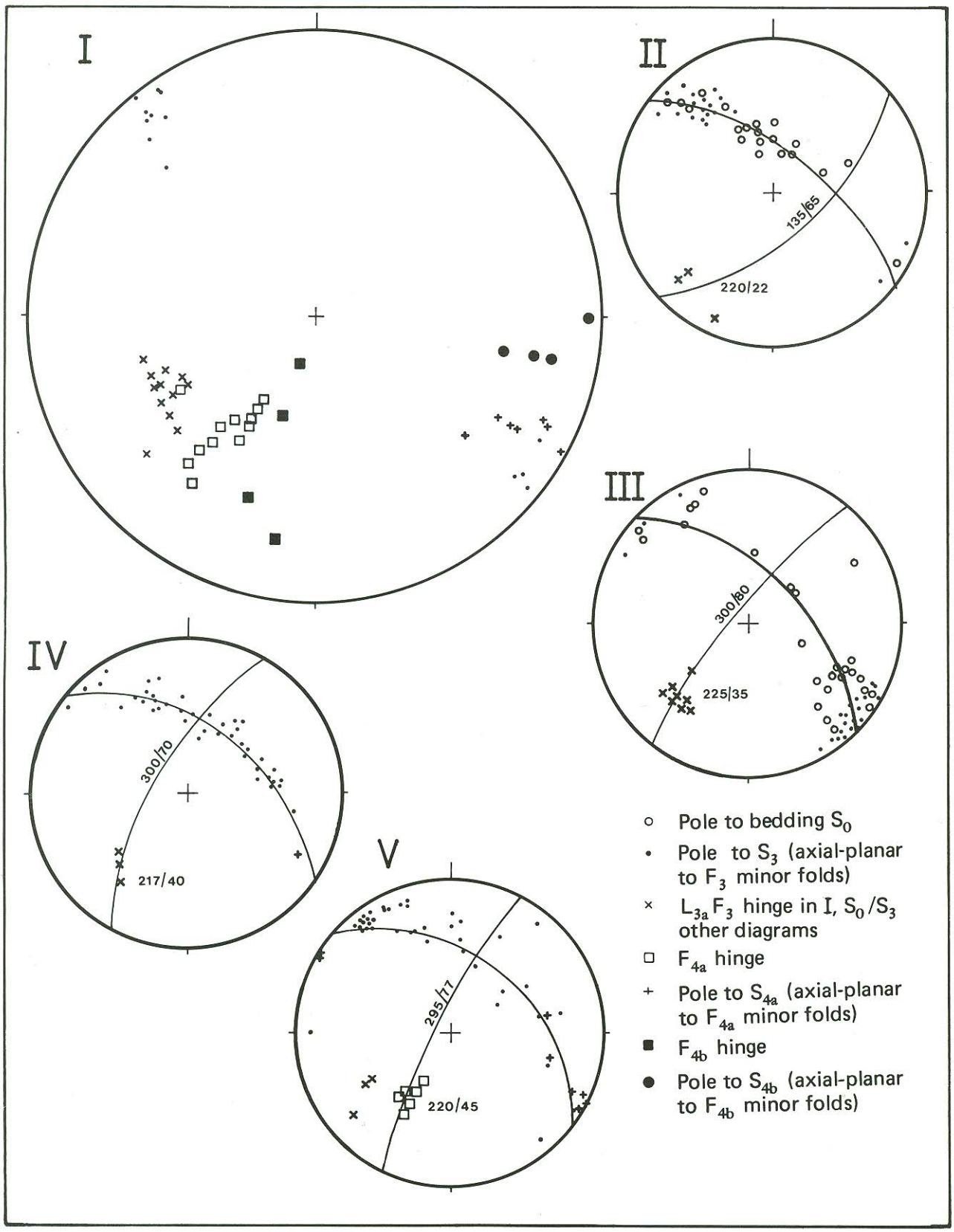

Fig. 3.8 — Fabric-element orientations in subzone OLZ/1. I - minor folds and axial planes from the whole subzone. II — V refer to domains shown in Figure 3.7. See Table 4.1 for correlation of fabric elements. *Maakselelementoriëntasies in subsone OLZ/1. I - ondergeskikte plooie en asvlakke van die subsone in geheel. II — V verwys na domeine in Figuur 3.7 aangetoon. Verwys Tabel 4.1 vir korrelasie van maakselelemente.*

Tabular calcite crystals in many marbles also lie parallel to S_2. Transposition of bedding parallel to the S_3 planes is evident in fold closures where calc-silicate layers are commonly disrupted into cleavage mullions. The average orientation of S_3 is subvertical, striking north-north-eastwards (Fig. 3.8).

S_{4a}, a weak crenulation cleavage, is best seen in more micaceous rocks, in the hinge areas of F_{4a} folds.

The S_{4b} fracture cleavage is present in the synformal closures of F_{4b} folds, and is invariably fanned (Fig. 4.2E).

Linear Fabric Elements—The dominant linear element L_{3a} is defined by cleavage mullions of calc-silicate fels or marble, and F_3 fold hinges. In a few cases hornblende needles adjacent to cleavage mullions are also aligned parallel to L_{3a}. On calc-pelite bedding planes L_{3a} often appears as ripple-like structures. Variation of L_{3a} orientation is slight as shown on the stereograms of Figure 3.8.

L_4 is a weak biotite lineation on S_3 planes due to S_{4a} intersection. L_4 is found only close to F_{4a} hinges.

3.4.1.2 *Minor Folds*

F_3 minor folds are uncommon, except in major fold closures, probably due to transposition of S_0 by S_3, which may be so severe as to totally disrupt calc-silicate layers leaving thin 'smears' of calc-silicate fels on S_3 planes. Minor folds are thus destroyed on fold limbs but may be preserved in thick marble and calc-silicate layers. F_3 plunges are gentle, and typically 232/37 (Fig. 3.8). When asymmetric with respect to S_3 long limbs may be sheared out, and the short limbs locally overturned.

F_{4a} and F_{4b} folds are of similar orientation to F_3 although folding S_3 planes. Figures 3.7 and 3.8 I show the change in hinge and axial surface orientation between F_3, F_{4a} and F_{4b}. Pegmatites intruded parallel to S_3 are folded by F_{4b}.

3.4.1.3 *Major Folds*

Possible F_1 folds are present in the north of this subzone giving rise to the fold closure at A in Figure 3.7 and a dome-and-basin pattern 1 km south-west of A. There is no apparent axial-planar schistosity associated with these folds but these are strongly folded and cleaved by F_3 and S_3 respectively.

Large-scale F_3 folds are developed in the east of the subzone. Interlimb angles are generally less than 5°. Calc-silicate cleavage mullions (L_{3a}) are abundant in the fold closures and lie parallel to F_3 hinges. The folds are slightly asymmetric often with the short limb locally overturned. Bedding, hinge and axial-plane orientations for one F_3 fold are shown in Figure 3.8 III.

3.4.1.4 *Major Faults and Discontinuities*

There are no major faults, although northerly trending minor faults with sinistral displacement of a few metres are common.

3.4.2 Subzone OLZ/2

A structural map of the subzone is shown in Figure 3.9. The area lies athwart much of the Okahandja Lineament Zone and includes rocks of the Kuiseb Formation and part of the Tinkas Member.

3.4.2.1 *Fabric Elements*

There are essentially four planar fabric elements—the crenulation cleavage S_{4a}, however, is only of local importance. Linear elements are cleavage mullions, fold hinges, mineral lineations and S-surface intersections constituting three main trends.

Planar Elements—The lithological variation in the Tinkas Member rocks enables S_0 to be determined readily. Above the Tinkas Member, however, pelitic schists dominate and S_0 is not as easily located. Orientation of S_0 is shown in Figure 3.10 I for the area east of the Tinkas Member, and Figure 3.10 VI shows bedding around the synform X–X on Figure 3.9.

The pelitic schists above the Tinkas Member (i.e. east of the upper Tinkas boundary) occasionally contain the S_1 fabric. S_1 is not observed over any great extent since it is folded by F_3 and strongly crenulated by S_3 into which fabric the biotites of S_1 have recrystallised.

The orientation of the strongly penetrative S_3 schistosity is fairly uniform over the subzone (Fig. 3.10 III). The fabric is seen as a compositional layering in calc-silicate cleavage mullions.

A crenulation cleavage S_{4a} is rarely developed, but when present is often very intense in F_{4a} fold closures. Orientation is shown in Figure 3.10 IV and is nearly co-planar with S_3.

East of the Tinkas Member thin breccia bands are developed parallel to S_3. These bands are not more than a metre thick, commonly only 50 mm wide and impersistent along strike grading into thin mylonitic bands (S_5) still parallel to S_3. The breccias contain angular fragments of schist cemented by carbonate or epidote. Because the bands are thin only about 20 have been found but they appear to be widespread.

Linear Elements—The L_{3a} lineation is common throughout the subzone as elongated cleavage mullions and rare F_3 fold hinges. Quartz veins are generally scarce in this subzone and in the Okahandja Lineament Zone in general, but a few of those present are rodded parallel to L_{3a}. L_{3a} orientations are shown in Figure 3.10 III.

A biotite lineation L_{3b} on S_3 planes is frequently broken up into small elongated spots whose long axes define L_{3b} where S_1 transposition into S_3 has occurred. The orientation of this lineation which has not yet been observed in the Tinkas Member, varies as shown in Figure 3.10 II.

A biotite lineation microcrenulation on S_3 planes defines L_4, which trends 030/05–20.

3.4.2.2 *Minor Folds*

Minor F_3 folds are common having axial planes dipping steeply north-westwards or south-eastwards. The long limbs of a few folds occurring in the Tinkas Member are sheared (e.g. on 290/70).

F_{4a} folds are nearly co-axial with F_3 folds; the plunge is consistently to the south-west averaging 210/45 (Fig. 3.10 V). These folds are frequently markedly asymmetric.

Minor F_5 kink folds, commonly in conjugate sets and having various orientations, are found adjacent to breccia bands.

3.4.2.3 *Major Folds*

Many of the F_3 folds are elongated basins or domes (Fold X–X, Fig. 3.9) with plunges (L_{3a}) either to the north-east or south-west (Fig. 3.10 III and VI). This may be due to undulating hinges, i.e. the folds are not cylindrical, or it may result from interference with pre-F_3 folds.

3.4.2.4 *Major Faults and Discontinuities*

A thrust fault is proposed in the western part of this subzone, parallel to the strike of S_3, but the dip of the plane is unknown. Evidence for the fault comes from a

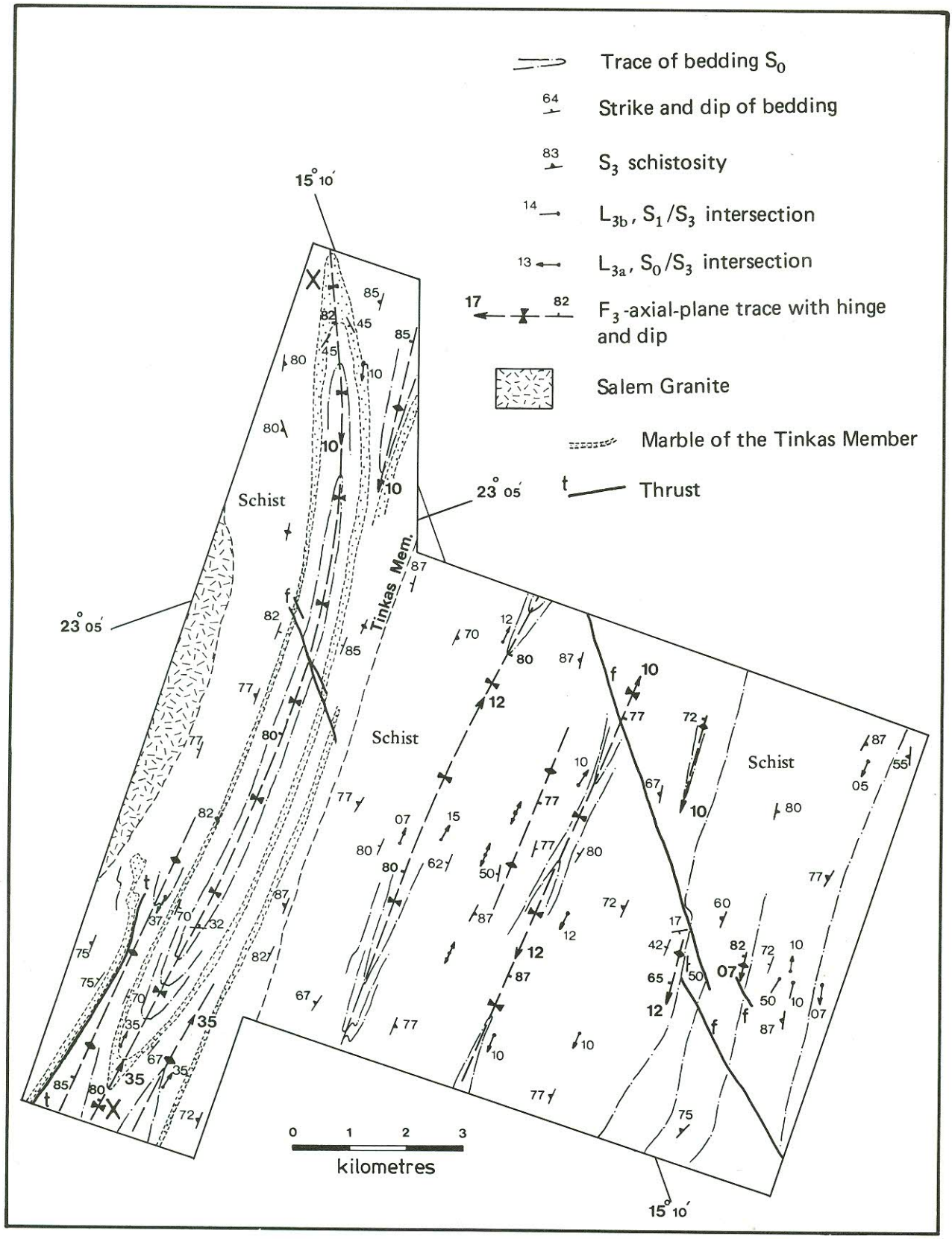

Fig. 3.9 — Structural details of subzone OLZ/2. For correlation of fabric elements see Table 4.1.
Struktuurgegewens van subsone OLZ/2. Vir korrelasie van maakselelemente verwys Tabel 4.1.

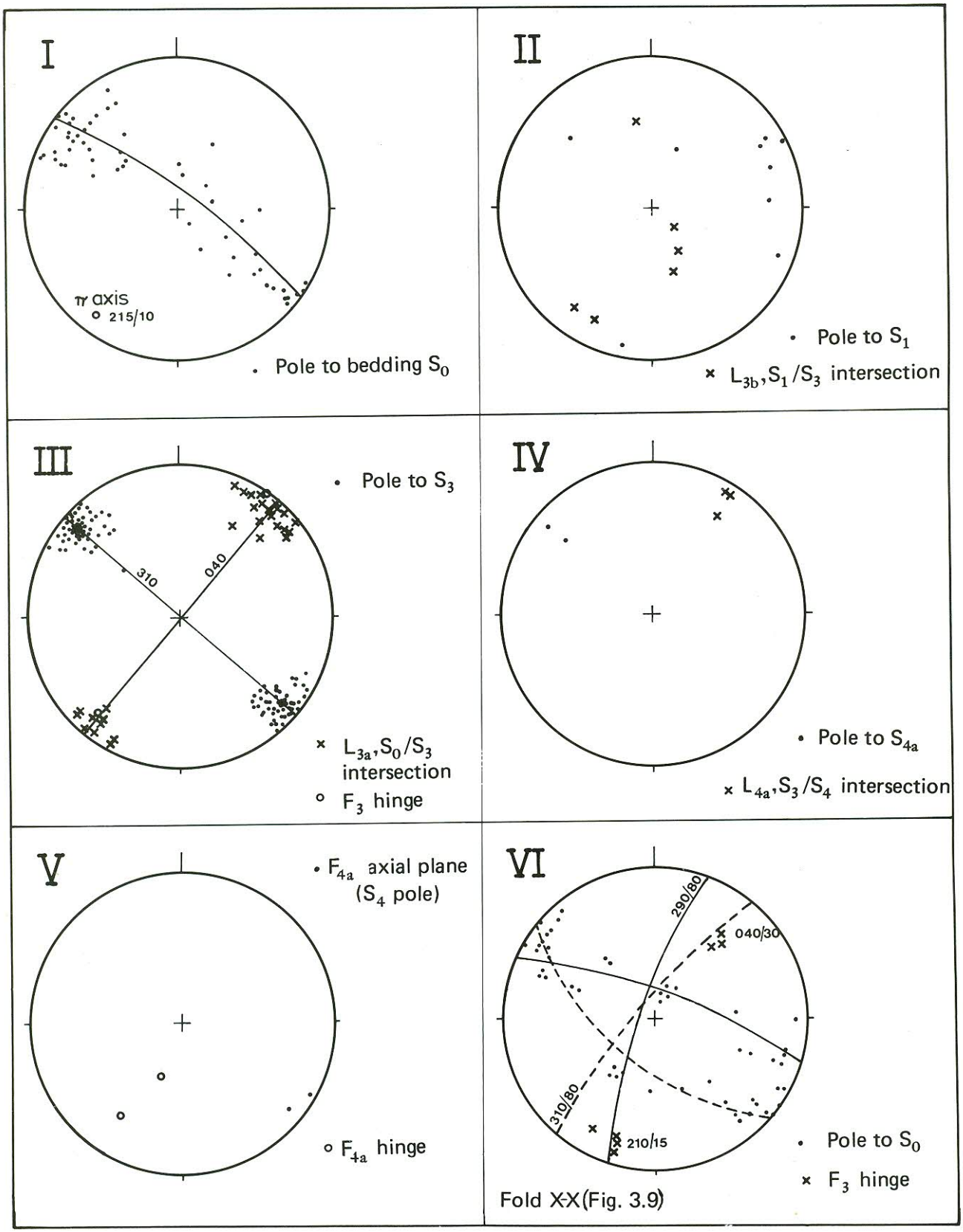

Fig. 3.10 — Fabric-element orientations in subzone OLZ/2. See Table 4.1 for correlation of fabric elements.
Maakselelementoriëntasies in subsone OLZ/2. Verwys Tabel 4.1 vir korrelasie van maakselelemente.

thin band of iron-stained metapelite accompanied by a grey brecciated quartz vein. In addition, part of the stratigraphic succession appears to be absent, and below the fault plane imbricate-type structures are present in dark massive rocks interbedded with semipelites. In the vicinity en echelon tension gashes indicate a dextral shear couple. This structure may be associated with the breccia bands. It is not known whether this thrust is present beneath the folded marble band east of the known outcrop of the fault plane.

Numerous small-scale northerly trending fractures are present often with metre-scale sinistral displacements.

3.4.2.5 *Other Structures*

A locally penetrative second schistosity S_f is visible in some of the more micaceous schists. In these rocks muscovite lies parallel to S_3 whereas biotite defines the S_f fabric, or may be irregularly oriented. S_f is generally subhorizontal (approximately 315/15) and includes biotites grown in associated tension-gash-like structures. The texture on S_3 planes is similar to that of a garbenschiefer as a result of the new biotite orientation. The relationship between S_f and S_3 is not known. S_f is enclosed helicitically in both andalusite and cordierite porphyroblasts which generally grow in bands parallel to S_3 (Section 7). No fold structures are obviously associated with S_f which may be of metamorphic origin. This fabric has been observed as far north-east as Gross Barmen.

3.4.3 Subzone OLZ/3

This subzone lies at the eastern edge of the Okahandja Lineament Zone adjacent to the Donkerhuk Granite, and contains several features not seen elsewhere in the zone. Figure 3.11 shows the main structural details.

3.4.3.1 *Fabric Elements*

Four main penetrative fabric elements are seen. The crenulation cleavage, however, may represent several 'events'. Linear elements are abundant and include fold hinges, rods, mineral lineation and S-plane intersections. Orientations of the various elements are shown in Figure 3.12.

Planar Elements—Bedding is generally transposed parallel to S_3 making precise orientation of S_0 difficult.

The S_1 fabric is fairly common although confined to mica-rich metapelites. S_1 is oblique to bedding and crenulated by S_3. S_1 may be a metamorphic banding or a pressure-solution cleavage.

S_3, the dominant planar fabric, is a schistosity in which most platy minerals are aligned. There is also a tendency for amphibole crystals to lie in S_3 at the edge of calc-silicate cleavage mullions. Towards the contact with the Donkerhuk Granite coarse-grained muscovite flakes, cauliform andalusite and nodular cordierite grow randomly across S_3. Crenulation cleavage is very common over the whole subzone with orientation differing from point to point. Thus the crenulations may represent several events and are only locally significant fabric elements, i.e. S_{4a} is associated with F_{4a}, S_{4b} with F_{4b} and S_6 with F_6. Some crenulations are axial-planar to similar type folds, whilst others belong to kink fold sets. The crenulations are best seen in the finer-grained micaceous schists. S_5, a mylonitic banding, commonly grades along strike from breccia bands, and is often of papery appearance and parallels S_3.

Linear Elements—The L_{3a} lineation of cleavage mullions, F_3 fold hinges and occasional mineral orientation has a uniform strike of 030° (Fig. 3.12 I) over the subzone.

Elongated biotite spots and biotite striping on S_3 surfaces define L_{3b}.

Northerly trending crinkles on S_3 planes due to S_{4a} define L_4 and are found in the hinge areas of F_{4a} folds.

Quartz rods due to boudinage or pinch-and-swell structures in quartz veins have various orientations, other than the lineations above. In general, however, quartz rods trend and plunge northwards.

3.4.3.2 *Minor Folds*

In one instance the S_1 fabric is folded into a nearly isoclinal recumbent F_2 minor fold and later crenulated by S_3. The fold is apparently rootless and may originally have had a subhorizontal axial plane. Biotite spots (L_{3b}) elongated along 210/35, are abundant nearby (Fig. 4.2C).

Minor F_3 folds are not abundant but often occur as rootless intrafolial folds parallel to S_3. F_3 orientations are shown in Figures 3.11 and 3.12 I.

The F_{4a} folds are almost co-axial with F_3 folds (Fig. 3.12 I and II). The F_{4b} folds show the same slight change in orientation from F_{4a} as in OLZ/1, (Fig. 3.12 II and III). Quartz veins are locally rodded parallel to the F_{4b} hinge.

Locally penetrative kink-and-buckle folds belong to F_6 and often occur in conjugate sets, close to the Donkerhuk Granite. Small to meso-scale asymmetric folds also belong to F_6, but do not occur in conjugate sets being parallel close-to-tight gently inclined folds with hinges 210/12 and axial planes 300/35 (Fig. 3.11).

3.4.3.3 *Major Folds*

Observed F_3 folds are very tight with interlimb angles of less than 10° (Figs 3.11 and 3.12 I).

3.4.3.4 *Major Faults and Discontinuities*

Very frequently bands of breccia are observed parallel to S_3. These are laterally impersistent and grade into mylonitic rocks. A thin band of marble is parallel to one such breccia and calc-silicate layers within the marble show small-scale folding (F_5), often with limbs sheared out. The shear couple producing these minor drag folds appears to have been sinistral. In another case en echelon tension gashes adjacent to a breccia band wholly in metapelitic schists indicate a dextral shear couple.

Close to the Donkerhuk Granite pegmatites are intruded either parallel to, or at high angles to S_3. In five instances where pegmatites are perpendicular to S_3-parallel breccia bands, the pegmatites are displaced sinistrally by up to 25 m. An S_3-parallel fracture cleavage (S_5) is developed in the brecciated pegmatite within the dislocation zone. Medium-grained muscovite pegmatites (early set) parallel to S_3 are occasionally boudinaged or show pinch-and-swell (L_5) structures having subvertical long axes typically plunging 200/70. Quartz veins may be present at boudin necks. Although at several localities S_3-parallel surfaces of breccia bands are exposed, no slickenside markings have been found. Breccia bands are numerous and in one instance persistent for 3 km along strike. Fracture cleavage and kink folds are often associated with the bands.

Post-Damara, northerly trending fractures with minor sinistral displacement are frequent and in a few places have been intruded by dolerite dykes.

3.5 CENTRAL ZONE STRUCTURAL GEOMETRY

The main characteristics of the fabric elements observed in the Central Zone are shown in Table 3.3.

3.5.1 Subzone CZ/1

This zone lies immediately to the west of the Okahandja Lineament Zone and contains structural elements common to both zones (Fig. 3.13).

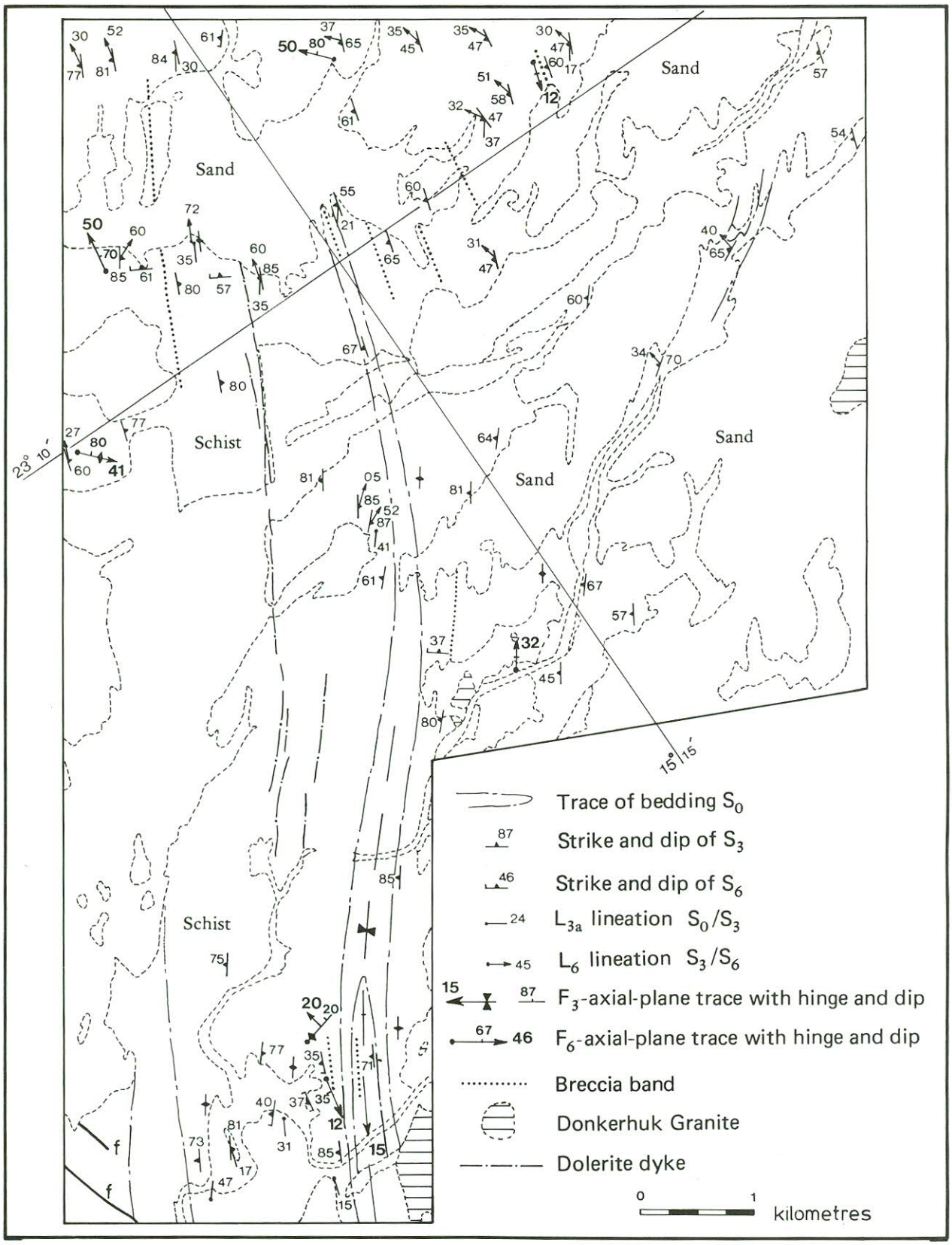

Fig. 3.11 – Structural details of subzone OLZ/3. For correlation of fabric elements see Table 4.1.
Struktuurgegewens van subsone OLZ/3. Vir korrelasie van maakselelemente verwys Tabel 4.1.

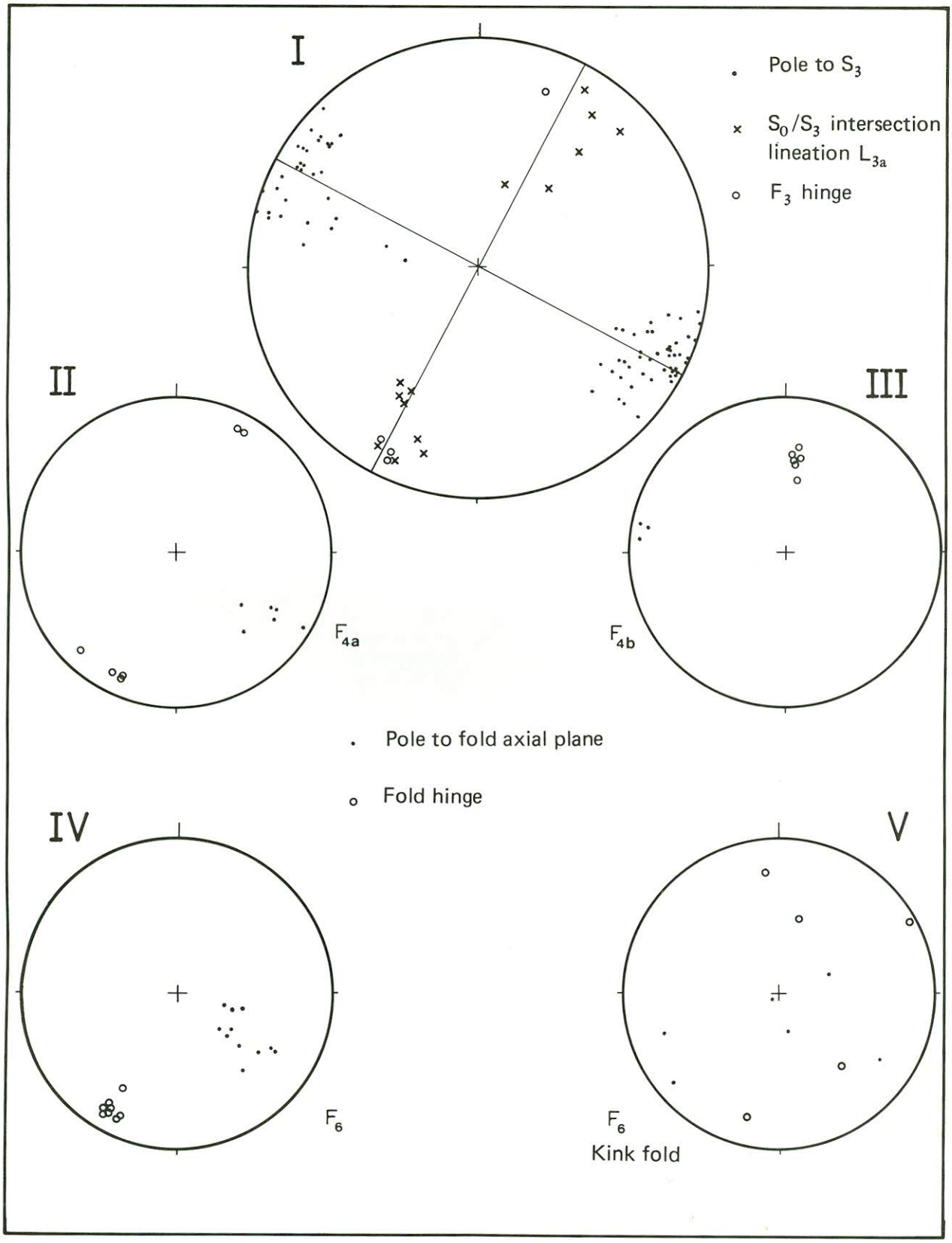

Fig. 3.12 — Fabric-element orientations in subzone OLZ/3. For correlation of fabric elements see Table 4.1.
Maakselelementoriëntasies in subsone OLZ/3. Vir korrelasie van maakselelemente verwys Tabel 4.1.

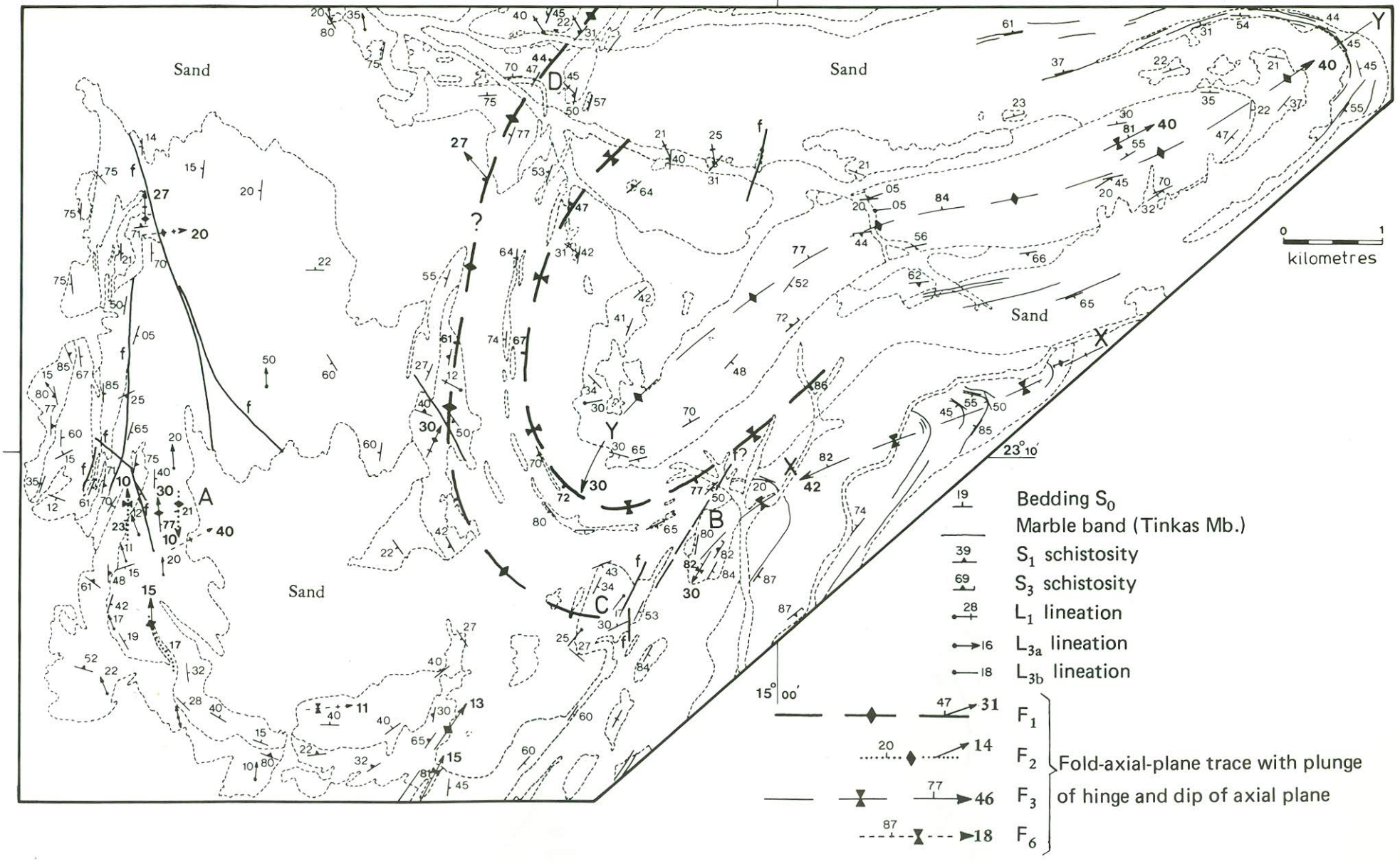

Fig. 3.13 — Structural details of subzone CZ/1. See Table 4.1 for correlation of fabric elements. A, B, C, D, X–X and Y–Y refer to localities and folds mentioned in the text.
Struktuurgegewens van subsone CZ/1. Verwys Tabel 4.1 vir korrelasie van maakselelemente. A, B, C, D, X–X en Y–Y verwys na lokaliteite en plooie in teks genoem.

Table 3.3—MAIN CHARACTERISTICS OF CENTRAL ZONE PENETRATIVE FABRIC ELEMENTS

Element	Occurrence	Main features	General orientation	Effect on pre-existing fabrics
S_0	CZ/1 and 2	Bedding, variation of lithology, mineralogy, grain size or colour	Variable	—
S_1	CZ/1 and 2	Schistosity in metapelites, parallelism of biotite and muscovite where present. Many granitic neosomes parallel S_1	Variable, generally north-westerly dipping	Subparallel to S_0 in most areas except F_1 fold closures
F_1	CZ/1 and 2	Tight to isoclinal moderately inclined gently plunging folds, S_1 is axial-planar, hinge parallel to L_1	Hinge north or north-westerly plunge	Folds S_0 which it locally inverts. Elongation of clasts in Chuos Formation defines L_1
S_2	CZ/1	Extremely weak alignment of biotite in F_2 closures	Subhorizontal	Reorientates biotites of S_0 and S_1
F_2	CZ/1 and 2	Tight to isoclinal gently inclined subhorizontal folds, S_2 axial-planar	Hinge (L_2) 350/10	—
S_3	CZ/1 and 2	Schistosity or crenulation cleavage, locally very strong replacing S_1. Alignment of the platy minerals, some granite neosomes parallel to S_3 planes	300/80	Intersection with $S_0 = L_{3b}$ (in east); mineral and lineation L_{3DC} elsewhere
F_3	CZ/1 and 2	Tight to isoclinal steeply inclined to upright gently plunging class 1C folds. S_3 axial-planar. Folds modified by diapirism	L_{3a} hinge 350/10-20 and L_{3b} hinge 210/30	Folds S_0, S_1, F_1 and F_2
F_4	CZ/2	Tight asymmetric moderately inclined, moderately plunging folds, class 1C	Axial plane 025/55 and hinge 355/40–025/60	Folds S_0, S_1, F_1, F_2, F_3 present mainly in Karibib marble
F_5	CZ/2	Close-tight moderately inclined moderately plunging class 1C folds	Axial plane 320/55 and hinge 010/40	Not observed folding F_4
F_6	CZ/1 and 2	Open parallel upright moderately plunging folds	Axial plane subvertical hinge 000–070/45	Folds F_3 and F_4

3.5.1.1 *Fabric Elements*

A number of planar fabric elements can be discerned of which two are clearly pre-Damara, but only the Damara structures will be considered. Linear fabric elements of Damara age are abundant and include fold hinges, mineral lineations, deformed clasts and intersection lineations.

Planar Elements—The Nosib Group rests unconformably upon the pre-Damara, in effect burying a pre-Nosib topography. Within the Nosib Group, bedding is recognised by heavy-mineral layering, presence of pebble bands, schist intercalations and sedimentary structures such as cross-laminations, channel fills and graded bedding. No bedding-plane structures appear to be preserved. The bedding is inverted at Fold C in Figure 3.13.

Bedding (S_0) within the Chuos and Kuiseb Formations is less easy to define but nevertheless, can generally be found as lithological variations although sedimentary structures are scarce. A compositional layering seen in the Karibib marbles is probably bedding.

The S_1 schistosity is well developed in pelites but very weakly developed in the quartzo-feldspathic rocks of the Nosib Group. S_1 is generally subparallel to S_0, but can be seen to lie oblique to S_0 locally (D in Fig. 3.13).

S_2 is a very weak schistosity confined to the closures of F_2 folds where biotites of S_0 or S_1 are reoriented (Fig. 4.3C.)

The S_3 schistosity or crenulation cleavage changes strikes from 350° to 035° from west to east as the Okahandja Lineament Zone is approached (Fig. 3.14 II and III). Flattened sillimanite knots also lie parallel to S_3 and oblique to S_1.

Linear Elements—The L_1 lineation is defined by the elongation of clast in the Chuos Formation and rarely by a lineation on S_1 planes. The orientation of L_1 is variably due to later folding, notably by F_3.

F_2 fold hinges define the L_2 lineation.

The change in orientation of S_3 from west to east is reflected in the orientation of associated lineations (Fig. 3.14 II and III). The L_{3a} lineation found in the western part of CZ/1 is due to elongation of augen in pre-Damara rocks, elongation of sillimanite knots and minor F_3 fold hinges in the Nosib. L_{3b}, present adjacent to the Okahandja Lineament Zone, is defined by clast elongation in the Nosib and Chuos rocks and occasional minor F_3 fold hinges. Typical orientations are: L_{3a} 355/30 and L_{3b} 040–220/00–20. L_{3b} in the Central Zone parallels L_{3a} of the Okahandja Lineament Zone.

3.5.1.2 *Minor Folds*

This subzone contains minor folds crucial to the correlation of Central Zone structures with those of the Okahandja Lineament Zone.

Recumbent, nearly isoclinal F_2 minor folds occur at A in Figure 3.13. The folds deform the fabric in pre-Damara gneisses and S_1 in the lowermost rather micaceous Nosib Group rocks. Axial planes are subhorizontal dipping either to the west or east.

F_3 folds deform F_2 structures (Fig. 4.3C) in the west of the subzone. In one example of an F_3 fold (Fig. 4.3A) a pegmatite vein intrudes across the fold and is deformed co-axially with F_3 suggesting post-pegmatite flattening of the F_3 fold. In other cases pegmatite and granitic leucosomes are intruded parallel to F_3 axial planes.

F_3 minor folds change orientation from west to east across the subzone as shown in Figure 3.13. The change of F_3 hinges from west (L_{3a}) to east (L_{3b}) is shown in Figure 3.14 II and III.

F_6 minor folds are frequently found in the western part of the subzone, but do not significantly affect the outcrop pattern.

3.5.1.3 *Major Folds*

Two major pre-F_3 axial plane traces are shown on Figure 3.13. These folds have S_1 axial-planar and L_1 defining hinge directions. The folds are F_1 since the axial-planar schistosity S_1 is folded by another pre-F_3 fold trend in the west of the subzone. F_1 folds invert the stratigraphy locally (B and C in Fig. 3.13, Section 4). The non-inverted limb is characterised by subhorizontal Nosib rocks north-west of Chungochoabberg.

F_3 folds in the western part of the subzone commonly have faults developed parallel to their limbs.

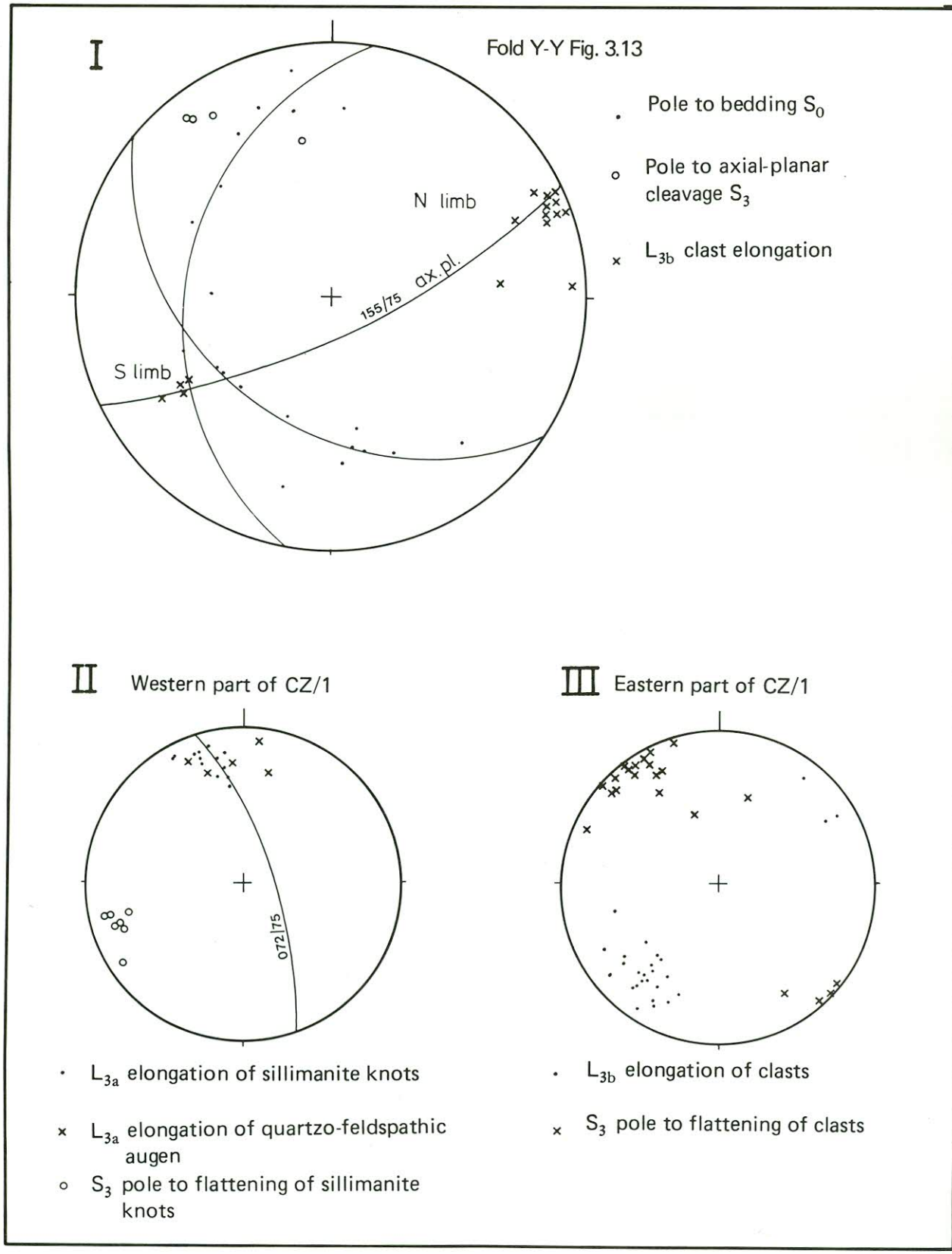

Fig. 3.14 — Fabric-element orientations in subzone CZ/1. For correlation of fabric elements see Table 4.1.
Maakselelementoriëntasies in subsone CZ/1. Vir korrelasie van maakselelemente verwys Tabel 4.1.

At the boundary with the Okahandja Lineament Zone an F_3 brachy-antiform Y–Y on Figure 3.13 deforms F_1 axial-plane traces. The shape of the fold results from F_1/F_3 interference, but may also be due to the intrusion of a large body of Salem Granite 5 km north of the fold deflecting the northern part of the Y–Y fold-axial trace. An axial-planar fracture cleavage is developed in the Nosib rocks of the fold and parallels S_3 in the Okahandja Lineament Zone. Fold X–X is indicated to be a synform from the attitude of marble bands in the Tinkas Member, but contains older rocks in the core, indicating the stratigraphy to be inverted.

3.5.1.4 *Major Faults and Discontinuities*

The fold Y–Y (Fig. 3.13) has a well-developed fracture cleavage which appears to be closely axial-planar. It is noted (Fig. 3.13) that the elongation of pebbles on the northern limb plunges north-eastwards, whilst the elongation plunges south-westwards for the other limb. In addition, poles to S_0 on a band of marble (Tinkas Member) outlining the northern closure fall on separate great circles (Fig. 3.14 I), suggesting some degree of axial-planar movement.

Faulting in Nosib Group rocks north-west of Chungochoabberg is often accompanied by a distinct red colouration of rock adjacent to the fault plane, due to growth of microcline.

3.5.2 Subzone CZ/2

This subzone covers an area dominated by fold structures in the Karibib Formation (Fig. 3.15).

3.5.2.1 *Fabric Elements*

Two penetrative planar-fabric elements are seen in the area. Linear elements include mineral lineations, clast elongations and fold hinges. The orientation of the latter is to some extent dependent on later folding.

Planar Elements—Differing lithologies in the Chuos and Karibib Formations make S_0 bedding readily apparent. Calc-silicate layers frequently parallel to S_0 in the Karibib marble are boudinaged and/or folded.

In areas of local partial melting, granitic neosomes are often found parallel to S_1 (e.g. red gneissic granite). Later folding-and-diapir formation gives rise to a highly variable orientation to S_1.

The subvertical S_3 fabric is occasionally seen in pelites folded by F_3. S_3 crenulates S_1 and contains flattened sillimanite knots. Locally partial-melt neosomes may intrude along S_3.

Linear Elements—The L_1 lineation is defined by elongation of clasts within the Chuos Formation, forming a lineation on S_1 planes.

The L_2 lineation is formed by F_2 fold hinges occasionally seen as folded calc-silicate bands within the Karibib marble.

Mineral lineation L_{3a} due to elongated aggregates of sillimanite, cordierite or quartzo-feldspathic neosomes (augen) lies parallel to F_3 hinges and all plunge gently northwards. In many cases cordierite porphyroblasts lie along the S_1/S_3 intersection but parallel to L_{3a}. The orientation of L_{3a} lineations is shown in Figure 3.16 I and II.

3.5.2.2 *Minor Folds*

Folded interference patterns at B in Figure 3.15, suggest a gently inclined set of F_1 minor folds to be present in the subzone.

Recumbent F_2 minor folds are occasionally seen where marble and pelite are interbedded, e.g. A in Figure 3.15. The subhorizontal axial planes dip gently eastwards with a northerly trending hinge line.

Minor F_3 folds are abundant in the Karibib marble, commonly accompanied by parasitic Z-, M- and S-shaped microfolds. F_3 interlimb angles are generally 5° or less. F_3 refolds F_2 giving rise to numerous interference fold patterns (Fig. 4.3).

F_4 minor folds are particularly common in the central part of the subzone, reorienting earlier structures (Figs 3.16 I and II).

F_6 concentric buckles with rare axial-planar fractures are common over the whole subzone.

3.5.2.3 *Major Folds*

The major F_3 folds trend north to north-eastwards and are locally modified by diapirism into north-trending dome structures (e.g. C, D, E in Fig. 3.15). The F_3 folds have essentially vertical limbs and appear to plunge northwards. Diapirically modified forms still plunge northwards, but often have a cylindrical form with bulbous antiforms and tightly pinched adjacent synforms, e.g. Sopiehoogte Antiform, C in Figure 3.15.

F_4 folds give rise to the north-westerly strike of the Karibib Formation south of Vogelfederberg.

F_5 folds are only present in the western part of the subzone and are arranged in en echelon fashion along the outcrop of the Karibib Formation.

3.5.2.4 *Major Faults and Discontinuities*

No major faults have been recognised in this subzone.

4. KINEMATIC INTERPRETATION

For the purposes of this chapter the fabric elements in each of the subzones are combined into an overall scheme for each zone; in Table 4.1 the elements present in the different zones are correlated. The relationship between the various elements observed is discussed and illustrated below enabling the overall histories of the subzones to be compiled (Tables 4.2, 4.3 and 4.4).

4.1 TROUGH ZONE

Bedding is common to all areas, although it is rarely traceable over any distance in the field. The Matchless Member, although an excellent marker, may not reflect S_0 in all areas, notably the metagabbro bodies and ultramafic types which are probably intrusive into either pelites or metabasites.

In all three subzones there is a single dominant penetrative fabric, which has a fairly uniform orientation dipping moderately steeply north-westwards. In thin section the fabrics in Matchless Member rocks are marked by alignment in y-z planes of phyllosilicates in metapelites and amphiboles. A large proportion of all quartz veins observed lie parallel to this fabric. Transposition of bedding, notably calc-silicate layers, is characteristic of this fabric. The schistosity is common to all three subzones and is termed S_2 since it can be seen to crenulate an earlier fabric in TZ/2.

The S_1 biotite folia in TZ/2 are regularly spaced biotite-rich layers, possibly of pressure solution origin. It is not known whether the biotite has mimetically grown in S_1 or was there originally. All biotite flakes defining S_1 now lie parallel to S_2. Since S_1 lies oblique to bedding in aluminous schists it is probably of structural or metamorphic origin (Fig. 4.1A).

There is also evidence of pre-S_2 folding for TZ/2 where small tight F_1 folds are obliquely cut and crenulated by

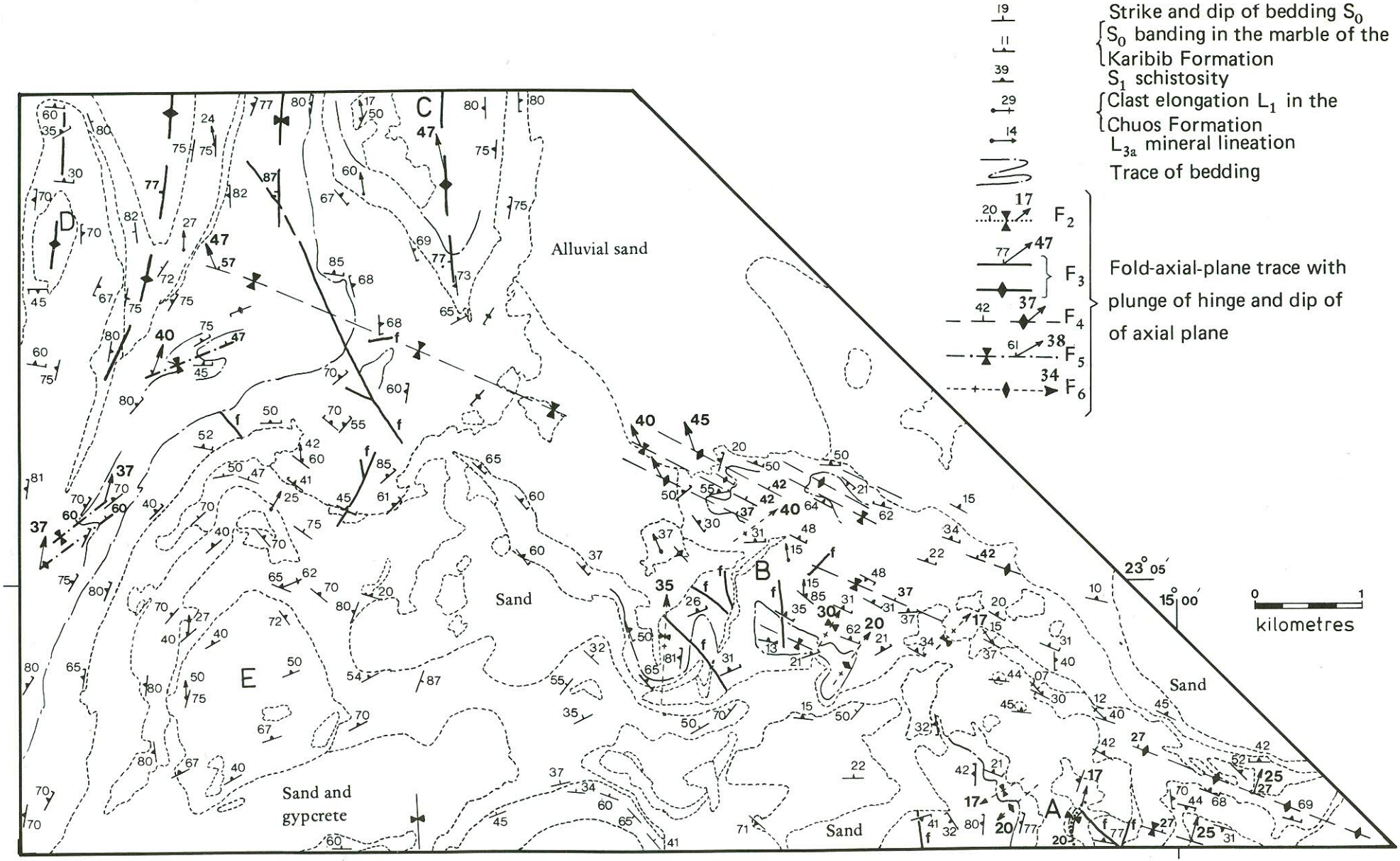

Fig. 3.15 — Structural details of subzone CZ/2. See Table 4.1 for correlation of fabric elements. A—E: localities referred to in the text.
Struktuurgegewens van subsone CZ/2. Verwys Tabel 4.1 vir korrelasie van maakselelemente. A—E: lokaliteite waarna in teks verwys word.

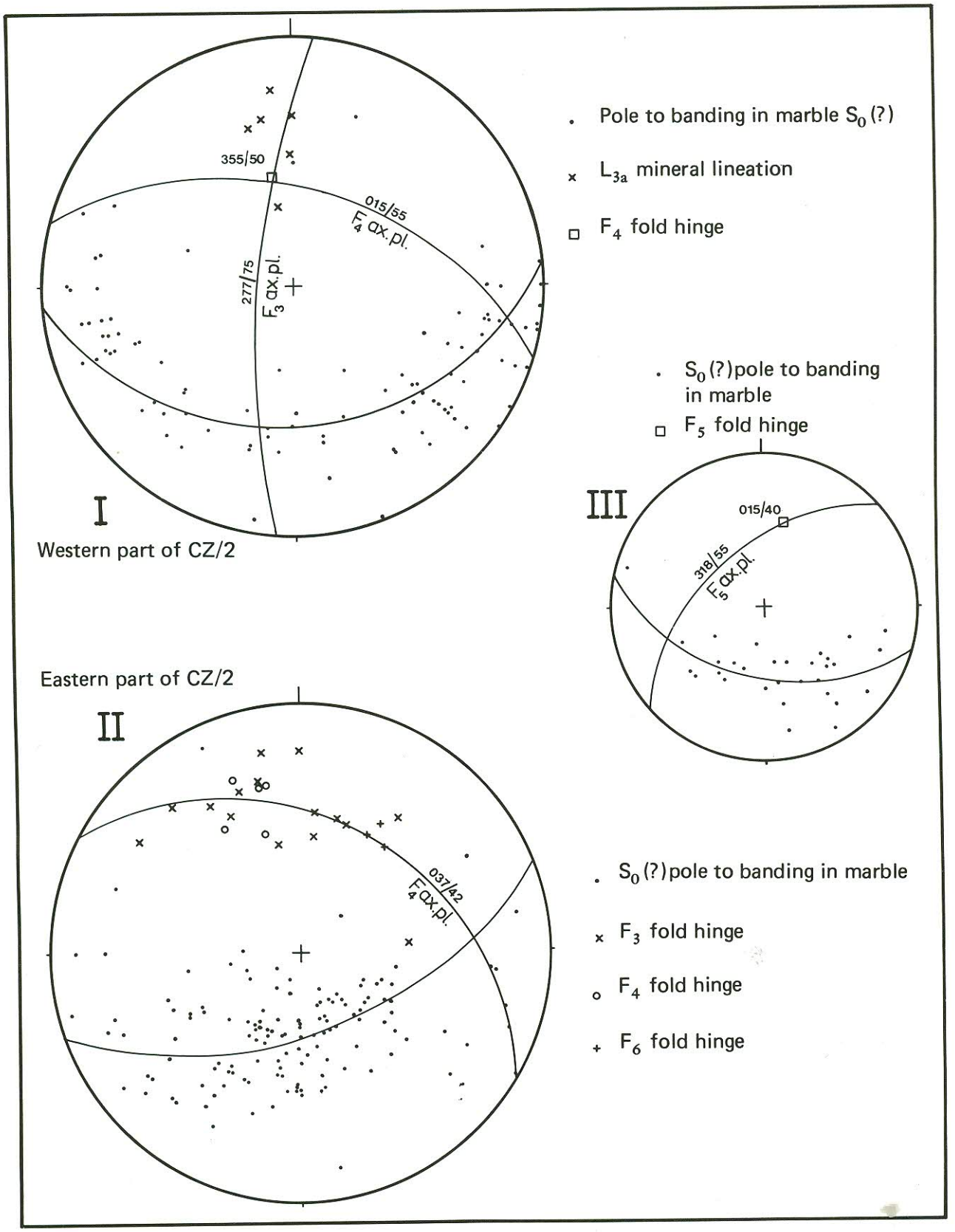

Fig. 3.16 – Fabric-element orientations of subzone CZ/2. For correlation of fabric elements see Table 4.1.
Maakselelementoriëntasies van subsone CZ/2. Vir korrelasie van maakselelemente verwys Tabel 4.1.

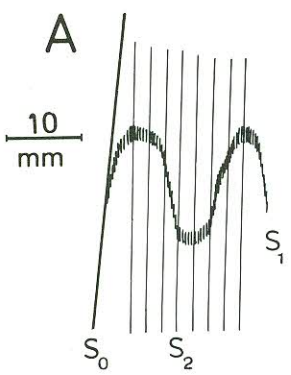

S_1 fabric crenulated by S_2. Biotite flakes parallel S_2 (TZ/2)

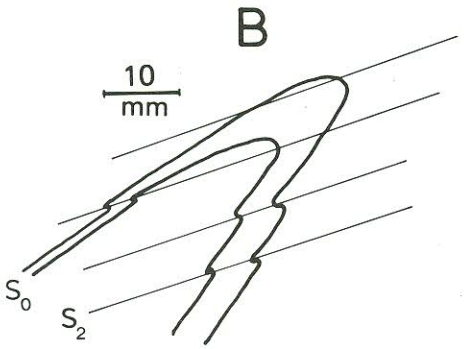

F_1 fold deformed by S_2 schistosity (locality G, Fig. 3.3, TZ/2)

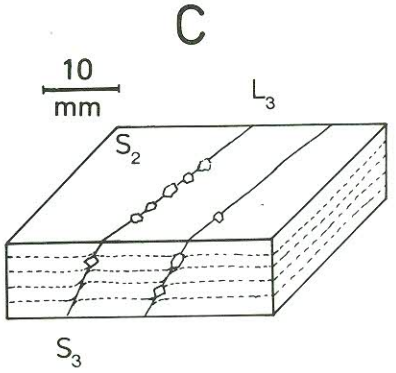

Garnet porphyroblasts grown along L_3 (TZ/2)

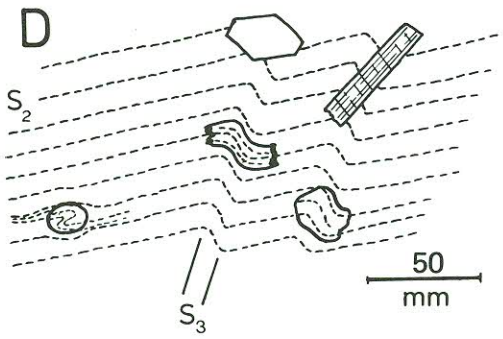

Kyanite and staurolite porphyroblasts pre- and post-dating S_2 (locality D, Fig. 3.3, TZ/2)

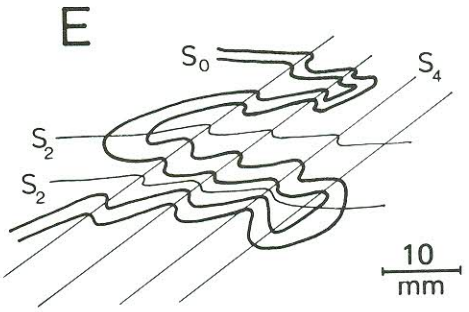

F_2 fold crenulated by S_4 in southern limb of Hope Synform (TZ/1)

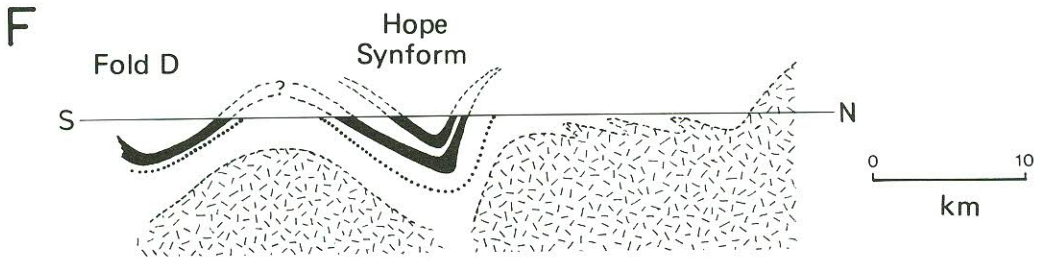

Hypothetical N–S section across Hope Synform (TZ/1) and fold D (TZ/3) showing the Matchless Member (black) on the low-temperature side of the Donkerhuk Granite aureole sillimanite isograd (dotted line). Donkerhuk Granite shown hachured

Fig. 4.1 – Structural and fabric-element relationships in the Trough Zone.
Struktuur-en maakselelementverhouding in die Trogsone.

Table 4.1—CORRELATION OF FABRIC ELEMENTS FOUND WITHIN EACH SUBZONE INTO OVERALL SCHEME FOR EACH MAJOR TECTONIC ZONE

Deformation event	Planar elements			Linear elements			Folds		
TROUGH ZONE	TZ/1	TZ/2	TZ/3	TZ/1	TZ/2	TZ/3	TZ/1	TZ/2	TZ/3
D_{T1}		S_1						F_1	
D_{T2}	S_2	S_2	S_2	L_2	L_2	L_2	F_2	F_2	F_2
D_{T3}		S_3			L_3			F_3	
*D_{T4}	S_4		S_4	L_4		L_4	F_4		F_4
*D_{T5}	S_{5a}		S_{5a}			L_5	F_{5a}, F_{5b}		F_{5a}
Post-Damara							F_6		
OKAHANDJA LINEAMENT ZONE	OLZ/1	OLZ/2	OLZ/3	OLZ/1	OLZ/2	OLZ/3	OLZ/1	OLZ/2	OLZ/3
D_{L1}		S_1	S_1				F_1?		
D_{L2}		S_f?	S_f?						F_2
D_{L3}	S_3	S_3	S_3	L_{3a}	L_{3a}, L_{3b}	L_{3a}, L_{3b}	F_3	F_3	F_3
D_{L4}	S_{4a}, S_{4b}	S_{4a}	S_{4a}, S_{4b}	L_4	L_4	L_4	F_{4a}, F_{4b}	F_{4a}	F_{4a}, F_{4b}
D_{L5}		S_5	S_5			L_5		F_5	F_5
*D_{L6}			S_6						F_6
CENTRAL ZONE	CZ/1	CZ/2		CZ/1	CZ/2		CZ/1	CZ/2	
D_{C1}	S_1	S_1		L_1	L_1		F_1	F_1	
D_{C2}	S_2			L_2			F_2	F_2	
D_{C3}	S_3	S_3		L_{3a}, L_{3b}	L_{3a}		F_3	F_3	
D_{C4}								F_4	
D_{C5}								F_5	
D_{C6}							F_6	F_6	

* Deformation events associated with the emplacement of the Donkerhuk Granite.

Table 4.2—SUMMARY OF DEFORMATION HISTORY OF THE TROUGH ZONE

Trough Zone Damara deformations:

D_{T1}	S_1	Biotite fabric oblique to bedding
	F_1	Tight rootless folds, hinge 310/17 axial plane 355/40; rare quartz veins parallel S_1
D_{T2}	S_2	Schistosity axial-planar to F_2; mean orientation 330/30
	F_2	Tight to isoclinal class 1C folds, hinge 325/25–015/20 depending on later folding; many quartz segregation veins parallel S_2
D_{T3}	S_3	Crenulation cleavage and micro-folding axial plane 260–330/30–70; garnets grow along S_2/S_3 intersection

Donkerhuk Granite emplacement (Late Damara):

D_{T4}	S_4	Weak crenulation cleavage 332/32 axial planar to F_4
	F_4	Close-tight asymmetric folds, hinge 050/10–230/30
D_{T5}	S_5	Crenulation cleavage 340/10–000/07 west of Hope
	F_5	Minor folds chevron-type hinge 320/05–060/12 west of Hope
	F_5	Minor folds of variable orientation on northern limb of Hope Synform

Post-Damara:

	F_6	N–S-trending faults, joints and minor kink bands

Table 4.3—SUMMARY OF DEFORMATION HISTORY OF THE OKAHANDJA LINEAMENT ZONE

Okahandja Lineament Zone Damara deformations:

D_{L1}	S_1	Biotite lamination, pressure solution cleavage (?) oblique to S_0
	S_f?	
D_{L2}	F_2	Tight to isoclinal, north-trending, gently inclined folds
D_{L3}	S_3	Axial-planar schistosity 312/80, transposing S_0 and S_1 local tectonic striping
	F_3	Tight to isoclinal class 1C/2 upright folds, locally with overturned short limb. Hinge 030–040/15 to 220/20; some long limbs sheared
D_{L4}	S_4	Weak axial-planar cleavage 300/75 or crenulation cleavage 280/70

Early Donkerhuk pegmatites:

	F_{4a}	Open-tight upright folds hinge 200/25–240/50
	F_{4b}	Open-tight upright folds hinge 195/45 or 007/37 folds early Donkerhuk pegmatites
D_{L5}		S_3 parallel breccia and mylonite bands. Reactivation of S_3 planes. Sinistral offset of early Donkerhuk pegmatites Boudinaging of pegmatites parallel to S_3. Minor kink folds

Main Donkerhuk Granite emplacement (Late Damara):

D_{L6}	S_6	Crenulation cleavage of various orientations
	F_6	Concentric open folds hinge 210/12, axial plane 300/25. Many kink folds; only adjacent to Donkerhuk Granite

Post-Damara:

N–S-trending fractures and joints sinistral offset

Table 4.4—SUMMARY OF DEFORMATION HISTORY OF THE CENTRAL ZONE

Central Zone Damara deformations:		
D_{c1}	S_1	Schistosity, axial-planar to F_1
	F_1	Moderately inclined folds with westward-dipping axial planes and north-westerly trending hinges
D_{c2}	F_2	Gently inclined folds with westerly dipping axial planes. North–south-trending hinges. Folds and reorientates S_1 biotites. Thrusting with north–south strike
D_{c3}	S_3	Crenulation cleavage or axial-planar schistosity; subvertical
	F_3	Tight to isoclinal class 1C upright folds S_3=axial plane c 300/80; hinge 355/20
		Late modification by diapiric rise gives domes and bulbous antiforms
D_{c4}	S_4	Very, very weak axial-planar fracture cleavage
	F_4	Close-tight class 1C folds axial plane variable 025/50; hinge 355/40–025/60
D_{c5}	F_5	Close tight small- to medium-scale folds, axial plane 320/55; hinge 010/40
D_{c6}	F_6	Small-scale open concentric folds: axial plane subvertical; hinge 000/50–070/40

the S_2 fabric (Fig. 4.1B). No axial-plane structures were observed in the F_1 folds. Evidence of large-scale F_1 folds can be seen on aerial photographs covering the area around G in Figure 3.3 which indicate a large synformal structure (F_1) refolded by F_2 and cleaved by S_2. The north-eastern part of this fold at G in Figure 3.3 shows no pre-S_2 axial-planar fabric.

No evidence has been found to relate S_1 and F_1; these are, however, combined into D_{T1}.

S_3 and S_4 are observed to crenulate S_2 in TZ/2 and TZ/1 respectively (Fig. 4.1C, D and E). S_3 is considered to be older than S_4 on the grounds (Fig. 4.1C and D) of kyanite, staurolite and garnet growth across S_3 or along its L_3 lineation with S_2. S_4, however, has only been observed crenulating minerals, most notably post-S_2 random growth of actinolite (at F in Fig. 3.3). This suggests that S_3 pre-dates a regional metamorphism, whereas S_4 post-dates it. It is unlikely that the mineral growth across S_3 planes is related to the Donkerhuk Granite since thin sections fail to show muscovite replacement of kyanite or staurolite, typical of thermally affected Trough Zone rocks near the Donkerhuk Granite.

No reason can be offered as to why S_3 is absent from TZ/1 and TZ/3, but within TZ/2 the S_3 fabric becomes stronger from west to east.

Large-scale folds deforming S_2 (i.e. F_4) are unique to TZ/1 and TZ/3 since they are absent from TZ/2 and further east on sheet area 2315B*. Hence F_4 folding is only a local phenomenon. Figure 8.1 shows both major F_4 folds (the Hope Synform and Fold D in Figure 3.5) to lie on the low-temperature side of the sillimanite isograd (6). The proximity of the Donkerhuk Granite to the F_4 folds suggests a relationship. A schematic N—S cross-section through Hope Synform and Fold D (Fig. 3.5) is drawn (Fig. 4.1F) bearing in mind the position of the sillimanite isograd. As shown in Figure 3.5, S_2 orientations are irregular between the Hope Synform and the Kuiseb River but define a post-S_2 antiform between the Hope Synform and Fold D. This suggests that the amphibole schists of the Hope area and at Fold D are the same band. The Matchless Member rocks in the eastern part of TZ/3 are largely metagabbros and are probably separate bodies. Whether the curvature of the sillimanite isograd is due to F_4 folds or to the increased thickness of rocks in the synform is uncertain. The second alternative is preferred.

The similar axial-plane orientations of the Hope Synform and Fold D suggest a common direction of maximum stress during formation, the plunges being controlled by the form of the intruding Donkerhuk Granite. Within this scheme the complex folds east of D are interpreted as disharmonic structures associated with the doming north of Fold D.

* Personal communication: R. S. Hill, Geological Survey.

S_4 and S_{4a} have similar dip directions but Figure 3.6 I shows the F_5 hinge defining L_5 on the S_5 axial surface to have a completely different orientation to F_4 folds to which S_4 is axial-planar. This may, however, be related to variable orientation of the folded surface. The F_{5a} folds of TZ/3 are found only in extensively recrystallised migmatitic schists where they fold the S_2 fabric. These also fold small Donkerhuk pegmatites intruded parallel to the S_2 fabric. Folds of similar orientation and geometry occur in the closure of the Hope Synform, but affect non-migmatised rocks.

The folds designated F_{5b} along the northern edge of the Hope Synform are unique to that area, clearly post-dating F_4 by folding the L_4 lineation (Fig. 3.2). Pegmatites intruded along F_{5b} axial planes are boudinaged*, suggesting that folds formed during pegmatite emplacement. There is no interrelationship between the F_{5b} folds of the Hope Synform's northern flank and those just south-east of its closure. Both are considered to have originated through the emplacement of Donkerhuk Granite.

Late F_6 kink folds and crenulations are associated with joints and fractures and are of post-Damara age.

4.2 OKAHANDJA LINEAMENT ZONE

Bedding, S_0, is readily discernible in the Tinkas Member, but is more difficult to recognise in the remainder of the Kuiseb Formation. Within the Tinkas Member graded bedding, turbidite structures (similar to those described by Allen 1970), and possible flute casts can be recognised locally. The sedimentary structures all indicate a sediment transport direction largely from the west.

S_1 biotite laminae are seen over much of the zone (especially in OLZ/2 and OLZ/3) east of the Tinkas Member. S_1 is strongly deformed being crenulated and transposed by S_3 giving rise to the L_{3b} lineation. Figure 4.2A shows the general appearance of S_1 whilst Figure 4.2B from OLZ/3 shows S_1 to be oblique to S_0, and that both are disrupted by S_3. This and the very regular spacing suggest that S_1 is of structural origin. An origin as a pressure solution-type structure is preferred. In all cases the biotite defining S_1 has recrystallised parallel to S_3.

Evidence for pre-S_3 folding can be seen in OLZ/1 (Fig. 3.7, locality A) and OLZ/3 (Fig. 4.2C). In the first case a macroscopic fold is clearly crossed by the S_3 fabric which is not axial-planar to the fold; F_3 and F_4 also fold the structure. The resulting Type 3-interference pattern (Ramsay 1967) suggests that the earlier fold was gently inclined and had a northerly plunge ($\alpha \simeq 0$, $\beta < 70°$, Ramsay 1967, Fig. 10–2). The second case shows another Type 3-interference pattern, but on a microscopic scale. Figure 4.2C shows a gently inclined rootless fold crenu-

* Personal communication: A Killick, Johannesburg Consolidated Investment Co. Ltd.

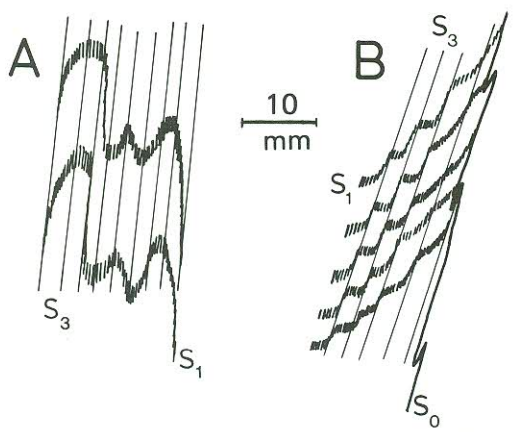

S_1 crenulated and transposed by S_3; note biotite flakes parallel to S_3 (OLZ/3)

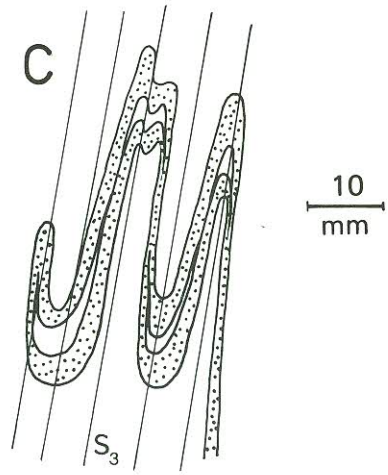

F_2 fold refolded along S_3 planes (OLZ/3)

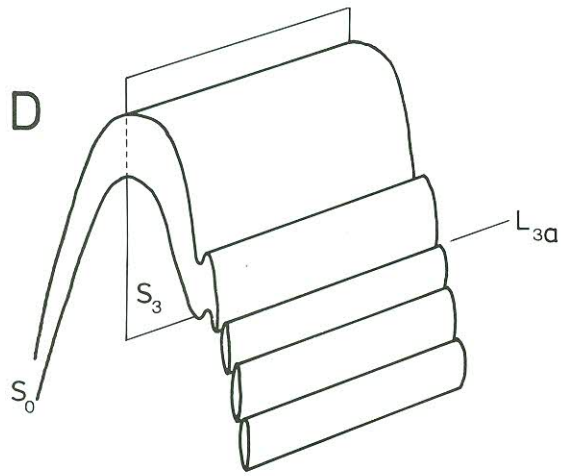

Relationship between F_3, S_3 and L_{3a} showing cleavage mullions formed by S_0/S_3 intersection (OLZ/1)

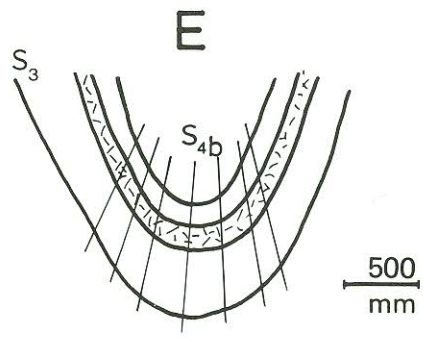

Fracture cleavage in F_{4b} synform deforming a pegmatite vein parallel to S_3

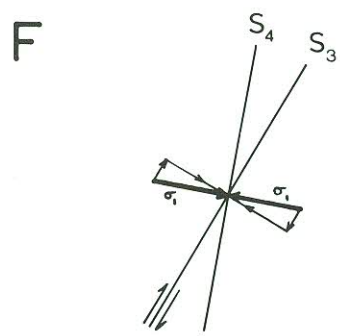

Sense of shear on S_3 planes during F_4 fold formation

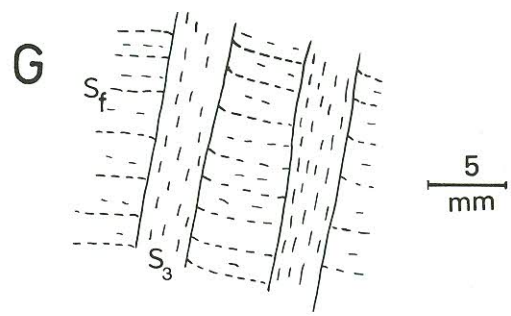

S_3 schistosity cutting the S_f fabric (OLZ/2)

Fig. 4.2 — Fabric-element relationships in the Okahandja Lineament Zone.
Maakselelementverhoudings in die Okahandja-lineamentsone.

lated by S_3. The geometry of this interference pattern and the known orientation of F_3 suggest that F_2 may have had a northerly trend. This microscopic interference fold deforms the S_1 biotite fabric, the biotites of which now lie parallel to S_3.

S_3 is common to all three subzones; correlation is based upon similar orientations, similar microscopic relationships to micas, similar associated folds and continuity observable in the field. It is the principal fabric imparting a fissility to the rocks of the Okahandja Lineament Zone. The fabric is a schistosity although it probably originated as a crenulation cleavage (Fig. 4.2A). Williams (1972) notes that a schistosity may initially begin as a crenulation cleavage becoming modified to a true schistosity. The relationship between S_3, F_3 and L_{3a} is shown schematically in Figure 4.2D.

The S_3 schistosity is folded (OLZ/1, Figure 3.8 IV and V) by F_{4a} and F_{4b}. These two folds have very similar profiles but slightly differing orientations. F_{4a} and F_{4b} are distinguished because F_{4b} folds have been observed to fold and cleave pegmatites intruded parallel to S_3 (Fig. 4.2E) whereas no such relationship has been observed with F_{4a} folds. It is believed that both fold trends represent minor changes in trend during the same deformation during which pegmatite intrusion took place.

Although the relationship between F_2, F_3 and F_4 can be established, the status of the 'breccia bands' and associated mylonites is uncertain. The sense of shear on S_3 planes from offset pegmatites, drag folds and rotated porphyroblasts is sinistral during breccia band deformation. One set of en echelon tension gashes does, however, indicate a dextral sense of shear. The sense of shearing induced along S_3 planes during F_4 deformation would be dextral (Fig. 4.2F).

Breccia and mylonite bands post-date the Samut Granite and early Donkerhuk pegmatites, yet pre-date the late Donkerhuk pegmatites and main Donkerhuk Granite, and may thus in part overlap the F_4 deformation. The sense of shear on S_3 planes during F_4 would mitigate against such a correlation.

The breccia bands could perhaps be the result of the emplacement of the Donkerhuk Granite, as they are more numerous near to the Donkerhuk Granite, that is towards the eastern edge of the Okahandja Lineament Zone. Crenulations and conjugate kink bands are commonly associated with the breccia bands. Because of the problem of assigning the breccia bands to either D_{L4} or D_{L6} they are given separate status as D_{L5} and probably are related to a stage of uplift occurring late in the Damaran orogenesis (Section 9).

Numerous crenulations and minor folds occur close to the Donkerhuk Granite and are considered to belong to the phase of granite emplacement on the following grounds:

(1) They occur close to the granite and die out westwards (cf. Pitcher and Read 1960. Fig. 4).

(2) They occur in migmatised pelites adjacent to the Donkerhuk Granite.

(3) They fold and boudinage many pegmatites.

Therefore these structures are assigned to D_{L6}.

The S_f fabric is problematical in that it has not been observed in direct association with any folds. Its relationship to S_3 is shown in Figure 4.2G, which indicates that S_f pre-dates S_3 (see also Turner and Weiss 1963, Figs 2–8 and 4–29). Muscovites in the aluminium-rich pelites are generally parallel to S_3 planes whereas biotites tend to parallel S_f or are irregularly oriented. In a few cases S_f traces appear to curve slightly into S_3 planes. S_f is crenulated by the various crenulation cleavages near the Donkerhuk Granite. Regional metamorphic andalusite and cordierite often enclose S_f helicitically since these minerals tend to grow in aluminium-rich pelites.

The orientation of S_f is such that it may represent an axial-planar fabric to the F_2 folds. It is also interesting to note that S_f bears a similar orientation to S_2 of the Trough Zone (Section 9).

4.3 CENTRAL ZONE

The relationship between fold phases is based largely upon interference structures which are very common in CZ/2.

In CZ/2, and the rest of the Central Zone, folds with a northerly or north-easterly trend are common, and are accompanied by a crenulation cleavage or schistosity (S_3). In the CZ/1 subzone, however, the orientation of these folds and S_3 changes markedly from west to east across the subzone, trending more north-east at the Okahandja Lineament Zone boundary. The relationship of these folds and the peak of metamorphism is illustrated in Figure 4.3A and G. In the former case a pegmatite is intruded across an F_3 fold and deformed co-axially with that fold, whilst in the latter example granitic neosomes are intruded parallel to fold-axial planes. This relationship to metamorphism can be seen throughout the Central Zone. The peak of metamorphism during late or just after F_3 corresponds with an episode of diapir formation. The rise of the domes, detailed in the next chapter, has in many cases modified F_3 folds making antiforms bulbous or cylindrical in form.

Evidence for two deformation events prior to F_3 comes largely from CZ/2 and may be summarised thus:

(1) Figure 4.3B shows the enveloping surface of an F_3 fold containing and deforming a train of basin-and-dome structures (Type 1-interference pattern) indicating two fold phases pre-dating F_3 assuming that the basins and domes are due to fold interference and not non-cylindrical inhomogeneous folding.

(2) Figure 4.3D and E show Type 2-interference patterns in which one of the deforming fold episodes is F_3. Since the geometry of F_3 is well known the geometry of the other fold set can be inferred from the interference pattern ($\alpha > 20°$, $\beta < 70°$). This suggests the other and earlier fold set to have had gently inclined axial surfaces, which is confirmed by direct observation at A in Figure 3.15. Hinges probably plunge northwards.

(3) If Figure 4.3B represents a folded interference pattern it is possible to state that one of the fold sets involved in the Type 1-interference pattern had a gently inclined axial surface. Therefore with $\alpha \neq 0°$, $\beta > 70°$ for Type 1-patterns it is possible that the other fold set also had moderate to gently inclined axial planes. Hinge trends of F_1 and F_2 are probably at a fairly large angle from the shape of domes and basins.

Evidence from CZ/1 supplements that of CZ/2 thus:

(4) S_1 is folded by a gently inclined fold (F_2) trending north—south which is in turn folded by F_3 (Fig. 4.3C).

(5) S_1 is axial-planar to F_1 folds and intersects S_0 at a high angle in F_1 closures. F_1 folds invert the stratigraphy at B and C in Figure 3.13, the former locality is a Type 1-interference pattern of basin form. These folds have a north-westerly plunge and are gently to moderately inclined although strongly deformed by F_3.

The fabric and structural relationships in both CZ/1 and CZ/2, therefore tend to suggest two fold episodes prior to F_3 as shown in Table 4.4.

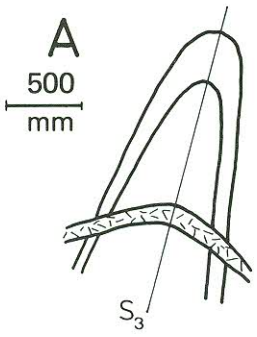

Pegmatite vein intruded across and deformed with an F_3 fold (CZ/1)

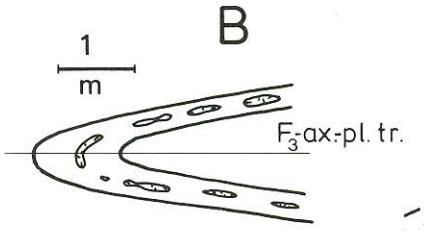

F_1/F_2 interference pattern (domes and basins) refolded by an F_3 fold (CZ/2)

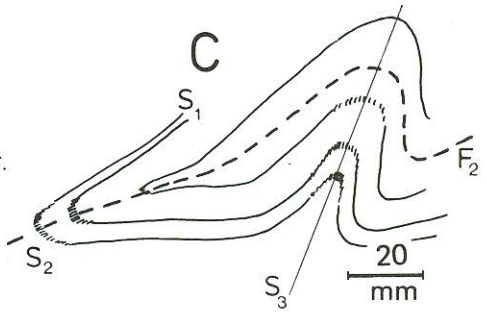

F_2 fold refolded by F_3 — note orientation of biotite flakes of S_1 (CZ/1)

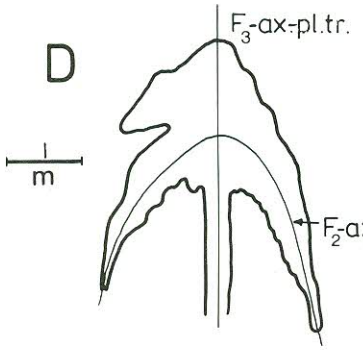

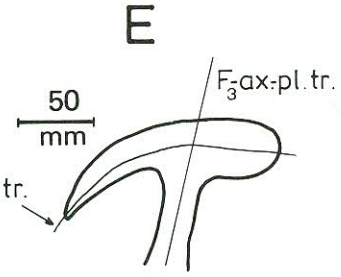

F_2/F_3 (type 2) interference patterns.
D from Swartbank, E from CZ/2

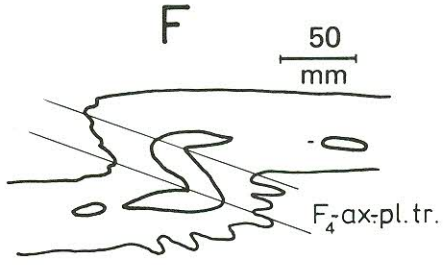

F_1/F_2 interference pattern (domes and basins) refolded by F_4 (CZ/2)

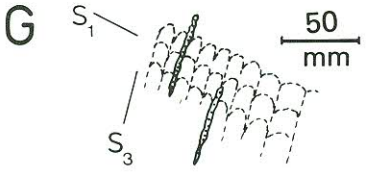

Granitic neosomes intruded along S_3 planes, crenulating S_1 (near Rooibank)

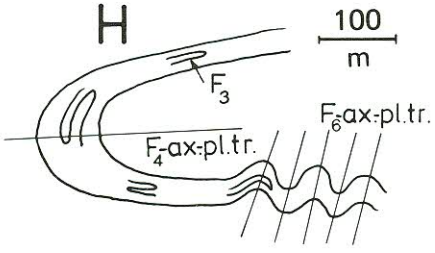

F_4 fold deforming F_3 closures.
F_6 folds fold the F_4 limb (CZ/2)

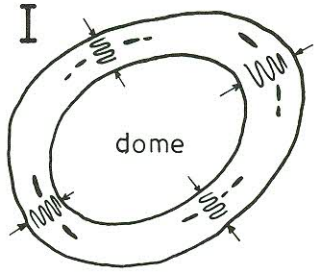

Schematic representation of the deformation around diapiric domes

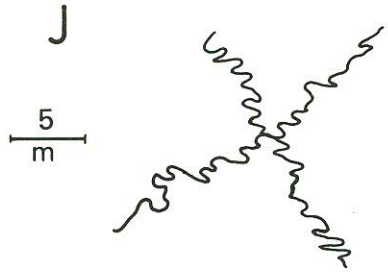

Shortened post-F_3 quartzo – feldspathic veins near Rooibank

Fig. 4.3 – Structural and fabric-element relationships in the Central Zone.
Struktuur- en maakselelementverhouding in die Sentraalsone.

S_3 is a locally strong crenulation cleavage which deforms S_1 (Fig. 4.3G). On F_3 fold limbs, however, S_1 and S_3 are subparallel, a fact observed in the Rooibank area where a thin section of a pelite from an F_3 fold limb shows S_1 and S_3 to be about 5° apart. Thus mineral lineations and mineral-fabric relations on F_3 fold limbs are difficult to determine accurately since both S_1 and S_3 schistosities are virtually parallel. At F_3 fold closures, however, S_1 and S_3 are virtually perpendicular and clearly visible as separate fabrics.

The S_1 schistosity is in general concentrically folded around F_3 dome structures.

Over most of the Central Zone, dome structures are accompanied by layer-parallel extensional features such as boudins or elongated clasts, and compressional features such as shortened veins perpendicular to layering (Fig. 4.3 I). This represents the expected strains developed during diapiric rise of domes (Fletcher 1972; Dixon 1975).

In the area north of Rooibank quartz veins intersecting at right angles show shortening in all directions on the horizontal plane, indicating constrictional strain with possible extension in the vertical sense. Such a deformation scheme is not compatible with diapiric dome formation seen further eastwards in the Central Zone. Any domes within the western extremity of the mapped area may thus be of interference origin.

F_4 folds in the CZ/2 subzone deform both F_1/F_2 interference patterns (Fig. 4.3F) and F_3 folds (e.g. Fig. 4.3H, which shows schematically a thick marble unit containing F_3 minor folds deformed by F_4).

F_5 minor folds are of local occurrence and are considered to be separate from F_4 because of differing axial plane orientation.

Minor F_6 folds occur throughout the subzone deforming F_3 and F_4 fold limbs (Fig. 4.3H). These are parallel folds and generally of small amplitude.

Several large-scale dislocations are present west of Hamilton Beacon. These structures generally have vertical dips, as a result of subsequent folding by F_3. In one example the dislocation plane cuts Salem Granite and induces a locally strong schistosity parallel to the shear plane (Ramsay and Graham 1970). The age of these structures is believed to be D_2 as they appear to have been low-angle thrusts subsequently refolded by F_3. The sense of movement on the dislocation planes indicates overriding from the west or north-west.

5. SOME ASPECTS OF QUANTITATIVE STRUCTURAL ANALYSIS

Several aspects of the structural geology in the area mapped are of special interest because of relevance to the broad-scale development of the Damara Orogen. Several aspects will be dealt with, one from each of the major structural areas:

(1) Structures due to gravity tectonics in the Central Zone.

(2) F_2 fold development in the Trough Zone.

(3) Strain determinations in the Trough Zone and the Okahandja Lineament Zone.

5.1 STRUCTURES DUE TO GRAVITY TECTONICS IN THE CENTRAL ZONE

5.1.1 General Description

During mapping of the Central Zone eight dome or brachy-antiforms were recognised (Fig. 5.1). Two of these structures are rather elongated with length to breadth ratios of about five whereas for the other domes the ratio is about two. In general the domes are elongated approximately north–south, with the exception of the structure A–A in Figure 5.1 which has a north-easterly trend. Several of the structures have slightly curved axial-plane traces probably due to deformation during D_{C4} or D_{C5}. The structure A–A in Figure 5.1 is possibly a D_{C1}–D_{C3} interference fold whilst the other domes further west are diapirs of late D_{C3} age.

The domes all have near-vertical, vertical or even overturned margins and are surrounded by pinched synformal areas. The domal nature is shown by the outcrop distribution of either Nosib Group or Karibib Formation rocks. The structures may be divided into two groups, an eastern and a western one separated by the Hamilton Mountain range. The eastern group is characterised by having a core of pre-Damara rocks which is overlain unconformably by Damara metasediments. This contact is not tectonised. In the Leeukop Antiform, for example, the basal Nosib metarudite contains clasts of the underlying pre-Damara and can be traced around the whole structure north of the area mapped. The pre-Damara core rocks consist of high-grade paragneiss, ortho-augen gneiss and minor amounts of schist, quartzite and calc-silicate rocks. The pre-Damara and parts of the Nosib sequence are extensively migmatised forming red gneissic, red homogeneous and buff leucocratic granites. Some red homogeneous granite bodies and veinlets intrude the Nosib Group rocks across the unconformity.

The western domes lack the core of pre-Damara rocks although red homogeneous and red gneissic granite derived from Nosib Group rocks are present in the cores. The Nosib Group rocks forming these domes frequently have vertical dips throughout much of the dome structure.

The difference in the two dome levels may be due simply to erosion, but it seems more likely to be due to level of diapir rise controlled by such factors as cover thickness, degree of heating with resultant viscosity contrasts or basement control in the location of the domes.

The Damara domes closely resemble the mantled gneiss domes of the Karelidies (Eskola 1948) and those of the Appalachians (Thompson *et al.* 1968; Naylor 1968).

In the original description, Eskola considered that mantled gneiss domes formed over granite plutons in the basement of a later cover sequence, these granites being remobilised during the "orogenic revolutions" which deformed the cover sequence, and the basement granites then rising into the cover. Since Eskola, further work (e.g. Thompson *et al.* 1968; Naylor 1968) have shown that many mantled gneiss domes do not contain basement plutons in their cores, but all do contain high-grade rocks of essentially granitic composition.

An alternative origin for the Damara domes is that they are interference structures. Evidence (see below) suggests they are diapiric structures.

5.1.2 Model for Damara Domes

Mapping has shown the Damara to be deposited on an essentially flat terrain, with occasional topographic highs of up to 800 m (Sawyer 1979). The nature of the Nosib sediments, however, suggests deposition on a highly eroded basement (Smith 1965; Sawyer 1979). The underlying pre-Damara rocks consist of high-grade granitic gneisses of igneous and sedimentary origin, together with pelitic schists and minor amounts of other rock

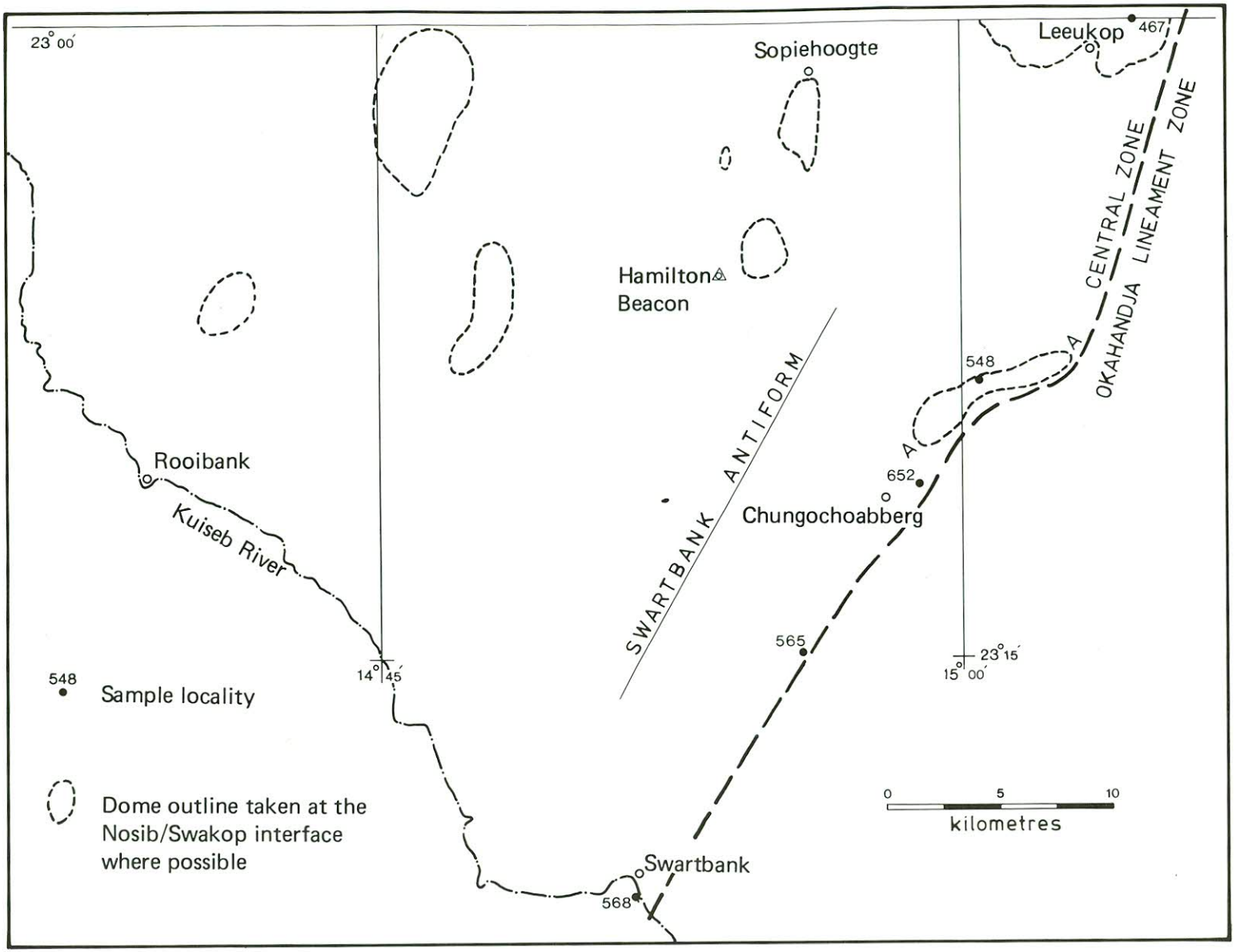

Fig. 5.1 — Location of dome structures in the Central Zone. A—A represents an interference fold. Sample localities are those referred to in Section 5.3.2.
Ligging van koepelstrukture in die Sentraalsone. A—A stel 'n interferensieplooi voor. Monstervindplekke soos na verwys in Seksie 5.3.2.

types. In contrast, the Damara metasediments consist of quartzites and marbles overlain by a considerable thickness of pelitic schist. The approximate thickness of the Damara pile above the Karibib Formation can be estimated from the metamorphic mineral assemblages contained within the metapelites. For the Central Zone, pressures are of the order of 4 kb (Section 8) giving an approximate thickness of 13,5 km above the Karibib Formation or 16 km above the pre-Damara—Damara contact. Thus in a pre-orogenic state with a normal geothermal gradient (say 25 °C. km^{-1}) the rocks at the contact would be at about 400 °C.

At the pressure and temperature of burial it is reasonable to assume that the Damara cover will be largely dewatered and compacted, losing much of its pore space. The bulk density will then be of the order 2,70 g. cm^{-3}. Bean (1953) shows that there is an increase in density from about 2,77 g. cm^{-3} to 2,82 g. cm^{-3} between medium- and high-grade metapelitic rocks. The implication is that during ensuing metamorphism the Damara cover will become progressively denser. The mean density of granitic rocks is about 2,67 g. cm^{-3} (Johnson and Wenk 1974), so even before tectonism and metamorphism the Damara cover and the pre-Damara floor constituted a layered sequence with marked density contrast and with denser material over lighter.

The lowermost Damara, the Nosib Group, presents a slight complexity. The quartz-microcline dominant Etusis Formation is of granitic composition and hence of granitic density. The Khan Formation, however, is essentially calc-silicate material and would have a bulk density comparable to the metapelites. Mechanically the Nosib as a whole is "competent" and similar to the underlying basement.

A situation with denser material resting upon less dense material is gravitationally unstable. The unstable state is relieved by "spontaneous overturn" of the inverted density stratification (Ramberg 1967, 1968a, 1973; Fletcher 1972; Dixon 1975). The relief of instability takes the form of the development of small amplitude waves at the interface between the two media due to rise of the buoyant less dense layer. Several groups of waves will be established (Ramberg 1968, 1968a and 1968b) but a dominant wavelength based on layer thickness will produce bulges on the interface as the less dense material is forced upwards. The initiation of the dominant wavelength is dependent on the viscosity contrast, with the only condition that the overlying layer is not perfectly rigid. However, for rapid development and sustained rise, an optimum viscosity contrast is required.

Thus by establishing a model based on this principle it is possible to predict the spacing of the incipient waves developed on the interface, waves which could be established before any significant deformation and more important metamorphism.

5.1.3 Simple Model for Dome Initiation

If the Damara cover sequence above the Etusis Formation has a minimum thickness of 15 km and a bulk mean density of $\rho=2,76$ g. cm^{-3} (Johnson and Wenk 1974, Table II), and overlies a granitic basement (including the Etusis Formation) of mean density $\rho=2,67$ g. cm^{-3}, a two-layer model can be assumed in the initial case. The thickness of the pre-Damara is not known, but a minimum value can be set by halving the diameter of the largest dome—this gives about 4 km. In addition approximately 1 km is required for the Etusis Formation giving 5 km.

Within a crustal sequence it is noted that a discontinuity — the Conrad — separates granitic crust $\rho=2,67$ g. cm^{-3}, from dioritic to gabbroic material $\rho=3,1$ g. cm^{-3}. This boundary is concidered to be rigid and gravitationally stable with light material above more dense material. Although not always present as a marked discontinuity (change in seismic velocity of 6,0 km. s^{-1} to 6,5 km. s^{-1}) it has an average depth of about 20–25 km (Rast 1969).

In the non-orogenic case a two-layer model is not too unrealistic, but during an orogenic episode probably a four-layer model is required to describe all the density and viscosity variations expected. For the model chosen the upper surfaces of the top layer (Layer 1) will be assumed to be free since the thickness of the cover is large, compared to the basement thickness (15 km against 5 km). The model scheme is shown in Figure 5.2.

In Ramberg's consideration of the simple two-layer model (1968a, 1968b), growth of the instability at the Layer 1/Layer 2-interface has been calculated for various viscosity contrasts η_1/η_2. The wavelength of the dominant perturbation is dependent upon viscosity η, density ρ, layer thickness h, rate of change of amplitude and number of layers. For the above model, curves relating the various factors have been calculated by Ramberg (1968a, 1968b) and are shown in Figure 5.3. The maximum for each curve corresponds to the dominant wavelength.

The viscosity contrast between Layer 1 and Layer 2 (pelitic and granitic respectively) has to be estimated. Examination of the structures within the domes shows that the core rocks are relatively undeformed with most of the deformation being confined to small ductile shear zones. The marble and pelitic sequence above is strongly deformed. These factors indicate that the Layer 2-rocks are far more viscous than the cover rocks, i.e. $1>\eta_1/\eta_2>0$. This is in marked contrast to salt domes where the rising salt is both less dense and less viscous than the mantle rocks. Fletcher (1972) has suggested that the bulk viscosity of core gneisses may be up to 100 times that of the mantling rocks, so that η_1/η_2 is of the order 0,01.

For the calculation of the dominant wavelength forming on the Layer 1/Layer 2-interface, data can be obtained from Figures 5.3 where:

h_2 = thickness of Layer 2

λ = dominant wavelength

$\phi = \frac{2\pi h_2}{\lambda}$

v = vertical velocity component

y = amplitude

$q = \frac{(\rho_1-\rho_2)h_2 g}{2\eta_2}$

$k = \frac{v}{yq}$ = growth factor, i.e. time required to enlarge the original amplitude 100 times

thus for:

(a) $\eta_1/\eta_2=1$ $\phi=1,95$ and

(b) $\eta_1/\eta_2=0$ $\phi=2,49$

let $h_2=5$ km

$\lambda_a=16,1$ km and $\lambda_b=12,6$ km

The dominant wavelength range of 16,1 km to 12,6 km, depending on the viscosity contrast is in good agreement with the observed dome separations of 13,5 km (one very small dome with length of less than 2,5 km is ignored, as the remainder have a mean length of $6\pm2,5$ km).

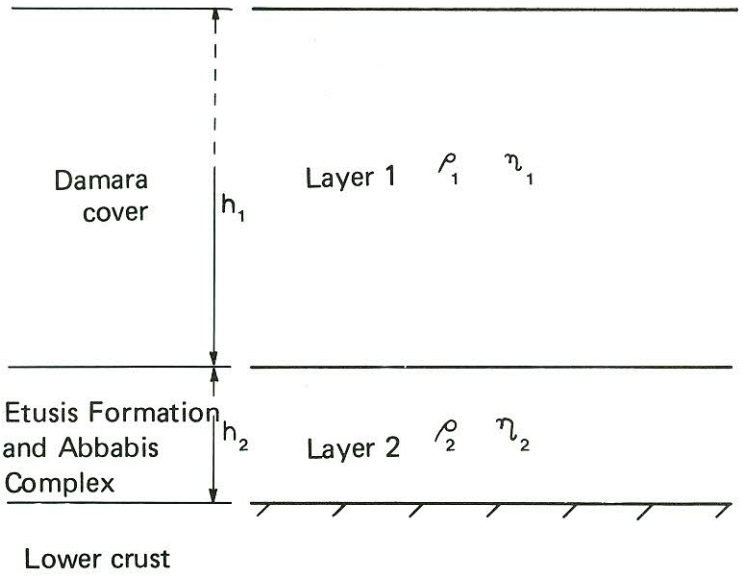

Fig. 5.2 – Simple two-layer model for Damara dome formation by diapirism. Base of layer 2 is rigid.
Eenvoudige tweelaagmodel om Damara-koepelvorming deur middel van diapirisme te verduidelik. Basis van laag 2 is star.

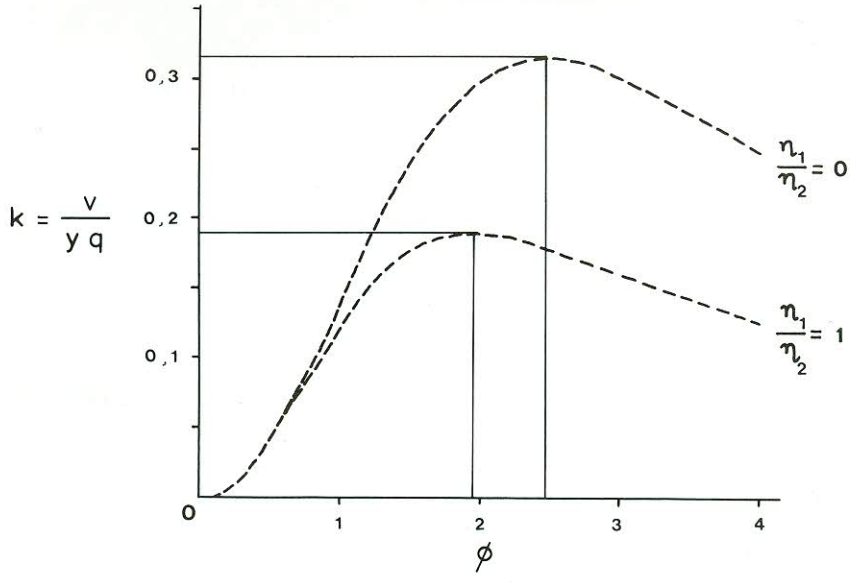

Fig. 5.3 – Growth factor k plotted against ϕ for a simple two-layer model (Fig. 5.2) with selected viscosity ratios η_1/η_2. Maxima show ϕ values of dominant perturbation (after Ramberg 1968b).
Groeifaktor k uitgestip teen ϕ vir 'n eenvoudige tweelaagmodel (Fig. 5.2) met geselekteerde viskositeit-verhoudings η_1/η_2. Maksima toon ϕ-waardes van dominante versteuring (volgens Ramberg 1968b).

The effect of making the granitic Layer 2 thicker, to say, 7 km, is to change the dominant wavelengths, thus

(a) $\eta_1/\eta_2=1$ $\lambda_a=22,5$ km

(b) $\eta_2/\eta_2=0$ $\lambda_b=17,7$ km

An expression derived by Ramberg (1968b) estimates the time taken for a 100 times amplification of the wave amplitude:

$$t=\frac{4,6}{kq}$$

for (a) $\eta_1/\eta_2=1$ $h_2=5$ km $t_a=70\times10^6$ y

(b) $\eta_1/\eta_2=0$ $h_2=5$ km $t_b=42\times10^6$ y

assuming $\eta_2=2,2\times10^{21}$ poise, and $\rho_1-\rho_2=0,1$ g. cm^{-3} the time for growth is longer than would occur in practice, since changes in density and viscosity within increasing temperature all tend to accelerate dome growth since η_2 would decrease and $\rho_1-\rho_2$ would increase.

These estimates are intended to establish the spacing between sites of potential dome formation. Establishment thereof could well have begun before metamorphism, although the Damaran metamorphic events would provide the impetus for rapid dome formation. Assumptions made in establishing the model are (i) Newtonian viscosity, (ii) small amplitude/wavelength ratio (sinusoidal), (iii) negligible internal forces, (iv) two-dimensional flow, and (v) orthogonal gravity-field symmetry (Ramberg 1968a).

5.1.4 Origin of the Damara Domes

Deposition of a thick sequence of largely metapelitic rocks upon a granitic pre-Damara basement, initiated a gravitational instability even before orogenic activity. The instability is relieved by flexing of the interface, taken as the top of the Etusis Formation, the perturbations being the site for future rapid diapiric dome rise, spaced between 12,6 km and 16,1 km. During ensuing Damara metamorphism the density contrast would increase as the metapelites progressively recrystallised and lost water whereas the viscosity of the granitic layer would tend to be lower although still higher than that of the cover rocks. These two factors would tend to accelerate dome rise at pre-established interface perturbations.

The irregularities in the pre-Damara—Damara interface would have had an effect on compaction of the overlying Damara sediments giving rise to incipient antiforms and potential sites of dome rise. However, by considering the Etusis Formation as mechanically part of the granitic Layer 2, large-scale irregularities will not be present. The effect of compaction over topography is merely to give a locus for later diapiric rise of granitic material.

The shape of many domes with overturned margins, or, as in the case of the Sopiehoogte Antiform, a flattened inclined cylindrical shape, is suggestive of diapir structures. Folding during F_4 and F_5 has affected the dome outcrop pattern, e.g. at Leeukop.

Dixon (1975) has studied the states of finite strain within diapir core and mantle rocks and finds distinct structural patterns to be expected at different erosion levels within an individual diapir. From this evidence it would appear that progressively lower levels are seen to the west.

Evidence suggesting a diapiric rather than interference fold origin are:

(a) initial gravity instability,

(b) dome spacing,

(c) dome rise during peak of metamorphism with granite generation (Section 7),

(d) dome shape and form,

(e) highly irregular pattern of associated synforms, which appear to be marginal synformal development as a result of intrusion through density inversion,

(f) lack of systematic lines of fold axes and large-scale interference pattern.*

Viscosity contrast structures are common in the central zone as a whole, with large-scale antiforms having a bulbous shape, but synforms generally tightly pinched.

5.2 F_2 FOLD DEVELOPMENT IN THE TROUGH ZONE

Tight to nearly isoclinal F_2 folds (of D_{T2}) are very common in the Trough Zone. These invariably have a strong axial-planar schistosity, S_2, which transposes bedding S_0. Hinges are defined by the intersection lineations S_0/S_2. In most cases the folds are observed by the folding of calc-silicate bands in a metapelitic matrix. There is probably a significant difference in viscosity between the calc-silicate bands and enclosing schists. Such a difference in relative viscosity appears to be a prerequisite for fold development and for similar folds in particular.

5.2.1 F_2 Fold Morphology

Figure 5.4 (A, B) shows the outline of two F_2 folds from the Trough Zone. It is noted that the dip isogons are mildly converging and that the layer thickness parallel to the axial plane does not vary greatly, a fact suggesting that the folds are of class 1C approaching class 2 (Ramsay 1967). By plotting t′ against angle of dip α (Hudleston 1973; Ramsay 1967) the various classes of folds are delineated. In addition the ratio of the principal quadratic elongation of superposed strain $\sqrt{\lambda_2/\lambda_1}$ can be determined. Figure 5.5A shows such a plot and the folds lie in the class 1C (Fig. 5.5B) field close to similar folds.

Transposition of bedding S_0 in the axial-planar schistosity is very common giving rise to cleavage mullions as shown in Figure 5.4C. Thin sections show the metapelites to have a very good fabric defined by biotite, muscovite and frequently by the elongation of quartz and feldspar. In the calc-silicate rocks, however, a planar fabric is not always developed, although many minerals are elongated in S_2. In the calc-silicates the fabric is sometimes mylonitic.

5.2.2 Similar Fold Development

The formation of similar folds is generally considered to result from the flattening of parallel buckle folds (Ramsay 1962, 1967; Dieterich 1970; Hudleston 1973, 1973a; Hudleston and Stephansson 1973; Parrish *et al.* 1976). Ramsay (1967, p. 415) notes that the effect of imposed homogeneous strain upon various fold classes, e.g. 1A, 1B and 1C, is to produce folds of class 1C morphology which approach class 2-type.

During the development of a fold, whilst still essentially concentric, an axial-planar cleavage develops, which will be refracted in layers of differing bulk viscosity. The cleavage forms essentially perpendicular to the maximum compressive strain σ_1, and will lie in the X–Y plane of the finite strain ellipsoid (Dieterich 1969; 1970; Ramsay 1967; Hudleston 1973, 1973a; Ramsay and Graham 1970). However, cases have been cited where the cleavage is oblique to the axial plane and the X–Y plane of the strain ellipsoid (Williams 1977).

* Personal communication: J. G. Ramsay.

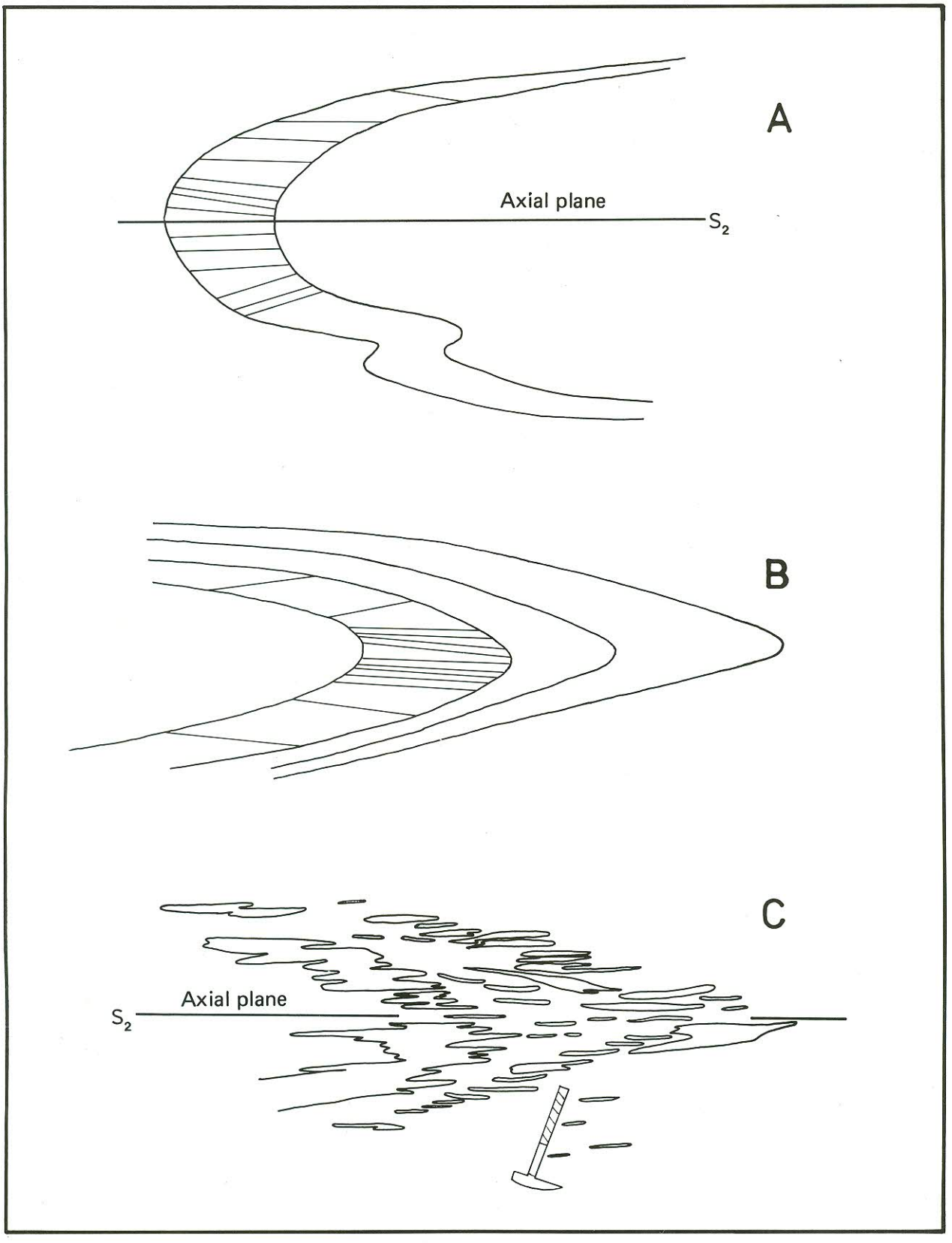

Fig. 5.4 – Trough Zone F_2 folds. A and B show dip isogons to the folded surface at 10° intervals. C shows calc-silicate bands in metapelite transposed into S_2 parallel cleavage mullions.
F_2-plooie van die Trogsone. A en B toon hellingisogone teen die plooi-oppervlak op intervalle van 10°. C dui kalksilikaatbande in metapeliet, getransponeer in S_2 parallelle splytroeistrukture, aan.

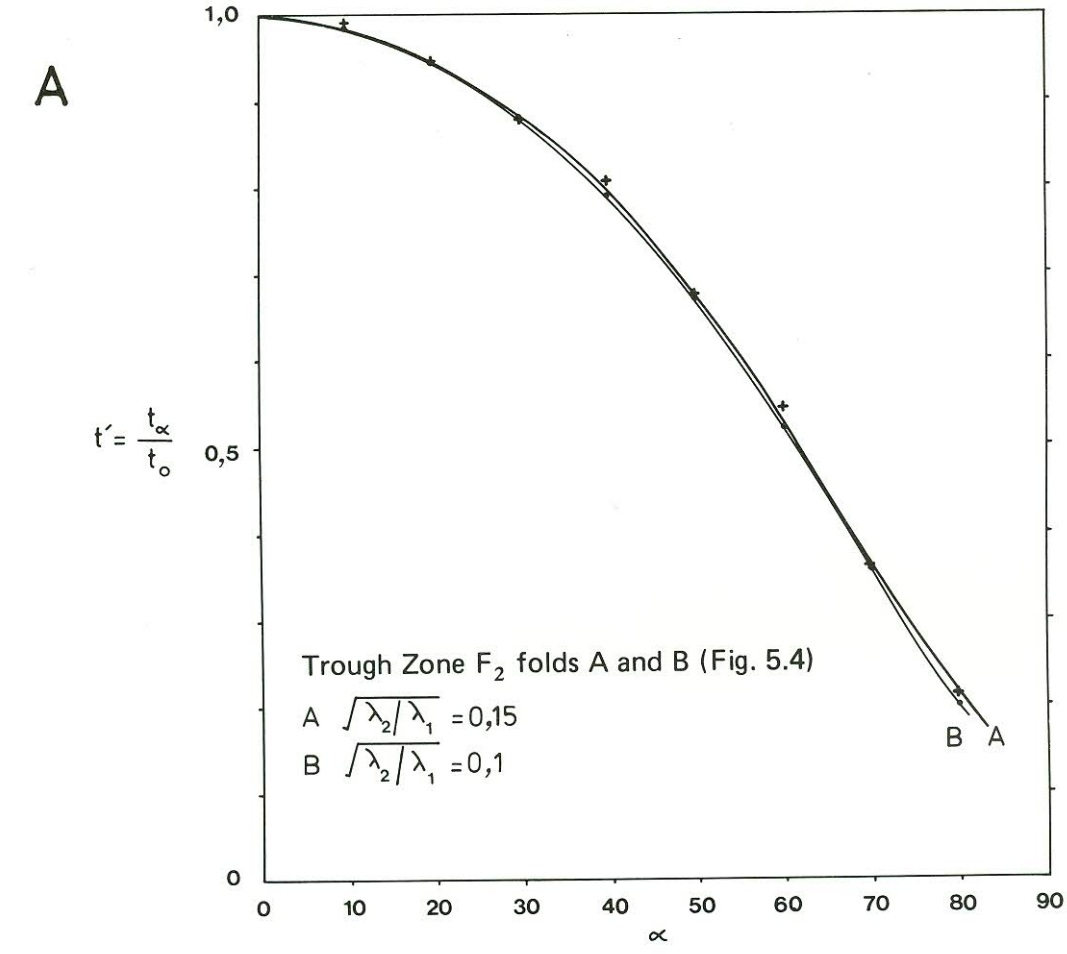

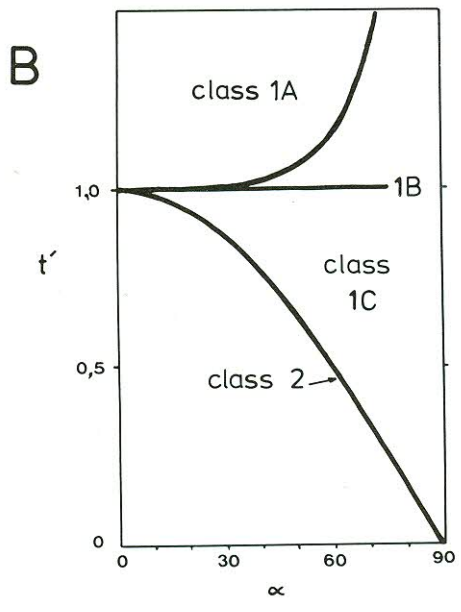

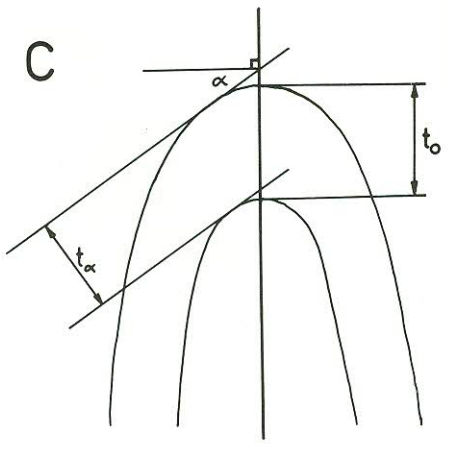

Fig. 5.5 – A: plot of t′ against α for Trough Zone F_2 folds shown in Figure 5.4;B and C define terms used in A and in the text (after Ramsay 1967).
A: uitstipping van t′ teen α vir F_2-plooie van die Trogsone aangetoon in Figuur 5.4;B en C definieer terme soos gebruik in A en in die teks (volgens Ramsay 1967).

As folds become tighter the cleavage tends to become parallel from initially being fanned (Dieterich 1969; 1970). Shearing or slip along cleavage planes is a well-known phenomenon (Ramsay 1967, Fig. 7–90) and can occur only after cleavage has formed; shearing along cleavage is a feature of late-stage fold development, the cleavage offering a mechanical anisotropy for relief of stress as the stress field changes in orientation (Dieterich 1969, 1970; Ramsay 1967; Schwerdtner 1973; Parrish *et al.* 1976).

Parrish *et al.* (1976) conducted a series of folding experiments with a wet quartzite band in a marble matrix with an initial viscosity contrast of 10 (i.e. $\eta_q/\eta_m=10$). Initial buckling produced concentric folds at 375 °C. With rising temperature and flattening of the folds, 'similar-type' geometries developed with a concomitant decrease in the viscosity contrast to as little as 0,6 especially on fold limbs (Parrish *et al.* 1976 Figs 9 and 10). They conclude that 'similar' folds can only develop when the viscosity contrast is reduced to 2 or less.

'Similar' folds produced by a process of shearing along discrete planes (slip folds) or by bulk movement (flow parallel to axial planes, i.e. flow folds) has often been cited (Whitten 1966; Ramsay 1967; Hobbs *et al.* 1976).

Whilst explaining the geometry of similar folds adequately, such processes present problems concerning the mechanical generation of the folds (Ramsay 1967). Production of similar folds by flow-folding and especially slip-folding is probable under certain conditions, although these processes may just be modifications to generally flattened buckle folds.

5.2.3 Formation of Trough Zone F_2 Folds

During D_{T1} a mineral banding was developed (S_1) which can now be seen sporadically as a biotite lamination. There is no evidence to suggest that the biotite formed during S_1 but the rocks were metamorphosed to greenschist facies at approximately 450 °C before or during early D_{T2} (Section 7 and Fig. 7.1). Thus before D_{T2} deformation commenced, the rocks would be crystalline and practically dewatered with the calc-silicate rocks having a higher bulk viscosity than the enclosing metapelites.

As F_2 folds developed, it is reasonable to assume that temperature was also rising since the peak of metamorphism is post-F_2 (porphyroblastic garnet, staurolite and kyanite enclose S_2). As deformation commenced, buckle folds of concentric geometry formed as the calc-silicate rocks are the more viscous. With increasing temperature and continued stress the viscosity contrast between metapelite and calc-silicate bands decreased allowing the folds to be flattened to near-similar geometry. Cleavage planes approach parallelism and an axial-planar cleavage in the X–Y plane of the strain ellipsoid is formed.

After formation of the schistosity planes perpendicular to σ_1, a plane of low-bulk viscosity existed in the rock, acting as a locus for late-stage shearing in the fold. Some cleavage planes remained 'active' long after F_2 folds had formed and post-dated the metamorphism (Section 7).

Thus the folds are seen as flattened buckle folds modified by late slip-fold processes.

5.2.4 F_3 Folds in the Okahandja Lineament Zone

F_3 folds of D_{L3} are rather frequent in the Okahandja Lineament Zone, both on a large and small scale. The folds have an appearance very similar to Trough Zone F_2 folds as described above. There is, however, a greater slip-fold component to the Lineament Zone folds, although the mode of origin is essentially similar to that of the Trough Zone. Figure 5.6A, B and C shows several typical fold profiles, and Figure 5.6D shows plots of t′ against α indicating the folds to be class 1C and class 2.

5.3 STRAIN DETERMINATIONS

5.3.1 Folds

By considering the folds of F_3 age in the Okahandja Lineament Zone and the F_2 folds of the Trough Zone to be flattened concentric folds (not necessarily of the same age) it becomes possible to estimate the degree of flattening. The method used is that of Ramsay (1962, 1967) and Hudleston (1973). It is assumed that the original folds had concentric profiles and that one of the principal directions of the three-dimensional strain ellipsoid is parallel to the fold axis. The latter assumption is reasonable since fold hinges parallel the stretching lineations defined by elongate variolites. The modification of the fold shape by a homogeneous flattening is a measure of $\sqrt{\lambda_2/\lambda_1}$ the ratio of the principal quadratic elongations of the superimposed strain.

From plots of t′ against α (terms defined in Fig. 5.5C) the class of fold (Ramsay 1967) can be determined as well as $\sqrt{\lambda_2/\lambda_1}$ (Table 5.1). Thus plots of t′ against α have been made for two Trough Zone F_2 folds (Figs 5.4A and B) and three Okahandja Lineament Zone F_3 folds (Figs 5.6A, B and C).

Table 5.1—RATIO $\sqrt{\lambda_2/\lambda_1}$ FOR TROUGH ZONE F_2 AND OKAHANDJA LINEAMENT ZONE F_3 FOLDS (FIGS 5.5A AND 5.6D)

Structural Zone	Fold	Class	$\sqrt{\lambda_2/\lambda_1}$
Trough	Fig. 5.4A	1C	0,15
	Fig. 5.4B+C	1C	0,10
Okahandja Lineament	Fig. 5.6A	1C	0,23
	Fig. 5.6B	1C	0,13
	Fig. 5.6C	2	—

5.3.2 Deformed Pebbles and Variolites

In the Trough Zone near Gorob, pillow structures can be seen in epidote-banded amphibole schists of the Matchless Member. In addition, outcrops show pillow outlines by variolite-bearing margins now observed as highly flattened spots. Both pillows and spots which have pressure shadows in thin section and are thus pre-tectonic, enable an estimate of strain to be made. Measurements from 20 pillows in epidote-banded amphibole schists were made near D in Figure 3.3, whilst 100 variolite measurements were made from oriented samples of spotted schists at F in Figure 3.3. For the variolites an initial spherical shape is assumed. Cuts parallel to the three principal axes of the strain ellipsoid were made. The measurements are shown in Table 5.2 after making Z=1. Orientation of the axes are also given.

Table 5.2—DEFORMED VARIOLITES AND PILLOWS NEAR GOROB (TROUGH ZONE)

	n	$\overline{X}$	$\overline{Y}$	$\overline{Z}$
Pillows (C – Fig. 3.3).	20	15	6	1
Orientation (S_2=330/35)		005/30	275/22	150/55
Variolites (F – Fig. 3.3)	100	19,1	5,8	1
Orientation (S_2=340/45)		355/45	260/10	150/45

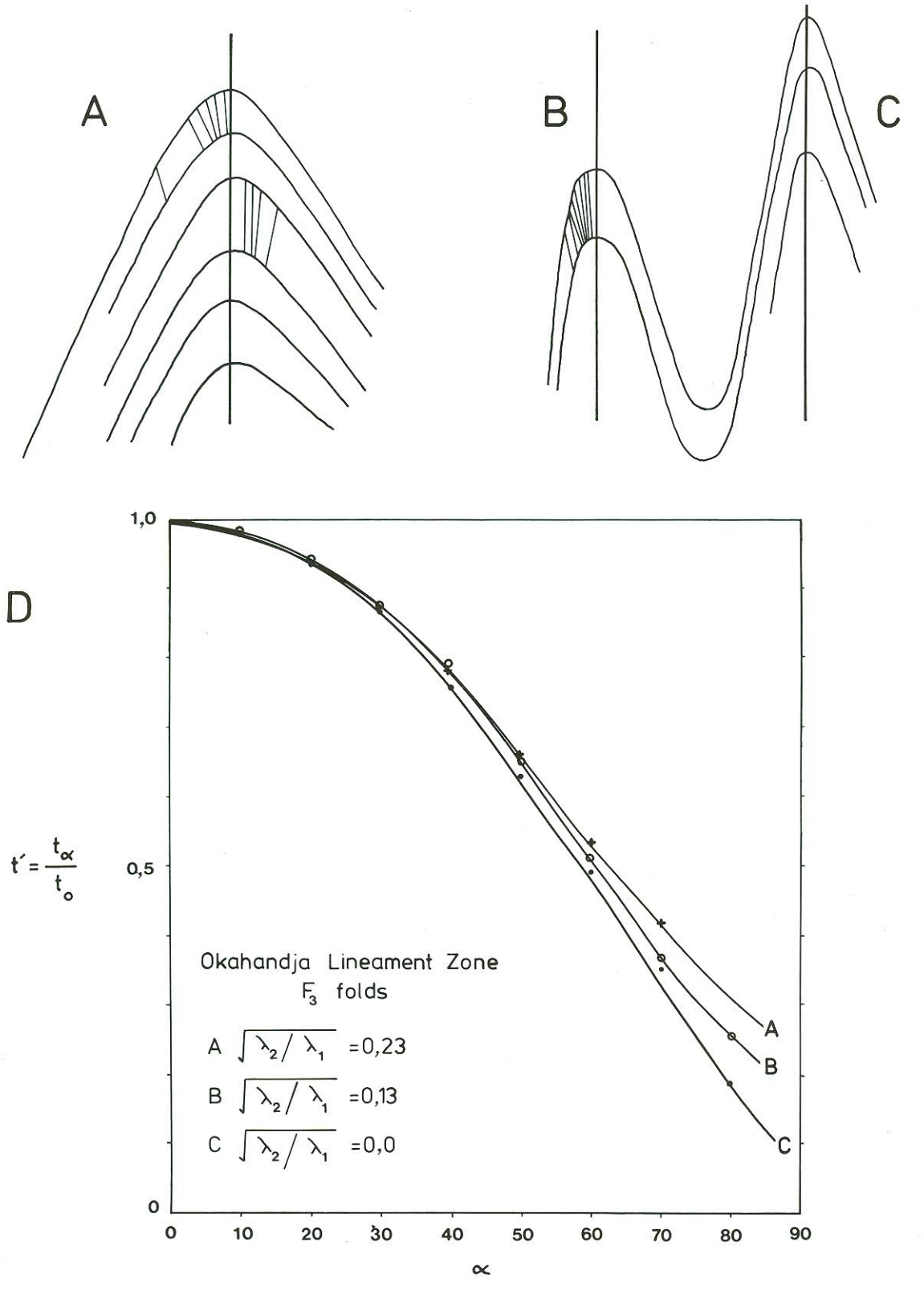

Fig. 5.6 — Sections of typical F_3 folds of the Okahandja Lineament Zone with dip isogons and plot of t′ against α for the sections.
Snitte van tipiese F_3-plooie van die Okahandja-lineamentsone met hellingisogone en uitstipping van t′ teenoor α vir die snitte.

Table 5.3—CLAST DEFORMATIONS AT THE EASTERN EDGE OF THE CENTRAL ZONE (SAMPLE LOCALITIES SHOWN IN FIG. 5.1)

Locality	n	$\overline{X}$	$\overline{Y}$	$\overline{Z}$	Formation/Group	Matrix
467	20	3,50	1,67	1,00	Khan	Calc-silicate
652	26	2,46	1,66	1,00	Etusis	Feldspathic quartzite
568	18	3,43	1,72	1,00	Etusis	Musc-bte-qtz-fsp schist
548	10	4,16	1,49	1,00	Nosib (undifferentiated)	Slightly micaceous quartzite
565	17	3,88	1,52	1,00	Chuos	Calc-silicate and quartzite

No rudaceous beds are developed in the Lineament Zone, although the eastern edge of the Central Zone contains many rudites and is deformed by Lineament Zone deformations since these possess a near-vertical planar fabric and have lineations parallel to those of the Lineament Zone further east. Figure 5.1 shows the locations where pebble measurements were made.

Measurements taken at each site include the long (X), intermediate (Y) and short (Z) axes. The orientations of X and where possible also the X–Y plane and together with clast type and matrix type were also noted. As far as possible only quartzite clasts were measured. The mean axial ratios for the quartzite clasts together with matrix type are shown in Table 5.3.

X, Y and Z are plotted on modified Flinn diagrams with axes $\log_e a$ and $\log_e b$, where $a=X/Y$ and $b=Y/Z$. Such a diagram is used since it allows the type of strain ellipsoid, deformation path (Ramsay 1967, p. 138) and volume change to be determined (Hobbs *et al.* 1976, p. 39). Also plotted is the line $K=1$ where $K=\frac{a-1}{b-1}$ which corresponds to no-volume-change plane strain. Below the line $K=1$ lies the field of flattened ellipsoids ($1>K>0$) whilst above $K=1$ are the constricted ellipsoids ($1<K<\infty$). Figure 5.7 shows modified Flinn diagrams for the measured clasts together with the orientation data for each locality cited in Table 5.3 above. The diagrams show the orientation of X, the orientation of the X–Y plane (shown as poles to flattening) and the orientation of S_0 bedding (as poles) where known. The poles to the X–Y plane define Z, thus with X and Z defined, Y can be found knowing X, Y and Z to be mutually perpendicular.

5.3.3 Strain Data: Conclusions

The degree of shortening of F_2 and F_3 folds is a minimum value since the degree of shortening, whilst still concentric, has not been allowed for and may amount to 36 per cent (De Sitter 1958).

The ratio $\sqrt{\lambda_2/\lambda_1}$ of 0,1 and 0,15 from F_2 folds of the Trough Zone agrees well with the value of 0,16 (Z/Y) determined from pillows and 0,17 from deformed variolites with the maximum elongation direction parallel to F_2 hinges (Z/Y) 0,05. The orientation of the strain ellipse from pillows and variolites is given in Table 5.2 above. The strain from flattened F_2 folds may be in error since movement along the cleavage planes is evident, although this may have occurred after fold formation. In addition, the variolites may not have been initially spherical and the pillows almost certainly were not of regular shape.

The $\sqrt{\lambda_2/\lambda_1}$ value of F_3 folds in the Okahandja Lineament Zone varies from 0,23 to 0,0, the latter reflecting class 2 folds. Change in the orientation of the strain ellipsoid during deformation is evident from the change in fold orientation from F_2 to F_4.

There is no direct evidence for large-scale vertical movements within the Okahandja Lineament Zone, and all elongations of clasts, fold hinges and lineations are subhorizontal. The cleavage and clast-flattening planes suggest that during the main deformation (D_{L3}), σ_1 was essentially horizontal, perpendicular to S_3 whilst σ_3 parallelled the clast elongations and fold hinges. Minor structural evidence suggests that sinistral, and, to a much lesser extent, dextral shear couples existed for the late movement (D_{L5}) on S_3. Whilst the possibility of moderate-scale lateral movement in the Okahandja Lineament cannot be discounted, there appears to be no single zone of intense shear movement apart from a thrust in OLZ/2 and its continuation southwards.

Clast deformation at the edge of the Central Zone shows that the intense vertical fabric of the Okahandja Lineament Zone (D_{L3}) affects the eastern edge of the Central Zone and is correlated with D_{C3}. Clasts, however, are far less deformed than the Okahandja Lineament Zone rocks as determined from the F_3 folds, although clasts are flattened parallel to S_3 i.e. parallel to F_3 axial planes in the Okahandja Lineament Zone (D_{L3}).

6. MINERAL ASSEMBLAGES

The three separate regional metamorphic zones have characteristic mineral assemblages, reflecting difference in P–T–X conditions and bulk chemistry. The aureole of the Donkerhuk Granite also has a distinctive appearance since the Kuiseb Formation pelitic schists show extensive migmatisation and recrystallisation.

Metapelites and calc-silicate rocks are common to all three regional metamorphic areas, thus more of these rock types are examined than metabasites or marbles. Mineral parageneses are given in order of increasing abundance (Winkler 1976, p. 326). Pre-Damara rocks are not included because of the possibility of pre-Damara metamorphism affecting present assemblages. Mineral assemblages are tabulated in Appendix II. The description that follows is intended to draw attention to the differences between characteristic assemblages in the three zones.

6.1 METAPELITES

The most common pelitic assemblage in the Trough Zone and the Okahandja Lineament Zone is muscovite-plagioclase-biotite-quartz, and in both zones probably comprises 75 per cent of all the pelites by volume. Occasionally small idioblastic garnets are also present.

In the Central Zone assemblages containing $\pm$sillimanite $\pm$ garnet $\pm$ cordierite-plagioclase-K feldspar-biotite-quartz are common. These rocks are generally not porphyroblastic. On rare occasions quartz and muscovite are found co-existing as primary minerals. Secondary muscovite is, however, common. A few metapelites are very dark in colour, being depleted in quartz, K feldspar and plagioclase, these minerals being removed in a melt

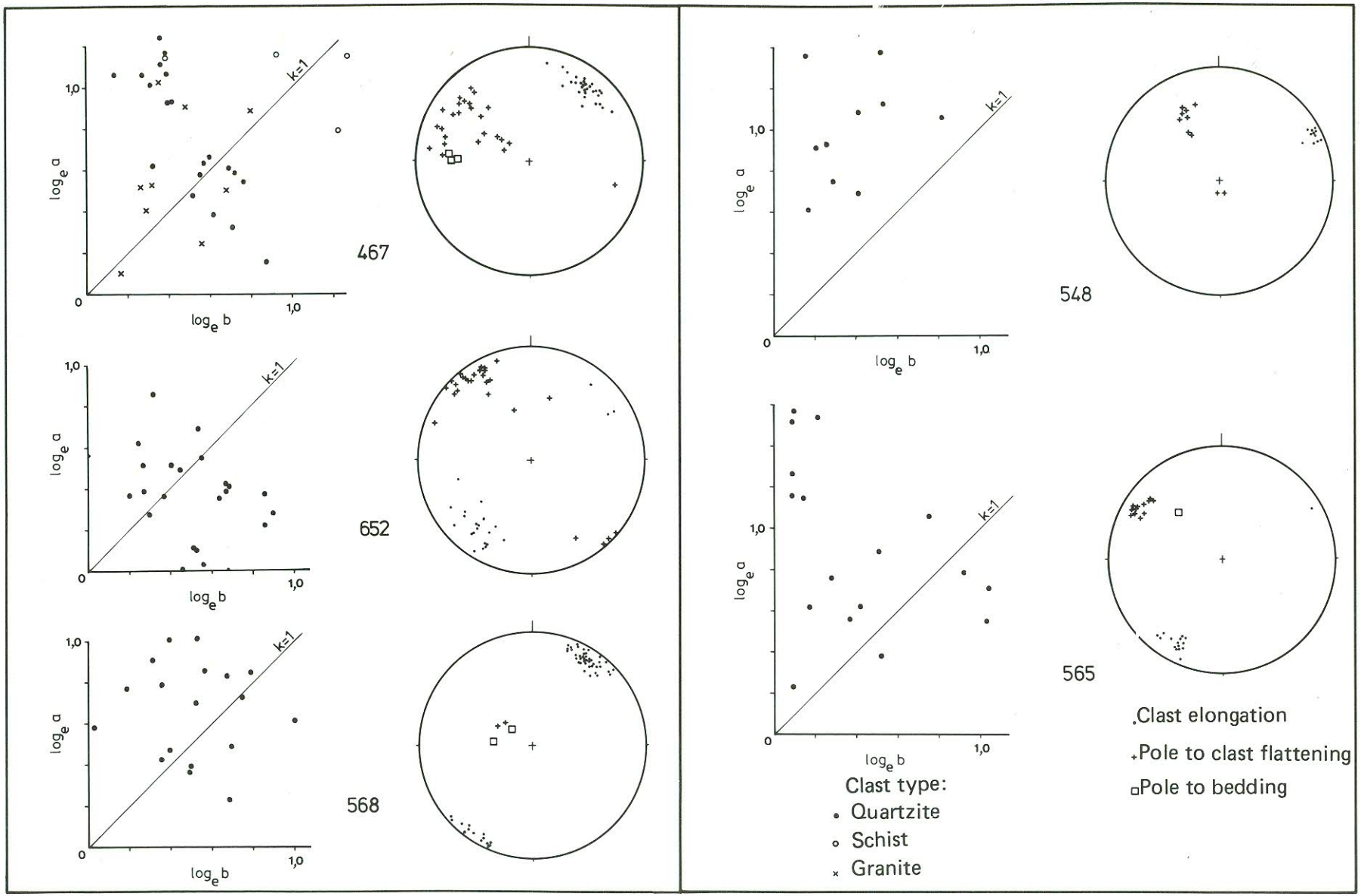

Fig. 5.7 – Clast deformation and orientation at the boundary between the Central Zone and the Okahandja Lineament Zone. Clast deformation is plotted on modified Flinn diagrams, whilst orientations are shown on stereograms.
Klastdeformasie en -oriëntasie op die grens tussen die Sentraalsone en die Okahandja-lineamentsone. Klastdeformasie is uitgestip op gemodifiseerde Flinn-diagramme terwyl oriëntasies op stereogramme aangedui word.

component during high-grade metamorphism. Quartzo-feldspathic leucosomes are often interlayered with cordierite-biotite melanosomes in migmatitic schists.

Diagnostic mineral assemblages of the Trough Zone and the Okahandja Lineament Zone are kyanite-garnet-staurolite-plagioclase-biotite-muscovite-quartz, and andalusite-cordierite-plagioclase-muscovite-biotite-quartz, respectively. Both these assemblages are found in the more aluminium-rich schists, actual mineral proportions depending on bulk rock chemistry and X_{H_2O}.

Fine-grained graphite-bearing schists are common in both the Trough Zone and the Okahandja Lineament Zone. The assemblage graphite-muscovite-biotite-plagioclase-quartz is common to both zones, but Trough Zone rocks often contain kyanite, staurolite and/or garnet in addition.

Calc-pelites in the Tinkas Member contain the assemblages ± K feldspar-white mica-chlorite-plagioclase-biotite (phlogopite)-quartz.

Small idioblastic crystals of tourmaline are present in many pelites from all three zones. Common accessory minerals are apatite, zircon and opaque ore.

6.2 CALC-SILICATE ROCKS

Calc-silicate rocks present a wide variety of mineral assemblages commonly with eight or more mineral species present. However, quartz and plagioclase (generally andesine or labradorite) are present in virtually all samples, and frequently comprise large portions of the rock by volume.

Thin calc-silicate bands commonly form cleavage mullions in the Okahandja Lineament Zone and the Trough Zone. Those of the former are commonly blue-green in colour, having the assemblage ± calcite ± garnet ± biotite-epidote and/or clinozoisite-hornblende (blue-green)-plagioclase-quartz. Thicker bands (over 150 mm wide) are commonly zoned having light-green cores containing the assemblage garnet-diopside-calcite-plagioclase-quartz. From core to margin, diopside is progressively replaced by hornblende, whilst calcite and plagioclase are replaced by epidote/clinozoisite. Garnet may or may not persist from core to margin. The calc-silicate bands of the Trough Zone are less commonly zoned and contain the assemblage ± chlorite ± biotite-calcite-hornblende-garnet-plagioclase-quartz with occasional colourless amphibole rims to hornblende.

Thicker (up to 5 m) bands of fine-grained, pale-green calc-silicate rocks in the Tinkas Member have the assemblage ± epidote-tremolite-diopside-carbonate-plagioclase-quartz, with tremolite replacing diopside. Thick (over 10 m) bands in the Trough Zone with the assemblage epidote-clinozoisite-carbonate-hornblende-diopside/hedenbergite-biotite-plagioclase-quartz are of glassy appearance and resemble the calc-silicate bands in the Chuos Formation of the Central Zone.

Massive calc-silicate rocks of the Khan Formation, like the Etusis Formation rocks (see Section 6.5), often contain high proportions (up to 60 per cent) of microcline which is probably of detrital origin. Typical assemblages are ± scapolite ± chlorite-epidote/clinozoisite-hornblende-diopside/hedenbergite-microcline-plagioclase-quartz. Biotite, garnet, tremolite and wollastonite may also be present.

Garnets of the Trough Zone and Okahandja Lineament Zone are pink in hand specimen and colourless in thin section whereas those of the Central Zone are brownish and strongly honey coloured in thin section. Furthermore, epidote in contact with Central Zone garnets is distinctly pleochroic and contains up to 24 per cent pistacite. The garnet thus may have a high andradite component. Epidotes from the other zones are generally weakly pleochroic.

Scapolite (mizzonite) is fairly abundant in the Central Zone, but rare in both the other zones, and commonly intergrown with plagioclase in a myrmekite-like manner.

In virtually all cases (except cores of zoned Okahandja Lineament Zone rocks) diopside is replaced by tremolite at its margins. Fe content varies considerably from rock to rock within the calc-silicates, and is reflected in the wide range of pleochroic schemes of clinopyroxene (diopside/hedenbergite) and amphibole (tremolite/actinolite).

Sphene, often rimming ilmenite, is a common accessory. Chlorite is usually secondary.

6.3 MARBLES

Marbles of the Okahandja Lineament Zone are principally carbonate (usually calcite) with minor (less than 5 per cent) quartz, talc, phlogopite, plagioclase and microcline. In contrast, the Karibib marble of the Central Zone shows considerable variation from calc-silicate to pure calcite and pure dolomite-types. A common and distinctive assemblage is ± chondrodite/clinohumite-antigorite-forsterite-dolomite-calcite. Dolomite exsolution-textures from high Mg-calcite are common. Other minerals occurring are tremolite, phlogopite, talc, garnet and sulphide.

Late, possibly post-Damara, siliceous alteration affects marbles in the Central Zone, notably near Hamilton Beacon.

6.4 METABASITES

Metabasites are only of significance in the Trough Zone. Assemblages are listed by fabric type in Appendix II.

Blue-green hornblende is abundant in all types whilst clinopyroxene (diopside or augite) occurs infrequently but is intergrown with hornblende in metagabbro types. Epidote-rich bands with minor amounts of pink calcite are frequent and in some cases have the form of closed loops, albeit very elongated. The epidote bands resulted from Ca metasomatism (analogous to Na metasomatism in spilites) of the material interstitial to pillows. Deformed variolites at some pillow margins consist of plagioclase and quartz with minor hornblende. Small (up to 7 mm) quartz-plagioclase knots of metamorphic origin (lacking pressure shadows) are also present.

The gradation from amphibole schist to metagabbro is accompanied by a progressive decrease in epidote and quartz content whilst plagioclase content rises. Relict ophitic textures are seen in some metagabbros between hornblende and plagioclase.

6.5 FELDSPATHIC QUARTZITES

Feldspathic quartzites of the Etusis Formation may contain up to 80 per cent microcline; typical assemblages are ± biotite ± muscovite ± sillimanite-microcline-quartz. Plagioclase is generally rare.

6.6 DONKERHUK GRANITE AUREOLE

In the Trough Zone rocks, sillimanite is developed at the expense of muscovite and perhaps staurolite. In some cases cordierite appears to replace staurolite and some samples contain four or five AFM phases, indicating relict minerals from the regional metamorphic assemblage.

Within the Okahandja Lineament Zone, andalusite and cordierite have formed close to the granite, in both zones partial melting of pelites took place very close to the granite, whilst growth of randomly oriented muscovite flakes has occurred for some considerable distance from the granite body.

7. RELATIONSHIP BETWEEN MINERALS AND FABRIC ELEMENTS AND TEXTURE

When discussing the relationship between metamorphic minerals and the fabric it must be borne in mind that the minerals are components of an assemblage and ought not to be thought of as separate entities. Thus, although garnet porphyroblasts overgrow biotite parallel to S_2 in the Trough Zone, it is most likely that the biotite has progressively changed its composition and/or perhaps recrystallised mimetically in S_2, thus remaining in equilibrium with the garnet (Vernon 1977). An important point to consider from fabric-mineral relationships is the effect of early fabrics upon later mineral growth. Over most of the area mapped an early fabric (e.g. S_1 of the Central Zone) is present and gives rise to a marked chemical anisotropy in the rock which may persist through subsequent events. The anisotropy once established may force later minerals to grow mimetically in this pre-existing mechanical and chemical anisotropy (Spry 1969, p. 9, 194 and 218; Etheridge and Hobbs 1973; Ferguson and Harte 1975, p. 469; Vernon 1976) complicating the metamorphic-structural relationships.

Similarly, the sequence of metamorphic crystallisation cannot be unambiguously determined, although the sequence of completion of growth is more readily discerned. Taking another example, some staurolite porphyroblasts of the Trough Zone enclose idioblastic garnets, indicating that staurolite finished growth after garnet. Nothing is, however, known about the sequence of the nucleation.

If mineral growth is considered to take place in sequential episodes, one species at a time, it is frequently necessary to invoke metasomatic introduction or removal of material for crystallisation of the final phase (e.g. Rast 1958). Consideration of the metamorphic assemblage as a whole generally obviates the need to invoke metasomatism.

Relationships between mineral species and fabric elements are given in Appendix II; the important conclusions are summarised below.

7.1 TROUGH ZONE

A locally penetrative planar fabric S_1 takes the form of biotite laminae 10 to 20 mm apart and could be a pressure-solution cleavage. No significant degree of metamorphism appears to accompany S_1.

The main regional schistosity S_2 is characterised by a strong-preferred orientation of prismatic and platy minerals. Much of this mineral alignment is the result of mimetic recrystallisation after D_{T2}. At one locality, however, clear evidence is available for the sequence of events. At D in Figure 3.3 kyanite and staurolite are rotated by up to 90° and cleaved along S_2 indicating these to be syn-S_2 mineral growths (Fig. 7.1A). A later S_3 crenulation cleavage further deforms these crystals, but a later growth of both staurolite and kyanite (and probably biotite also) post-dates the S_3 fabric. The syn-S_2 staurolites contain biotite crystals defining the internal fabric; thus some biotite is either pre- or syn-S_2 in age. Therefore not all biotite can post-date S_2 and grow mimetically in S_2 planes (Hoffer 1975, considers biotite growth to be entirely post-S_2). A few hundred metres further north a strong S_2-planar fabric in Matchless Member rocks is defined by oriented hornblende crystals, some of which are polygonised by S_3 crenulations. Here, also, a randomly oriented mineral growth (ortho-amphibole) post-dates S_3.

Further east garnets and staurolite crystals helicitically enclose straight inclusion trails of quartz and plagioclase elongated in S_2. In other instances garnets growing in S_3 planes helicitically enclose S_2. In the Hudaub area (Fig. 7.1B) a garnet showing about 90° discordance of included S_1 (?) fabric is probably pre-S_2; however, most of the garnet, kyanite and staurolite also helicitically enclose a fabric (S_2) but are slightly deformed, probably by a weak flattening of the S_2 fabric.

Calc-silicate rocks show garnet porphyroblasts enclosing the mylonitic cleavage but are themselves not deformed. Amphiboles also grow randomly across the S_2 fabric.

Thus, for the Trough Zone, S_1 may have developed through pressure solution during low-grade, but waxing metamorphism. The first metamorphic event reached its peak during S_2 and gave rise to the very strong regional fabric during intense deformation. The work of Parrish *et al.* (1976) shows that medium- to high-grade metamorphism is conducive to the formation of similar style folds, e.g. F_2 structures. Locally kyanite and staurolite assemblages were developed. A second metamorphic peak occurred post-dating D_{T2} and D_{T3}, this event giving rise to the widespread biotite-muscovite-staurolite-garnet-kyanite-bearing assemblages of garbenschiefer appearance. In this scheme the muscovite felt-mat fabric may belong to the first event and a plagioclase fabric representing the second event.

During cooling chlorite formed at the expense of biotite, garnet and rarely staurolite. The conditions of the second thermal event are considered in Section 8.

7.2 OKAHANDJA LINEAMENT ZONE

In this zone mimetic growth of minerals and a late reactivation of S_3 planes during D_{L5} cause difficulty. An early schistose fabric S_1 may be the result of pressure solution processes or may in part represent banding of metamorphic origin.

Evidence clearly indicates two metamorphic events separated by an intense deformational event. It is unlikely that the metamorphic (thermal) events are entirely separate. They actually represent two peaks of a broad thermal episode. Similar folds formed during D_{L3} indicating a "hot rock" deformation (Section 5). In an example of a massive schist which has not undergone reactivation of S_3 planes, cordierite porphyroblasts enclose an earlier fabric (S_f) at a high angle to S_3. In addition, S_3 schistosity planes wrap around the cordierite porphyroblasts, which show no sign of rotation. A banding or irregular spacing (S_0?) is also present within the rock and is also helicitically included by the cordierite, passing straight through the porphyroblast with no rotation or disruption (hence no D_{L5} rotations – Fig. 7.1C). Thus there is clear evidence of a cordierite growth post-dating S_f but pre-dating S_3 in aluminous schists.

Elsewhere pre-existing cordierite porphyroblasts are flattened into S_3 with the S_3 schistosity planes wrapping around the porphyroblasts, and subsequently being deformed during D_{L5}.

The intense deformation of D_{L3} gives rise to a pervasive schistosity. In most metapelitic rocks the biotite and muscovite fabrics are essentially parallel. In such pelites it is common for cordierite porphyroblasts to be elongated parallel to S_3 and enclose S_3 helicitically as straight

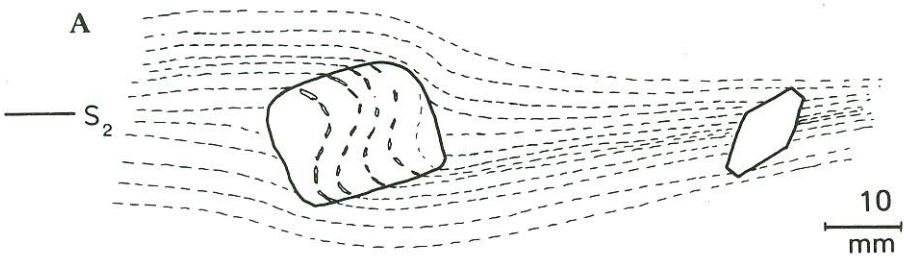

Syn-S_2 staurolite poikiloblast with curved inclusion trains of biotite (left) and post-S_2 staurolite (right) (TZ/2)

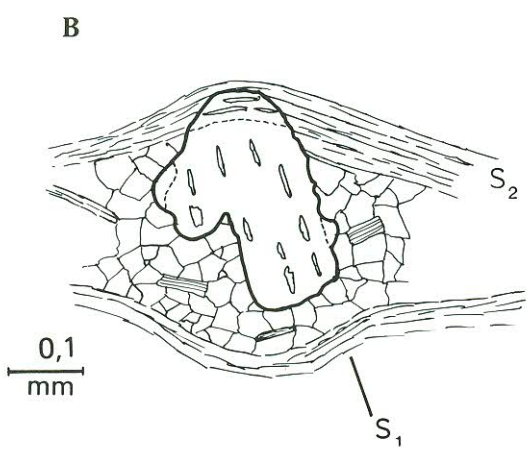

Pre-S_2 garnet enclosing S_1 fabric with post-S_2 overgrowths (TZ/2)

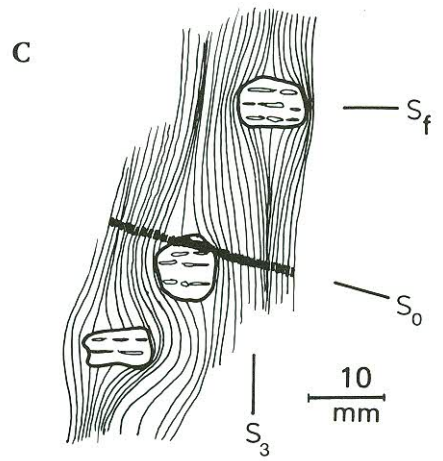

Pre-S_3 cordierite poikiloblasts enclosing the S_f fabric (OLZ/2)

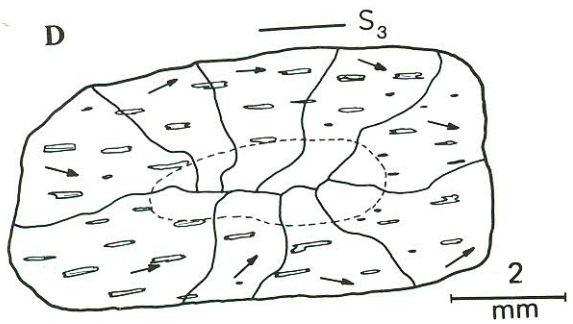

Andalusite poikiloblast with inclusion-free core. Arrows show extinction directions of subgrains (OLZ/3)

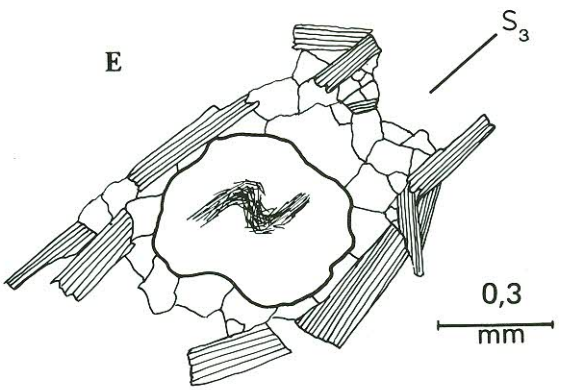

Sillimanite inclusions in cordierite outlining micro-crenulations (CZ/2)

Fig. 7.1 — Mineral-fabric relationships.
Mineraalmaakselverhoudings.

inclusion trails. There are often biotite-rich rims around such porphyroblasts (including andalusite), possibly the result of slow porphyroblast growth being able to remove other reaction products from the site of the growing crystal (Spry 1969). Andalusite porphyroblasts are often ramdomly oriented across S_3, although mimetic growth in S_3 chemical anisotropy is common. In a few cases both cordierite and andalusite have sigmoidally curved inclusion trails suggesting a late S_3 age.

In one example from fairly close to the Donkerhuk Granite, yet showing no outward signs of textural change, andalusite poikiloblasts grow across S_3 and exhibit an unusual texture. The poikiloblast margins contain abundant S_3-parallel inclusions whilst the cores are devoid of inclusions. The optical pattern bears little relationship to the poikiloblast outline being made up of large subgrains as much as 45° out of optical coincidence. Individual subgrains contain both an inclusion-free and inclusion-bearing part of the poikiloblast (Fig. 7.1D). The origin for this texture may be:

(a) Regional metamorphic growth of an inclusion-free core followed by overgrowth of thermal andalusite due to intrusion of the Donkerhuk Granite followed in turn by subsequent granulation by movement in the Okahandja Lineament Zone, or

(b) slow growth of a clear core followed by rapid spongy growth of the outer part during regional metamorphism, subsequent deformation and/or recrystallisation giving rise to the present texture.

Aluminium-rich schists, however, show the metamorphic history rather more clearly. Muscovites lie parallel to S_3, yet biotites are often oriented at various angles to S_3 (at a consistent angle on outcrop scale) forming the S_f fabric (see OLZ/2, Sections 3 and 4). Both cordierite and andalusite porphyroblasts enclose the S_f fabric helicitically. In many cases the porphyroblasts are markedly tabular, being confined to the aluminous layers. Rarely, small idioblastic staurolite porphyroblasts grow randomly across S_3 and S_f. At the very western edge of the Okahandja Lineament Zone sillimanite has developed from quartz and muscovite in Chuos Formation rocks. Thus sillimanite forms radiating knots parallel to S_3 planes since that is the plane containing the reactant minerals.

Some calc-silicate rocks show a mylonitic compositional layering (Vernon 1974) which is helicitically enclosed in garnet and randomly overgrown by amphibole. The majority of calc-silicate rocks do not show this mylonitic layering at all, although these are commonly zoned, containing cores of oriented diopside showing peripheral alteration to amphibole. This apparently retrograde texture is discussed in Section 8. The randomly oriented amphibole is ubiquitous among the calc-silicate rocks.

The Okahandja Lineament Zone textures are thus best explained by a thermal event, possibly during D_{L2} and a second, very late event, essentially post-D_{L3}.

Conditions of the second metamorphism are discussed in Section 8.

7.3 CENTRAL ZONE

Sillimanite crystals defining microfolds are occasionally observed in the cores of cordierite crystals. The cordierite appears to post-date D_{C3} and is rarely associated with garnet porphyroblasts growing across the schistose S_1 and S_3 fabrics. As the cordierite post-dates D_{C3}, the sillimanite evidently must pre-date at least D_{C3}.

Elsewhere (e.g. CZ/1 near Chungochoabberg) sillimanite porphyroblasts growing in the S_1 layering are flattened together with most of the S_1 biotites and reoriented into the F_3 axial-planar cleavage (S_3). In most cases where the sillimanite knots are not highly flattened the S_3 fabric tends to wrap around the porphyroblasts, a few of which have pressure shadows. This suggests that sillimanite growth occurred prior to F_3 folding and flattening.

The schistosity in rocks of the Kuiseb Formation cropping out just north of Rooibank represents S_1 modified into parallelism with S_3 on the flanks of F_3 folds. The microclines of a sample taken from such an F_3 flank contain the S_1 fabric as biotite inclusion trains, but are wrapped around by the S_3 schistosity. The inclusion fabric is subparallel to the external one, although occasional crystals show up to 40° discordance.

The Rooibank area shows further clear evidence of a metamorphic event, either late or post-dating D_{C3}. Garnet porphyroblasts grow across both S_1 and S_3 and commonly are associated with undeformed quartzo-feldspathic veinlets. Cordierites from the same area do not appear to contain S_1 inclusions and commonly grow mimetically along S_1 and S_3. In some cases equant, roundish cordierite crystals grow across the mica fabric. Small randomly oriented quartz veins are strongly shortened, indicating a constrictional deformation with the long axis of the strain ellipsoid approximately vertical, this occurring late- to just post-F_3.

Further east in the Central Zone, quartzo-feldspathic leucosomes intrude along S_3 planes, and in one case a pegmatite is slightly folded during final flattening of an F_3 fold. In addition, both garnet and cordierite grow across the S_3 fabric, which in several cases has been almost totally destroyed. In situ partial melting, giving rise to red homogeneous granite which intrudes F_3 structures but itself lacks any fabric, also suggests a strong post-F_3 thermal event which produced the diapiric structures of the area.

Within calc-silicate rocks, amphibole formed at the expense of diopside, and wollastonite developed with random orientation at calcite-quartz contacts. These factors may indicate changes in fluid-phase composition (Section 8).

Thus the Central Zone is characterised by a sillimanite-producing event during D_{C2} and a garnet-cordierite grade thermal event which largely outlasted D_{C3}.

7.4 DONKERHUK GRANITE AUREOLE

The general effect of the intrusion of Donkerhuk Granite upon regionally metamorphosed schists is to induce the random growth of large muscovite poikiloblasts across the schistose fabric. Approaching the granite the schists become progressively coarser grained due largely to mimetic recrystallisation of the biotite parallel to the regional schistosity. Still closer to the granite partial melting gives rise to migmatites and lit-par-lit injection of granitic material.

Most of the mineralogical changes occur where coarsening of grain size or migmatite development has taken place. The pre-existing fabric has exercised a strong influence on the orientation of newly formed minerals. Thus sillimanite on the eastern and southern boundaries forms parallel to the S_2 fabric (D_{T2}) since the reactants necessary for sillimanite formation lie in S_2. Along the western edge new growth of andalusite and cordierite has occurred with the former frequently growing in and helicitically enclosing crenulated S_3 (D_{L3}) schistosity, the crenulation cleavage apparently being caused by granite emplacement.

Early Donkerhuk pegmatites are deformed by D_{L5}.

The Donkerhuk Granite is undeformed and shows clearly cross-cutting contacts with country-rock fabrics. The existence of a large thermal aureole is confirmed by the presence of sillimanite on the eastern side, and post-regional-fabric andalusite along the western margin. The time of intrusion post-dates Trough Zone regional tectonism but is clearly synchronous with the very final stages of significant tectonism in the Okahandja Lineament Zone.

7.5 PRE-DAMARA ROCKS OF THE CENTRAL ZONE

Large-scale mineralogical and fabric evidence strongly suggests at least one high-grade pre-Damaran metamorphic event.

In pre-Damara outcrops a strong foliation can be seen in pelites and gneisses. This foliation tends to strike in an east–west direction away from contacts with the overlying Damara cover. As the Damara–pre-Damara contact is approached the pre-Damara foliation is generally reoriented into near parallelism with the Damara trend. Close to contacts a Damara foliation is impressed upon the pre-Damara rocks, often showing two gneissic fabrics at 5–10° and giving rise to a lineation and rarely a pencil-gneiss fabric. Thus a very coarse-grained gneissic fabric was in existence in pre-Damara rocks before the Damara metamorphism and deformation.

8. CONDITIONS OF METAMORPHISM

Mineral assemblages in the three main structural-metamorphic zones enable some constraints to be placed upon the conditions of metamorphism within the respective areas. In all cases the last metamorphic event (M_2), i.e. largely post-deformational, is investigated. When considering the conditions of metamorphism an attempt at assessing X_{H_2O} and changes in fluid-phase composition is also made.

Both pelitic and calc-silicate rocks offer assemblages and mineral reactions from which the various parameters may be determined. However, only the pelitic rocks were investigated by microprobe analysis and thermodynamic considerations. In some cases the parameters P and T derived from pelites are used to augment data derived from calc-silicates. In applying thermodynamics to mineral reactions and assemblages the following assumptions are made:

(1) The minerals in contact or in small domains are in equilibrium with each other unless disequilibrium textures (Zen 1963) are present;

(2) the present composition of the minerals concerned is the same as that attained at the peak of metamorphism;

(3) volume change of reaction, $\triangle V°$, is *not* a function of pressure and temperature over the range of interest;

(4) any fluid phase present is assumed to be an ideal mixture;

(5) minerals are ideal solid solutions (i.e. ideal on-site mixing is assumed) except for Reaction I where allowance has been made for non-ideality of the solid solutions; and

(6) errors in $\triangle H°$, $\triangle S°$ and $\triangle V°$ are considered in calculating reaction curves, but errors in microprobe analysis are not considered.

Mineral margins were analysed since these can be assumed to have been in equilibrium with adjacent minerals and the fluid phase, bearing in mind that at least two metamorphic events have occurred over the area. Mineral-core analyses are not used in the thermodynamic considerations below. Calculation was made on the basis of mean values for the composition of each mineral species of interest in each rock and not by individual mineral pairs (e.g. if five garnet-cordierite pairs were analysed in a rock, then the mean garnet and mean cordierite compositions were used). Thermodynamic data has been extracted either from published data using the method of Weisbrod (1968), or from unpublished data.*

8.1 TROUGH ZONE

8.1.1 Introduction

No chlorite or chloritoid was observed in any of the rocks other than as minor retrograde alteration of biotite, garnet or rarely staurolite. In addition, kyanite is present in rocks over the whole area examined. Furthermore, there is no evidence of partial melting in any of the rocks. These three field observations are combined to provide a lower and upper temperature and a lower pressure estimate. Figure 8.2 shows the field delineated by the observations. The breakdown of chlorite and chloritoid is from the investigations of Richardson (1968), Hoschek (1969) and Ganguly (1972). The beginning of partial melting is taken from Winkler (1976), and the aluminium-silicate triple point from Richardson *et al.* (1969). The various determinations of the Al_2SiO_5 triple point are shown in Vernon (1976, Figure 4–3).

In order to define the metamorphic conditions further, three pelitic schists (EWS 115, 235 and 316) have been investigated (see Figure 8.1 for localities). All three rocks contain the assemblage:

Quartz + kyanite + staurolite + garnet + plagioclase + muscovite + biotite, which in equilibrium with fluid represents eight phases. The assemblage may be described by the seven components:

$(K,Na)_2O$, CaO, (Fe,Mn)O, MgO, Al_2O_3, SiO_2, H_2O

Thus by application of the phase rule the assemblage has a variance of one, i.e. it is isobaric invariant. If one phase (plagioclase) and one component (CaO) are temporarily removed from consideration, the variance remains as one, but the phases can now be linked by the reaction:

$$\text{Staurolite} + \text{muscovite} + \text{quartz} \rightleftharpoons \text{garnet} + \text{biotite} + \text{kyanite} + H_2O$$

Since staurolite has an Fe/Mg ratio intermediate between garnet and biotite (Carmichael 1970; Thompson 1976) the reaction is discontinuous (Thompson 1976) and as such ought to define an isograd. However, the assemblage occurs widely in the Trough Zone. This may be explained by several factors:

(1) If the fluid were not pure H_2O, and H_2O not perfectly mobile, then the equilibrium assemblage may buffer the fluid composition (Greenwood 1975; Vernon 1976), allowing the full-phase assemblage to occur over a wide but undefined range of temperature.

(2) The effect of extra components: the garnets in all three samples contain significant amounts of Mn and Ca. The effect of Mn on the Mg-Fe discontinuous reaction above would be to make it an Mn-Fe-Mg continuous reaction, and therefore present over a range of temperature (Thompson 1976; Tracy *et al.* 1976). Ca may affect the stability of the assemblage through garnet-plagioclase continuous reactions (Tracy *et al.* 1976).

Of the five continuous reactions (Thompson 1976) which can be written between minerals in the above assemblage the following Fe end-member equilibria are important:

Fe staurolite + quartz $\rightleftharpoons$ almandine + kyanite + H_2O;
almandine + muscovite $\rightleftharpoons$ annite + 2 kyanite + quartz

* Personal communication: D. Waters.

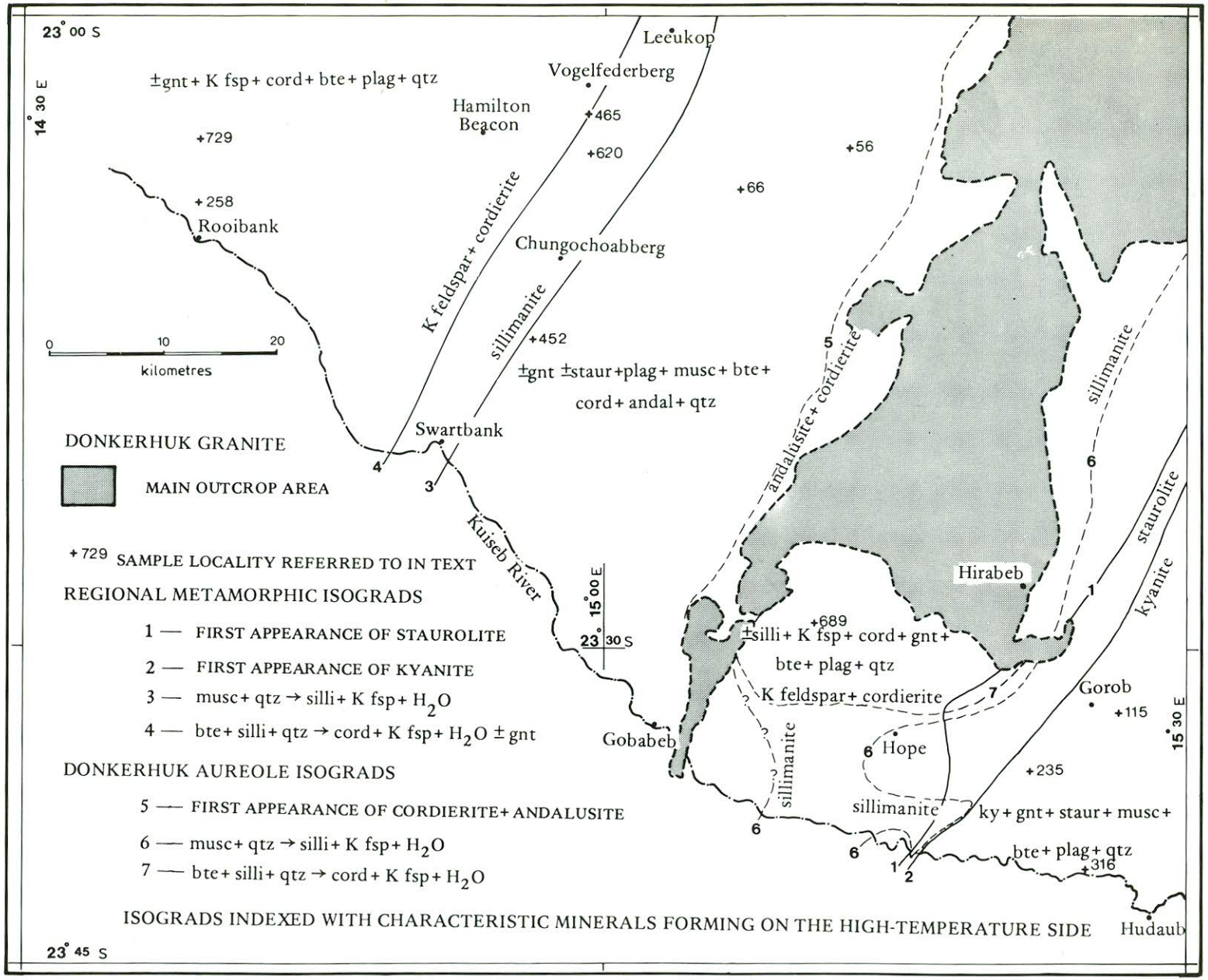

Fig. 8.1 — Metamorphic sketch map based on pelitic rocks showing distribution of major pelitic assemblages (see Appendix I for abbreviations).

Metamorfe sketskaart gebaseer op pelitiese gesteentes wat die verspreiding van die belangrikste pelitiese versamelings aandui (verwys Aanhangsel I vir afkortings).

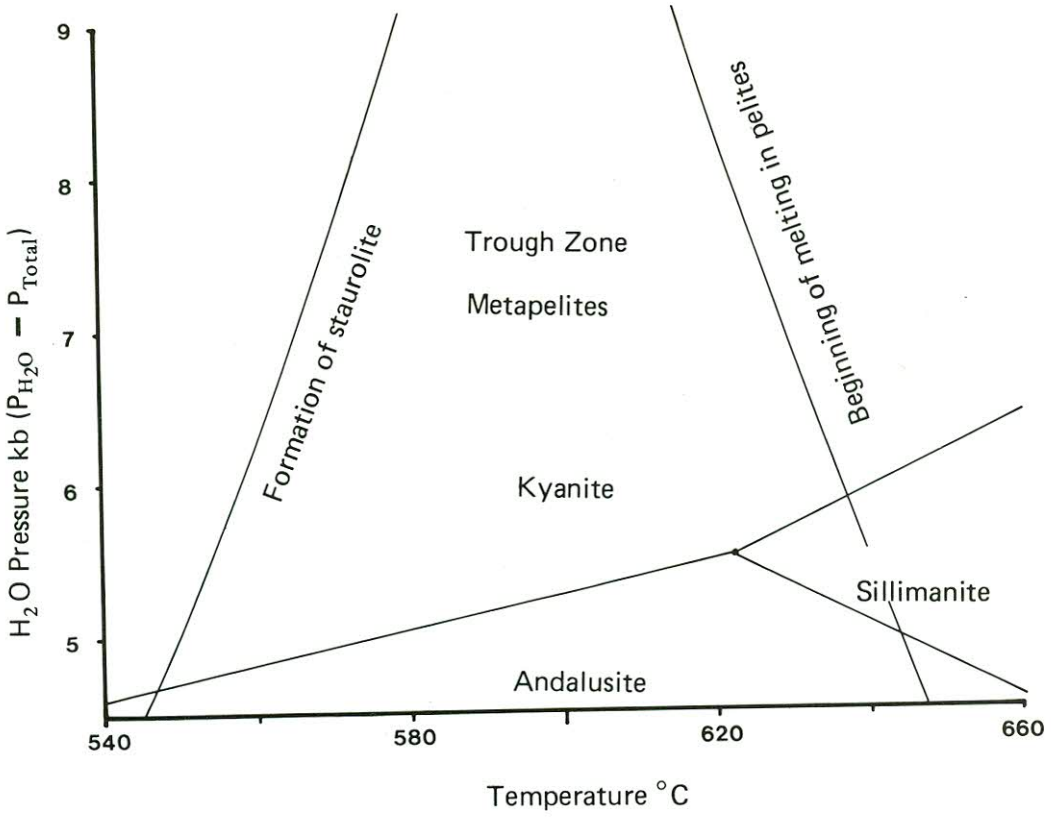

Fig. 8.2 – Pressure and temperature constraints based on field observations in the Trough Zone (see Section 8.1).
Druk- en temperatuurbeperkinge gebaseer op veldwaarnemings in die Trogsone (verwys Seksie 8.1).

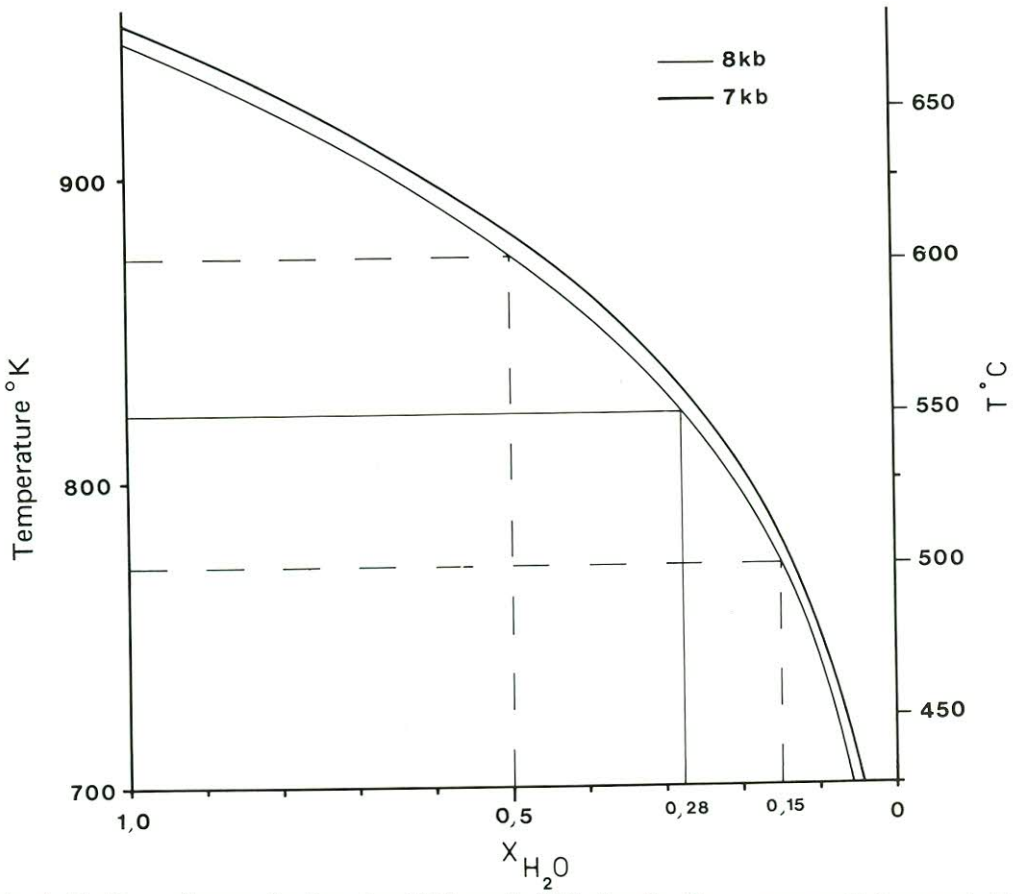

Fig. 8.3 – Isobaric T–X_{H_2O} diagram for Reaction IV (sample 235) showing X_{H_2O} range with temperature estimates (±50 °C) from Reaction III.
Isobariese T–X_{H_2O}-diagram vir Reaksie IV (monster 235) wat die bestek van X_{H_2O} met benaderde temperature (±50 °C) van Reaksie III aandui.

8.1.2 Reaction Equilibria

The pelitic schists analysed all contain plagioclase, kyanite and garnet, enabling the plagioclase-garnet-Al_2SiO_5-quartz geobarometer to be used. The reaction:

3 anorthite $\rightleftharpoons$ grossular + 2 Al_2SiO_5 + quartz

has been investigated experimentally by Hays (1967) and Hariya and Kennedy (1968), whilst its potential as a geobarometer was discussed by Ghent (1975, 1976). In this case the following reaction is applicable:

(I) 3 anorthite $\rightleftharpoons$ grossular + 2 kyanite + quartz

Thermochemical data used are from Waters (Appendix I), but do not differ greatly from those of Ghent (1976), and Schmid and Wood (1976). Since the phases present are impure (e.g. anorthite in oligoclase and grossular in garnet) activities in terms of the pure phases were calculated for the observed minerals. Plagioclase activity data were taken from Orville (1972).

The equilibrium equation (Appendix I) contains both P and T as variables and was solved by fixing T at values within the range of interest. The results are shown in Table 8.1 below. Uncertainties are estimated at ±1 kb.

Table 8.1—EQUILIBRIUM DATA, REACTION I

Sample	550 °C	600 °C	650 °C
	bar	bar	bar
115	7 258	8 183	9 093
235	6 304	7 158	8 018
316	7 546	8 480	9 418

A further check on pressure is given by the reaction:

(II) almandine + muscovite $\rightleftharpoons$ annite + 2 kyanite + quartz

Although potentially an extremely useful reaction together with its Mg counterpart enabling both P and T to be established, the thermochemical data have very large errors at present. Attempts to calibrate the reactions have been made (Thompson 1976, 1976a); those used here are from Waters.* As the errors are large (±300 °C for the Mg end member) only the Fe end-member reactions have been calculated and are shown in Table 8.2. Activities of the minerals present have been calculated in terms of the end-member compositions.

Table 8.2—EQUILIBRIUM DATA, REACTION II

Sample	8 000 bar		7 000 bar		6 000 bar	
	T °C	Error	T °C	Error	T °C	Error
115	637	554 745	590	509 692	544	464 640
235	622	539 727	576	498 675	531	457 624
316	592	514 689	548	474 640	504	435 590

Temperature may be determined from Fe-Mg exchange between garnet-biotite mineral pairs. Determination of K_D values from mean garnet and biotite composition for mineral pairs in contact give temperatures of the order of 525 °C, using the calibrations of Thompson (1976a) and Ferry and Spear (1977). Using the data of Holdaway and Lee (1977) for the reaction:

(III) 1/2,52 Mg biotite + 1/3almandine $\rightleftharpoons$ 1/2,52Fe biotite + 1/3pyrope

Garnet–biotite K_D values give the temperatures shown in Table 8.3. These values are still considered to be low and have an error limit of ±50 °C.

Table 8.3—TEMPERATURES DETERMINED FROM Fe-Mg EXCHANGE, REACTION III

P bar	Sample 115	Sample 235	Sample 316
	T °C	T °C	T °C
6 000	544	546	535
7 000	548	549	538
8 000	551	552	541
9 000	554	555	545

Temperature is potentially determinable from the reaction:

(IV) 6 Fe staurolite + 25 quartz $\rightleftharpoons$ 8 almandine + 46 kyanite + 12H_2O

The thermodynamic data given in Appendix I are derived from the experimental data of Ganguly (1972) using the staurolite formula of Richardson (1968) as the analytical data indicate this to be more appropriate than the formula used by Ganguly.

The equilibrium temperature for Reaction IV is dependent upon X_{H_2O} as the isobaric T–X diagram (Figure 8.3) shows (calculated from the re-arranged equation of state, Appendix I). Assuming temperatures determined by Reaction III to be correct (±50 °C) it can be seen from Figure 8.3, that X_{H_2O} has the range 0,15 to 0,50 at 7 to 8 kb (pressure estimates from Tables 5.1 and 5.2).

Wells (1976) finds P_{H_2O} to be about half P_{total} in upper amphibolite-grade rocks of Greenland. French (1966) suggests X_{H_2O} to be of the order of 0,5 in graphite-bearing pelites. Ohmoto and Kerrick (1977) consider that under typical moderate- to high-metamorphic grades, X_{H_2O} must be less than 0,9 in the presence of graphite. Graphite-bearing pelites are common within the Kuiseb Formation especially in subzone TZ/2 where the three samples were collected. Should graphite have been present then the reaction:

2 graphite + 2H_2O $\rightleftharpoons$ CO_2 + CH_4

may well have occurred, consuming H_2O and thereby reducing X_{H_2O} in the fluid phase.

In view of the indicated X_{H_2O} range of 0,15 to 0,5 and the findings of other workers the value X_{H_2O}=0,5 has been chosen and the equilibrium for Reaction IV calculated accordingly (Table 8.4).

Table 8.4—REACTION IV EQUILIBRIA AT X_{H_2O}=0,5

P bar	Sample 115		Sample 235		Sample 316	
	T °C	Error	T °C	Error	T °C	Error
9 000	596	565 617	593	559 614	595	562 615
8 000	604	575 622	601	570 619	602	572 621
7 000	610	583 627	608	580 623	609	581 626
6 000	614	590 631	611	585 627	612	589 630
5 000	616	594 632	612	588 630	615	594 632

Temperature may also be estimated by the reaction:

(V) paragonite + quartz $\rightleftharpoons$ albite + kyanite + H_2O

where paragonite and albite are involved in solid solutions.

* Unpublished data, see Appendix I.

Microprobe analysis of the white micas (samples 115 and 235) show them to be muscovites with 17–20 per cent paragonite, which is close to the maximum possible crystalline solution of paragonite in muscovite (Thompson 1974).

Several metapelites (e.g. sample 694) have a felt-like mat fabric of white mica, whereas other samples (e.g. 115 and 235) have a groundmass consisting largely of oligoclase. The difference in mineralogy between the two rocks is attributed to the occurrence of Reaction V.

Chatterjee (1972) and Thompson (1974) show that the breakdown of paragonite+quartz occurs at lower temperatures than that of muscovite+quartz. The sub-assemblage oligoclase-muscovite-kyanite found in samples 235 and 115 corresponds to the K feldspar-deficient part of the phase diagram in section E, Figure 1 of Thompson (1974). At 7 kb, Reaction V occurs at 630 °C ($X_{H_2O} = 1$) and therefore after the beginning of melting in pelites. With reduced X_{H_2O} the reaction is displaced to lower temperatures, e.g. 576 °C at 6 kb and 591 °C at 7 kb for $X_{H_2O} = 0,5$ (Wintsch 1975). The occurrence of muscovite-rich and plagioclase-rich assemblages in Trough Zone pelites may be attributed to the occurrence of Reaction V in rocks of suitably low X_{H_2O}.

8.1.3 Conclusions

The reaction equilibria for the three samples investigated are plotted on Figures 8.4A, B and C. Reaction I tends to give lower-pressure determinations when the bulk Ca content of the co-existing garnet and plagioclase is low (Table 8.5).

Table 8.5—MEAN Ca CONTENT OF GARNET AND PLAGIOCLASE FROM ANALYSED SAMPLES

Sample	X_{Ca}^{garnet}	$X_{Ca}^{plagioclase}$
115	0,082	0,318
235	0,042	0,230
316	0,079	0,280

Reactions I and II are in reasonable agreement for sample 235 and in excellent agreement for 316, however, the discrepancy between the two equilibria for sample 115 may be due to the upward displacement of Reaction I due to higher Ca content.

Temperature estimates from Reaction III give consistent results for the three samples, although temperatures are considered low, in spite of large errors (±50 °C).

Figure 8.3 shows that X_{H_2O} could not have been greater than about 0,8 since partial melting ought then to have been widespread. Reaction III with its large errors suggests $X_{H_2O} = 0,15$ to 0,5. Taking the value of $X_{H_2O} = 0,5$, since graphite is common in Trough Zone rocks, Reaction IV gives temperatures of about 600 °C, which is in very good agreement with Reaction V, also assuming $X_{H_2O} = 0,5$.

Quartz veins parallel to S_2 contain abundant fluid inclusions, a high proportion of which are CO_2-filled, thus lending support to the suggestion that H_2O was diluted in the fluid phase by CO_2.

The eight-phase isobaric invariant assemblage is expected to occur over a limited area in outcrop; on the contrary, however, it is rather widespread. This is probably due to the buffering effect of the assemblage on the fluid phase. In a closed system, or where H_2O is not perfectly mobile, the occurrence of devolatilisation reactions yield internal control of the chemical potentials of fluid components. The process of buffering in rocks undergoing devolatilisation is considered to be commonplace (Greenwood 1975; Ohmoto and Kerrick 1977; Fyfe *et al.* 1978). Other explanations for the apparent low variance of the assemblage are: (i) The presence of Mn in the system makes the discontinuous reaction:

staurolite + muscovite + quartz ⇌ garnet + biotite + H_2O

divariant in which Mn stabilises garnet at lower temperatures than in the Fe–Mg range; (ii) Harte (1975) notes the refractory (non-reactive) nature of garnets in particular. It may thus be that garnet is a refractory mineral having formed at lower temperatures.

Metamorphic conditions experienced by samples 115 and 235 during M_2 (last regional metamorphism post-dating S_2) appear to be a pressure of 7,3±1,2 kb and a temperature of 605±25 °C. Sample 316, collected 16 km further south-eastwards indicates pressures of 8,2 ±1,2 kb and temperatures of 600±25 °C.

8.2 CENTRAL ZONE

8.2.1 Introduction

High-grade metapelites of the Central Zone often contain the assemblage:

±garnet±sillimanite+K feldspar+plagioclase+cordierite+biotite+quartz

The K feldspar is always microcline and the plagioclase an oligoclase. Furthermore, partial melting in metapelites and Etusis Formation feldspathic quartzites begins in the vicinity of sample 465 and is widespread at sample 729, the two samples chosen for investigation (Fig. 8.2).

Sample 465 contains the assemblage (with all phases in contact):

sillimanite + garnet + oligoclase + microcline + biotite + quartz + cordierite

which with a fluid phase represents eight phases in the seven component system:

$(Na,K)_2O$, CaO, (Fe,Mn)O, MgO, Al_2O_3, SiO_2, H_2O

This indicates isobaric invariance. Excluding plagioclase and CaO from consideration the variance is still one, but the reaction:

biotite + sillimanite + quartz ⇌ cordierite + garnet + K feldspar + H_2O

can be written linking all phases. This reaction is discontinuous (Thompson 1976) and thus ought to define an isograd.

Sample 729, however, contains the isobaric univariant assemblage:

garnet + biotite + cordierite + oligoclase + microcline + quartz

for which the reaction:

biotite + cordierite + quartz ⇌ garnet + K feldspar + H_2O

can be written (neglecting plagioclase and CaO).

8.2.2 Reaction Equilibria

Estimates of temperature can be made using the Fe–Mg exchange reactions:

(III) 1/2,52 Mg biotite + 1/3 almandine ⇌ 1/2,52 Fe biotite + 1/3 pyrope

(VI) 1/2 Mg cordierite + 1/3 almandine ⇌ 1/2 Fe cordierite + 1/3 pyrope

of Holdaway and Lee (1977). Both reactions have been calibrated by Thompson (1976) but yield temperatures below 600 °C. Wells (1976) gives thermodynamic data for Reaction VI with results similar to those obtained from the data of Holdaway and Lee (1977).

I 3 anorthite ⇌ grossular + 2 kyanite + quartz

II almandine + muscovite ⇌ annite + 2 kyanite + quartz

III 1/2,52 Mg biotite + 1/3 almandine ⇌ 1/2,52 Fe biotite + 1/3 pyrope

IV 6 Fe staurolite + 25 quartz ⇌ 8 almandine + 46 kyanite + 12 H_2O

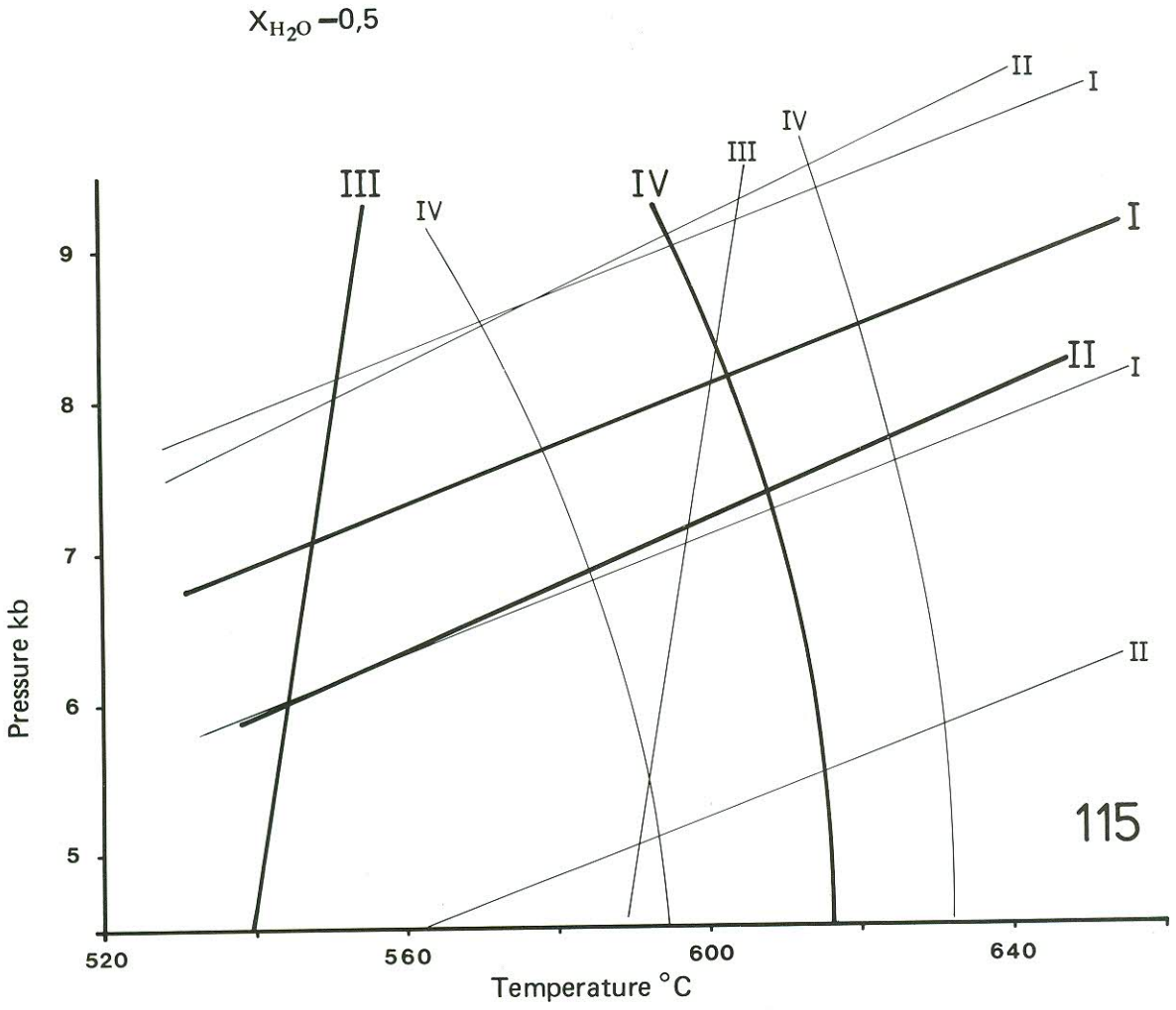

Fig. 8.4A – Reaction equilibria for sample 115 from the Trough Zone plotted on a P–T diagram with $X_{H_2O} = 0,5$. Heavy lines show equilibria calculated from the 'best fit' thermodynamic data (see Appendix I). Light lines indicate errors due to uncertainties in the thermodynamic data.
Reaksie-ekwilibria vir monster 115 van die Trogsone uitgestip op 'n P–T-diagram met $X_{H_2O} = 0,5$. Dik lyne toon ekwilibria bereken vanaf die 'mees toepaslike' termodinamiese data (verwys Aanhangsel I). Dun lyne dui foute te wyte aan onsekerhede in die termodinamiese data aan.

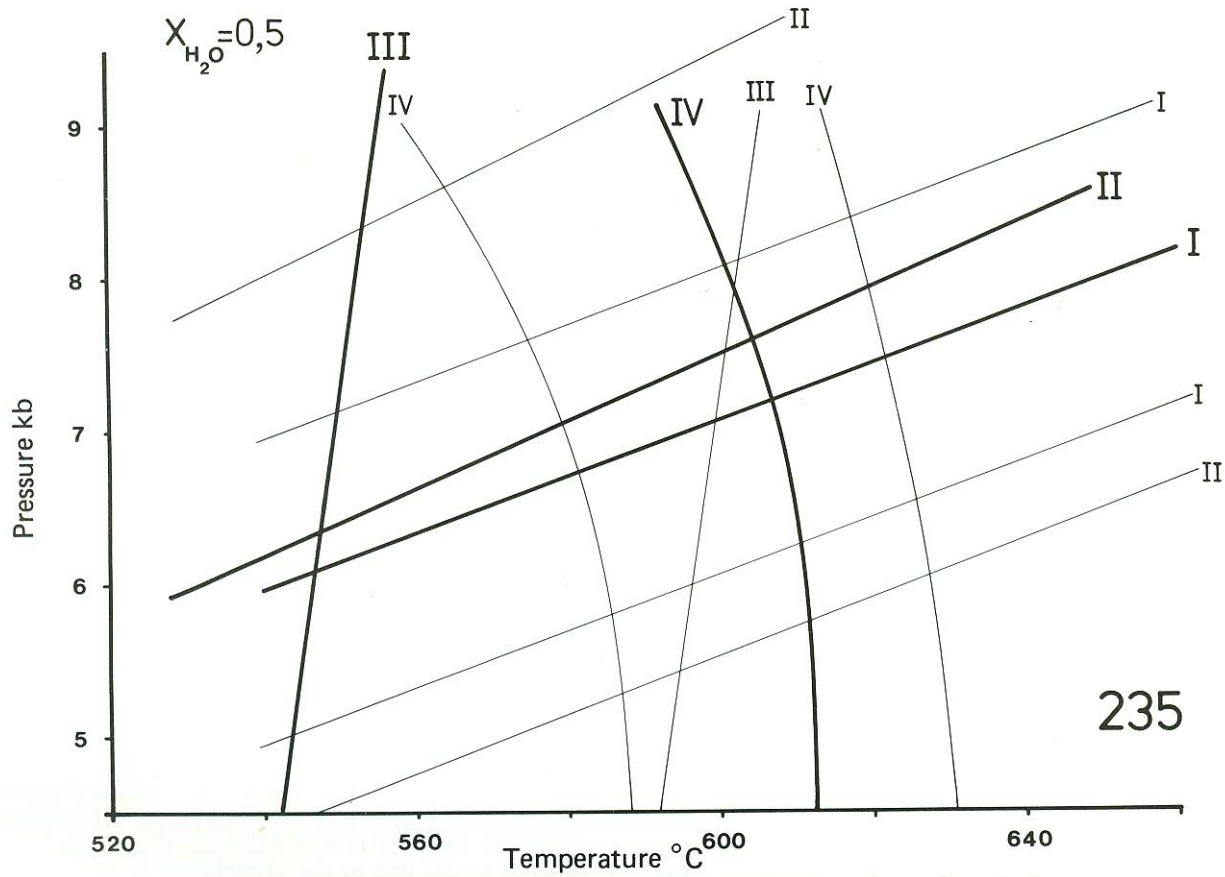

Fig. 8.4B – Reaction equilibria for sample 235 (see Fig. 8.4A for explanation).
Reaksie-ekwilibria vir monster 235 (kyk Fig. 8.4A vir toeligting).

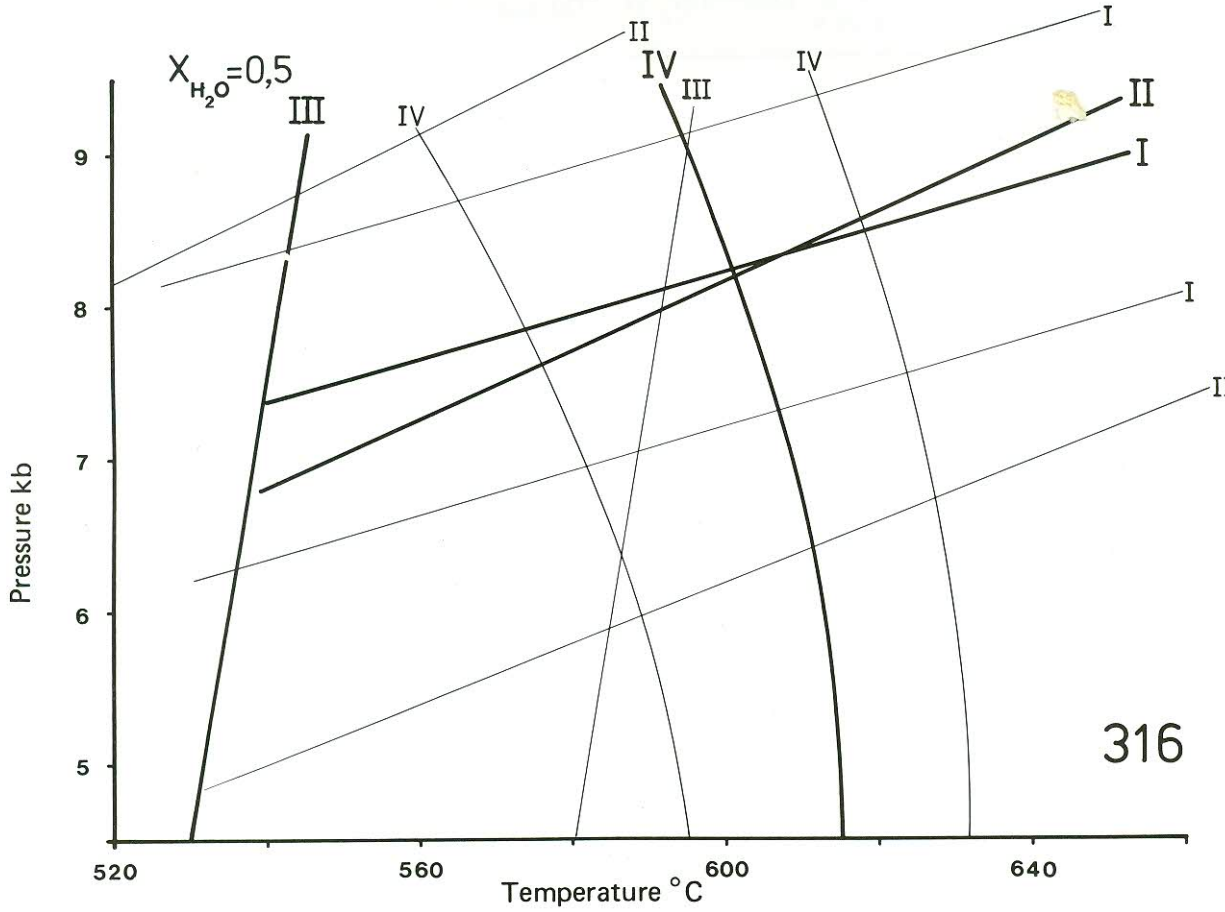

Fig. 8.4C – Reaction equilibria for sample 316 from the Trough Zone (see Fig. 8.4A for explanation).
Reaksie-ekwilibria vir monster 316 uit die Trogsone (kyk Fig. 8.4A vir toeligting).

K_D values for Reactions III and VI are shown in Table 8.6 and are used to calculate the temperatures shown in Table 8.7, using the data of Holdaway and Lee (1977). Temperatures for Reaction VI from the data of Wells (1976) are shown in Table 8.8.

Table 8.6—K_D VALUES FOR REACTIONS III AND VI (HOLDAWAY AND LEE 1977)

Sample	465		729	
Reaction	III	VI	III	VI
K_D.....	0,1826	0,0928	0,1846	0,1046

Table 8.7—TEMPERATURE DETERMINATIONS FROM REACTIONS III AND VI USING DATA IN TABLE 8.6

P bar	Sample 465		Sample 729	
	T °C (III)	T °C (VI)	T °C (III)	T °C (VI)
3 000.....	646	568	649	597
4 000.....	650	572	653	601
5 000.....	654	577	656	605
6 000.....	658	582	660	609

Table 8.8—EQUILIBRIUM DATA FOR REACTION VI USING DATA OF WELLS (1976)

P bar	Sample 465	Sample 729
	T °C	T °C
3 000.....	626±5	657±4
4 000.....	622±5	653±4
5 000.....	618±5	649±4
6 000.....	614±5	645±4

Since partial melting of metapelites occurs at both sample localities, the higher temperatures from Reaction III are preferred, and a temperature of 652 °C (925 °K) is assumed for both samples. An error of ±25 °C is also assumed, and thus encompasses the results from Reaction VI using the data of Wells (1976)—Table 8.8.

The combination of garnet and cordierite offers a potentially useful geobarometer (Currie 1971, 1974; Hutcheon *et al.* 1974; Hensen 1977). However, considerable variation in the thermochemical data exists. Seifert (1976) experimentally investigated the Mg reaction:

6 muscovite + 2 phologopite + 15 quartz ⇌
3 Mg cordierite 0,5 H_2O + 8 K feldspar + 6,5 H_2O

whilst Hoffer (1976), using natural minerals, experimentally investigated the reaction:

2 biotite+6 sillimanite+9 quartz⇌
3 cordierite+2 K feldspar+0,5 H_2O

Fe end-member reactions experimentally determined are:

(VII) 3 Fe cordierite. $3nH_2O$⇌
2 almandine+4 sillimanite+5 quartz+$3nH_2O$

by Weisbrod (1973, 1973a) and Holdaway and Lee (1977) (n=number of mols H_2O in cordierite); and

(VIII) Fe biotite+2,08 sillimanite+4 quartz⇌
1,26 Fe cordierite+0,84 K feldspar+(1–1,26n) H_2O

by Holdaway and Lee (1977). Although both experimental determinations of Reaction VII give similar results (Appendix I) the data of Holdaway and Lee are used for compatibility.

With temperature known, an isothermal P–X_{H_2O} diagram can be constructed for sample 465, enabling Reactions VII and VIII to be solved simultaneously yielding values for both P and X_{H_2O}. To ensure both reactions are compatible, the experimental data of Holdaway and Lee (1977) are used since both experimental determinations (for VII and VIII) used similar buffers (QFM) and experimental procedure. A further complication arises from the problem of water in cordierites. The number of mols of H_2O (n) in cordierite is approximately 0,5 at 2 kb P_{H_2O} and 0,7 at 5 kb P_{H_2O} (Weisbrod 1973a, Fig. 61). Since the experiments of Holdaway and Lee (1977) are in the pressure range 2–3,5 kb, and the expected pressure is about 4 kb in the Central Zone $X_{H_2O}<1$; a value of n=0,5 has been chosen as realistic for the amount of water in cordierite.

Figure 8.5 shows the isothermal P–X_{H_2O} diagram for Reactions VII and VIII and sample 465. Equilibria are shown for temperatures of 652±25 °C and also take into account errors due to the uncertainty in the thermochemical data (Appendix I).

Neither Reaction VII nor VIII are applicable to sample 729 since sillimanite is not present. However, the reaction:

(IX) 4 annite+3 Fe cordierite+3 quartz⇌
6 almandine+4 K feldspar+5,5 H_2O

can be written for the assemblage of 729. The experimental data of Holdaway and Lee (1977) can be combined to yield thermochemical data for Reaction IX*.

Although no detailed work was carried out on calc-silicate rocks, the following observations are significant:

In one case (EWS 620, see Figure 8.1 for locality) the isobaric invariant assemblage:

clinozoisite+quartz+anorthite+grossular+calcite

was found. Since clinozoisite and not zoisite is present the reaction:

4 zoisite+quartz⇌grossular+5 anorthite+H_2O

is displaced upwards to higher temperature (Holdaway 1972) whilst the reaction:

2 clinozoisite+CO_2⇌calcite+3 anorthite+H_2O

is little altered (Thompson 1975a). Thus the isobaric invariant assemblage lies at approximately 650 °C at 4 kb and is indicative of a very low X_{CO_2}.

A common subassemblage in calc-silicate rocks is:

diopside/hedenbergite+tremolite/actinolite+quartz+calcite

generally with the amphibole forming at the expense of the clinopyroxene, possibly by the reaction investigated by Slaughter *et al.* (1975):

5 diopside+3 CO_2+H_2O⇌
tremolite+3 calcite+2 quartz.

* The data used are those obtained by D. Waters (personal communication). See Appendix I.

In many such rocks diopside comprises over 20 per cent of the rock volume. During progressive metamorphism of a rock containing quartz, dolomite and calcite, it is reasonable to assume that the fluid composition will be driven to a fairly high CO_2 content by reactions involving talc and tremolite (Greenwood 1975). Thus diopside may form by:

$$\text{tremolite} + 3\ \text{calcite} + 2\ \text{quartz} \rightleftharpoons 5\ \text{diopside} + 3\ CO_2 + H_2O$$

at low to moderate X_{CO_2} or at high X_{CO_2} by:

$$\text{dolomite} + 2\ \text{quartz} \rightleftharpoons \text{diopside} + 2\ CO_2.$$

Frequently the rocks also contain the subassemblage:

$$\text{epidote/clinozoisite} + \text{quartz} + \text{calcite} \pm \text{plagioclase}$$

which is indicative of a low X_{CO_2}. Thus a change of fluid composition is indicated during metamorphism of the calc-silicate rocks, possibly due to:

(i) Two metamorphic events, the first at high X_{CO_2} producing diopside and the second event at low X_{CO_2} producing the epidote/clinozoisite + tremolite assemblage.

(ii) A change of fluid composition during a single metamorphic event by the continuous gain of water from adjacent pelitic rocks effectively reducing X_{CO_2} and thus affecting the stability of certain minerals in favour of low X_{CO_2} assemblages.

Three rocks taken from close to bodies of red granite contain the subassemblage:

$$\text{calcite} + \text{quartz} + \text{wollastonite}.$$

In one case (sample 258, see Fig. 8.1) the assemblage:

$$\text{plagioclase} + \text{quartz} + \text{calcite} + \text{scapolite} + \text{garnet} + \text{microcline} + \text{wollastonite} + \text{diopside}$$

is present. This contains the isobarically invariant assemblage:

$$\text{grossular} + \text{quartz} + \text{wollastonite} + \text{anorthite} + \text{calcite}$$

as well as products of the reactions:

$$\text{calcite} + \text{quartz} \rightleftharpoons \text{wollastonite} + CO_2$$

and,

$$\text{plagioclase} + \text{calcite} \rightleftharpoons \text{scapolite (mizzonite)}.$$

Mizzonite is the scapolite stable at the lowest temperatures (Orville 1975). The isobarically invariant assemblage suggests a pressure of about 3,8 kb at 652 °C. The pressure and temperature estimates suggest that wollastonite formed at $X_{CO_2} \simeq 0{,}20$ (Winkler 1976, Fig. 9-8).

8.2.3 Conclusions

Unlike the Trough Zone, Fe–Mg exchange reactions give temperatures considered to be realistic from the occurrence of partial melting in pelitic rocks. The Fe–Mg exchange reaction between garnet and cordierite gives satisfactory results when the thermodynamic data of Wells (1976) are used. A range of ±25 °C covers the calculated temperatures from Reaction III and Wells' Reaction VI.

The experimental data of Hoffmann (1976a) for the Central Damara rocks suggest that partial melting begins at 655 °C in pelitic rocks (excess H_2O at 4 kb total pressure) and most samples contain melt by 670 °C. The Nosib feldspathic quartzites at Rooibank will begin to produce red homogeneous granite at 662 °C and have produced 20 per cent melt by 670 °C (Hoffmann 1976).

The derived temperature of 652±25 °C therefore appears to be realistic.

The production of large amounts of melt at a eutectic will have the effect of buffering the temperature, since addition of heat leads to continued melting (until one of the phases is consumed) rather than a rise in temperature (Bailey 1976, p. 27). Thus it is unlikely that temperatures would exceed 675 °C except locally where melting did not occur.

The isobaric invariant assemblage of sample 465 enables both P and X_{H_2O} to be determined by plotting Reactions VII and VIII (assuming n=0,5) on an isothermal P–X_{H_2O} diagram such as Figure 8.5. The pressure so indicated is 4,25±0,3 kb with X_{H_2O} ranging from 0,082 to 0,169. At 652 °C values are 4,24 kb and X_{H_2O}= 0,124 respectively. Although X_{H_2O} and n (number of mols H_2O in cordierite) are related, assuming n=0,7, raises X_{H_2O} to a maximum value of 0,237 at T= 652±25 °C.

An assemblage in a calc-silicate rock (EWS 620) taken near to sample 465 indicates the same order of pressure and temperature.

Calc-silicate sample 258 suggests a pressure of just below 4 kb at 652 °C which, when applied to the isothermal P–X_{H_2O} plot for sample 729 (Fig. 8.6), suggests an X_{H_2O} of about 0,18.

Holdaway and Lee (1977) state that the assemblage:

$$\text{almandine} + \text{cordierite} + \text{K feldspar} + \text{quartz}$$

requires $P_{H_2O} < P_{total}$ to form, and that with cordierite of Mg_{50} requires $X_{H_2O} \leq 0{,}4$. (X_{Mg} cordierite are 0,6047 and 0,6107 for samples 465 and 729 respectively). The determined values of X_{H_2O} thus appear to be reasonable.

8.3 OKAHANDJA LINEAMENT ZONE

Chloritoid has not been found in any metapelites, whilst chlorite is generally retrograde, the sole exception being the prograde continuous reaction:

$$\text{chlorite} + \text{muscovite} + \text{quartz} \rightleftharpoons \text{garnet} + \text{biotite} + H_2O$$

observed texturally in one sample (locality 56 Fig. 8.1).

The most characteristic pelitic assemblage encountered is:

$$\text{plagioclase} + \text{quartz} + \text{muscovite} + \text{biotite} + \text{cordierite} + \text{andalusite}$$

which with a fluid phase has a variance of two in the seven-component system $(Na,K)_2O$, CaO, (Fe,Mn)O, MgO, Al_2O_3, SiO_2, H_2O.

In a few instances staurolite is also present making the system isobarically invariant.

Since both garnet and staurolite are very rare in metapelites the disappearance of chlorite probably involved cordierite through the continuous reactions:

$$\text{chlorite} + \text{andalusite} + \text{quartz} \rightleftharpoons \text{cordierite} + H_2O;$$

$$\text{chlorite} + \text{muscovite} + \text{quartz} \rightleftharpoons \text{cordierite} + \text{biotite} + H_2O$$

for which the two Mg-end-member reactions have been carried out by Seifert and Schreyer (1970) and Seifert (1970) respectively. However, Guidotti *et al.* (1975) suggest that the actual disappearance of chlorite takes place via the terminal univariant reaction:

$$\text{chlorite} + \text{muscovite} + \text{quartz} \rightleftharpoons \text{cordierite} + Al_2SiO_5 + \text{biotite} + H_2O$$

which thus sets a lower temperature limit to pelites (Fig. 8.7).

The pelitic assemblages are characteristic of Buchan-type low-pressure metamorphism (Harte 1975).

Calc-silicate rocks often contain the isobaric invariant assemblage:

$$\text{clinozoisite} + \text{grossular} + \text{calcite} + \text{quartz} + \text{anorthite}$$

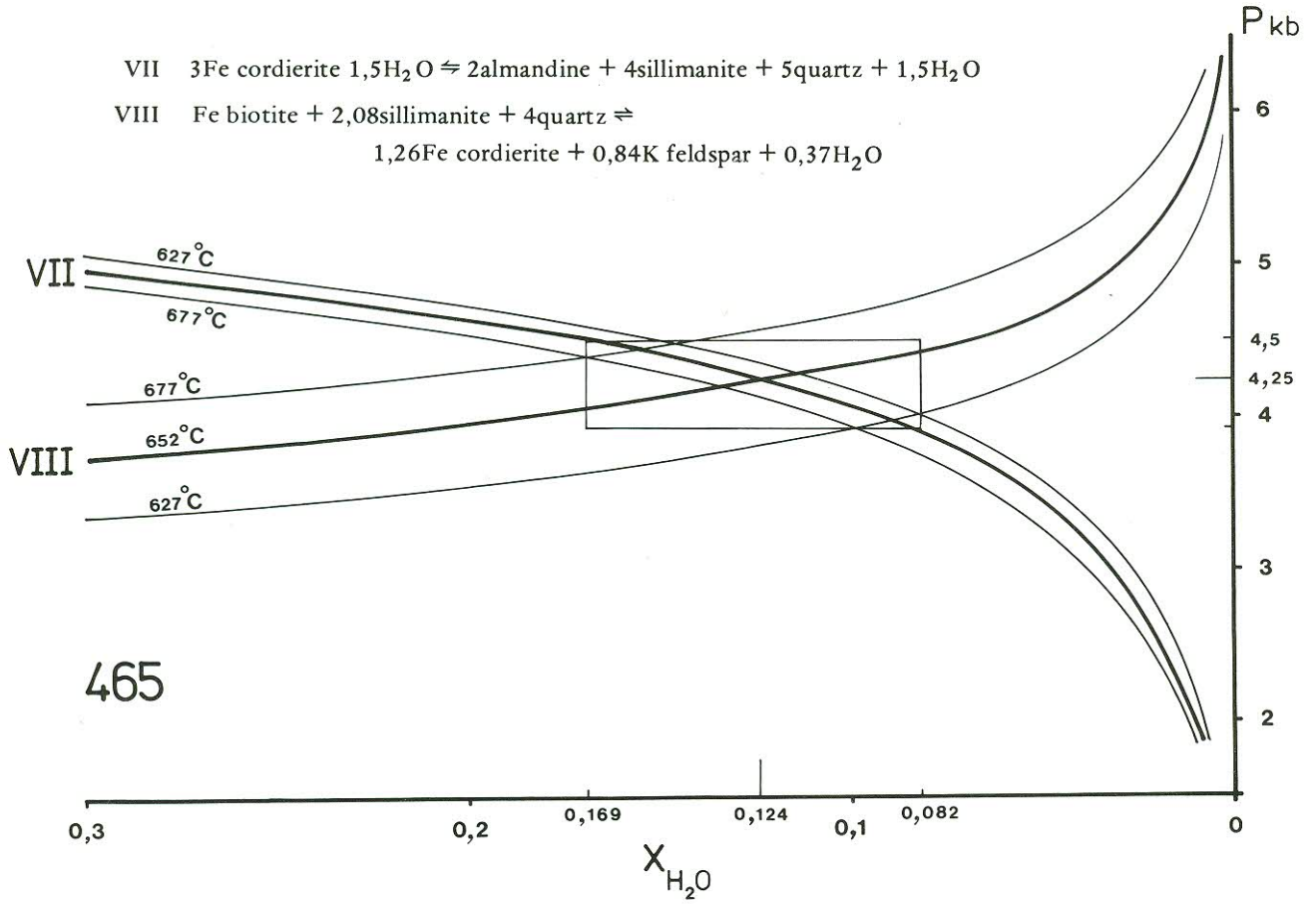

Fig. 8.5 – Isothermal P–X_{H_2O} diagram for Reactions VII and VIII for sample 465 showing errors for a temperature of 652±25 °C.
Isotermale P–X_{H_2O}-diagram van Reaksies VII en VIII vir monster 465 wat foute by 'n temperatuur van 652±25 °C uitwys.

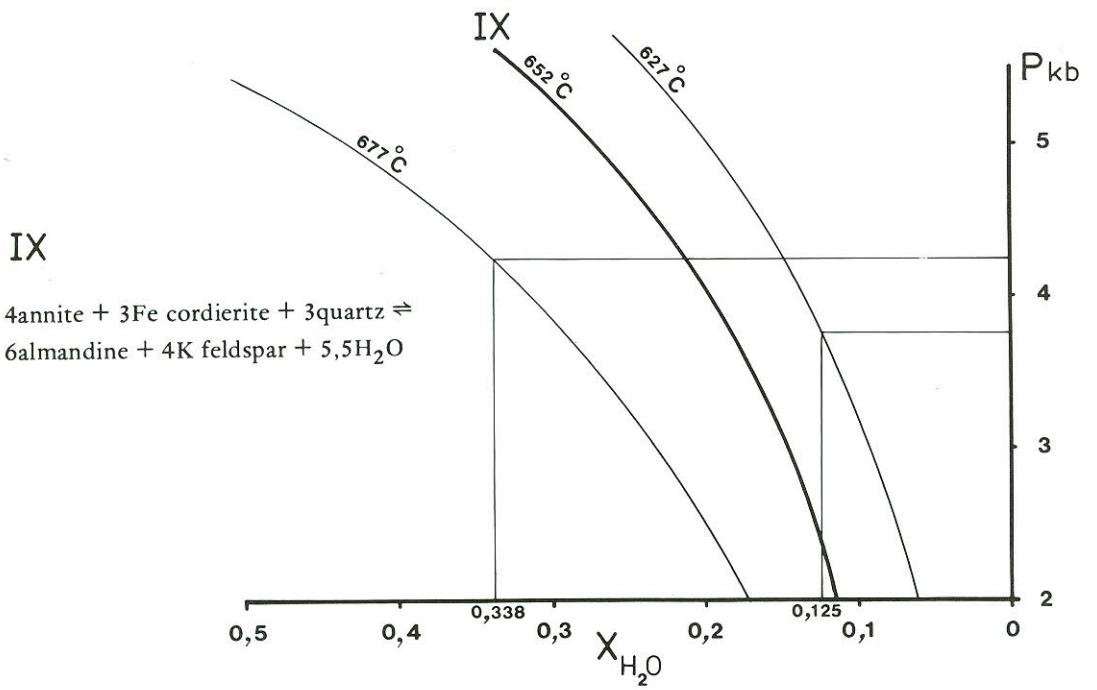

Fig. 8.6 – Isothermal P–X_{H_2O} diagram for Reaction IX for sample 729 at a temperature of 652±25 °C. Pressure estimate from sample 258.
Isotermale P–X_{H_2O}-diagram van Reaksie IX vir monster 729 by 'n temperatuur van 652±25 °C. Benaderde druk van monster 258.

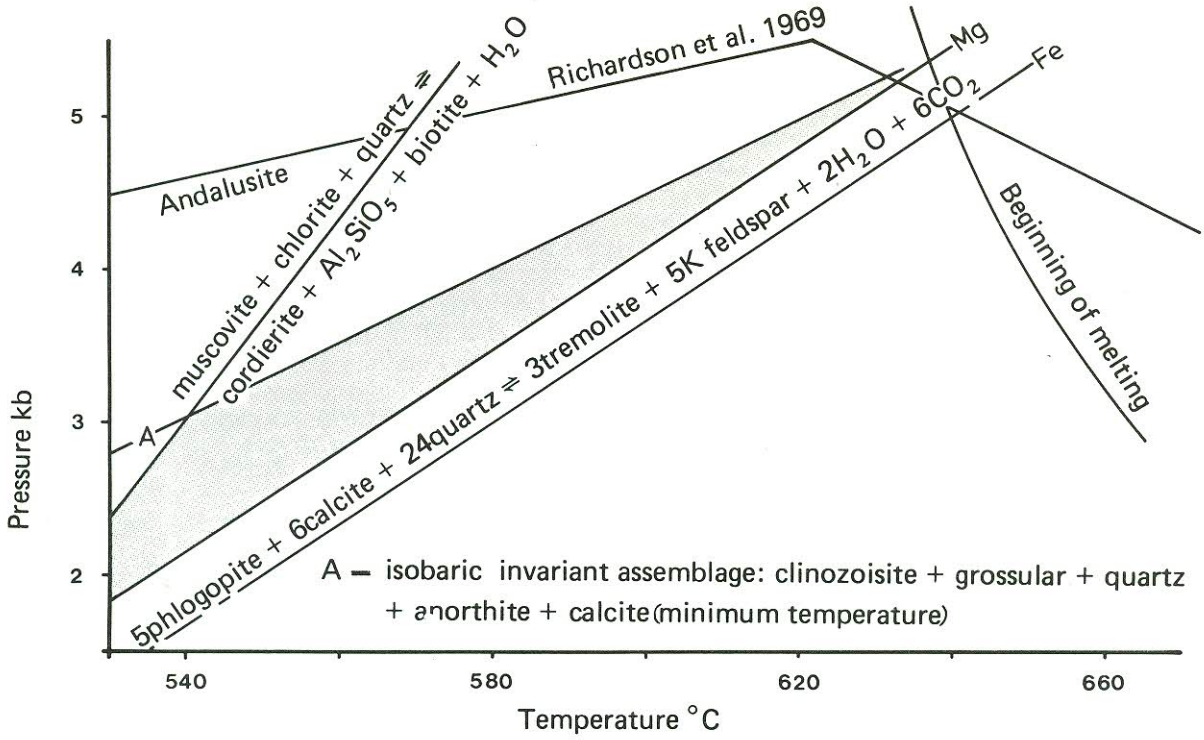

Fig 8.7 — Pressure and temperature constraints at locality 66 in the Okahandja Lineament Zone.
Druk- en temperatuurbeperkinge by lokalitiet 66 in die Okahandja-lineamentsone.

a 5dolomite + 8quartz + H_2O ⇌ tremolite + 3calcite + $7CO_2$
b chlorite + 3calcite + 7quartz ⇌ tremolite + anorthite + $3H_2O$ + $3CO_2$
c 5phlogopite + 6calcite + 24quartz ⇌ 3tremolite + 5K feldspar + $3H_2O$ + $6CO_2$
d tremolite + 3calcite + 2quartz ⇌ 5diopside + H_2O + $3CO_2$
e calcite + 3anorthite + H_2O ⇌ 2clinozoisite + CO_2
f 2clinozoisite + tremolite + 2quartz ⇌ 5diopside + 3anorthite + H_2O

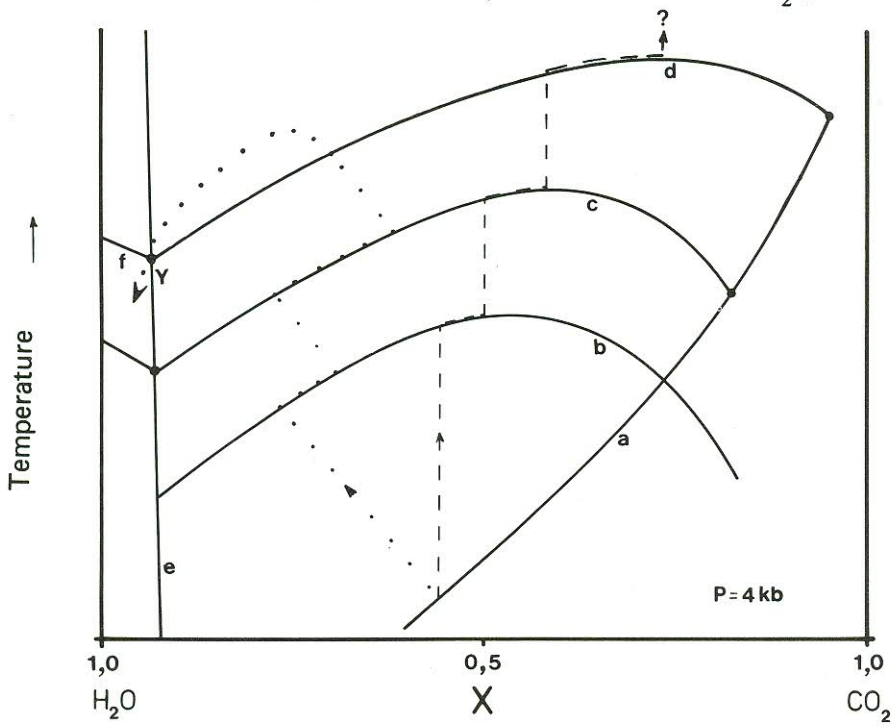

Fig. 8.8 — Possible paths of fluid-composition change in sample 452. Dashes: closed-system path; dots: open-system path to the isobaric invariant assemblage Y in a single metamorphic event.
Moontlike paaie van verandering in fluïdumsamestelling in monster 452. Strepe: geslote sisteempad; kolletjies: oop-sisteempad na die isobariese, onveranderlike versameling Y in 'n enkele metamorfe gebeurtenis.

for which the minimum temperature is shown on Figure 8.7. Increasing the Fe content of the epidote mineral displaces the equilibria to higher temperatures (Holdaway (1972).

Calc-pelites are fairly common in the Tinkas Member. Five examples from locality 66 (Fig. 8.1) show the subassemblage:

phlogopite + calcite + quartz

i.e. tremolite which could have formed via the Fe–Mg continuous reaction:

5 phlogopite + 6 calcite + 24 quartz ⇌
3 tremolite + 5 K feldspar + 2 H_2O + 6 CO_2

is absent. This enables a maximum to be placed upon temperature of (Thompson 1975a)

610 °C at 5 kb H_2O pressure
580 °C at 4 kb H_2O pressure
550 °C at 3 kb H_2O pressure

assuming pure Mg end members. However, the addition of Fe could raise these temperatures by 30 °C (Hewitt 1975; Thompson 1975a). These temperatures lie just above the minimum temperatures of the assemblage:

clinozoisite + grossular + calcite + quartz + anorthite.

Many calc-silicate rocks contain diopside grains rimmed by acicular, disoriented amphibole crystals. Sample EWS 452 (see Fig. 8.1 for location) shows such an amphibole accompanied by clinozoisite; the full assemblage is:

plagioclase + biotite + clinozoisite + tremolite + calcite + diopside + quartz + K feldspar.

Textural evidence suggests that the following reactions have occurred:

5 phlogopite + 6 calcite + 24 quartz ⇌
3 tremolite + 5 K feldspar + 2H_2O + 6 CO_2;

2 clinozoisite + quartz ⇌ calcite + 3 anorthite + H_2O;

5 diopside + 3 anorthite + H_2O ⇌
2 clinozoisite + tremolite + 2 quartz.

Since diopside comprises about 20 per cent of the rock by volume it is evident that the reaction:

tremolite + 3 calcite + 2 quartz ⇌
5 diopside + 3 CO_2 + H_2O

was the diopside-producing reaction since it occurs at lower temperatures than the reaction:

3 tremolite + 6 calcite + K feldspar ⇌
phlogopite + 12 diopside + 6 CO_2 + 2 H_2O.

(Rice 1977, Fig. 3).

The generation of tremolite and diopside would tend to enrich the fluid phase in CO_2 in a closed system (Greenwood 1975). However, the subassemblage:

diopside + plagioclase + tremolite + clinozoisite + quartz + calcite

is isobaric invariant at about 580 °C at 4 kb with X_{CO_2} less than 0,1. Thus the composition of the fluid phase has changed from relatively rich in CO_2 to being CO_2-deficient. This is difficult to explain in a closed system, but may occur in an open system where CO_2 is lost to and H_2O gained from adjacent pelites. Calc-silicate bands commonly show zoning with core, intermediate and rim assemblages:

diopside + calcite + plagioclase + quartz + garnet;

diopside + tremolite + clinozoisite + calcite + quartz + garnet;

tremolite + clinozoisite + quartz + calcite + garnet

respectively, suggesting increasing X_{H_2O} from core to margin. Thompson (1975) and Vidale and Hewitt (1973) considered such zoned calc-silicate rocks to be the result of diffusion of volatile components (e.g. CO_2, H_2O) and non-volatile components (e.g. KCl, $CaCl_2$) down activity gradients between the calc-silicate rock and a large external pelite reservoir.

Hence by considering sample 452 as an open system it is possible to derive the present assemblage by constant diffusion of CO_2 from H_2O into the rock. Figure 8.8 shows two suggested paths of open and closed systems assuming a single metamorphic event.

A further explanation may be sought by considering the diopside to result from an earlier metamorphism in which X_{CO_2} was high, which has been subsequently retrograded by the M_2 event with high X_{H_2O}.

8.3.1 Conclusions

A lower limit to temperature for M_2 metamorphism can be established by the absence of chlorite in metapelites, and by the assemblage (isobaric invariant):

clinozoisite + grossular + calcite + anorthite + quartz

in calc-silicate rocks. The upper limit can be established at locality 66 by the reaction:

5 phlogopite + 6 calcite + 24 quartz ⇌ 3 tremolite + 5 K feldspar + 2H_2O + 6 CO_2

which has not occurred, whereas it has occurred at locality 452. Thus locality 452 must have been at higher temperature and/or lower pressure than locality 66, or else contained less Fe in the bulk composition than at 66. This together with the only occurrence of prograde chlorite (locality 56) indicates increasing temperatures from east to west across the Okahandja Lineament Zone.

Thus temperature has a range of 535 to 610 °C and pressure a range of 2,0–5,25 kb with the andalusite ⇌ kyanite transition as the upper limit and the occurrence of staurolite as a lower limit. At locality 66, $P = 4{,}0 \pm 0{,}9$ kb and $T = 585 \pm 25$ °C.

8.4 DONKERHUK GRANITE AUREOLE

The following comments are confined to the area between Hope Mine and Hirabeb Mountain (Fig. 8.1).

Donkerhuk Granite has intruded Kuiseb Formation schists of the Trough Zone containing the assemblage:

garnet + staurolite + muscovite + biotite + quartz + plagioclase.

Compositionally the granite is a peraluminous adamellite containing both muscovite and biotite with almandine garnet also frequently present. Whitney *et al.* (1976) describe a similar granite from Georgia, U.S.A., and have used the muscovite + quartz-out reaction, together with the minimum melting of granite to indicate a minimum pressure of intrusion of about 3,3 kb. Carmichael *et al.* (1974, p. 65) suggest a minimum pressure of about 4 kb.

In many of the country rocks partial melting has occurred and thus the minimum melting temperature in metapelites has been exceeded, although the

muscovite + quartz ⇌ sillimanite + K feldspar + H_2O

reaction can still occur up to 6 kb and 730 °C.

An assemblage occasionally found is:

plagioclase + sillimanite + quartz + biotite + staurolite + cordierite + almandine + K feldspar

whilst one sample contains a cordierite porphyroblast enclosing sillimanite, biotite, staurolite and quartz suggesting the reactions:

staurolite + muscovite + quartz ⇌
sillimanite + biotite + H_2O

and,

sillimanite + biotite + quartz ⇌
cordierite + K feldspar + H_2O

occurred. Cordierite and almandine do not appear to be produced together in any reaction involving staurolite breakdown since almandine and cordierite have not been observed in contact. In several cases small idioblastic staurolite crystals appear to be forming at the edge of cordierite porphyroblasts. The final assemblage and the remaining staurolite suggests $P_{min}=3,7$ kb at 680 °C and $P_{max}=5,5$ kb at 720 °C depending on Fe/Mg ratios (Thompson 1976a) and X_{H_2O}. Furthermore the assemblage:

plagioclase+sillimanite+cordierite+biotite+garnet+hercynite+ilmenite±quartz±K feldspar±corundum

found in sample 689 suggests temperatures in the range 650–800 °C (Loomis 1976).

8.4.1 Conclusions

The data indicate that the Donkerhuk Granite has a marked thermal aureole, contrary to the view of Faupel (1973, p. 335) and that in the southern part of that aureole the country rocks underwent very high-grade thermal metamorphism in the range $P=4,6\pm1,0$ kb and $T=700\pm20$ °C. The western and eastern margins underwent lower-grade thermal metamorphism with andalusite and sillimanite developed respectively. The degree of metamorphism experienced in the aureole is probably a function of angle of contact and contacts are relatively steep on the east and west flanks, but of low angle in the south.

9. CONCLUSIONS

9.1 PRESENT STUDY

9.1.1 Damara Deposition

Within the area mapped a marked contrast exists between the Central Zone with its fairly thin cover sequence of Nosib and Swakop Group rocks consisting of feldspathic quartzites, marbles and pelites, and the thick, largely pelitic succession in the Okahandja Lineament and Trough Zones.

Sedimentary structures such as cross-lamination, cross-bedding and channel fills in the Nosib Group suggest a derivation from the west and north-west. In addition an intraformational rudite in the Karibib Formation marbles suggest shallow-water deposition (Sawyer 1979). The Trough Zone rocks show layering similar to that of distal turbidites (Allen 1970) whilst submarine volcanism gave rise to pillow lavas and associated gabbro and dolerite intrusions of the Matchless Member.

The Okahandja Lineament Zone and the eastern Central Zone contain the peculiar Tinkas Member, partly interfingering with and partly overlying the Karibib Formation. The contact between the Tinkas Member and the Kuiseb Formation is fairly sharp, although rocks east of the boundary often are as dark and fine grained as those of the Tinkas Member. Sedimentary structures in the Tinkas Member include flute casts and slump structures whilst sedimentary layering tends to become finer grained and more pelitic from west to east in the manner of distal turbidites (Allen 1970). All the sedimentary features thus indicate a derivation from the west or north-west for the Tinkas Member. Mapping shows that the Tinkas Member thickens from nothing about eight km west of the Okahandja Lineament to over 3 000 m just a few kilometres into the Lineament.These facts suggest that the Tinkas Member is a local, thick accumulation of pelite and carbonate of turbidite origin at the edge of the Central Zone, that was deposited in moderately deep water on the continental slope with the Karibib Formation as a shelf edge reef (Dietz and Holden 1966, Fig. 3).

Taking a broader view of the Damara Orogen it is apparent that the lower Damara succession in the Hakos–Rostock area 70 km to the south-east bears little resemblance to the rocks of the Central Zone of the mapped area.* In the Rostock area, thick metarudites and quartzites are developed which together with amphibolites and graphitic schists have no counterpart in the Central Zone. The only exception is the useful marker, the Chuos Formation, a schistose rudite of wide distribution. The rocks of the Hakos–Rostock area seem to be of local provenance representing local outwashes of predominantly clastic sediment derived from a pre-Damara highland area further south-east towards Rehoboth and deposited in a tectonically active environment.

The flysch-like Kuiseb Formation (minus the Tinkas Member) is envisaged filling the Trough Zone, and separating two distinct Damara successions resting unconformably upon the respective pre-Damara gneissic basements. In this scheme the Tinkas Member would require separate formation status within the depositional sequence of the Central Zone, forming a wedge-shaped accumulation of sediment at the edge of the shallow-water depositional regime of the Central Zone and the deep water Trough Zone.

9.1.2 Metamorphic Geology

Two metamorphic events have been established in the Central and Trough Zones through mineral-fabric relations.

In the Central Zone sillimanite porphyroblasts are flattened and rotated during F_3 folding, whilst in one case sillimanite folded by the S_3 crenulation cleavage is enclosed in a cordierite porphyroblast. The M_1 metamorphism hence reached at least sillimanite grade. In the Khan–Swakop area garnet–cordierite assemblages formed during M_1 suggesting that (if $X_{H_2O}=1$) pressure could not have exceeded 6 kb, the upper stability limit of Mg cordierite. Pressure was probably well below this maximum since muscovite and quartz would still be stable until beyond the beginning of melting if pressure was above about 4 kb. Furthermore, some partial melting appears to be associated with M_1. Pressures during M_1 were probably similar to those during M_2 although temperatures may have been somewhat less (600–625 °C). Fabric relations indicate M_1 to be syn-D_{C2}.

The M_2 metamorphic event in the Central Zone occurred partly during but largely after D_{C3}, giving rise to wide-spread partial melting in pelites. Mineral assemblages and reaction equilibria suggest temperatures of 652 ± 25 °C and pressures of $4,25\pm0,3$ kb at sample locality 465 with X_{H_2O} in the range 0,08–0,17. The fluid phase in calc-silicate rocks was low in CO_2 since epidote and wollastonite are frequently present. The increasing degree of partial melting from east to west suggests a temperature rise in that direction.

In the Trough Zone staurolite and kyanite porphyroblasts are rotated and deformed by both D_{T2} and D_{T3} in the same outcrop. Later post-S_3 growth of both minerals is across the pre-existing fabric indicating two metamorphic events, M_1 being syn-S_2 and M_2 being late- but largely post-S_3.

The M_1 event produced staurolite–kyanite-bearing assemblages as did M_2. However, the presence of M_2 ortho-amphibole (anthophyllite) porphyroblasts in an ultrabasic unit of the Matchless Member suggests that

* Field work: R. S. Hill and E. W. Sawyer.

M_2 was of higher temperature than M_1. Conditions for M_2 are pressures of $7,3\pm1,2$ kb and temperatures of 605 ± 25 °C with X_{H_2O} approximately 0,5 in metapelites.

Conditions for M_1 in the Okahandja Lineament are difficult to establish. Some M_2 andalusite porphyroblasts have a bladed habit which may be indicative of inversion from kyanite. If this is so, then M_1 was at higher pressure (hence greater depth) than the M_2 metamorphism which could indicate uplift after M_1 due to erosion. If diopside in the calc-silicates was formed during M_1 rather than during M_2 then a higher temperature and X_{CO_2} during M_1 is indicated. M_1 occurred during the D_{L2} deformation event.

The M_2 syn- to post-D_{L3} metamorphism shows increased temperatures from east to west as in the Central Zone. Pressures were probably about 4 kb and temperature approximately 580 °C as deduced from calc-silicate assemblages.

The common occurrence of diopside altering to tremolite in Central and Okahandja Lineament Zones calc-silicate rocks cannot be adequately explained by assuming a single metamorphic event and a system closed to exchange of fluids with adjacent rocks. The alteration can be explained by either considering the system open to fluid exchange with adjacent metapelites, or by considering the assemblage to be derived from two metamorphic events. The open system is preferred since it can be used to explain the zoning commonly seen in thick calc-silicate bands in the Tinkas Member.

Five Trough Zone and Central Zone metapelites were examined by microprobe and thermodynamic considerations. In all cases it was found that the X_{H_2O} of the fluid phase in equilibrium with the mineral assemblages was 0,5 or less. Thus when dealing with metapelites of the Damara it cannot be assumed that $X_{H_2O}=1$, with the consequence that reaction equilibria will be displaced to lower temperatures, the exceptions being melting reactions.

Figure 8.1 shows the distribution of the main pelitic assemblages, characteristic of the zones. The compilation is based upon 300 thin sections and approximately 2 000 field observations. The regional isograds are shown where possible. Partial melting in regionally metamorphosed rocks begins at curve 3, and increases westwards until it is widespread beyond curve 4. The isograds are indexed with the characteristic minerals shown on the side of the curve on which these occur.

Curves 1 and 2 mark the first occurrences of kyanite and staurolite respectively. The change-over to regional cordierite-andalusite assemblages occurs roughly parallel to lines 1 and 3, some 10 km east of Gobabeb, but is obscured by the Donkerhuk Granite. In addition this boundary also marks the north-western limit of abundant garnet.

Isograds of the Central and Okahandja Lineament Zones are virtually parallel to the structural trends, whereas those of the Trough Zone are oblique to the regional fabric by up to 30°.

The M_2 regional metamorphism characterises both the Central Zone and the Okahandja Lineament Zones as low-pressure metamorphic facies series (Miyashiro 1973) having geothermal gradients of $42,1\pm3,7$ °C. km^{-1} (locality 465) and $39,8\pm9$ °C. km^{-1} (locality 66, large errors due to poor pressure determination) respectively. These estimates assume the density of pelite to be 2,80 g. cm^{-3} (Bean 1953). If a pressure of $4,0\pm0,25$ kb is assumed from the evidence of sample 258 at 652 ± 25 °C the geothermal gradient at locality 729 is $45\pm4,5$ °C. km^{-1}. This shows that both the Central and Okahandja Lineament Zones belong to the same metamorphic regime and have similar geothermal gradients.

M_2 regional metamorphism in the Trough Zone took place with a geothermal gradient of $22,8\pm4,0$ °C. km^{-1}, that is just within the high-pressure metamorphic zone of Miyashiro (1973) which is drawn at the 25 °C. km^{-1} geotherm.

Figure 9.1 summarises the P–T conditions established for each zone and the intrusion of the Donkerhuk Granite.

9.1.3 Structural Geology

In broad terms the three subzones represent an antiformal region (Central Zone) separated from a synformal region (Trough Zone) by a monoclinal region (Okahandja Lineament Zone).

Both the Okahandja Lineament Zone and the Central Zone show the same deformation event (D_{L3} and D_{C3} respectively) producing structures of similar orientation and morphology, although much more intense in the Okahandja Lineament Zone. In both zones two earlier fold phases having subhorizontal and moderately inclined axial planes are postulated. It is assumed, therefore, that the deformation history of the two zones was similar up to and including D_{L3} and D_{C3}. Indeed, all of its history from deformation sequence, timing of metamorphic events and geothermal gradients are closely related up to the post-D_{L3} and D_{C3} M_2 metamorphic event. The main difference between the two zones appears to be largely sedimentological with thin cover over partly exhumed basement in the Central Zone and very thick cover on an unseen basement in the Okahandja Lineament Zone. The other main distinguishing feature is that metamorphic temperatures were rather higher in the Central Zone.

Later deformations, i.e. post-D_{L3} and -D_{C3}, cannot be correlated between the two subzones. In the Central Zone the D_{C4} and D_{C5} folding episodes, although probably of local significance, show thickened hinge regions (i.e. class 1C) and may be indicative of quasi-plastic 'hot rock' deformation (Parrish *et al.* 1976) whereas it is not until D_{C6} that parallel folds with associated fracture cleavage develop. The Okahandja Lineament Zone, however, shows increasingly brittle deformation during D_{L4} with the early folds having an axial-planar crenulation cleavage and the later folds a fanned-fracture cleavage. Also during D_{L3} the intense S_3 schistosity (with locally considerable shearing along S_3 planes) produced a mylonitic fabric parallel to S_3 in calc-silicate rocks, mylonitic cleavage planes being 1–3 mm apart. During D_{L5} deformation, however, an essentially brittle deformation-style produced the 'breccia bands' parallel to S_3 and developed associated kink folds. The change in deformation-style from quasi-plastic (D_{L3}) to elastico-viscous (D_{L5}) (Sibson 1977) may be due to cooling in response to uplift.

The S_f fabric of the Okahandja Lineament Zone does not appear to have a counterpart in the Central Zone, but it does have a similar orientation to the S_2 (D_{T2}) schistosity of the Trough Zone. No deformational event has been proved to be related to S_f, which retains a similar orientation as far north-eastwards as Okahandja. Thin-section evidence has so far failed to show conclusively what the relationship between S_f and S_3 (D_{L3}) is, although it indicates S_f to pre-date S_3. In aluminous schists S_f is defined by biotite whilst S_3 is defined by muscovite. Andalusite and cordierite of M_2 commonly enclose S_f helicitically. The orientation of S_f is similar to axial planes of D_{L2} folds, and is thus correlated with D_{L2}. Also the orientation of S_f is similar to that of the S_2 Trough Zone schistosity and the two are tentatively

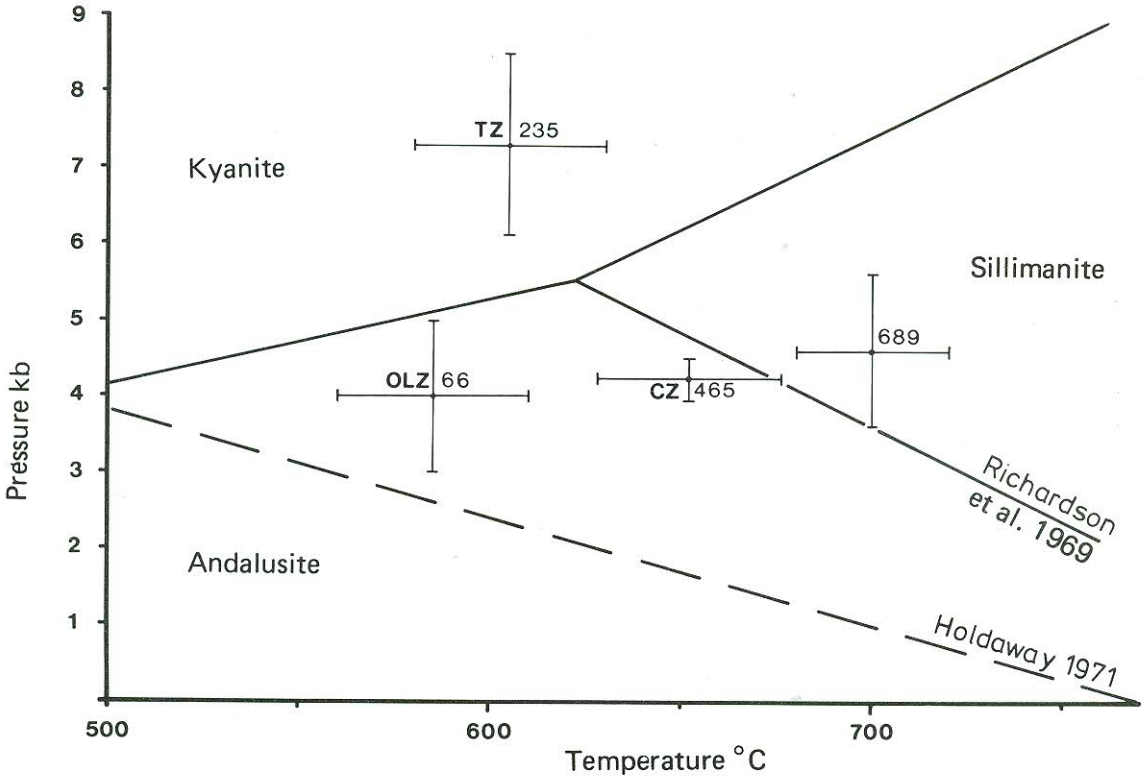

Fig. 9.1 — Determined P–T conditions during M_2 with reference to the Al_2SiO_5 phase diagram.
P–T-toestande soos vasgestel gedurende M_2 met verwysing na die Al_2SiO_5-fasediagram.

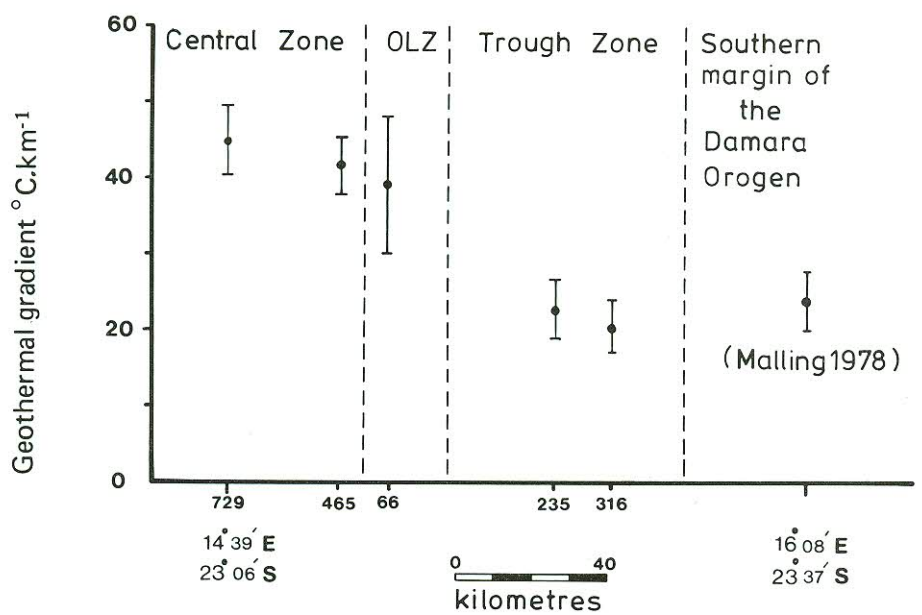

Fig. 9.2 — Calculated geothermal gradients (mean rock density = 2,80 g.cm^{-3}) for M_2 projected onto a section across the area mapped from locality 729 (14°39′E, 23°06′S) to the southern margin of the Damara Orogen (16°08′E, 23°37′S).
Berekende geotermale gradiënte (gemiddelde gesteentedigtheid = 2,80 g.cm^{-3}) vir M_2 geprojekteer op 'n snit geneem dwarsoor die gekarteerde gebied vanaf vindplek 729 (14°39′O, 23°06′S) tot by die suidgrens van die Damara-orogeen (16°08′O, 23°37′S).

correlated. Lines of evidence supporting this are: (i) although the relationship between the Okahandja Lineament Zone and the Trough Zone fabrics is not clearly visible since the Donkerhuk Granite intrudes along the boundary between the two zones, outcrops some seven km east of Gobabeb indicating the subvertical S_3 fabric of the Lineament Zone to post-date the gently inclined Trough Zone S_2 schistosity; (ii) it is known that M_1 is contemporaneous with D_{L2} and M_2 syn- to post-D_{L3} in the Lineament Zone, and that M_1 is syn-D_{T2} and M_2 post-D_{T3} in the Trough Zone. Now by assuming that both the M_1 and M_2 metamorphic events are the same in both zones then it follows that D_{T2} and D_{L2} could be the same event.

Correlation of deformation events between the three zones suggests that all experienced the same three (pre-M_2) deformation episodes within the tectono-metamorphic framework, although the style and orientations of structures produced in the Central and Okahandja Lineament Zones differ markedly from those in the Trough Zone. Later deformations (post-M_2) differ in each zone, but all indicate a progressive transition to elastico-viscous and brittle behaviour.

The degree of shortening determined from F_2 folds, deformed pillows and flattened variolites in the Trough Zone is 50–80 per cent. A similar although less reliable amount of shortening is obtained for F_3 folds in the Okahandja Lineament Zone.

An initial gravity instability of denser Damara metasediments upon a granitic pre-Damara basement in the Central Zone caused diapiric domes to form during the M_2 metamorphic event. An origin by interference folding is discounted in the mapped area because of the lack of regional interference patterns, presence of rim synclines around the domes, shortening across bedding concentric to the dome, whilst extension parallel to such layers has occurred, and finally by the close agreement between actual dome spacing and that calculated for a simple gravitationally unstable model.

The large-scale synforms in the Hope area are considered to have formed through the emplacement of the Donkerhuk Granite. It is envisaged that these folds were compressed between granite bodies during the ascent of the Donkerhuk Granite. Sufficiently large in volume the cores of these synforms did not undergo high-grade thermal metamorphism thus causing the muscovite + quartz thermal aureole isograd to curve around every synform (Figs. 4.1F and 8.1).

9.2 CONSIDERATION OF PREVIOUS WORK

At Swartkrans 224, Rehoboth Gebiet, on the southern margin of the Damara Orogen mineral assemblages indicate a decline in temperature and pressure from the Trough Zone (Malling 1978). Using the garnet–biotite calibration of Ferry and Spear (1977) and the phengite content of muscovite (Velde 1967), Malling (1978) has obtained $T=545\pm50$ °C and $P=6{,}3\pm0{,}5$ kb for a biotite-muscovite-garnet-chlorite-albite-quartz schist. Assuming a mean rock density of 2,8g. cm^{-3} these P–T estimates indicate a geothermal gradient of 24 ± 4 °C. km^{-1}. Figure 9.2 shows the different geotherms obtained from the mapped area and from the data of Malling (1978).

Within the mapped area no radiometric dating has been carried out save a biotite K–Ar cooling age at Gorob (Clifford 1967). The following data are, however, significant in interpreting the area mapped (all Rb–Sr whole rock ages):

(i) Syn- or pre-tectonic Salem granite: 700 Ma: Haack (1977).

(ii) Post-tectonic Salem Granite: 550 Ma: Hawkesworth *et al.* (in prep.).

(iii) Donkerhuk Granite: 528 ± 7 Ma: Haack (1977).

(iv) Khan Formation, Central Zone: 663 ± 14 Ma: Kröner *et al.* (prep.).

(v) Khan Formation, Central Zone: 475 ± 6 Ma: Kröner *et al.* (in prep.).

Within the Trough Zone it is evident that the regional metamorphism pre-dates the Donkerhuk Granite, and furthermore, in the Okahandja Lineament an unfoliated post-tectonic variety of the Salem Granite is intruded by Donkerhuk Granite indicating M_2 to pre-date the 550 Ma age. The 663 ± 14 Ma age (iv above) may represent M_1 since it is noticeably younger than the date obtained by Haack for syn- or pre-tectonic granite of the Salem Suite. Thus an age of 170 Ma covers the intrusion of syn- or pre-tectonic varieties of the Salem Granite Suite and the emplacement of the post-tectonic Donkerhuk Granite.

The second Khan Formation Rb–Sr whole-rock age of 475 Ma and the Rössing alaskite age of 468 ± 8 Ma (Kröner and Hawkesworth 1977) date a later, post-tectonic thermal event. The cause of this late thermal episode may be high-level radiogenic heating. An alternative cause of the heating is discussed in Section 9.3.

Fission-track data on garnet, idocrase and apatite (Haack 1976) together with K–Ar biotite ages (Clifford 1967; Haack and Hoffer 1976) reflect the times at which the various minerals cooled through the respective blocking temperatures.

The K–Ar data on biotites show no systematic regional variation and give ages of 513 to 420 Ma over much of the Damara belt. This led Haack and Hoffer (1976) to conclude that any differential uplift within the Damara belt must have taken place before the rocks cooled below 300–350 °C some 485 Ma ago.

Fission-track ages which indicate the time when annealing processes became so slow as not to destroy tracks, show a marked change across the Okahandja Lineament Zone with older ages to the south-east. This suggests that slower cooling north-west of the Lineament Zone are possibly due to:

(i) higher geothermal gradient north-west of the Lineament;

(ii) uplift south-east of the Lineament;

(iii) continued heat supply north-west of the Lineament.

Pressures determined (Section 8) suggest that the depth of M_2 metamorphism in the Trough Zone was $26{,}6\pm4{,}4$ km, whilst the depth of emplacement of the Donkerhuk Granite was $16{,}7\pm3{,}6$ km. Hence an uplift of about 10 km (assuming mean density=2,80 g. cm^{-3}) took place after M_2 and before 528 Ma (Haack 1977), the age of the Donkerhuk Granite, thus giving a more precise age to the uplift than the 485-Ma limit set by Haack and Hoffer (1976).

It is also noted that the pressure obtained for the metamorphism in the Okahandja Lineament Zone and that for the Donkerhuk Granite (Section 8) are of the same order, thus the uplift must have occurred at the very eastern boundary of the Okahandja Lineament Zone (Fig. 1.1) where it adjoins the Trough Zone, a site now occupied by the Donkerhuk Granite, which may have used the crustal discontinuity as a locus for its ascent.

Since the age of the Donkerhuk Granite is known all that is required to calculate the rate of uplift is the date of the M_2 metamorphic event. It is known that M_2 must

be older than 550 Ma (age of post-tectonic Salem Granite). If an age of 560 Ma is assumed for M_2 the rate of uplift is approximately 300 m per million years, a rate comparable with the Upper Triassic uplift in the Appalachians or the Eocene to Recent uplift of the Himalayas (Sutton 1969).

Detailed mapping along a traverse from Okahandja to Windhoek enabled Hälbich (1977) to present clear evidence that the subvertical schistosity of the Okahandja Lineament Zone is overprinted by the main schistosity of the Trough Zone. Some 200 km to the south-west in the area mapped, the subvertical schistosity of the Okahandja Lineament Zone is considered to post-date the main schistosity of the Trough Zone. Blaine (1977) shows in his Figure 30 the subvertical schistosity of the Okahandja Lineament Zone (termed by him a metamorphic banding cleavage) to post-date the tight-inclined folding of the Khomas Trough below the basal unconformity of the fore-arc deposits. Within the Okahandja Lineament Zone pre- and syn-D_{L3} granites (Salem and Aussinanis) are common in the Gobabeb area, whereas Blaine (1977) observes no such granites. Thus with reference to Blaine (1977, Fig. 30b) the conflicting observations of Hälbich (1977) and the author can be reconciled by considering Hälbich to have mapped structural relations within the fore-arc basin deposits, and the present study to have examined structural relationships below the fore-arc basin metasediments at a deeper structural level.

The structural elements associated with D_{C1}, D_{C2} and D_{C3} are essentially the same as those observed by Jacob (1974). However, he (p. 37) considers that his F_1 folds produced two foliations, one (S_0) parallel to bedding (SS) and the other (S_1) axial-planar to F_1, i.e. these two fabrics would be perpendicular in F_1 hinges. The contention of two fabrics forming at right-angles during the same fold-forming event is untenable (Dieterich 1969, 1970; Hudleston 1973a, 1973b; Ramsay 1967; Ramsay and Graham 1970). It is preferred to consider the S_0 fabric of Jacob (1974) to result from a deformation event and term this fabric element S_1 belonging to the D_{C1} deformation. Thus F_1 and F_2 of Jacob (1974) correspond to D_{C2} and D_{C3} of this study.

Bickle and Coward (1977) show the existence of large-scale thrusting along the southern edge of the Khomas Trough, a feature indicative of considerable crustal shortening, as determined for the Trough Zone.

The location of the Al_2SiO_5 triple point has long been a topic of controversy. Experimental data are in fair agreement for the andalusite $\rightleftharpoons$ kyanite and the sillimanite $\rightleftharpoons$ kyanite reaction boundaries (Anderson *et al.* 1977). The andalusite $\rightleftharpoons$ sillimanite boundary has been variously determined, Richardson *et al.* (1969), Althaus (1967), and Holdaway (1971) being the most quoted.

The use of field data, e.g. Froese and Gasparini (1975), has been made to determine the location of the triple point. The data in Section 8 indicate that andalusite $\rightleftharpoons$ sillimanite reaction boundary lies between those of Richardson *et al.* (1969) and that of Holdaway (1971).

9.3 DISCUSSION OF A MODEL FOR THE DAMARA OROGENIC BELT

It has been noted by Martin and Porada (1977) and Kröner (1977) that the Damara Orogen consists of three arms, two essentially parallel to the coast, and a third striking roughly east-north-east (the so-called intracratonic arm), with the hypothetical triple junction being off the present coastline. The area investigated lies entirely within the 'intracratonic arm'.

The authors mentioned above all consider the intracratonic branch of the Damara to be an aulacogen or rift-like system in which a cratonic area has rifted into a sequence of parallel graben structures, of which the Trough Zone is perhaps the most important. The aulacogen model is considered below.

Martin and Porada (1977) consider the site of Nosib sedimentation to be a graben structure, and cite palaeocurrent data which indicate infilling of the basin. During Kuiseb times however, they postulated thick schists to be deposited on the adjacent horsts, which ultimately became the Khomas Trough. Several questions arise: firstly, if the Nosib grabens filled with sediment derived from adjacent horsts, where did the material for the Kuiseb Formation come from? Secondly, the proposed model requires that structures that were grabens originally ultimately become horsts, and that horsts become grabens. The vertical movement being of the order of 20 km, what process is involved in generating such extreme reversals of uplift?

The palaeocurrent data of Martin and Porada (1977) are considered suspect, since within the mapped area cross-laminations and cross-bedding in the Nosib at the eastern edge of the Central Zone indicate westward or northerly source areas (Sawyer 1979). Furthermore, evidence from the Karibib Formation and Tinkas Member suggests a transport direction from the west. It is therefore contended that the Central Zone was always a positive area with respect to the Khomas Trough during the Damaran orogenesis.

In contrast, Kröner (1977) states that particular lithostratigraphic units are continuous across the whole orogen. This is possibly true of the Chuos Formation but for the other formations there is no positive correlation between Central Zone rocks and Southern Margin rocks. Similarities are outweighed by dissimilarities, i.e. the Auas quartzite is confined to the Southern Margin whilst the Tinkas Member is confined to the eastern edge of the Central Zone. Martin and Porada (1977) and Kröner (1977) base their correlation of the Damara stratigraphy on similarity of lithology, always a dubious method in highly deformed terrains with a complicated sedimentological history. Kröner (1977) following Miller (1973) considers that large volumes of granodioritic and adamellitic intrusives (i.e. the Salem Granite) are derived from partial melting of the Kuiseb Formation. Yet field evidence especially in the area mapped shows the Salem to be largely intrusive into the Kuiseb Formation. Miller* now considers the Salem Granite Suite to be at least of lowermost crustal origin. The deep-level origin, range of compositions, zonation, age spread and size of the Salem Granite indicate a similarity with batholiths such as the Sierra Nevada.

The presence or absence of continental crust below the Khomas Trough during the Damaran orogenesis is crucial to the aulacogen model, since all well-documented examples, (Hoffmann *et al.* 1974) are floored by an unbroken layer of granitic crust. Furthermore, true aulacogens are devoid of ultramafic rocks. Whilst there is no direct geophysical evidence of oceanic crust flooring the Khomas Trough, the presence of alpine-type serpentinites† strongly suggests the presence of oceanic crust during the Damaran orogenesis. The presence of ultramafic rocks immediately separates the Damara Belt from a true aulacogen.

The model of Martin and Porada (1977) requires rifting accompanied by acid volcanism in parts of the

* Personal communication: R. McG. Miller.

† Personal communication: S. J. Barnes.

Nosib sequence. They consider rifting with an asthenolith cushion developed but their scheme allows only moderate crustal extension (10 per cent in the Kenya rift, Bailey 1972) which after Damara deformation and closing cannot adequately explain the observed degree of deformation (50–80 per cent shortening) in the Trough Zone and large-scale thrusting along the Southern Margin (Bickle and Coward 1977).

Secondly, heating comes from below the crust, yet the oldest granites formed – the Salem Granite Suite – are considered by Kröner (1977) as having developed from the top of the sedimentary pile, dismissing any deeper origin. If near-surface temperatures were high enough to partially melt large amounts of sediment (ca 720 °C) why did the Red Granites not form then, as its source-rock was at still deeper levels, rather than at about 550 Ma ago? The Red Granites would thus have been pre- or syn-tectonic.

There is, in conclusion, no adequate explanation for two metamorphic events some 100 Ma apart. The degree of deformation permissible in the aulacogen model seems to be far too low for that observed. The generation of large volumes of Salem Granite is not adequately explained, nor is the late formation of the Red Granites. Lastly, there is no proof that continental crust floored the Khomas Trough, rather evidence favours a floor of oceanic material. The aulacogen model is thus seen to be wanting.

One alternative lies in a plate-tectonic model leading to continent–continent collision. Evidence for continental rifting during the Nosib is poor, the Naauwpoort volcanics suggested to belong to the graben or rifting episode of Martin and Porada (1977) actually interfinger with Ugab and Chuos metasediments in the Fransfontein area (South African Committee for Stratigraphy 1978, Table 4 in prep.) making a correlation with a rifting episode suspect. Furthermore, pre-Damara rocks of the Southern Margin (De Waal 1966) and those of the Central Zone (Blaine 1977; Sawyer 1979) have distinctly different sedimentological and deformational histories. Bailey (1972, 1974) notes that intracratonic rifting is often, but not always, accompanied by alkali magmatism. Assuming rifting to have occurred, then a period of spreading leading to the creation of oceanic crust is postulated, the resulting ocean taking the site of the Khomas Trough. During the spreading phase the Central Zone and the southern margin of the Khomas Trough developed their own characteristic sedimentary sequences, having only the Chuos Formation in common. The Central Zone sedimentation was generally of shallow-water type with turbidite sequences being deposited in deeper water of the Okahandja Lineament Zone continental slope.

Generation of the first granites of the Salem Suite approximately 700 Ma ago indicates the early history of the northward-dipping subduction zone beneath the Central Zone. As heat was conducted or convected up into the crust and sedimentary pile, the M_1 metamorphic event took place. During heating it can be expected that the rocks would become ductile, and flow, giving rise to the sub-similar recumbent folds of F_1 and F_2 (Central Zone and Okahandja Lineament Zone) in the manner of Hudleston (1977).

A period of relative quiescence followed M_1 until renewed plate descent caused the D_{C3} and D_{L3} deformations and related M_2 event during the final stages of closure, plate descent occurring at the same site as for M_1. Mitchell and Reading (1971) note that intermittent plate descent may lead to narrow zones of differing structural trends. Hartnady (1977) and Porada and Wittig (1975) have recognised several linear belts of differing tectonic style within the Khomas Trough.

During M_2 a region of high-geothermal gradient was separated from a region of low-geothermal gradient by the eastern edge of the Okahandja Lineament Zone. Disregarding the post-tectonic Donkerhuk Granite, Damara granites occur only in and west of the Okahandja Lineament Zone, making the comparison with paired metamorphic belts separated by a median tectonic line (e.g. Japan and New Zealand, Miyashiro 1973, 1973a) more striking. In this case the median tectonic line is represented by the eastern edge of the Okahandja Lineament Zone. The Central Zone metamorphic conditions with large granite intrusions correspond well with those expected beneath a volcanic arc (Mitchell and Reading 1971, Table 1). The distribution of geothermal gradients across the Damara (Fig. 9.2) shows a pattern typical of that found in plate tectonic environments (Miyashiro 1973, Fig. 2; Ernst 1974, Figs 1 and 3).

Martin and Porada (1977) ask the pertinent question for a plate-tectonic model: "Where is the suture line?" Miyashiro (1973a) and Turcotte and Oxburgh (1972) show that high-pressure metamorphism takes place in the down-going slab, that is, in or near the trench. Thus the Trough Zone rocks and those further to the east on the Southern Margin with similar geothermal gradients must have been near to the trench. The low-pressure metamorphic belt occurs on the continent side of the high-pressure belt (Miyashiro 1973, 1973a; Mitchell and Reading 1971; Ernst 1974). The metamorphic pattern dictates that the trench must lie east of the Okahandja Lineament Zone. The south-easternmost position of the trench would be the pre-Damara outcrop of Rostock. The occurrence of serpentinite and talc schist on the farm Schlesien 483, together with large-scale thrusting in the Hakos–Rostock area (Bickle and Coward 1977) having a north-over-south sense may indicate that the suture zone lies along the northern edge of the Hakos Anticline of De Waal (1966). The suture line would be placed close to the red band (De Waal 1966) and its continuation eastwards. In the Windhoek area and further eastwards the suture line follows a line of ultramafic intrusions extending as far east as Amerongen 181, Windhoek District, and passing just north of the Rietfontein and Seeis Inliers. The proposed trace of the suture zone separates two distinctly different structural zones, the Trough Zone and the Southern Margin (Hartnady 1977).

If the highest regional metamorphism in the Central Zone is considered to mark the centre of the volcanic arc (Ernst 1974) then the distance to the eastern edge of the Okahandja Lineament Zone in the area mapped is 80 km. Allowing for 50–80 per cent crustal shortening during D_{C3} and D_{L3} the arc-trench gap becomes 280 ± 120 km giving reasonable agreement with the computed thermal structure in a convergent plate (Turcotte and Oxburgh 1972; Ernst 1974, Fig. 3).

The eastern edge of the Okahandja Lineament Zone in the area mapped has the characteristics of a median tectonic line (Miyashiro 1973a), being a subvertical line of uplift. The origin for the uplift and hence the " median tectonic line" may be the isostatic rebound associated with partial subduction of continental crust belonging to the southern continental block. During the process of final closure a considerable amount of pelite was drawn down into the subduction zone. However, since the geothermal gradient in the Southern Margin rocks is low and the rocks underwent high-pressure metamorphism (7 kb) it is apparent that these too were deeply buried. It is considered that during the final stages of closure of the Damara Orogen the southern continent's leading edge of

Table 9.1—SUGGESTED SEQUENCE OF EVENTS IN THE HISTORY OF THE DAMARA OROGEN

1. Deposition of early Nosib on gneissic basement; possible rifting.
2. Deposition of Nosib complete, local uplift and erosion give rise to many unconformities; Chuos deposition; formation of oceanic crust.
3. Uplift and minor folding before deposition of Karibib Formation in shallow sea on the northern continent (Central Zone). Tinkas deposited on continental slope; separate sedimentation on southern continent.
4. Matchless Member volcanism during deposition of Kuiseb Formation at margins to ocean basin.
5. Beginning of ocean closure.
6. 700–600 Ma: Heating of Central Zone (northern continent) by a north-westward-dipping subduction zone; intrusion of early granites of the Salem Suite (700 Ma); D_1 and D_2 with M_1 metamorphism; emplacement of serpentinites.
7. 560 Ma: Final closure of ocean, D_3 deformation in Central Zone and Okahandja Lineament Zone; thrusting in Trough Zone; overriding of leading edge of southern continent by northern continent; deep burial of granitic crust of southern continent.
8. 550–528 Ma: Isostatic rebound of Trough Zone and Southern Margin of Orogen; uplift of 10 km accomplished before 528 Ma; formation of subvertical lineament (median tectonic line) at eastern edge of the Okahandja Lineament Zone due to Trough Zone uplift against northern continent.
9. 528–475 Ma: Late thermal event responsible for formation of Donkerhuk Granite and late alaskite emplacement in Central Zone.
10. Erosion and uplift of orogen.

granitic crust (Southern Margin) was pulled by the downgoing slab (Molnar and Gray 1979) and was overridden by the northern (Central Zone) continental crust and hence forced to considerable depth (>26 km). After compression had ceased and the downgoing slab of oceanic lithosphere had separated from the continental lithosphere (Fig. 9.3), the low-density granitic and pelitic rocks were rapidly uplifted and the 'median tectonic line' marks the western edge of that uplift against the continental crust of the northern continent.

Expression of the uplift at the western edge of the Trough Zone as a deformation in the Okahandja Lineament Zone is considered to be the D_{L5} breccia bands and reworking of S_3 schistosity planes into locally very thin slate-like cleavage sheets. Kojima and Suzuki (1958) describe such a fabric associated with the Sanbagawa metamorphic median tectonic line in Japan.

In an active subduction zone, the sediments passing into the trench are pushed upwards into a higher temperature/lower pressure environment, being welded to the continental plate, in this case the Central Zone/Okahandja Lineament Zone. In the area mapped this process of adding material to the low-pressure side of the trench may account for the width of the Okahandja Lineament Zone (30 km) east of the Tinkas Member. Furthermore, this process may explain the bladed andalusite porphyroblasts, by considering these to have been inverted from kyanite after passing through the trench, being uplifted and welded to the Central Zone crust. In a continent–continent collision it is common for the subducting oceanic slab to drag continental crust down with it into the subduction zone as in the Zagros Mountains (Bird *et al.* 1975). Detachment of the oceanic slab near to the leading edge of the subducted crust terminates the downward motion of the subducted continental crust, allowing it to rise by isostatic rebound. The process of detachment and sinking of the oceanic slab enables hot asthenosphere to upwell and heat the base of the crust causing a thermal event in the crust (Bird *et al.* 1975; Toksoz and Bird 1977). This late, post-tectonic event is considered responsible for the formation of the Donkerhuk Granite and perhaps the late Rössing alaskites as well.

The sequence of events outlined above is summarised in Table 9.1.

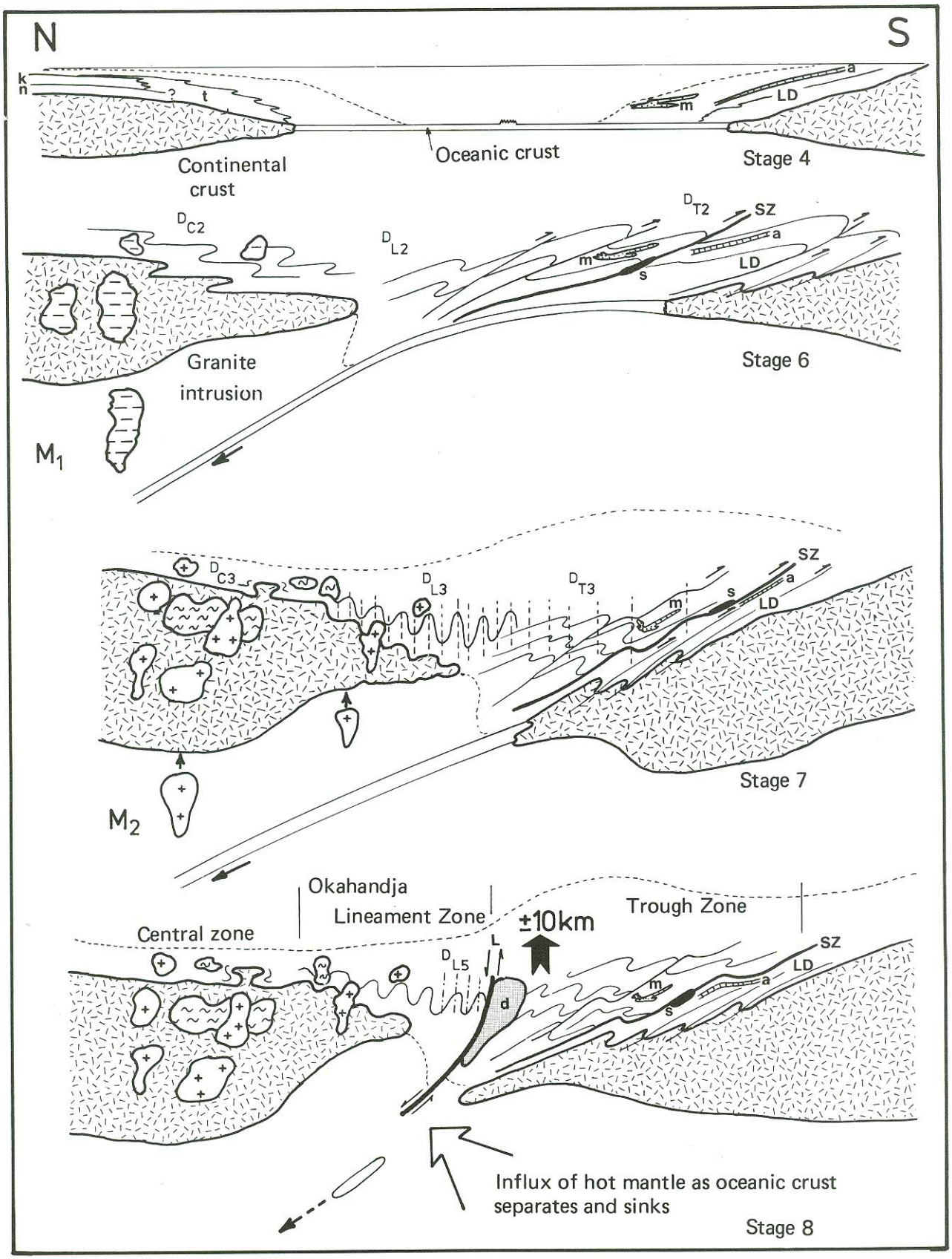

LEGEND : **n – Nosib Group, k – Karibib Formation, t – Tinkas Member, m – Matchless Member, a – Auas quartzite, s – serpentinite (e.g. Schlesien), d – Donkerhuk Granite, SZ – Suture Zone, L – line of uplift (median tectonic line) at eastern edge of the Okahandja Lineament Zone, LD – Lower Damara succession of the southern margin.**

Fig. 9.3 – Suggested sequence of events in the evolution of the Damara Mobile Belt shown schematically (not to scale) at Stages 4, 6, 7 and 8 respectively of Table 9.1.
Skematiese voorstelling van opeenvolging van gebeure in die evolusie van die Damara Mobiele Gordel (nie volgens skaal nie) op Stadiums 4, 6, 7 en 8 onderskeidelik van Tabel 9.1.

APPENDICES

I. MINERAL FORMULAE AND REACTION EQUILIBRIA

Abbreviations for solid-solution minerals mentioned in Appendix I

cordierite=cord staurolite=staur white mica=w.mica garnet=gnt biotite=bte plagioclase=plag

Mineral compositions and abbreviations

Almandine.....	alm.....	$Fe_3 Al_2 Si_3 O_{12}$
Annite.....	ann.....	$K Fe_3 AlSi_3 O_8 (OH)_2$
Anorthite.....	anorth.....	$Ca Al_2 Si_2 O_8$
Fe cordierite.....	Fe cord....	$Fe_2 Al_4 Si_5 O_{18} \cdot nH_2O$
Mg cordierite.....	Mg cord...	$Mg_2 Al_4 Si_5 O_{18} \cdot nH_2O$
Grossular.....	gross.....	$Ca_3 Al_2 Si_3 O_{12}$
K feldspar.....	Kfsp.....	$K AlSi_3 O_8$
Kyanite.....	Ky.....	Al_2SiO_5
Muscovite.....	musc.....	$K Al_3 Si_3 O_{10} (OH)_2$
Phlogopite.....	phl.....	$KMg_3 AlSi_3 O_{10} (OH)_2$
Pyrope.....	py.....	$Mg_3 Al_2 Si_3 O_{12}$
Quartz.....	qtz.....	SiO_2
Sillimanite.....	Silli.....	Al_2SiO_5
Fe staurolite.....	Fe staur...	$2 Fe_2 Al_9 Si_{3,75} O_{22} (OH)_2$
Fe biotite (III,VIII)		$K_{0,84} Fe_{2,52} Al_{1,72} Si_{2,74} O_{10} (OH)_2$
Mg biotite (III)...		$K_{0,84} Mg_{2,52} Al_{1,72} Si_{2,74} O_{10} (OH)_2$

$\triangle G^\circ_{P,T}$ —standard state Gibbs energy of reaction at the P and T of interest.

$\triangle H^\circ_{1,T}$ —enthalpy of the reaction at one bar and T of interest.

$\triangle S^\circ_{1,T}$ —entropy of the reaction at one bar and T of interest.

$\triangle V^\circ_{solids}$—volume change of reaction at one bar and 298 °K assuming volume changes of reactions are not functions of pressure and temperature.

A. GENERAL

Consider the reaction: $bW+cX \rightleftharpoons dY+eZ$

Then at equilibrium,

$$\triangle G^\circ_{P,T} = -RT\ 1n \left(\frac{(a^y_Y)^d \quad (a^z_Z)^e}{(a^w_W)^b \quad (a^x_X)^c} \right) = -RT\ lnK = 0$$

where a^y_Y refers to the activity of component Y in pure phase y, also,

$$\triangle G^\circ_{P,T} = \triangle H^\circ_{1,T} - T\triangle S^\circ_{1,T} + (P-1)\ \triangle V^\circ_{1,298} = 0$$

at equilibrium i.e.

$$\triangle G^\circ_{P,T} = \triangle H^\circ_{1,T} - T\triangle S^\circ_{1,T} + (P-1)\ \triangle V^\circ_{1,298} + RT\ lnK = 0$$

Let the mineral $A_nF_mSi_xO_y$ be a component of the solid solution series

$$(A,B,C)_n(D,E,F)_mSi_xO_y$$

Then assuming ideal solution, the activity of the solid solution is:

$$a^{(A,B,C)_n\ (D,E,F)_mSi_xO_y}_{A_n\ F_m\ Si_x\ O_y} = (X_A)^n(X_F)^m$$

where $X_A = \left(\frac{A}{A+B+C}\right)$ and $X_F = \left(\frac{F}{D+E+F}\right)$

see Wood and Fraser (1976).

Now the general equation at equilibrium for an H_2O-producing reaction is:

$$\triangle G^\circ_{P,T} = \triangle H^\circ_{1,T} - T\triangle S^\circ_{1,T} + (P-1)\ \triangle V^\circ_{solids} + RT\ ln f_{H_2O} + RT\ lnK = 0$$

rearranging

$$ln f_{H_2O} \cdot X_{H_2O} = \left(\frac{-\triangle H^\circ_{1,T} + T\triangle S^\circ_{1,T} - (P-1)\ \triangle V^\circ_{solids}}{RT} \right) - lnK$$

hence

$$X_{H_2O} = \frac{\exp\left(\frac{-\triangle H^\circ_{1,T} + T\triangle S^\circ_{1,T} - (P-1)\ \triangle V^\circ_{solids}}{RT} \right) - lnK}{f_{H_2O}}$$

B. REACTION EQUILIBRIA

I. 3 anorthite $\rightleftharpoons$ grossular + 2 kyanite + quartz

$$3 \ln\left(\frac{X^{gnt}_{gross}\ \gamma^{gnt}_{gross}}{X^{plag}_{anorth}\ \gamma^{plag}_{anorth}}\right)=\frac{7\,444}{T}-19{,}38+\frac{0{,}7947\ (P-1)}{T}$$

Data: D. Waters (pers. comm.); see also Ghent (1975, 1976 and 1978); γ^{plag}_{anorth} from Orville (1972);

$\ln\ \gamma^{gnt}_{gross}=\frac{(1-X^{gnt}_{gross})^2 W}{RT}$ Ghent (1976); W = 950 cal. mol.$^{-1}$ Schmid and Wood (1976).

II. almandine + muscovite $\rightleftharpoons$ annite + 2 kyanite + quartz

$$\triangle G^{\circ}_{P,T}=\triangle H^{\circ}_{1,T}-T\triangle S^{\circ}_{1,T}+(P-1)\ \triangle V^{\circ}_{solids}+RT\ln\left(\frac{a^{bte}_{ann}}{a^{gnt}_{alm}\ a^{w.mica}_{musc}}\right)=0$$

$\triangle V^{\circ}_{solids}=0{,}2199$ cal. bar^{-1}

$\triangle S^{\circ}_{1,T}=0{,}45\pm0{,}55$ cal. mol.$^{-1}$ deg.$^{-1}$

$\triangle H^{\circ}_{1,T}=2\,550\pm45$ cal. mol.$^{-1}$

$$a^{gnt}_{alm}=(X^{gnt}_{Fe})^3,\qquad a^{bte}_{ann}=(X_K)(X^{oct}_{Fe})^3(X_{Si})^3,\qquad a^{w.mica}_{musc}=(X_K)(X^{oct}_{Al})^2(X_{Si})^3$$

Data: D. Waters (pers. comm.).

III. 1/2,52 Mg biotite + 1/3 almandine $\rightleftharpoons$ 1/2,52 Fe biotite + 1/3 pyrope

$$\triangle G^{\circ}_{P,T}=6\,150-3{,}93\ T+0{,}0246\ P+RT\ln K_D=0$$

where $$K_D=\frac{X^{bte}_{Fe}\ X^{gnt}_{Mg}}{X^{bte}_{Mg}\ X^{gnt}_{Fe}}$$

Data: Holdaway and Lee (1977).

IV. 6 Fe staurolite + 25 quartz $\rightleftharpoons$ 8 almandine + 46 kyanite + 12 H_2O

$$\triangle G^{\circ}_{P,T}=296\,653-463{,}0\ T-7{,}1076(P-1)+12\ RT\ln f_{H_2O}+24RT\ln\left(\frac{X^{gnt}_{alm}}{X^{staur}_{Fe\ staur}}\right)=0$$

$\triangle S^{\circ}_{1,T}=465\pm55$ cal. mol.$^{-1}$ deg.$^{-1}$

$\triangle H^{\circ}_{1,T}=298\,727\pm53\,305$ cal. mol.$^{-1}$

$$a^{gnt}_{alm}=(X^{gnt}_{Fe})^3,\qquad a^{staur}_{Fe\ staur}=(X^{staur}_{Fe})^4$$

Data: Ganguly (1972); Richardson (1968).

VI. 1/2 Mg cordierite + 1/3 almandine $\rightleftharpoons$ 1/2 Fe cordierite + 1/3 pyrope

$$\triangle G^{\circ}_{P,T}=6\,150-2{,}69\ T+0{,}0303\ P+RT\ln K_D=0$$

where $$K_D=\frac{X^{cord}_{Fe}\ X^{gnt}_{Mg}}{X^{cord}_{Mg}\ X^{gnt}_{Fe}}$$

Data: Holdaway and Lee (1977).

Also 3 Fe cordierite + 2 pyrope $\rightleftharpoons$ 3 Mg cordierite + 2 almandine (i.e. 6 times VI)

$$\triangle G^{\circ}_{P,T}=-40\,291+15{,}88T+0{,}1768(P-1)+RT\ln\left(\frac{(a^{cord}_{Mg\ cord})^3\ (a^{gnt}_{alm})^2}{(a^{cord}_{Fe\ cord})^3\ (a^{gnt}_{py})^2}\right)=0$$

$\triangle V^{\circ}_{solids}=0{,}1768$cal. bar.$^{-1}$

$\triangle S^{\circ}_{1,T}=15{,}88\pm2$cal. mol.$^{-1}$deg.$^{-1}$

$\triangle H^{\circ}_{1,T}=40\,291\pm2\,000$cal. mol.$^{-1}$

where $a^{cord}_{Mg\ cord}=(X_{Mg})^2$, $a^{cord}_{Fe\ cord}=(X_{Fe})^2$, $a^{gnt}_{py}=(X_{Mg})^3$, $a^{gnt}_{alm}=(X_{Fe})^3$

Data: Wells (1976).

VII. 3 Fe cordierite. $3nH_2O \rightleftharpoons 2$ almandine $+4$ sillimanite $+5$ quartz $+3nH_2O$

$$\triangle G^{\circ}_{P,T} = 30\,837 - 41{,}3\,T - 4{,}0061\,(P-1) + 1{,}5\,RT \ln f_{H_2O} + RT\left(\frac{(a^{gnt}_{alm})^2}{(a^{cord}_{Fe\ cord})^3}\right) = 0$$

$\triangle V^{\circ}_{solids} = -4{,}0061$ cal. bar.$^{-1}$ $\quad n = 0{,}5$

$\triangle S^{\circ}_{1,T} = 41{,}3 \pm 5{,}8$ cal. mol.$^{-1}$deg.$^{-1}$

$\triangle H^{\circ}_{1,T} = 30\,837 \pm 5\,500$ cal. mol.$^{-1}$

$a^{gnt}_{alm} = (X_{Fe})^3$, $\quad a^{cord}_{Fe\ cord} = (X_{Fe})^2$

Data: Holdaway and Lee (1977).

Also: $\triangle G^{\circ}_{P,T} = 28\,394 - 38{,}2T - 3{,}95\,(P-1) + 1{,}5\,RT\,1n f_{H_2O} + 6\,RT \ln\left(\frac{X^{gnt}_{Fe}}{X^{cord}_{Fe}}\right) = 0$

$\triangle V^{\circ}_{solids} = -3{,}95$ cal. bar.$^{-1}$ $\quad n = 0{,}5$

$\triangle S^{\circ}_{1,T} = 37{,}9 \pm 4{,}5$ cal. mol.$^{-1}$ deg.$^{-1}$

$\triangle H^{\circ}_{1,T} = 28\,165 \pm 4\,410$ cal. mol.$^{-1}$

Data: Weisbrod (1973, 1973a).

VIII. Fe biotite $+2{,}08$ sillimanite $+4$ quartz $\rightleftharpoons 1{,}26$ Fe cordierite $+0{,}84$ K feldspar $+(1-1{,}26n)\ H_2O$

$$\triangle G^{\circ}_{P,T} = 11\,599 - 20{,}12T + 1{,}0024(P-1) + 0{,}37RT \ln f_{H_2O} + RT \ln\left(\frac{(a^{cord}_{Fe\ cord})^{1{,}26}\ (a^{K\ fsp}_{KAlSi_3O_8})^{0{,}84}}{(a^{bte}_{Fe\ bte})}\right) = 0$$

$\triangle V^{\circ}_{solids} = 1{,}0024$ cal. bar.$^{-1}$ $\quad n = 0{,}5$

$\triangle S^{\circ}_{1,T} = 20{,}12 \pm 3{,}59$ cal. mol.$^{-1}$ deg.$^{-1}$

$\triangle H^{\circ}_{1,T} = 11\,599 \pm 3\,403$ cal. mol.$^{-1}$

$a^{cord}_{Fe\ cord} = (X_{Fe})^2$, $\quad a^{K\ fsp}_{KAlSi_3O_8} = (X_K)$, $\quad a^{bte}_{Fe\ bte} = (X_K)(X^{oct}_{Fe})^3$ Thompson (1976).

Data: Holdaway and Lee (1977).

IX. 4 annite $+3$ Fe cordierite $+3$ quartz $\rightleftharpoons 6$ almandine $+4$ K feldspar $+5{,}5\ H_2O$

$$\triangle G^{\circ}_{P,T} = 146\,360 - 214{,}66T - 6{,}4351(P-1) + 5{,}5RT \ln f_{H_2O} + RT \ln\left(\frac{(a^{gnt}_{alm})^6\ \ (a^{K\ fsp}_{KAlSi_3O_8})^4}{(a^{bte}_{ann})^4\ \ (a^{cord}_{Fe\ cord})^3}\right) = 0$$

$\triangle V^{\circ}_{solids} = -6{,}4351$ cal. bar^{-1}

$\triangle S^{\circ}_{1,T} = 214{,}66 \pm 32{,}7$ cal. mol.$^{-1}$ deg.$^{-1}$

$\triangle H^{\circ}_{1,T} = 146\,360$ (± 148 at $S = 214{,}66$) cal. mol.$^{-1}$

$$a^{cord}_{Fe\ cord} = (X_{Fe})^2, \quad a^{K\ fsp}_{KAlSi_3O_8} = (X_K), \quad a^{gnt}_{alm} = (X_{Fe})^3, \quad a^{bte}_{ann} = (X_K)\ (X_{Fe})^3$$

Data: D. Waters (pers. comm.) after Holdaway and Lee (1977).

A. MINERAL ASSEMBLAGES (Tables 11a–11h)

Table IIa – TROUGH ZONE PELITES

	97	111	112	115	116	233	235	236	237	239	316	693	694	695	231	327
quartz	O	+	X	O	X	X	O	X	X	X	X	O	X	X	X	X
plagioclase	O	X	X	X	X	X	X	X	X	X	X		X	X	X	X
biotite	X	X	X	X	X	X	X	X	X	X	X	X	X	X	X	O
garnet	O	+		X	O		X			O	O	O	O	O	O	O
staurolite	X	X		X			X				X	X		O	X	
kyanite	X	O		O			O				O					
muscovite	X	X	X	X	X	X	X	+	O	O	O	X	O	+	X	
chlorite	X	O		O					+		O	O	+			
graphite	+				X			+	X				+	+	+	
opaque ore	O	+	+	O	+	+	+	+	+		+	O	+	+	O	+
apatite			+			+	+	+	+		+		+		+	
tourmaline			+	+		+	+	+	+		+		+	+	+	
zircon	+	+	+	+	+	+	+	+	+	+	+	+	+			
cummingtonite																X

X abundant (> 5%); O minor (1–5%); + trace (< 1%)
Sample localities shown on Folder 2.1.

Table IIb – TROUGH ZONE MATCHLESS MEMBER

	120	121	122	123	229	320	328	365	119	230	697	699	118	234	317	323		691		695A
quartz	X	X	X	X	X	X	X	X	O	X	X	+	X	X	X	O		O		+
plagioclase	X	X	X	X	X	X	X	X	X	X	X	X	X	X	X	X				O
hornblende	X	X	X	X	X	X	X	X	X	X	X	X	X	X	X	X		X		X
anthophyllite																				X
clinopyroxene						X		X								X				
epidote	+		O	+	X	X	+	+	O	X						X		X		
clinozoisite		X					+			+			X							
sphene		O	X	X	O	+	O	O	O	+	X	O	O	+	O	O		O		
opaque ore	X									+		O			O					
carbonate		X				X			O	O		O	X					X		
scapolite						X														
chlorite																				X
talc																				+

amphibole schists — metagabbro

X abundant (> 5%); O minor (1–5%); + trace (< 1%)
Sample localities shown on Folder 2.1.

Table IIc – TROUGH ZONE CALC SILICATES (359–113) AND OKAHANDJA LINEAMENT ZONE CALC SILICATES (39–68: TINKAS MEMBER; 33–592: KUISEB FORMATION)

	39	47	50	64	80	440	452	527	636	646	647	68	33	35	56	281	591	592		359	586	700	113
quartz	X	X	X	X	X	X	X	X	X	X	X	X	X	X	X	X		X		X	X	X	X
microcline							X	O		+						X	O				O		
plagioclase	X		X	X	X	X	O	X	X	X	X	X	X	X	X	X	X	X		X	X	X	X
biotite	O			O		O	O				O	X			X			X		O			X
garnet	O								X					X	X							X	X
hornblende	X		X	O	X	X			X	X	X		X					X		O		X	X
tremolite		+					X	O						X		X	O				X		O
clinopyroxene						X	X	X	X				+			X	X			O	X	X	
carbonate	+	+		X		O	X	X	X	X	O	X		X		X	O			O	X		X
epidote		X	X		X	X		+		O			O							O			
clinozoisite			X	+	X	+				O						+				O	O		+
chlorite	+	X		X			O				O	X		O	+					O			O
sphene	+		+				+	+	O	O	O		+	O				+		O	O	+	+
opaque ore			+	+			+			+	+	+		+	O		+						+
scapolite																+	X				X		
white mica				+								+			+								+

X abundant (> 5%); O minor (1–5%); + trace (< 1%)
Sample localities shown on Folder 2.1.

Table IId – OKAHANDJA LINEAMENT ZONE PELITES (604 from a breccia band)

	34	40	41	48	66	70	156	276	279	280	436	439	538	631	16	28	31	32	57	62	578	604	658	660	662	663
quartz	X	X	X	X	X	X	X	X	X	X	X	X	X	X	X	X	X	X	X	X	X	X	X	X	X	X
microcline			X		O	O			O		X															
plagioclase	X	X	X	O	X	X	X	X	O	O	X		O	O	X		X	X		O		X	X	X	X	O
biotite	X	X	X	X	X	X	X	X	X	X		X	X	X	X	X	X	X	X	X	X		X	X	X	X
muscovite			X	O	O	O	+	O	O		+	O	X	X	+	X	X		X	X	X	X	X	X		X
andalusite				X						X		X	O	X					X				X	O		
cordierite	X			O						O		X	O	O		X								X	X	X
garnet	+							O																		
staurolite																								+		+
chlorite					O	+		+			X			O							O	O				
carbonate					X	O		+														X				
graphite							O	+																		
opaque ore	+	+	+	+	+	+			+	+	O	O			+	O	+	+	+				+	+	+	+
apatite	+		+						+								+						+	+		+
tourmaline	+	+			+							+				+	+		+				+			+
	Tinkas Member														Kuiseb Formation											

X abundant (> 5%); O minor (1–5%); + trace (< 1%)
Sample localities shown on Folder 2.1.

Table IIe – CENTRAL ZONE AND OKAHANDJA LINEAMENT ZONE MARBLES

	170	175	192	212	256	470		43	44	65	67	82
carbonate	X	X	X	X	X	X		X	X	X	X	X
quartz	+							O	O	O	O	+
plagioclase					+						O	+
white mica	+	+			O	O						
phlogopite					O					O	O	
talc								+	+	+	+	+
tremolite		O		O		O						
forsterite		X	X	X		X						
chondrodite			O	X								
garnet						O						
chlorite			O								O	
antigorite		X	O	X		X						
scapolite									+			
	Central Zone							Okahandja Lineament Zone				

X abundant (> 5%); O minor (1–5%); +trace (< 1%)
Sample localities shown on Folder 2.1.

Table IIf – CENTRAL ZONE FELDSPATHIC QUARTZITES AND PELITES

	88	89	90	91	92	181	184	260	614	615	635		190		722		453	472	543		447		465	728	729	733
quartz	X	X	X	X	X	X	X	X	X	X	X		X		X		X	X	X		X		X	X	X	X
microcline	X	X	X	X	X	X	X	X		X	O		O				O	X	X		O		X	X	X	X
plagioclase							O	X	O		O		O		X		O	X	X		X		X	X	X	X
biotite	O	O	+	O	+		O						O				X	X	X		X		X	X	X	X
muscovite	+	+	O	O	O	+	O	+	O	O	O						X	+	+		+		+	+	+	+
cordierite																					X		X	X	X	X
garnet																							O	O	O	
sillimanite			O	O	O			+	+	O			X				X	O	+		+		O			O
opaque ore	O	+		O	+			+	+		+		X		O		+	+			O		+	+	+	+
apatite									+		+				+		+		+		+		+	+	+	+
zircon	+	+	+	+				+	+						+		+				+		+	+	+	+
chlorite							O																			
allanite															+											
tourmaline			+														+		+		+		+			+
	Etusis Formation feldspathic quartzites												Etusis Fm		Khan Fm		Chuos Fm metapelites				Karibib Fm		Kuiseb Fm			

X abundant (> 5%); O minor (1–5%); +trace (< 1%)
Sample localities shown on Folder 2.1.

Table IIg – CENTRAL ZONE CALC SILICATES

	164	208	213	258	418	628	634	640	642	708	725	541	454	468	513	542	620	626	197	199	264	421	476	494	516	270
quartz	X	X		X	X	X	X		X	X	X	+	X	X	X	X	X	X	X		X	X	O		X	X
microcline	X	X		X		O		X	X		X		+										X			
plagioclase	X	X	X	+	X	X	X	O	X	X	X	X	X	X	X	X	X	O	X		X	X	O		X	
biotite		X				O	O				O		O			O										
white mica						O	O			O		X	O			O	O					O	+	X	X	O
tremolite	O		X									O		O	X	O	X									
hornblende		X			X		+	O	X	O	O		+					X				+	X			
clinopyroxene	+		X	X	O	+		O	X	O	O	X	X	X	X		O	O	X	X	X	X	X	X	X	X
garnet				X				X									O	O								X
forsterite			O									X														
calcite	O	+	O	X	O		O	O	O	+	+	+	O	+	O		O		O	+			X		O	O
wollastonite				X																X				X		
epidote	O				O	O	O	X	+	+			X					X				O				
clinozoisite	O				O	O								X	O		O	X					O			X
chlorite	O				O		O		+	O			O			O					X		+			
sphene	+		O		O	+		+		O	+			+	O	+	O	O	O	O	O	O	O	O	O	O
opaque ore	+	X			O	+			O	O	O				+	+	+				+				+	
scapolite			X	X		O									O					X				X		
	Khan Fm											Rössing / Fm \			Chuos Fm						Karibib Fm					

X abundant (> 5%); O minor (1–5%); + trace (< 1%)
Sample localities shown on Folder 2.1.

Table IIh — DONKERHUK THERMAL AUREOLE IN TROUGH ZONE PELITES

	98	99	105	329	331	332	347	352	689
quartz	X	X	X	X	X	X	X	X	O
microcline					O	O	X		O
plagioclase	X	X	X	X	X	X	O	X	O
biotite	X	X	X	O	X	X	X	X	X
muscovite	O	X	X	O			X	O	
sillimanite	+	O	+	O	O	X			X
cordierite				X	X	X			X
staurolite				O		O			
garnet	+	+			O	+			X
chlorite				X		O			
opaque ore	+		+	O	O	O		+	O
tourmaline		+	+						+
hercynite									O

X abundant (> 5%); O minor (1–5%); + trace (< 1%)
Sample localities shown on Folder 2.1.

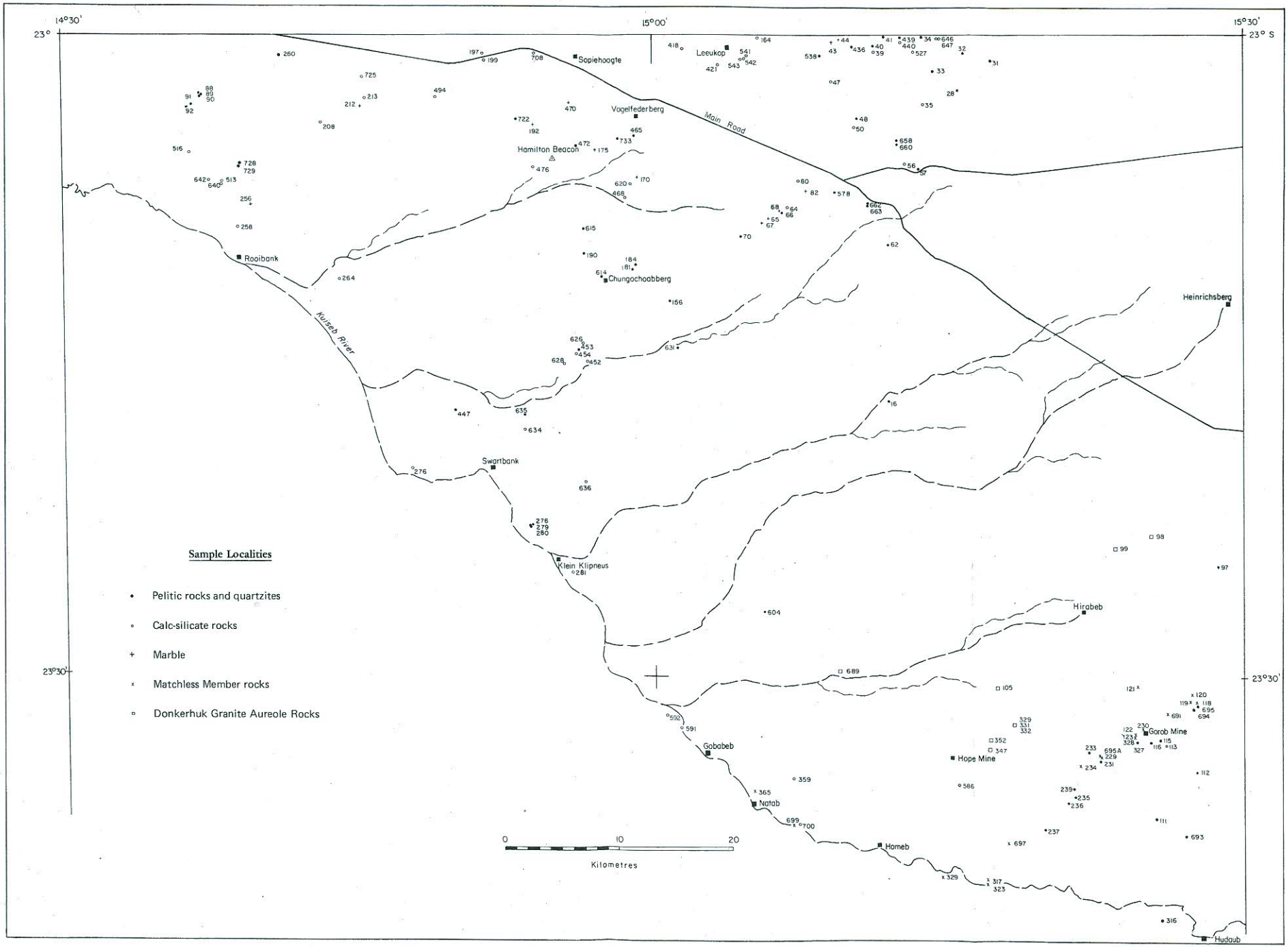

Folder 2.1 — Location of samples referred to in Appendix IIA (MINERAL ASSEMBLAGES).

Voufiguur 2.1 — Monstervindplekke waarna in Aanhangsel IIA (MINERAL ASSEMBLAGES) verwys word.

B. MINERAL-FABRIC RELATIONSHIPS

TROUGH ZONE

Observations were made on rocks throughout the Trough Zone, and were not confined to the three subzones of Section 3. The fabric elements cited refer to those of the Trough Zone only, as indicated in Table 4.2, Section 4.

A. Pelitic Rocks

(i) *Muscovite*—In the majority of metapelites muscovite flakes lie in the S_2 plane, and in some cases these are the only oriented mica. Sections of muscovite showing cleavage traces are generally far more elongated than biotite crystals. Generally muscovite comprises less than 10 per cent of the rock by volume. In some Al-rich schists, however, muscovite may comprise over half of the rock, forming a felt-like mat fabric parallel to S_2. Recrystallisation of the mica produces larger, less elongated grains generally parallel to the S_2 fabric. Such recrystallisation post-dates the biotite poikiloblasts. Muscovite derived from the alteration of staurolite and kyanite occurs as scaly randomly oriented aggregates. In the Al-rich schists with a largely plagioclase groundmass disoriented elongated muscovite laths are commonly present, possibly resulting from alteration of the plagioclase. Near the Donkerhuk Granite large muscovite poikiloblasts have grown randomly over the S_2 fabric.

(ii) *Biotite*—In most quartz-rich schists north and south of the Matchless Member small flakes of dark-brown, almost black biotite parallel S_2 and together with muscovite delineate the schistosity. Those biotites forming the S_1 mineral laminations are undeformed and now also lie parallel to S_2 suggesting recrystallisation rather than rotation. Those schists with the muscovite mat fabric or containing kyanite and staurolite have randomly developed porphyroblastic biotite, occasionally enclosing S_2 poikiloblastically. This fabric clearly post-dates the schistosity S_2. The biotites are prismatic and resemble hornblende in hand specimens.

(iii) *Garnets*—Some rocks from Hudaub in the very south-east show garnet growth to be pre-S_2 since one garnet contains straight inclusion trails of quartz and plagioclase at 90° to S_2. There is evidence of a later overgrowth of new garnet upon the old, and later flattening of the S_2 fabric around the porphyroblast [see (iv) below and Fig. 7.1B]. Elsewhere garnets are usually idioblastic and grow across the S_2 schistosity. In some instances zones around the garnets are depleted in S_2 parallel muscovite and biotite, and rarely also graphite. Frequently post-S_2 garnets occur in embayments in post-S_2 biotite but without touching the biotite, elsewhere idioblastic garnets are enclosed by biotite blades parallel to and touching garnet crystal faces without apparent replacement textures. In an example where S_3 crenulation cleavage is present garnets grow in S_3 and enclose S_2 helicitically.

(iv) *Staurolite*—Around Hudaub staurolite growth may be syn- to late-S_2. Elongated inclusions within the staurolites make a slight angle with the external fabric (S_2) which is undulose around the poikiloblasts (S_2 is defined by biotite lying in the schistosity). It is also possible that this texture was produced by the following sequence of events: (a) development of S_2 schistosity; (b) growth of staurolite; (c) flattening of the fabric essentially perpendicular to S_2 deforming the schistosity and causing slight rotation of the poikiloblasts. Elsewhere staurolite porphyroblasts may attain lengths of up to 20 mm and grow randomly across the S_2 schistosity. Such staurolites may enclose idioblastic garnets, small grains of biotite and plagioclase. At locality D in Figure 3.3 staurolite (and kyanite) orientated essentially parallel to S_2, are sheared and rotated by S_2 and crenulated by S_3. Later growth of staurolite (and kyanite) crosses both S_2 and S_3 randomly without being deformed. This locality, however, is considered unique as far as conditions of mineral nucleation and growth are concerned since some crystals reach 150 mm in length.

(v) *Kyanite*—With the exception of pre-S_3 kyanite at locality D in Figure 3.3 [see (iv) above] kyanite is the last prograde mineral to complete its growth. Whilst generally in the S_2 plane, kyanite is randomly oriented (Spry 1969, p. 259). A kyanite growth across S_2 at Hudaub shows undulose extinction and bent cleavage traces possibly confirming late compression perpendicular to S_2 planes.

(vi) *Quartz*—In quartz-rich schists and especially the graphitic schists, quartz is often elongated parallel to S_2 schistosity. In Al-rich schists quartz is generally rare and of granoblastic form. However, in Al-rich schists numerous S_2-parallel quartz veins are present (amounting to 15 per cent of rock volume) and suggest migration of quartz, perhaps through pressure solution and metamorphic reactions.

(vii) *Plagioclase*—Plagioclase (oligoclase) in the quartz-rich and graphite schists is often elongated in S_2 whereas the Al-rich schists have either a fairly fine-grained granoblastic–polygonal or fairly coarse-grained fabric with shape determined by impingement boundaries upon staurolite, biotite, garnet or kyanite. For Al-rich schists the groundmass is largely plagioclase, possibly derived from the muscovite mat fabric.

(viii) *Chlorite*—All chlorite present results from the retrograde alteration principally of biotite but also of staurolite and garnet, in the latter along fractures.

B. Matchless Member

Only the amphibole schists are considered, since the coarser varieties tend to have a decussate texture and little or no fabric. Quartzo-feldspathic knots of metamorphic origin are abundant in some rocks and show progressive elongation adjacent to minor shear zones.

(i) *Blue-green amphibole (hornblende)*—Much of the hornblende lies parallel to the S_2 schistosity, often with the y–z crystallographic plane in the fabric. Occasionally, however, crystals are oriented virtually perpendicular to S_2 and some have grown in the lineation caused by S_3 intersecting S_2. In other instances hornblende needles are oriented parallel to the strike of S_2.

(ii) *Ortho-amphibole*—Undeformed porphyroblasts of ortho-amphibole (anthophyllite) reaching 15 mm in length grow across a fabric defined by blue-green hornblende parallel to S_2.

C. Calc-silicate Rocks

Thin garnet-bearing calc-silicate bands are often transposed into the S_2 cleavage in F_2 folds, and frequently show a planar fabric of elongated recrystallised quartz and plagioclase. The fabric is a mylonitic compositional layering (Vernon 1974) parallel to the S_2 schistosity. Porphyroblasts of garnet, hornblende and biotite are often elongated in S_2 and contain abundant S_2-parallel inclusions, but do not show an optical-preferred orientation parallel to S_2. These minerals post-date S_2 and may grow along the S_0/S_2 lineation.

Massive glassy calc-silicate rocks west of Homeb contain small segregations or pods of epidote, diopside/hedenbergite or green amphibole parallel to S_2. These minerals often occur as inclusions in quartz parallel to S_2, suggesting development of quartz porphyroblasts by boundary migration after the main fabric formed.

OKAHANDJA LINEAMENT ZONE

A. Pelitic Rocks

(i) *Muscovite*—Muscovite generally parallels the main S_3 fabric, but close to the Donkerhuk Granite and adjacent to the unfoliated type granite of the Salem Suite porphyroblastic muscovite grows across S_3. Scattered small flakes oriented across the S_3 fabric are present in many porphyroblastic (andalusite and cordierite) schists, and these are not thermal aureole muscovites.

(ii) *Biotite*—In many cases biotite lies parallel to the S_3 schistosity, but in some cases the biotite schistosity lies at 5–10° to the muscovite and quartz fabric. Biotite growth across S_3 is common either as randomly oriented scattered flakes or more commonly as a well-defined locally penetrative fabric S_f almost at right angles to S_3 and occurring in thin Al-rich bands. The biotites defining the schistosity (S_f) are locally deformed on planes parallel to S_3.

Schists containing biotite spots due to S_1/S_3 intersections have a muscovite-defined S_3 schistosity in which all biotite spots are disrupted, the spots frequently being small fold closures.

(iii) *Cordierite*—Poikiloblastic cordierites up to 150 mm long frequently enclose the S_3 schistosity of biotite and quartz, in a few cases also enclosing the S_f biotite fabric. The external fabric may differ slightly in orientation, but on examination of microscopic quartz veinlets the slight rotation appears to be due to the late compression of, and movement parallel to S_3 causing poikiloblasts to rotate (Ramsay 1962, Fig. 16). In other cases the S_e and S_i discordance varies from poikiloblast to poikiloblast and may result from crystallisation effects. Whilst the majority of inclusion trails are straight a few are slightly sigmoidal. Orientation of retrograde alteration products (e.g. muscovite) in cordierites appears to be generally irregular. Some cordierites are completely pseudomorphed by micaceous aggregates.

(iv) *Andalusite*—Andalusite poikiloblasts generally have straight inclusion trains parallel to S_3, in a very few places they are curved. In other cases andalusite crystals appear to be disrupted parallel to S_3. This may be the result of late movement on S_3 planes during D_{L5}.

(v) *Garnet*—Occasionally small idioblastic or subidioblastic garnets which have grown across the S_3 schistosity are found. Very rarely minute idioblastic garnets with high Mn content are present in the outer edges of cordierite porphyroblasts.

(vi) *Quartz and Plagioclase*—Xenoblastic polygonal or elongated grains often parallel to the S_3 schistosity tend to be elongated in muscovite- and/or graphite-bearing schists. In many andalusite- and cordierite-bearing schists both quartz and plagioclase are absent from the matrix adjacent to poikiloblasts.

(vii) *Staurolite*—Small squat idioblastic crystals have grown across the S_3 fabric and S_f schistosity.

(viii) *Chlorite*—Subidioblastic porphyroblasts traverse the S_3 schistosity. In most cases chlorite is a retrograde alteration of biotite. Chlorite is not common.

B. Calc-silicate Rocks

(i) *Quartz and Plagioclase (andesine–labradorite)*—The majority of the calc-silicate rocks forming cleavage mullions have a mylonitic compositional layering (Vernon 1974) delineated by thin lamellae of quartz and plagioclase of noticeably finer grain size than that between the cleavage planes, spaced 1–2 mm apart. Recrystallisation of the smaller grains has removed strained extinction and produced granoblastic-polygonal textured layers parallel to the S_3 fabric.

(ii) *Amphibole*—Sheaf-like aggregates of undeformed blue-green hornblende are common and grow randomly across the S_3 parallel fabric. Retrogressive alteration of clinopyroxene (diopside/hedenbergite) to amphibole gives rise to randomly oriented acicular crystals.

(iii) *Clinopyroxene*—Skeletal poikiloblasts up to 10 mm across show no optical-preferred orientations in the fabric although poikiloblasts tend to be elongated parallel to S_3.

(iv) *Garnet*—Skeletal xenoblastic poikiloblasts of garnet tend to be elongated in S_3, but post-date S_3 since these contain straight inclusion trails parallel to S_3. In addition the inclusions tend to be elongated in S_3. Small idioblastic garnets are often developed across S_3 in metapelites at contacts with calc-silicate rocks.

(v) *Epidote/Clinozoisite*—Epidote that replaces plagioclase often forms streaks parallel to the S_3 fabric, the epidote forming rounded granoblastic grains. Epidote may in rare cases replace randomly oriented amphibole in zoned calc-silicate rocks with a mosaic of extremely fine-grained equant crystals. Generally, however, clinozoisite is secondary (retrograde) and irregularly oriented, but where associated with carbonate and garnet lies in S_3, and may be prograde.

(vi) *Chlorite*—Chlorite forms irregular sheaf-like aggregates, in some cases retrograde after garnet. In general, however, chlorites are alteration products of amphibole or biotite.

C. Marbles

Many marbles have a strong fabric consisting of elongated and flattened carbonate grains in the S_3 fabric. Tremolite and phlogopite generally form at grain boundaries and hence have a parallelism to S_3.

CENTRAL ZONE

A. Pelitic rocks

(i) *Biotite*—Biotite flakes define the S_1 fabric in metapelites. Locally these show regrowth or reorientation into F_2 and F_3 axial planes. In some cases S_3 crenulates S_1 and biotites then lie parallel to S_3. Small biotite crystals (0,1 mm long) parallel to S_1 are frequently enclosed in poikiloblastic microcline and are also oriented subparallel to the external S_3 fabric. Rounded biotite crystals are commonly found in some cordierite porphyroblasts.

(ii) *Sillimanite*—Radially oriented sillimanite fibres occur as small flattened knots up to 40 mm across or as small aggregates of fibres. The flattened knots lie in the S_3 axial-planar cleavage (generally a strong crenulation of the S_1 fabric) of F_3 folds. Sillimanite also lies in the S_1 plane where it has formed at the expense of muscovite and quartz. This growth parallel to S_1 may, however, be mimetic. Sillimanite, when not occurring as knots, is often disharmonious (Vernon and Flood 1977) with respect to quartz and feldspar, but harmonious with respect to cordierite. In one example small sillimanite needles outline a polygonal fold within a porphyroblast of cordierite in a rock with fairly strong schistosity but with granoblastic quartzo-feldspathic minerals (Fig. 7.1E).

(iii) *Cordierite*—Cordierite may form small granoblastic grains or large poikiloblasts confined in the S_3 fabric e.g., north of Rooibank. The cordierites often contain inclusions which parallel the external fabric but S_1 and S_3 are subparallel in F_3 fold flanks from where the sample was taken. As far as the mapped area is concerned no cordierite has been observed which shows rotation. Rotated cordierites do exist further north in the Khan–Swakop area*. Cordierite may be bluish or greenish and

* Personal communication: S. J. Barnes and M. Coward.

in some cases is elongated along the intersection between S_1 and S_3 schistosities. In thin section many equant cordierites grow across the S_1 fabric.

(iv) *Garnet*—In thin section the garnets are irregular, commonly embayed and elongated in S_1. A few kilometres north of Rooibank garnet crystals can be seen to grow in the S_3 fabric whilst large garnet porphyroblasts or aggregates grow across the S_1 and S_3 fabrics. These occur in association with some late undeformed pegmatitic veins and are also disseminated throughout the rock. In the area mapped no rotated garnet porphyroblasts have been observed although these too are common in the Khan–Swakop area. Garnets in thin section appear to be late as they grow either across the fabric or are elongated parallel to S_3, yet include large S_1-parallel biotite grains. Garnet and cordierite are often in contact and associated with microcline.

B. Calc-silicate Rocks

The rocks are generally granoblastic-polygonal but those of the Chuos Formation often have a glassy appearance due to large elongated (parallel to S_1 fabric) quartz grains which enclose amphibole, diopside and epidote parallelling S_1. In most rocks a mineral layering or segregation parallels S_1, although a specific mineral-preferred orientation appears to be absent. Clinopyroxene (diopside/hedenbergite) invariably shows a degree of retrograde alteration peripherally to unoriented amphibole. Most mineral species are subidioblastic or xenoblastic.

C. Marbles

Carbonate minerals generally give rise to a granoblastic texture in which the various calc-silicate minerals have a random orientation, although a mineral banding (possibly S_0 or S_1) is generally present.

III. MINERAL ANALYSES

The 103 mineral analyses (Tables IIIa–IIIj) were all done by Mr R. S. Rickard of the Department of Geochemistry, University of Cape Town, using an electron microprobe.

Operating conditions were a 15-kv accelerating potential and a beam current of 0,15 μamps. The 0,5 micron-diameter beam was defocussed to 10–20 microns to obtain analyses for Na and K. Determinations were made as close as possible to the mineral margin (avoiding edge effects). Those minerals denoted by * were analysed at their respective *cores*. A short dash in the tabulated data indicates "not analysed for".

Total iron is represented as FeO for all minerals.

Table IIIa—CENTRAL ZONE BIOTITES, SAMPLES 465 AND 729

	465A	465B	465C	465D	729A	729B	729C	729E
SiO_2	34,54	34,32	34,21	33,99	33,81	33,93	34,25	34,14
TiO_2	3,17	3,38	3,32	3,65	2,94	2,36	2,35	2,86
Al_2O_3	19,38	19,31	19,27	18,92	18,43	18,53	18,35	18,51
FeO	19,63	19,90	19,06	19,81	18,58	18,88	18,81	18,66
MnO	0,02	0,05	0,03	0,04	0,05	0,06	0,06	0,06
MgO	8,54	8,40	8,89	8,36	9,18	9,59	9,66	8,99
CaO	0,00	0,00	0,01	0,01	0,00	0,00	0,02	0,03
Na_2O	0,11	0,09	0,09	0,09	0,13	0,09	0,15	0,09
K_2O	9,63	9,51	9,52	9,70	10,00	9,86	9,87	9,79
Total	95,02	94,96	94,40	94,57	93,12	93,30	93,52	93,11
	Atomic proportions (22 oxygens)							
Si	5,296	5,272	5,267	5,255	5,298	5,306	5,339	5,337
Ti	0,366	0,391	0,385	0,425	0,346	0,278	0,275	0,336
Al	3,496	3,497	3,498	3,450	3,404	3,416	3,373	3,411
Fe	2,517	2,556	2,454	2,562	2,435	2,469	2,452	2,439
Mn	0,003	0,006	0,004	0,005	0,007	0,007	0,008	0,009
Mg	1,952	1,922	2,040	1,927	2,145	2,235	2,245	2,094
Ca	0,000	0,000	0,002	0,002	0,000	0,000	0,003	0,002
Na	0,035	0,026	0,027	0,026	0,041	0,028	0,046	0,028
K	1,884	1,863	1,870	1,912	1,999	1,967	1,963	1,953
Total	15,549	15,533	15,547	15,564	15,675	15,706	15,704	15,609

Table IIIb—CENTRAL ZONE CORDIERITES, SAMPLES 465 AND 729

	465A	465B	465C	465D	465E	729A	729B	729C	729E	729G	729H
SiO_2	47,97	47,53	47,53	47,45	47,62	47,28	47,28	47,33	47,44	47,04	47,39
TiO_2	0,01	0,01	0,01	0,01	0,02	0,01	0,00	0,00	0,01	0,02	0,02
Al_2O_3	33,33	32,25	33,52	33,54	33,45	33,69	32,82	33,46	33,39	33,44	33,87
FeO	9,07	9,09	8,94	8,99	9,04	8,77	8,79	8,96	8,77	8,59	8,71
MnO	0,08	0,08	0,10	0,09	0,08	0,16	0,15	0,17	0,16	0,19	0,21
MgO	7,75	7,71	7,73	7,80	7,77	7,83	7,85	7,46	7,79	7,73	7,65
CaO	0,01	0,00	0,01	0,01	0,01	0,02	0,03	0,03	0,04	0,02	0,01
Na_2O	0,17	0,19	1,16	0,17	0,19	0,14	0,24	0,17	0,17	0,13	0,12
K_2O	0,03	0,01	—	—	—	0,00	0,00	—	—	—	—
Total	98,42	97,87	98,00	98,06	98,18	97,90	97,16	97,58	97,77	97,16	97,98
					Atomic proportions (18 oxygens)						
Si	4,954	4,939	4,928	4,919	4,939	4,907	4,946	4,904	4,929	4,915	4,911
Ti	0,001	0,000	0,001	0,001	0,001	0,000	0,000	0,000	0,001	0,001	0,002
Al	4,060	4,073	4,097	4,099	4,084	4,121	4,049	4,109	4,090	4,120	4,138
Fe	0,783	0,790	0,775	0,779	0,783	0,762	0,769	0,781	0,763	0,751	0,755
Mn	0,007	0,007	0,009	0,008	0,007	0,014	0,014	0,015	0,014	0,017	0,019
Mg	1,193	1,194	1,194	1,205	1,199	1,211	1,224	1,159	1,207	1,203	1,182
Ca	0,001	0,000	0,001	0,001	0,001	0,003	0,003	0,003	0,004	0,002	0,001
Na	0,035	0,038	0,033	0,033	0,038	0,028	0,048	0,034	0,034	0,027	0,024
K	0,003	0,002	—	—	—	0,000	0,000	—	—	—	—
Total	11,037	11,043	11,038	11,045	11,052	11,046	11,053	11,005	11,042	11,036	11,032

Table IIIc—CENTRAL ZONE GARNETS, SAMPLES 465 AND 729

	465Ai	465Aii	465B	465B*	465C	465D	729Aii	729B	729C	729C*	729D	729E
SiO_2	36,26	36,48	36,37	36,70	36,51	36,66	36,26	36,50	36,53	36,62	36,31	36,35
TiO_2	0,04	0,08	0,06	0,02	0,07	0,01	0,02	0,05	0,05	0,03	0,04	0,02
Al_2O_3	21,09	21,35	21,21	21,32	21,38	21,44	21,36	20,53	20,47	21,47	21,35	21,10
FeO	36,69	36,74	36,82	36,08	36,40	36,60	35,09	35,73	35,52	34,35	34,45	34,43
MnO	1,58	1,47	1,53	1,25	1,39	1,43	2,80	2,53	2,35	2,47	2,99	2,91
MgO	2,55	2,96	2,84	3,69	3,14	3,11	3,33	3,29	3,35	3,80	2,95	3,22
CaO	0,78	0,68	0,74	0,70	0,79	0,69	0,96	0,90	0,92	1,00	0,97	0,91
Na_2O	0,03	0,05	0,07	0,02	0,03	0,04	0,00	—	—	—	—	—
Total	99,02	99,81	99,64	99,78	99,71	99,98	99,82	99,53	99,19	99,74	99,06	98,94
					Atomic proportions (12 oxygens)							
Si	2,969	2,958	2,958	2,963	2,958	2,963	2,939	2,974	2,982	2,953	2,960	2,966
Ti	0,003	0,005	0,004	0,001	0,004	0,001	0,001	0,003	0,003	0,002	0,C02	0,001
Al	2,035	2,041	2,034	2,029	2,042	2,043	2,041	1,972	1,970	2,041	2,052	2,029
Fe	2,512	2,492	2,505	2,436	2,466	2,474	2,379	2,435	2,425	2,316	2,348	2,350
Mn	0,110	0,101	0,106	0,085	0,095	0,096	0,192	0,175	0,163	0,169	0,206	0,201
Mg	0,312	0,358	0,344	0,444	0,380	0,374	0,402	0,400	0,408	0,456	0,359	0,391
Ca	0,069	0,059	0,065	0,060	0,068	0,060	0,083	0,078	0,080	0,086	0,084	0,079
Na	0,004	0,008	0,011	0,003	0,004	0,007	0,000	—	—	—	—	—
Total	8,014	8,022	8,027	8,021	8,017	8,018	8,037	8,037	8,031	8,023	8,011	8,017

Table IIId—CENTRAL ZONE MICROCLINES AND PLAGIOCLASES, SAMPLES 465 AND 729

	MICROCLINE						PLAGIOCLASE				
	465A	465B	465C	729A	729B	729C	465A	465B	729B	729D	729E
SiO_2	63,61	63,57	63,26	63,14	65,99	66,21	62,79	62,68	60,48	59,97	60,34
TiO_2	—	—	0,03	0,03	0,03	0,01	—	—	0,01	0,01	—
Al_2O_3	19,55	19,50	19,36	19,28	19,05	19,03	23,66	23,61	25,22	24,50	24,54
FeO	0,02	0,04	0,04	0,00	0,01	0,11	0,02	0,02	0,01	0,03	0,11
MgO	—	—	0,00	0,00	0,00	0,00	—	—	0,00	0,00	—
CaO	0,03	0,02	0,01	0,03	0,04	0,08	3,80	3,87	5,32	5,36	5,20
Na_2O	2,20	2,00	1,82	1,83	1,85	2,35	10,01	9,82	9,87	9,61	9,50
K_2O	13,78	14,19	14,01	15,26	14,40	14,09	0,25	0,16	0,18	0,20	0,12
Total	99,19	99,32	98,53	99,57	101,37	101,88	100,53	100,16	101,09	99,68	99,81
	Atomic proportions (8 oxygens)						Atomic proportions (8 oxygens)				
Si	2,946	2,945	2,950	2,937	2,987	2,984	2,769	2,772	2,674	2,688	2,696
Ti	—	—	0,001	0,001	0,001	0,000	—	—	0,000	0,000	—
Al	1,067	1,065	1,064	1,057	1,017	1,011	1,230	1,231	1,314	1,294	1,293
Fe	0,001	0,002	0,002	0,000	0,000	0,004	0,001	0,001	0,000	0,001	0,004
Mg	—	—	0,000	0,000	0,000	0,000	—	—	0,000	0,000	—
Ca	0,001	0,001	0,001	0,001	0,002	0,004	0,180	0,184	0,252	0,258	0,249
Na	0,197	0,179	0,165	0,165	0,162	0,205	0,856	0,842	0,846	0,835	0,823
K	0,814	0,839	0,834	0,906	0,831	0,810	0,014	0,009	0,010	0,011	0,007
Total	5,026	5,031	5,017	5,067	5,000	5,018	5,050	5,039	5,096	5,087	5,072

Table IIIe—TROUGH ZONE BIOTITES, SAMPLES 115 AND 235 (115F IS AN INCLUSION IN A STAUROLITE PORPHYRO BLAST)

	115A	115B	115C	115D	115E	115F	235A	235B	235C	235D	235E	235F
SiO_2	35,56	35,79	35,69	34,60	35,29	34,86	35,62	35,72	35,38	35,30	35,11	35,69
TiO_2	1,44	1,46	1,40	1,44	1,54	1,77	1,42	1,47	1,46	1,34	1,46	1,48
Al_2O_3	20,14	20,19	19,88	19,77	19,85	20,19	20,29	20,05	19,76	19,76	20,01	20,55
FeO	16,28	16,91	17,08	17,11	16,63	15,78	16,93	17,28	17,60	16,75	17,41	16,64
MnO	—	—	—	—	—	—	0,07	0,06	0,05	0,06	0,07	0,07
MgO	11,15	11,10	11,31	10,51	11,04	12,29	11,33	11,09	10,79	11,00	11,05	11,06
CaO	0,02	0,00	0,01	0,02	0,00	0,03	0,01	0,02	0,01	0,02	0,02	0,04
Na_2O	0,01	0,16	0,16	0,15	0,18	0,01	0,39	0,41	0,34	0,28	0,39	0,42
K_2O	8,78	8,96	9,01	3,55	8,95	8,46	8,66	8,57	8,70	8,67	8,62	8,70
Total	93,38	94,57	94,54	87,15	93,48	93,39	94,72	94,67	94,09	93,18	94,14	94,65
	Atomic proportions (22 oxygens)											
Si	5,401	5,392	5,388	5,364	5,381	5,288	5,358	5,382	5,382	5,399	5,334	5,364
Ti	0,164	0,165	0,159	0,168	0,176	0,202	0,161	0,167	0,167	0,154	0,167	0,167
Al	3,606	3,587	3,537	3,613	3,569	3,610	3,597	3,561	3,543	3,563	3,585	3,640
Fe	2,068	2,130	2,157	2,218	2,121	2,001	2,129	2,177	2,239	2,143	2,212	2,091
Mn	—	—	—	—	—	—	0,009	0,007	0,007	0,007	0,009	0,009
Mg	2,524	2,492	2,544	2,428	2,508	2,778	2,540	2,490	2,446	2,508	2,502	2,477
Ca	0,003	0,000	0,002	0,004	0,000	0,005	0,001	0,002	0,002	0,003	0,004	0,006
Na	0,031	0,046	0,045	0,044	0,053	0,004	0,113	0,119	0,101	0,083	0,115	0,124
K	1,701	1,723	1,734	1,692	1,741	1,638	1,662	1,648	1,688	1,691	1,671	1,669
Total	15,488	15,535	15,566	15,531	15,549	15,526	15,570	15,553	15,575	15,551	15,599	15,547

Table IIIf—TROUGH ZONE GARNETS, SAMPLES 115 AND 235

	115Ai	115Aii	115B*	115B	115C	115D	1158	235A*	235A	235B	235C	235D
SiO_2	37,16	37,02	36,96	37,15	36,97	37,14	37,31	37,02	36,75	36,50	36,37	36,78
TiO_2	0,05	0,08	0,09	0,10	0,05	0,05	0,06	0,02	0,01	0,02	0,03	0,03
Al_2O_3	21,47	21,76	21,60	21,58	21,73	21,57	21,70	21,35	21,35	21,19	21,26	21,30
FeO	32,13	32,12	29,84	31,48	32,09	32,58	31,46	31,44	32,47	32,15	32,51	32,42
MnO	3,01	2,96	4,90	3,17	3,09	3,56	3,19	4,95	5,04	4,97	5,25	5,14
MgO	3,20	3,13	2,37	3,09	3,14	2,85	3,10	3,43	3,12	3,05	2,72	2,94
CaO	3,06	3,32	4,28	3,66	2,98	2,78	3,57	2,07	1,37	1,69	1,50	1,58
Total	100,08	100,39	100,04	100,23	100,05	100,53	100,39	100,28	100,11	99,57	99,64	100,19

Atomic proportions (12 oxygens)

Si	2,976	2,957	2,967	2,969	2,961	2,971	2,974	2,969	2,963	2,961	2,955	2,966
Ti	0,003	0,005	0,005	0,006	0,003	0,003	0,003	0,001	0,001	0,001	0,002	0,002
Al	2,027	2,049	2,045	2,033	2,052	2,035	2,039	2,018	2,029	2,026	2,037	2,025
Fe	2,152	2,145	2,003	2,104	2,149	2,180	2,097	2,109	2,189	2,181	2,209	2,186
Mn	0,204	0,200	0,333	0,215	0,210	0,241	0,216	0,336	0,344	0,341	0,361	0,351
Mg	0,382	0,373	0,284	0,367	0,374	0,340	0,368	0,410	0,375	0,368	0,330	0,353
Ca	0,262	0,285	0,368	0,313	0,256	0,239	0,305	0,178	0,118	0,147	0,131	0,136
Total	8,006	8,014	8,005	8,007	8,005	8,009	8,002	8,021	8,019	8,025	8,025	8,019

Table IIIg—TROUGH ZONE STAUROLITES, SAMPLES 115 AND 235

	115Ai	115Aii	115B	115C	235A*	235A	235B	235C	235D
SiO_2	27,17	27,43	26,98	26,98	27,15	27,32	27,34	27,35	27,03
TiO_2	0,57	0,59	0,51	0,76	0,60	0,50	0,59	0,65	0,64
Al_2O_3	54,91	54,04	54,77	54,96	55,07	54,77	55,04	55,22	55,01
FeO	13,10	11,81	13,11	13,12	13,12	13,21	13,12	13,17	13,30
MnO	0,19	0,20	0,19	0,20	0,26	0,24	0,26	0,25	0,26
MgO	1,94	1,77	1,84	1,72	1,74	1,65	1,54	1,54	1,67
CaO	0,02	0,01	0,01	0,00	—	—	—	—	—
Total	97,90	95,85	97,41	97,74	97,94	97,69	97,89	98,18	97,91

Atomic proportions (23 oxygens)

Si	3,756	3,847	3,750	3,738	3,753	3,786	3,779	3,769	3,742
Ti	0,060	0,062	0,053	0,079	0,062	0,052	0,061	0,068	0,067
Al	8,951	8,934	8,976	8,977	8,976	8,949	8,970	8,973	8,978
Fe	1,515	1,385	1,524	1,521	1,517	1,531	1,517	1,518	1,540
Mn	0,022	0,024	0,022	0,023	0,031	0,029	0,030	0,030	0,030
Mg	0,401	0,371	0,380	0,356	0,358	0,341	0,317	0,317	0,345
Ca	0,003	0,002	0,002	0,001	—	—	—	—	—
Total	14,708	14,625	14,707	14,695	14,697	14,688	14,674	14,675	14,702

Table IIIh—TROUGH ZONE BIOTITES, GARNETS AND STAUROLITES, SAMPLE 316

	BIOTITE				GARNET			STAUROLITE	
	316B	316C	316D	316E	316A*	316A	316BB	316A	316B
SiO_2	35,81	35,47	35,47	35,62	36,93	36,88	36,84	27,63	27,54
TiO_2	1,45	1,92	1,43	1,49	0,07	0,02	0,00	0,66	0,62
Al_2O_3	20,05	19,47	19,06	19,34	21,50	21,50	21,41	54,82	55,10
FeO	17,99	17,10	17,48	17,36	32,15	33,51	32,67	12,63	12,67
MnO	0,06	—	—	—	2,53	2,79	2,59	0,18	—
MgO	11,54	10,15	11,00	10,81	3,37	2,99	2,90	1,41	1,24
CaO	0,01	0,01	0,00	0,00	3,61	2,82	2,70	0,01	0,00
Na_2O	0,14	0,11	0,10	0,10	—	—	—	—	—
K_2O	9,18	9,32	9,16	9,42	—	—	—	—	—
Total	96,23	93,55	93,70	94,14	100,16	100,51	99,11	97,34	97,17
	Atomic proportions (22 oxygens)				Atomic proportions (12 oxygens)			Atomic proportions (23 oxygens)	
Si	5,340	5,399	5,429	4,933	2,955	2,957	2,982	3,827	3,818
Ti	0,162	0,222	0,165	0,155	0,004	0,001	0,000	0,069	0,064
Al	3,525	3,531	3,439	3,157	2,029	2,032	2,042	8,953	9,007
Fe	2,244	2,200	2,238	2,011	2,151	2,247	2,211	1,463	1,469
Mn	0,007	—	—	—	0,172	0,189	0,178	0,022	—
Mg	2,563	2,327	2,508	2,231	0,402	0,357	0,350	0,291	0,255
Ca	0,001	0,001	0,000	0,000	0,310	0,242	0,235	0,002	0,000
Na	0,040	0,033	0,028	0,028	—	—	—	—	—
K	1,747	1,830	1,789	1,664	—	—	—	—	—
Total	15,629	15,543	15,596	14,179	8,023	8,025	7,998	14,627	14,613

Table IIIi—TROUGH ZONE MUSCOVITES, SAMPLES 115, 235 AND 316

	115A	115B	115C	115D	235A	235C	235D	316A	316B
SiO_2	45,62	45,81	46,25	46,03	45,75	45,38	45,89	46,01	45,67
TiO_2	0,32	0,39	0,30	0,54	0,55	0,30	0,50	0,49	0,37
Al_2O_3	37,19	36,48	36,47	36,61	36,31	37,46	37,03	36,12	36,66
FeO	1,10	1,05	0,97	0,94	0,82	0,71	0,71	1,42	1,42
MgO	0,73	0,76	0,76	0,67	0,70	0,44	0,50	0,56	0,45
CaO	0,01	0,02	0,00	0,01	0,00	0,00	0,01	0,00	0,00
Na_2O	1,37	1,22	1,23	1,21	1,60	1,97	1,74	1,50	1,55
K_2O	9,30	9,03	9,32	9,30	8,87	8,41	8,54	9,05	8,86
Total	95,64	94,76	95,30	95,31	94,60	94,67	94,92	95,15	94,98
	Atomic proportions (22 oxygens)								
Si	6,019	6,082	6,110	6,081	6,081	6,015	6,062	6,102	6,062
Ti	0,031	0,039	0,030	0,054	0,055	0,029	0,050	0,048	0,037
Al	5,784	5,710	5,681	5,702	5,693	5,854	5,768	5,648	5,737
Fe	0,121	0,117	0,107	0,104	0,091	0,079	0,078	0,158	0,158
Mg	0,143	0,151	0,151	0,132	0,138	0,086	0,099	0,112	0,090
Ca	0,001	0,002	0,000	0,001	0,000	0,000	0,002	0,000	0,000
Na	0,351	0,314	0,314	0,311	0,412	0,506	0,446	0,385	0,399
K	1,566	1,530	1,570	1,568	1,506	1,421	1,439	1,531	1,501
Total	14,016	13,945	13,963	13,953	13,976	13,990	13,944	13,984	13,984

Table IIIj—TROUGH ZONE PLAGIOCLASES, SAMPLES 115, 235 AND 316

	115A	115B	115C	115D	235A	235B	235D	316A	316C	316BD
SiO_2.....	61,12	60,49	61,53	60,02	62,83	62,29	62,65	61,57	61,17	60,29
TiO_2.....	0,01	0,02	0,03	0,03	0,00	0,01	0,03	0,00	0,00	—
Al_2O_3.....	25,35	25,04	25,29	25,57	23,56	24,36	24,32	24,97	25,52	25,01
FeO.....	0,01	0,03	0,04	0,01	0,05	0,05	0,04	0,20	0,04	0,02
MgO.....	0,04	0,00	0,00	0,00	0,00	0,00	0,01	0,00	0,00	—
CaO.....	6,01	6,25	6,26	6,79	4,34	5,06	4,83	5,89	6,24	5,84
Na_2O.....	8,30	7,97	8,47	7,49	9,15	8,92	9,25	8,29	8,38	8,75
K_2O.....	0,15	0,33	0,08	0,07	0,07	0,05	0,06	0,09	0,04	0,07
Total.....	100,99	100,13	101,70	99,98	100,00	100,74	101,19	101,01	101,39	99,98
Atomic proportions (8 oxygens)										
Si.....	2,690	2,689	2,692	2,669	2,778	2,741	2,745	2,708	2,684	2,686
Ti.....	0,000	0,001	0,001	0,001	0,000	0,000	0,001	0,000	0,000	—
Al.....	1,316	1,312	1,305	1,340	1,228	1,264	1,256	1,295	1,320	1,313
Fe.....	0,000	0,001	0,001	0,000	0,002	0,002	0,001	0,008	0,001	0,001
Mg.....	0,002	0,000	0,000	0,001	0,000	0,000	0,001	0,000	0,000	—
Ca.....	0,283	0,298	0,294	0,324	0,206	0,239	0,227	0,279	0,293	0,279
Na.....	0,709	0,687	0,719	0,646	0,784	0,761	0,786	0,707	0,713	0,755
K.....	0,009	0,019	0,004	0,004	0,004	0,003	0,004	0,005	0,002	0,004
Total.....	5,009	5,007	5,016	4,985	5,002	5,010	5,021	5,002	5,013	5,038

REFERENCES

ALLEN, J. R. L., 1970. Physical Processes of Sedimentation: George Allen and Unwin Ltd, London, 248p.

ALTHAUS, E., 1967, The triple point andalusite-sillimanite-kyanite: Contr. Mineral. Petrol., *16*, 29–44.

ANDERSON, P. A. M., NEWTON, R. C., and KLEPPA, O. J., 1977. The enthalpy change of the andalusite-sillimanite reaction and the Al_2SiO_5 diagram: Am. J. Sci., *277*, 585–593.

BAILEY, D. K., 1972. Uplift, rifting and magmatism in continental plates: Earth Sci. J. Leeds Univ., *8*, 225–239.

BAILEY, D. K., 1974. Continental rifting and alkaline magmatism, *in* The Alkaline Rocks. (Ed. H. Sorensen): Wiley Interscience, London, 148–159.

BAILEY, D. K., 1976. Experimental methods and the uses of phase diagrams *in* The Evolution of the Crystalline Rocks (Ed. D. K. Bailey and R. MacDonald): Academic Press, London, 3–97.

BEAN, R. J., 1953. Relation of gravity anomalies to the geology of central Vermont and New Hampshire: Bull. geol. Soc. Am., *64*, 509–538.

BICKLE, M. J., and COWARD, M. P., 1977. A major thrust in the southern Damara belt, Namibia: 20th A. Rep. Res. Inst. Afr. Geol., Univ. Leeds, 8–13.

BIRD, P., TOKSOZ, M. N., and SLEEP, N. H., 1975. Thermal and mechanical models of continent-continent convergence zones: J. geophys. Res., *80*, 4 405–4 416.

BLAINE, J. L., 1977. Tectonic evolution of the Waldau Ridge structure and the Okahandja Lineament in part of the central Damara Orogen, west of Okahandja, South West Africa: Bull. Chamber Min. Precambr. Res. Unit., Univ. Cape Town, *21*, 99 p.

CARMICHAEL, D. M., 1970. Intersecting isograds in the Whetstone Lake area, Ontario: J. Petrol., *11*, 147–181.

CARMICHAEL, I. S. E., TURNER, F. J., and VERHOOGEN, J., 1974. Igneous Petrology: McGraw-Hill Inc., New York, 739 p.

CHATTERJEE, N. D., 1972. The upper stability limit of the assemblage paragonite+quartz and its natural occurrences: Contr. Mineral. Petrol., *34*, 288–303.

CLIFFORD, T. N., 1967. The Damaran episode in the upper Proterozoic–lower Paleozoic structural history of Southern Africa: Spec. Paper, Geol. Soc. Am., *92*, 100 p.

CURRIE, K. L., 1971. The reaction 3 cordierite=2 garnet+4 sillimanite+5 quartz as a geological thermometer in the Opinicon Lake region, Ontario: Contr. Mineral. Petrol., *33*, 215–226.

CURRIE, K. L., 1974. A note on the calibration of the garnet–cordierite geothermometer and geobarometer: Contr. Mineral. Petrol., *44*, 35–44.

DE SITTER, L. U., 1958. Boudins and parasitic folds in relation to cleavage and folding: Geologie Mijnb., *20*, 277–286.

DE WAAL, S. A., 1966. The Alberta Complex, a metamorphosed layered intrusion, north of Nauchas, South West Africa, the surrounding granites and repeated folding in the Damara System: D.Sc. thesis, Univ. Pretoria (unpubl.), 203 p.

DIETERICH, J. H., 1969. Origin of cleavage in folded rocks: Am. J. Sci., *267*, 155–165.

DIETERICH, J. H., 1970. Computer experiments on mechanics of finite amplitude folds: Can. J. Earth Sci., *7*, 467–476.

DIETZ, R. S., and HOLDEN, J. C., 1966. Miogeoclines (miogeosynclines) in space and time: J. Geol., *74*, 566–583.

DIXON, J. M., 1975. Finite strain and progressive deformation in models of diapiric structures: Tectonophysics, *28*, 89–124.

ERNST, W. G., 1974. Metamorphism and ancient continental margins *in* The Geology of Continental Margins (Ed. C. A. Burke and C. L. Drake): Springer Verlag, Berlin, 907–919.

ESKOLA, P. E., 1948. The problem of mantled gneiss domes: Q. Jl geol. Soc., Lond., *104*, 461–476.

ETHERIDGE, M. A., and HOBBS, B. E., 1974. Chemical and deformational controls on recrystallization of mica: Contr. Mineral. Petrol., *43*, 111–124.

FAUPEL, J., 1973. Geological and mineralogical investigation of the Donkerhoek-Granite, Karibib-District, South West Africa (Preliminary Report): Neues Jb. Miner. Geol. Paläont. Mh., 327–341.

FERGUSON, C. C., and HARTE, B., 1975. Textural pattern at porphyroblast margins and their use in determining the time of deformation and crystallization: Geol. Mag., *112*, 467–480.

FERRY, J. M., 1976. Metamorphism of calcareous sediments in the Waterville-Vassalboro area south-central Maine: Mineral reactions and graphical analysis: Am. J. Sci., *276*, 841–882.

FERRY, J. M. and SPEAR, F. S., 1977. Experimental calibration of the partitioning of Fe and Mg between biotite and garnet: Carnegie Instn, Wash. Yb., *76*, 579–581.

FLETCHER, R. C., 1972. Application of a mathematical model to the emplacement of mantled gneiss domes: Am. J. Sci., *272*, 197–216.

FLEUTY, M. J., 1964. The description of folds: Geol. Assoc. Proc., *75*, 461–492.

FRENCH, B. M., 1966. Some geological implications of equilibrium between graphite and a C-H-O gas phase at high temperatures and pressures: Rev. Geophysics, *4*, 223–253.

FROESE, E., and GASPARINI, E., 1975. Metamorphic zones in the Snow Lake area, Manitoba: Can. Miner., *13*, 162–167.

FYFE, W. S., PRICE, N. J., and THOMPSON, A. B., 1978. Fluids in the Earth's Crust: Elsevier, Amsterdam, 383 p.

GANGULY, J., 1972. Staurolite stability and related parageneses: Theory, experiments and application: J. Petrol., *13*, 335–365.

GHENT, E. D., 1975. Temperature, pressure, and mixed-volatile equilibria attending metamorphism of staurolite–kyanite-bearing assemblages, Esplanade Range, British Columbia: Bull. geol. Soc. Am., *86*, 1 654–1 660.

GHENT, E. D., 1976. Plagioclase-garnet-Al_2SiO_5-quartz: a potential geobarometer-geothermometer. Am. Miner., *61*, 710–714.

GHENT, E. D., 1978. Applications of activity-composition relations to displacement of a solid-solid equilibrium, anorthite = grossular + kyanite + quartz *in* Short Course in Application of Thermodynamics to Petrology and Ore Deposits (Ed. H. J. Greenwood): Mineral. Assoc. Canada, 99–108.

GREENWOOD, H. J., 1975. Buffering of pore fluid by metamorphic reactions: Am. J. Sci., *275*, 573–593.

GUIDOTTI, C. V., CHENEY, J. T., and CONATORE, P. D., 1975. Coexisting cordierite + biotite + chlorite from the Rumford quadrangle, Maine: Geology, *3*, 147–148.

HAACK, U., 1976. Rekonstruktion der Abkühlungsgeschichte des Damara-Orogens in Südwest-Afrika mit Hilfe von Spaltspuren-Altern: Geol. Rundschau, *65*, 967–1 002.

HAACK, U., 1977. Radiometrische Untersuchungen in Damara-Gebiet: Ber. Sonder Forsch Bers 48, Georg-August. Univ. Göttingen, 182–186.

HAACK, U., and HOFFER, E., 1976. K/Ar ages of biotites from the Damara-Orogen, South West Africa: Trans. geol. Soc. S. Afr., *79* (2), 213–216.

HÄLBICH, I. W., 1977. Structure and tectonics along the southern margin of the Damara mobile belt, South West Africa: Annale Univ. Stellenbosch, Serie A1 (Geol.), *2*, 149–247.

HARIYA, Y., and KENNEDY, G. C., 1968. Equilibrium study of anorthite under high pressure and high temperature: Am. J. Sci., *266*, 193–203.

HARTE, B., 1975. Determination of a pelite petrogenetic grid for the Eastern Scottish Dalradian: Carnegie Instn, Wash. Yb., *74*, 438–446.

HARTNADY, C. J., 1977. On the tectonic zonation of the Damara orogenic belt and the Khomas ridge province: Rep. Precambr. Res. Unit, Univ. Cape Town (unpubl.).

HAWKESWORTH, C. J., MILLER, R. McG., and RODDICK, J. C., (in prep.) Geochronology in the Damarides, South West Africa.

HAYS, J. F., 1967. Lime-alumina-silica: Carnegie Instn, Wash. Yb., *65*, 234–239.

HENSEN, B. J., 1977. Cordierite–garnet-bearing assemblages as geothermometers and barometers in granulite facies terraines: Tectonophysics, *43*, 73–88.

HEWITT, D. A., 1975. Stability of the assemblage phlogopite-calcite-quartz: Am. Miner., *60*, 391–397.

HIGGINS, M. W., 1971. Cataclastic Rocks: Prof. Pap. U.S. geol. Survey, *687*, 97 p.

HOBBS, B. E., MEANS, W. D., and WILLIAMS, P. F., 1976. An Outline of Structural Geology: Wiley Interscience, New York, 571 p.

HOFFER, E., 1975. Die zeitliche Beziehung zwischen Tektogenese und Metamorphose: Ein Beitrag zur Rekonstruktion der thermischen Geschichte des Damara-Orogens: Ber. Sonder Forsch Bers 48, Georg-August-Univ. Göttingen, 170–183.

HOFFER, E., 1976. The reaction sillimanite + biotite + quartz $\rightleftharpoons$ cordierite + K-feldspar + H_2O and partial melting in the system K_2O-FeO-MgO-Al_2O_3-SiO_2-H_2O: Contrib. Mineral. Petrol., *55*, 127–130.

HOFFMANN, C., 1976. Granites and migmatites of the Damara belt, South West Africa. Petrography and melting experiments: Geol. Rundschau, *65*, 939–966.

HOFFMANN, C., 1976a. Natural granitic rocks and the granitic systems Qz-Or-Ab-An-(H_2O) and Qz-Ab-An-(H_2O): Neues Jb. Mineral. Mh., 1976 (7), 289–306.

HOFFMANN, P., DEWEY, F. F., and BURKE, K., 1974. Aulacogens and their genetic relation to geosynclines, with a Proterozoic example from Great Slave Lake, Canada *in* Modern and Ancient Geosynclinal Sedimentation (Ed. R. H. Dott and R. H. Shaver): Spec. Publ., Soc. econ. Palaeont. Min., *19*, 38–55.

HOLDAWAY, M. J., 1971. Stability of andalusite and the aluminium silicate phase diagram: Am. J. Sci.,*271*, 91–131.

HOLDAWAY, M. J., 1972. Thermal stability of Al-Fe epidote as a function of f_{O_2} and Fe content: Contr. Mineral. Petrol., *37*, 307–340.

HOLDAWAY, M. J. and LEE, S. M., 1977. Fe-Mg cordierite stability in high-grade pelitic rocks based on experimental, theoretical, and natural observations: Contr. Mineral. Petrol., *63*, 175–198.

HOSCHEK, G., 1969. The stability of staurolite and chloritoid and their significance in metamorphism of pelitic rocks: Contr. Mineral. Petrol., *22*, 208–232.

HUDLESTON, P. J., 1973. Fold morphology and some geometrical implications of theories of fold development: Tectonophysics, *16*, 1–46.

HUDLESTON, P. J., 1973a. An analysis of "single layer" folds developed experimentally in viscous media: Tectonophysics, *16*, 189–214.

HUDLESTON, P. J., 1977. Similar folds, recumbent folds, and gravity tectonics in ice and rock: J. Geol., *85*, 113–122.

HUDLESTON, P. J. and STEPHANSSON, O., 1973. Layer shortening and fold-shape development in the buckling of single layers: Tectonophysics, *17*, 299–321.

HUTCHEON, I., FROESE, E., and GORDON, T. M., 1974. The assemblage quartz-sillimanite-garnet-cordierite as an indicator of metamorphic conditions in the Daly Bay Complex, N.W.T.: Contr. Mineral. Petrol., *44*, 29–34.

JACOB, R. E., 1974. Geology and metamorphic petrology of part of the Damara Orogen along the Lower Swakop River, South West Africa: Bull. Chamber Min. Precambr. Res. Unit, Univ. Cape Town, *17*, 201 p.

JOHNSON, L. R., and WENK, H. R., 1974. Anisotropy of physical properties in metamorphic rocks: Tectonophysics, *23*, 79–98.

KOJIMA, G., and SUZUKI, T., 1958. Rock structure and quartz fabric in a thrusting shear zone: the Kiyomizu Tectonic Zone in Shikoku, Japan: J. Sci. Hiroshima Univ., Series C, *2*, 173–193.

KRÖNER, A., 1977. Precambrian mobile belts of southern and eastern Africa—ancient sutures or sites of ensialic mobility? A case for crustal evolution towards plate tectonics: Tectonophysics, *40*, 101-135.

KRÖNER, A., HALPERN, M., CLAUER, N., HAWKESWORTH, C. J. and JACOB, R. E., (in prep.). Timing of polymetamorphism and deformation in the Pan African Damara belt of Namibia (South West Africa) as deduced from new Rb-Sr chronological data.

KRÖNER, A., and HAWKESWORTH, C. J., 1977. Late pan-African emplacement ages for Rössing alaskitic granite (Damara belt) and Rooi Lepel bostonite (Gariep belt) in Namibia and their significance for the timing of metamorphic events: 20th A. Rep. Res. Inst. Afr. Geol., Univ. Leeds, 14–17.

LOOMIS, T. P., 1976. Irreversible reactions in high-grade metamorphic rocks: J. Petrol., *17*, 559-588.

MALLING, S., 1978. Microprobe and XRD studies of Damaran metamorphosed rocks at the southern margin of the Damara Orogenic Belt, Windhoek District, South West Africa: Rep. CSIR (unpubl.).

MARTIN, H., and PORADA, H., 1977. The intracratonic branch of the Damara Orogen in South West Africa: I. Discussion of geodynamic models: Precambr. Res., *5*, 311–338.

MEHNERT, K. R., 1968. Migmatites and the Origin of Granitic Rocks: Elsevier, Amsterdam, 393 p.

MILLER, R. McG., 1973. The Salem Granite Suite, South West Africa: genesis by partial melting of the Khomas schist: Mem. geol. Surv. S. Afr., *64*, 97 p.

MITCHELL, A. H., and READING, H. G., 1971. Evolution of island arcs: J. Geol., *79*, 253–284.

MIYASHIRO, A., 1973. Paired and unpaired metamorphic belts: Tectonophysics, *17*, 241–254.

MIYASHIRO, A., 1973a. Metamorphism and Metamorphic Belts: George Allen and Unwin, London, 492 p.

MOLNAR, P., and GRAY, D., 1979. Subduction of continental lithosphere: Some constraints and uncertainties: Geology, *7*, 58–62.

NAYLOR, R. S., 1968. Origin and regional relationships of the core-rocks of the Oliverian Domes *in* Study of Appalachian geology: Northern and Maritime (Ed. E-An, Zen, W. S. White, and J. B. Hadley): Wiley Interscience, New York, 231–240.

OHMOTO, H., and KERRICK, D., 1977. Devolitization equilibria in graphitic systems: Am. J. Sci., *277*, 1 013–1 044.

ORVILLE, P. M., 1972. Plagioclase cation exchange equilibria with aqueous chloride solution: Results at 700 °C and 2 000 bars in the presence of quartz: Am. J. Sci., *272*, 234–272.

ORVILLE, P. M., 1975. Stability of scapolite in the system Ab-An-NaCl-$CaCO_3$ at 4 kb and 750 °C: Geochim. cosmochim. Acta., *39*, 1 091–1 105.

PARRISH, D. K., KRIVZ, A. L., and CARTER, N. L., 1976. Finite-element folds of similar geometry: Tectonophysics, *32*, 183–207.

PITCHER, W. S., and READ, H. H., 1960. The aureole of the Main Donegal granite: Q. Jl geol. Soc. Lond., *116*, 1–36.

PORADA, H., and WITTIG, R., 1975. Zur Tektonik des Südlichen Damara-Belts: Ber. Sonder Forsch Bers 48, Georg-August. Univ.-Göttingen, 51–70.

RAMBERG, H., 1967. Gravity, Deformation and the Earth's Crust, as studied by Centrifuge Models: Academic Press, New York, 214 p.

RAMBERG, H., 1968. Fluid dynamics of layered systems in the field of gravity. A theoretical basis for certain global structures and isostatic adjustment: Phys. Earth Planet. Interiors, *1*, 63–87.

RAMBERG, H., 1968a. Instability of layered systems in the field of gravity I: Phys. Earth Planet. Interiors, *1*, 427–447.

RAMBERG, H., 1968b. Instability of layered systems in the field of gravity II: Phys. Earth Planet. Interiors, *1*, 448–474.

RAMBERG, H., 1973. Model Studies of gravity controlled tectonics by the centrifuge technique *in* Gravity on Tectonics (Ed. K. A. de Jong, and R. Scholten): Wiley Interscience, New York, 49–68.

RAMSAY, J. G., 1962. The geometry and mechanics of formation of "similar" type folds: J. Geol., *70*, 309–327.
RAMSAY, J. G., 1967. Folding and Fracturing of Rocks: McGraw-Hill, New York, 568 p.
RAMSAY, J. G., and GRAHAM, R. H., 1970. Strain variation in shear belts: Can. J. Earth, Sci., *7*, 786–813.
RAST, N., 1958. Metamorphic history of the Schichallion Complex: Trans. R. Soc. Edinb., *63*, 413–431.
RAST, N., 1969. Orogenic belts and their parts *in* Time and Place in Orogeny (Ed. P. E. Kent, *et al.*): Geol. Soc. Lond., 197–214.
RICE, J. M., 1977. Progressive metamorphism of impure dolomitic limestone in the Marysville aureole, Montana: Am. J. Sci., *277*, 1–24.
RICHARDSON, S. W., 1968. Staurolite stability in a part of the system Fe-Al-Si-O-H: J. Petrol., *9*, 467–488.
RICHARDSON, S. W., GILBERT, M. C., and BELL, P. M., 1969. Experimental determination of kyanite-andalusite and andalusite-sillimanite equilibria: The aluminium silicate triple point: Am. J. Sci., *267*, 259–272.
SAWYER, E. W., 1979. The geology of an area south-east of Walvis Bay: Lithology and field relationships: Rep. geol. Surv. S.W. Afr. (unpubl.).
SCHMID, R., and WOOD, B. J., 1976. Phase relationships in granulitic metapelites from the Ivrea-Verbano Zone (Northern Italy): Contr. Mineral. Petrol., *54*, 255–279.
SCHWERDTNER, W. M., 1973. A scale problem in palaeostrain analysis: Tectonophysics, *16*, 47–54.
SEIFERT, F., 1970. Low-temperature compatibility relations of cordierite in haplopelites of the system K_2O-MgO-Al_2O_3-SiO_2-H_2O: J. Petrol., *11*, 73–99.
SEIFERT, F., 1976. Stability of the assemblage cordierite+K-feldspar+quartz: Contr. Mineral. Petrol., *57*, 179–185.
SEIFERT, F., and SCHREYER, W., 1970. Lower temperature stability limit of Mg cordierite in the range 1–7 kb water pressure: A redetermination: Contr. Mineral. Petrol., *27*, 225–238.
SIBSON, R. H., 1977. Fault rocks and fault mechanisms: J. geol. Soc. Lond., *133*, 191–214.
SLAUGHTER, J., KERRICK, D. M., and WALL, V. J., 1975. Experimental and thermodynamic study of equilibria in the system CaO-MgO-SiO_2-H_2O-CO_2: Am. J. Sci., *275*, 143–162.
SMITH, D. A. M., 1965. The geology of the area around the Khan and Swakop Rivers in South West Africa: Mem. geol. Surv. S. Afr., *3* (S.W.A. series), 113 p.
SOUTH AFRICAN COMMITTEE FOR STRATIGRAPHY, 1976. Draft proposals for nomenclature of the Damara Supergroup and associated granites (unpubl.).
SOUTH AFRICAN COMMITTEE FOR STRATIGRAPHY 1978 (in prep.). Stratigraphic sub-divisions: Geol. Surv. S. Afr.
SPRY, A., 1969. Metamorphic Textures: Pergamon Press, Oxford, 350 p.
SUTTON, J., 1969. Rates of change within orogenic belts *in* Time and Place in Orogeny, (Ed. P. E. Kent, *et al.*): Geol. Soc. Lond., 239–250.
THOMPSON, A. B., 1974. Calculation of muscovite-paragonite-alkali feldspar phase relations: Contr. Mineral. Petrol., *44*, 173–194.
THOMPSON, A. B., 1975. Calc-silicate diffusion zones between marble and pelitic schist: J. Petrol., *16*, 314–346.
THOMPSON, A. B., 1975a. Mineral reactions in a calc-mica schist from Gassetts, Vermont, U.S.A.: Contr. Mineral. Petrol., *53*, 105–127.
THOMPSON, A. B., 1976. Mineral reactions in pelitic rocks: I prediction of P-T-X(Fe-Mg) phase relations: Am. J. Sci., *276*, 401–424.
THOMPSON, A. B., 1976a. Mineral reactions in pelitic rocks: II calculation of some P-T-X(Fe-Mg) phase relations: Am. J. Sci., *276*, 425–454.
THOMPSON, J. B., ROBINSON, P., CLIFFORD, T. N., and TRASK, N. J., 1968. Nappes and gneiss domes in west-central New England *in* Study of Appalachian Geology: Northern and Maritime, (Ed. E-An Zen *et al.*): Wiley Interscience, New York, 203–218.
TOKSOZ, M. N., and BIRD, P., 1977. Modelling of temperatures in continental convergence zones: Tectonophysics, *41*, 181–193.
TRACY, R. J., ROBINSON, P., and THOMPSON, A. B., 1976. Garnet composition and zoning in the determination of temperature and pressure of metamorphism, central Massachusetts: Am. Miner., *61*, 762–775.
TURCOTTE, D. L., and OXBURGH, E. R., 1972. Mantle convection and the new global tectonics: Ann. Rev. Fluid Mech., *4*, 33–68.
TURNER, F. J., and WEISS, L. E., 1963. Structural Analysis of Metamorphic Tectonites: McGraw-Hill, New York, 545 p.
VELDE, B., 1967. Si^{+4} content of natural phengites: Contr. Mineral. Petrol., *14*, 250–258
VERNON, R. H., 1974. Controls of mylonitic compositional layering during non-cataclastic ductile deformation: Geol. Mag., *111*, 121–123.
VERNON, R. H., 1976. Metamorphic Processes, Reactions and Microstructure Development: George Allen and Unwin, London, 247 p.
VERNON, R. H., 1977. Relationships between microstructures and metamorphic assemblages: Tectonophysics, *39*, 439–452.
VERNON, R. H. and FLOOD, R. H., 1977. Interpretation of metamorphic assemblages containing fibrolite sillimanite: Contr. Mineral. Petrol., *59*, 227–235.
VIDALE, R. J. and HEWITT, D. A., 1973. "Mobile" components in the formation of calc-silicate bands: Am. Miner., *58*, 991–997.
WATERS, D. J., 1976. Structural, metamorphic and geochronological studies in the south-east Tauern: Ph.D. thesis, Univ. Oxford (unpubl.).
WEISBROD, A., 1968. Détermination rapide des variations reactionnelles d'entropie et d'enthalpie à partir des courbes expérimentales d'équilibre trace rapide des courbes théoreques d'équilibre: Bull. Soc. fr. Minér. Cristallogr., *91*, 444–452.
WEISBROD, A., 1973. Refinements of the equilibrium conditions of the reaction Fe cordierite=almandine+quartz+sillimanite (+H_2O): Carnegie Instn, Wash. Yb., *72*, 518–521.
WEISBROD, A., 1973a. The problem of water in cordierite: Carnegie Instn, Wash. Yb., *72*, 521–523.
WELLS, P. R. A., 1976. Late Archean metamorphism in the Buksefjorden region southwest Greenland: Contr. Mineral. Petrol., *56*, 229–242.
WHITNEY, J. A., JONES, L. M. and WALKER, R. L., 1976. Age and origin of the Stone Mountain Granite, Lithonia district, Georgia: Bull. geol. Soc. Am., *87*, 1 067–1 077.
WHITTEN, E. H. T., 1966. Structural Geology of Folded Rocks: Rand McNally, Chicago, 678 p.
WILLIAMS, P. F., 1972. Development of metamorphic layering and cleavage in low-grade metamorphic rocks at Bermagui, Australia: Am. J. Sci., *272*, 1–47.
WILLIAMS, P. F., 1977. Foliation: A review and discussion: Tectonophysics, *39*, 305–328.
WINKLER, H. G. F., 1976. Petrogenesis of Metamorphic Rocks: Springer-Verlag, New York, 334 p.
WINTSCH, R. P., 1975. Solid-fluid equilibria in the system $KAlSi_3O_8$-$NaAlSi_3O_8$-Al_2SiO_5-SiO_2-H_2O-HCl: J. Petrol., *16*, 57–79.
WOOD, B. J. and FRASER, D. G., 1976. Elementary Thermodynamics for Geologists: Oxford Univ. Press, Oxford, 303 p.
ZEN, E-An., 1963. Components, phases, and criteria of chemical equilibrium in rocks: Am. J. Sci., *261*, 929–942.